DOCTOR OF PHILOSOPHY

A qualitative and quantitative investigation of structural morphology in the neonatal ilium

Cunningham, Craig Andrew

Award date:
2009

DOCTOR OF PHILOSOPHY

A qualitative and quantitative investigation of structural morphology in the neonatal ilium

Craig Andrew Cunningham

2009

University of Dundee

A QUALITATIVE AND QUANTITATIVE INVESTIGATION OF STRUCTURAL MORPHOLOGY IN THE NEONATAL ILIUM

CRAIG ANDREW CUNNINGHAM

PhD in Anatomy and Forensic Anthropology
University of Dundee
September 2009

CONTENTS

Tables

Figures

Acknowledgements

I would first like to thank my supervisor Professor Sue Black, to whom I owe a great deal of gratitude, which can only be partly expressed here. Sue's constant support and enthusiasm toward my work has been truly inspirational and instrumental in igniting my own desire for furthering knowledge. Under her supervision I have gained many attributes which will remain with me and for which I will be forever grateful.

I also thank the following people who have directly aided data collection and analysis and have played a key role in the success of this research:

Dr Michael Fagan and Ms Sue Taft, Centre for Medical and Engineering Technology, University of Hull, for providing micro-computed tomography facilities.

Ms Margaret Low, for assistance with radiographic procedures.

Mr Scot Dundas, for assistance with clinical computed tomographic procedures.

Dr Steve Hubbard for statistical advice which was essential for the interpretation of the results obtained.

Additionally, I would like to thank the following people for helpful discussions and suggestions at various stages throughout this research:

Dr Sandy Chudek; Professor Rami Abboud; Dr Graeme Houston; Dr Chris Rowland; Dr John McGee; Professor Paul O'Higgins; Professor Terry Meyhew; Dr Soren Blau; Mr Kevin MacKenzie; Mr Nick Corps; Mr Andrew Connell; Mr Andrew O'Malley; Dr John Lucocq; and Dr Peter Taylor.

I would also like to acknowledge all staff within the Centre for Anatomy and Human Identification for providing a professional and approachable environment within which to work. This has greatly aided how enjoyable and productive my research has been.

I am grateful to the following funding sources: BBSRC; Leng Trust; Wenner-Gren Foundation

I would like to whole-heartedly thank my family who have provided endless support and encouragement throughout the duration of my studies. Their belief and pride in me has contributed significantly to enabling the completion of this work.

Finally, I thank my partner and future wife, Jennifer, who has tolerated my grumbles with sympathetic compassion and on many an occasion has re-invigorated my enthusiasm when things didn't appear to be proceeding well. It is to her that I dedicate this work.

Declaration

The candidate is the author of this thesis. Unless otherwise stated, all references cited have been consulted by the candidate. The work, of which the thesis is a record, has been completed by the candidate. No portion of the work referred to in this thesis has been submitted in support of an application for another degree or qualification of this or any other university, or other institute of learning.

Craig Cunningham

Copyright

Statement

I certify that Craig Cunningham has spent twelve terms of research under my supervision. Craig has fulfilled the conditions of Ordinance 39 and is qualified to submit the accompanying thesis in application for the degree of Doctor of Philosophy.

Professor Sue Black

Summary

Cortical and trabecular bone characteristics can be used to make predictions regarding previous loading regimes and developmental milestones which a bone has encountered. This has led to the suggestion that in the adult pelvis, bone patterning is related to the remodeling forces generated during bipedal locomotion. However, during the neonatal period the pelvic complex is non-load bearing, therefore, structural organisation of the ilium cannot reflect direct stance related forces. This study considers the cortical and trabecular bone structure in the ilium of the fetal and newborn infant, a structural configuration which until now has remained largely neglected in the literature.

Only recently, with the advent of imaging modalities, has a greater insight and understanding of previously unexplored human bone structural composition and developing bone structure been made possible. In this study, multiple imaging techniques were applied to establish the optimal modality for application to the assessment of bone microstructure. Plain plate macroradiography and micro-computed tomography were identified as the gold standard imaging modalities for bone structural analysis for respective qualitative and quantitative assessment. These techniques were applied to gain a perspective of bone form from a sample of fetal and neonatal ilia selected from the Scheuer collection of juvenile remains.

Initially, qualitative analysis highlighted consistent and well-defined patterns of cortical and trabecular bone organisation within the fetal and neonatal ilium, which corresponded with previously recognised regions in the adult that have been attributed directly to forces associated with bipedal locomotion. This was highly unexpected as the early developmental ilium is non-load bearing. Subsequently, quantification of the neonatal cortical and trabecular structure reinforced radiographic observations by identifying regions of significant architectural arrangement. Further investigation of this

precocious patterning led to a revised proposal for the mode of growth in the human ilium during the neonatal developmental period. Analysis revealed statistically significant differences in regional trabecular characteristics and cortical thicknesses which have formed the basis of a proposed growth model for the ilium. The presence of ‘progressive growth regions’ and ‘restricted growth regions’ which appear to relate to metaphyseal and non-metaphyseal borders of the ilium have been demonstrated.

Analysis of the early iliac bone pattern is important for understanding the relationship between trabecular bone patterning and cortical bone structure during the earliest stages of development in response to the specific functional forces acting during this period. It is suggested that the seemingly organised rudimentary scaffold observed in the early developmental ilium may be attributable to early ossification patterning, non-weight bearing anatomical interactions or even to a predetermined genetic blueprint.

It must also be postulated that whilst the observed patterning may be indicative of a predetermined inherent template, early non-load bearing locomotive influences may subsequently be superimposed upon this scaffolding and perhaps reinforced and likely remodelled at a later age. Ultimately, the analysis of this fundamental primary pattern has core implications for understanding the earliest changes in iliac trabecular architecture and provides a baseline insight into future ontogenetic development and bipedal capabilities. Finally, the structural data and statistical analysis presented challenge the current concept of implied centrifugal ossification within the human ilium and present evidence of an alternative pattern of ossification that is largely dictated and controlled by basic anatomical principles.

CHAPTER 1 – Introduction

1.1 Outline of thesis

Wolff's law and the fundamental principles around which it is formulated today, encompasses the works of many biomechanical investigators, who, although not afforded the great scientific accolade of a law in their name, have been instrumental in their contribution towards our current understanding of bone modeling and remodeling. Our current interpretation of Wolff's law has changed significantly from the first publication of his doctrine, and today it has been replaced by the more scientifically accepted term 'bone functional adaptation', which in essence excludes the strict mathematical rules that defined the original theory. However, regardless of the semantics of terminology the same basic principles apply. These are that bone is functionally adaptive to stresses and strains, in that it is laid down where there is an increase in stresses and strains and conversely where there is a lack of stresses and strains, it is resorbed. It is from this theory of functional adaptation that this research, investigating the external and internal architecture of the ilium during the earliest stages of development, will be based.

With emphasis on bone functional adaptation, it is postulated that throughout ontogeny, the developmental stresses and strains which are placed upon the pelvic complex will be reflected in the configuration of the internal architecture and external morphology for a specific temporal period. Therefore, this research aims to address how the iliac cortical and trabecular structure changes in response to progressive developmental demands and associated functional interactions during the early stages of ontogenetic periodicity. Based on the current knowledge of gross trajectory pathways which have been derived from the adult iliac structure (Aiello and Dean, 1990; Scheuer

and Black, 2000), it should be possible to monitor how these trajectory pathways develop from an ontogenetic perspective and observe how they change in response to natural progressive stages of physical maturation. Establishment of the gross positioning of these pathways and the mode by which they develop will allow the isolation of individual volumes of interest which can be quantified in terms of trabecular characteristics and cortical thicknesses in relation to bone maturity. Ultimately, this analysis will produce a detailed signature of morphological cortical and trabecular changes in relation to specific regional and functional alterations during the fetal and neonatal period of development.

This research will be carried out using a unique range of specimens to which a combination of imaging technologies appropriate to visualising the internal architecture of bone will be applied. Plain plate radiography will be utilised in the first instance for the qualitative visualisation of gross differences in bone density and characterisation of basic developmental bone patterning. This preliminary investigation will be supplemented and expanded upon by the application of micro-computed tomography (μCT) for the three dimensional visualisation of the internal architectural structure. Subsequently, raw data obtained from micro-computed tomography data sets will be transferred into model-independent stereological software packages for histomorphometric analysis and reconstruction into three dimensions. Stereological analysis will allow for quantification of important trabecular bone indices and cortical bone thicknesses, contributing to the detailed knowledge of trabecular characteristics within specific regions of the ilium. Finally, both qualitative and quantitative data will be related to developmental characteristics and events allowing for a detailed insight into early cortical and trabecular bone development within this fundamental skeletal structure. This advanced knowledge will contribute to a greater understanding of

developmental bone mechanics which can be applied and expanded upon in a variety of disciplines. However, the primary aim of this study is to make a significant contribution to the anthropological literature by documenting hitherto unknown human developmental bone growth in the ilium.

In summary, this study aims to document the trabecular architecture and cortical thickness of the ilium from an early developmental perspective taking into account the temporal biomechanical interactions which may influence bone form during the fetal and neonatal period. Therefore, it may be possible to determine the natural template of biomechanical alteration during the earliest developmental stages prior to the adoption of an obligate bipedal stance.

1.2 Biomechanical and Clinical Significance

Research based on the internal trabecular architecture of the human pelvic complex and the way in which it changes throughout development has an important bearing on many different scientific disciplines. The primary importance of this study is directed towards an advanced knowledge of biomechanical, anthropological and developmental theory.

The pelvic complex is a particularly significant structure within the biomechanical framework of the skeleton in that it is an extremely robust, semi-closed osteo-articular ring located at the base of the trunk. It acts as protective armour to internal soft tissues, is a structural conduit between the axial and appendicular skeleton, has a large surface area for muscular attachment, is a fundamental structure in the formation of the birth canal and has an important haemopoetic function. Specifically, it is the segmental link bridging the vertebral column at the sacrum, and the lower extremity at the femur, acting as a major conduit in the transfer of weight from the

upper body to the ground. In addition it must accommodate the dissipation of ground reaction forces from the head of the femur in the opposite direction as a result of standing and active locomotion (Dalstra and Huiskes, 1995).

The human pelvis has evolved into an efficient structure which is adapted to carry and distribute large repetitive forces (Kapandji, 1987). It is reasonable to infer that these forces must ultimately contribute to determining its external morphology and internal architecture. Skeletal tissues are able to respond to functional influences in a manner that leads to an optimal design for prevailing functional requirement. As such, the pelvic region is of particular interest in this regard as its complex dynamic development is multifunctional. The pelvic complex is directed by the influences of normal bone expansion that reflect standard growth requirements for muscle and ligament attachments associated with bipedalism. These are subsequently modified to accommodate an expanding cavity with soft tissue spatial requirements. In addition, it must retain sufficient pliability to undergo substantial alterations at a later stage in response to the secondary sexual development to prepare the structure as a birth canal in the female.

Assuming that Wolff's law of bone functional adaptation holds true, these progressive dynamic influences will be reflected in the way in which the internal and external architecture of the complex accommodates to such demands. The pelvis progresses through a series of phases that influence alterations to its biomechanical structure. These phases will be reflected not only in the relative size, shape and positioning of the pelvic components but also in the strength and direction of its internal trajectory architecture. The periods of greatest functional and biomechanical alteration are likely to occur within distinct periods of development. The ontogenetic temporal windows which are expected to represent greatest internal architectural differentiation

are; in the fetus and the neonate, six months post partum, 1-2 years, 3-5 years, and 6-9 years. Those which will be investigated in this study include the fetal and neonatal developmental cohorts. This specific age cohort has been chosen due to its hypothesised internal architectural changes and for the purposes of establishing a detailed baseline understanding for future ontogenetic investigation, (see section 1.6).

In the context of these developmental windows of investigation, and the skeletal morphological development which is predicted to occur in response to temporal functional influences, a fundamental insight into normal human locomotor development may be achieved. The establishment of a template of human locomotor behaviour, reflected in changing bone morphology, may then be related to the architectural variation between animals with different locomotive signatures and profiles.

In summary, the pelvis is a particularly important area of the skeleton for developmental and biomechanical studies. This is due to the fact that the development of the pelvis is a particularly complex aspect of skeletal form coupled with the requirement that the continuously changing forces that the pelvis must accommodate throughout life, have a direct and significant influence on the internal trabecular architecture and external cortical morphology. Relatively little work has been directed towards the overall structure and the variation in trabecular bone during ontogeny (Tanck *et al*, 2001; Ryan and Krovitz, 2006; Ryan *et al*, 2007). This has created a deficiency in the foundation upon which trabecular bone adaptation can be used for anthropological inferences (Gosman and Ketcham, 2009). A detailed knowledge of iliac trabecular and cortical bone form during early development will aid in our understanding of the developmental processes to which the ilium is subjected throughout an important growth period and provide a baseline data set for subsequent predictive studies of altered mechanical loading.

In addition to biomechanical and developmental studies, the investigation of pelvic morphology has particular importance in clinical medicine, as the way in which bone models and remodels is significant to paediatrics, orthopaedics and many other disciplines. The term paediatric is constructed from the Greek words ‘paedion’, meaning child, and ‘iatriki’, meaning medicine, literally translated as ‘medicine for children’ (Soutis, 2006). Paediatrics is the sub speciality of medicine which attends to the medical care of individuals from birth through to adolescence. This is a significant period of development for most structures within the body including the skeleton and from the early fetal period the skeleton is subject to constant modeling and remodeling pressures (Delaere and Dhem, 1999; Hadjidakis and Androulakis, 2006; Mulder *et al*, 2007). The rate of bone remodeling during the neonatal period and during the first two years of life has been reported to be much higher than is exhibited in the adult (Walker 1991). The remodeling pressures the skeleton endures are due to the constant changing temporal and spatial events which cause the bone to adapt and change in order to accommodate these requirements. As these internal changes are so fundamental and integral to the process of bone development it is imperative that the paediatric physician is acquainted with the normal pattern of internal structure present at each developmental stage. This knowledge is important for the purposes of monitoring normal growth in the child and for the ability to correct any anomalies which may arise within the pelvic complex. It is in the same ilk that the speciality of orthopaedics would be greatly supplemented with an increased knowledge of pelvic internal architecture.

Orthopaedics, coined by French physician Nicolas Andre in 1741, from Latin words meaning ‘straight child’ (Lee and Taylor, 1999), is the branch of medicine concerned with the correction or prevention of skeletal deformities. As a result of this research, the orthopaedic specialist would be equipped to augment their diagnostic

arsenal with an increased knowledge of the internal structure of the pelvic complex and the characteristic changes which it undergoes throughout the initial stages of development. At present, developmental anomalies of the pelvic complex, and traumatic alterations to its normal structure are managed with an array of corrective and stabilising devices which continue to develop in their ability to correct these abnormalities (Musemeche *et al*, 1987; Stanitski, 2005). Disorders which are regularly associated with pelvic orthopaedics relate to gait anomalies. Normal bipedal gait is necessary to carry out fundamental daily activities and due to this, much emphasis is placed on the correction of such disabilities due to the profound impact they have on an individual's physical and mental well being. Gait has been tracked from a developmental point of view from the first appearance of a bipedal stance, to the appearance of a mature gait pattern (Sutherland *et al*, 1980) (see section 2.2.4 for review) and many studies have further focused on the deterioration of gait with advancing age (Sudarsky, 1990). Through the investigation of normal gait and the ever increasing emphasis placed on research in the field of walking and exercise, a clear representation of the 'normal' has been postulated (Inman *et al*, 1981; Whittle, 1991). It is from this normal template that medical practitioners can distinguish compensatory patterns of gait from pathological gait and in cases where therapeutic intervention is required a more accurate diagnosis can be made. With a growing knowledge of how to correct anomalies of the pelvic complex and a drive for increased therapeutic application and better clinical outcome, a corresponding increase in understanding of this region's changing internal architecture must also be gained. It can be surmised that if an orthopaedic practitioner is presented with a natural template of biomechanical alteration throughout an ontogenetic series, a much better diagnostic platform may be achieved for optimal therapeutic application and surgical intervention.

It is also hoped that this research may be applied in a comparative anatomical manner, whereby the results obtained for the early developmental human pattern of iliac form, may be compared with other Hominin species. This is of importance as the architecture of the pelvis has regularly been used to infer origins of bipedality from specimens early in the Hominin lineage (Macchiarelli et al, 1999; Rook, 1999; Martinon-Torres, 2003). Therefore, a comprehensive investigation of the developing human pattern of iliac bone formation may aid in further understanding evolutionary origins of bipedality and indeed comparisons of general gross bone patterning across species.

Finally, and as an accessory application of this study it is proposed that if a characteristic and identifiable internal signature of developing trabecular architecture and cortical thickness is present, then this could potentially be applied in the forensic sense for aging juvenile material. The ability to determine at which developmental stage a particular trajectory pathway is laid down, altered, maintained or resorbed may have diagnostic implications for the aging of an individual when presented with a fragmented piece of the juvenile pelvic complex. It is frequent in the forensic recovery of skeletal remains that the pelvic complex does not survive inhumation intact, with the features of the innominate that exhibit the highest levels of dimorphism and the strongest correlation with chronological age, often being damaged or missing in exhumed material (MacLaughlin and Bruce, 1986). Thus, in many instances there may only be fragmentary, incomplete remains of a structure which would have proved useful, if intact, in aiding the identification procedure. As such, when presented with a small region of the pelvic bone, the internal trabecular pattern could be analysed and paralleled with the normal template of biomechanical alteration so that a prediction of age at death, or other features could be ascertained.

1.3 Motivation for this study

In recent studies, and indeed in the historical literature, much work has concentrated on the investigation of trabecular bone architecture with the aim of elucidating its mechanical role within the skeletal system (Evans, 1957, 1973; Lanyon, 1974; Carter and Hayes, 1977; Gibson, 1985; Goldstein, 1987; Frost, 1990a; Ciarelli *et al*, 1991; Biewener *et al*, 1996; Keaveny *et al*, 2001; Jee, 2005; Liu *et al*, 2006). Consistently, these investigative studies have made particular and continued reference to long bones and most specifically to the proximal femur (Ward, 1838; Osborne *et al*, 1980; Von Mayer, 1867; Wolff, 1986; Carter *et al*, 1989; Drapeau and Streeter, 2006; Rudman *et al*, 2006; Ryan and Krovitz, 2006; Skedros and Baucom, 2007). This is presumably due to a number of factors including the linear trajectories observed in the long bones and most likely, tradition has played a significant part in this tendency (Huiskes and Chao, 1983). More recent investigations have extended into other previously neglected areas of the skeleton, notably those which are subjected to significant tensile and compressive forces, including the calcaneus (Maga *et al*, 2006; Rupprecht *et al*, 2006), the talus (Pal and Routal, 1998), the proximal tibia (Gosman and Ketcham, 2008) and the vertebral column (Jensen *et al*, 1990; Haidekker *et al*, 1999; Rapillard *et al*, 2006).

Despite an increasing trend towards investigation of trabecular dynamics, surprisingly little is documented regarding the changes to the internal structure of the developing human pelvis (Dalstra *et al*, 1993). However, despite this, the pelvis has long been used in osteological studies for the aging and sexing of individuals due to its highly dimorphic nature and well documented ontogenetic alterations (Boucher, 1957; Weaver, 1980; Krogman and Íşçan, 1986). Likewise much emphasis has been placed on this poorly understood complex in the clinical context, as the way in which the pelvis

grows and matures can lead to many anomalies in the juvenile which span well into adult life (Tronzo and Okin, 1975). Due to its importance in both these fields there has been a constant drive to improve upon our current knowledge of this fundamental skeletal structure, with most studies and data concentrating on external morphological features for the determination of the age, sex and stature of an individual (Straus, 1929; Boucher, 1957; Jovanivic and Zivanovic, 1965; Bruzek and Soustal, 1981), as well as selection of the most appropriate orthopaedic devices (Tile and Pennal, 1980; Miller *et al*, 1990). This investigative drive has left a particularly large discrepancy in the knowledge of internal architectural structure and the bearing it may have on the predictive capacity of developmental, anthropological and clinical studies. This deficit in our knowledge of pelvic biomechanics requires to be supplemented with a comprehensive study of its changing internal and external structure from a developmental perspective.

Ontogenetic studies of trabecular architecture are important for furthering our understanding of the mechanical properties of bone as during life, bone develops into a load bearing structure (Mulder *et al*, 2007) requiring the trabecular architecture to be structurally arranged in order to accommodate and remodel in response to a life time of changing stresses (Martinon-Torres, 2003). This structural arrangement is fundamentally important as trabecular architecture has been shown to play a significant role in bone strength and in determining the skeleton's biomechanical properties (Majumdar *et al*, 1998; Ulrich *et al*, 1999b; Müller, 2005; Bevill *et al*, 2006). It is only recently that studies have been initiated in an attempt to compensate for the lack of knowledge of this intricate yet fundamental area of skeletal biology, with a view to determining the distribution of stresses throughout the skeletal structure (Goel *et al*, 1978; Dalstra *et al*, 1993; Dalstra and Huiskes, 1995). However, although these studies

have contributed to an increased understanding of theoretical pelvic stress distribution from a bioengineering perspective, they have continued to neglect the specific regional and developmental trabecular characteristics which give bone its strength. Their only contribution to understanding pelvic skeletal morphology has been to document the pelvic complex as a sandwich construction with a core of trabecular bone covered by an outer and inner layer of compact bone (Dalstra *et al*, 1993).

The pelvis should be a significant focus for developmental and biomechanical studies as it represents a junctional complex where the transfer of weight from the upper body to the lower extremity is redirected through a non-linear route. It is also an area within the skeleton which undergoes continually changing stresses throughout development therefore making it a functionally significant region for investigating trabecular structural integrity that leads to an understanding of biomechanical failure. As changes associated with body size and locomotor behaviour are reflected in trabecular bone architecture, the pelvic complex should be a key focus for such studies (Oxnard and Yang, 1981; Thomason, 1985; Carter *et al*, 1989; Galichon and Thackeray, 1997; Macchiarelli *et al*, 1999; Rook *et al*, 1999; Fajardo and Müller, 2001; MacLatchy and Müller, 2002; Ryan and Ketcham, 2002; Lai *et al*, 2005; Ryan and Krovitz, 2006; Fajardo *et al*, 2007).

However, recent studies offer only small pockets of information on this very large topic and have tended to consider only isolated temporal characteristics relating to a particular single behaviour and have a more phylogenetic rather than ontogenetic emphasis (Macchiarelli *et al*, 1999; Rook *et al*, 1999; Marchal, 2000; Fajardo and Müller, 2001; Fajardo *et al*, 2002; Ryan and Ketcham, 2002; Martinon-Torres, 2003; Ryan and van Rietbergen, 2005). At present no study has been dedicated to investigating the full human ontogenetic spectrum of the development of the internal

architecture of the pelvis, encompassing all stages of development that may influence the morphology of the internal characteristics. It is surprising that with the vast array of knowledge and research which has concentrated on orthopaedics and bone biomechanics that this region of the skeletal complex has remained neglected for so long. In understanding the way in which the iliac internal architecture is first laid down, through the differing stages of biomechanical alteration, which are dependant upon temporal stresses and strains, it is likely that a new perspective on developmental biomechanics, clinical diagnosis and forensic analysis may be obtained.

1.4 Scheuer Collection

This study was carried out using selected age cohorts from the Scheuer collection of juvenile skeletal remains. The Scheuer Collection is believed to be the only active repository for juvenile skeletal remains held anywhere in the world. It consists of the remains of over 100 subadult individuals, collected from archaeological and historical anatomical sources. Although some of the material is of documented identity, the majority has been aged and sexed using the dentition and various other metric and morphological evaluations of isolated bones. The collection is composed of a combination of complete skeletons and individual skeletal elements or partial skeletons. All specimens used in this study were in a good to excellent state of preservation with minimal damage to the cortical shells and underlying trabecular structure. Any specimens which displayed excessive damage or questionable pathology were excluded from the sample. The collection is housed within the Centre for Anatomy and Human Identification, College of Life Sciences, University of Dundee. The material offers significant opportunities to address areas of education and research into skeletal development that have largely been ignored in the past due to a paucity of material. In

using the Scheuer collection, the results and conclusions of this study must be treated in the context of the cross-sectional nature of the material. It is from this cross-sectional snapshot of ontogenetic growth that inferences about longitudinal development can be postulated, but in light of current imaging capabilities, have never been studied.

1.5 Objectives for this study

The objectives of this study are to investigate the external and internal structure of the ilium in response to local temporal forces experienced throughout early development. External and internal morphology will be investigated both quantitatively and qualitatively to provide a comprehensive perspective of early developmental skeletal alteration in the ilium. In summary, this study aims to characterise the temporal sequence and variation in trabecular bone structure and cortical bone thickness during the fetal and neonatal developmental period as related to the acquisition of normal functional activities. Specific objectives are:

1. To document, using radiographic procedures, the mature iliac density representation and relate this to muscular interactions and bipedal locomotive influences.

2. To investigate, using qualitative radiographic procedures, the general bone patterning of the fetal and neonatal ilium prior to the influences of weight bearing locomotion and compare this to the final mature adult template.

3. To investigate quantitatively, using micro-computed tomographic procedures, the ontogenetic trabecular architecture of the neonatal ilium.

4. To investigate, quantitatively, the gluteal and pelvic cortical thicknesses of the neonatal ilium.

5. To relate quantitative and qualitative data to normal developmental milestones and functional interactions.

1.6 Hypotheses for ontogenetic pelvic alteration

The focus of this study is aimed at characterising the changing external and internal morphology of the developing ilium taking into account the functional influences placed on the bone from an ontogenetic perspective. The premise of the hypothesis is based on the well documented knowledge that trabecular bone density and microarchitecture are influenced by mechanical forces during growth and development resulting in the adult configuration through the process of Wolff's law or the more commonly termed 'bone functional adaptation' (Martin *et al*, 1998; Huiskes *et al*, 2000; Carter and Beaupre, 2001; Ryan and Krovitz, 2005). Therefore, it is hypothesised that during early fetal development, trabecular bone architecture will be laid down in a generally disorganised template of randomly distributed bony struts reflective of normal endochondral ossification of cartilage septae (Byers *et al*, 2000). This pattern of generalised trabecular distribution, characterised by the absence of any preferential alignment or differentiated regional characteristics is hypothesised due to the absence of any weight bearing influences or any significant mechanically functional anatomical influences *in utero*. This pattern of generalised trabecular distribution is predicted to continue into the neonatal period as the absence of any direct stance related weight transfer is characteristic of this developmental period. Further to this, any developing

anatomical interactions associated with the iliac portion of the innominate are hypothesised to have a minimal influence on the basic structural composition of the bone. Initial changes and organisation to trabecular structure and external cortical thickness are hypothesised to occur during the subsequent developmental window, around the age of six months. During this developmental period trabecular characteristics are hypothesised to reflect the shift in the child's centre of gravity from a predominantly supine dynamic to that of a sitting posture. This dramatic change in the centre of gravity, redirecting the line of weight transfer through the ischial tuberosities, and the muscular interactions involved is reported to set-up a sacro-ischial trajectory (Kapandji, 1987; Aiello and Dean, 1990; Scheuer and Black, 2000). This force trajectory is hypothesised to be reflected in the trabecular characteristics in the underlying trabecular bone and the thickness of the overlying cortex. Following on from this developmental milestone, the period between 1 and 2 years of age is considered to be a significant temporal milestone for investigation. During this developmental period, a child is purported to adopt a bipedal stance altering the entire dynamic of forces passing through the ilium. This change in the centre of gravity and the redirection of forces within the ilium is reported to set up the superior and inferior auriculo-acetabular stress trajectories (Kapandji, 1987; Aiello and Dean, 1990; Scheuer and Black, 2000). In addition to these compressive weight-bearing trajectories it is expected that compensatory tensile trabecular trajectories will also be developed. These force trajectories are hypothesised to alter the trabecular characteristics towards a structurally competent morphology quantified by strengthened trabecular arrangements and reinforced cortical thickness along weight bearing lines. Subsequently, the external and internal structure of the ilium at 3-5 years of age is likely to respond to the physical effects of visceral descent. The descent of the viscera into the true pelvis from the

abdomen is considered to have profound implications on the structural dynamics of the complex as a whole and the ilium in particular. It is hypothesised that a significant shift in the centre of gravity, combined with the required change in iliac dimensions and positioning required to accommodate the migrating organs, will be reflected in the trabecular architecture and cortex thickness due to realignment of the lines of stress and resultant strengthening of trabecular characteristics. Finally, the iliac trabecular and cortical structure between the ages of 6-9 years are also considered to be functionally significant windows for investigation. These developmental periods are thought to be reflective of the attainment and reinforcement of mature gait (Popova, 1935; Inman *et al*, 1981; Keen, 1993; Li *et al*, 1996; Verhulst, 2003; Kubo and Ulrich, 2006). During this period, the dynamics of stress transference and the lines of weight transfer are thought to be redirected once again and will be reflected in both the trabecular morphology and the local cortical thickness. As well as the primary developmental events described, consideration was also given to other general anatomical interactions which develop alongside the ilium and are hypothesised to have varying degrees of influence on the changing dynamic of the ilium which are reflected in the changing structural morphology. These include muscular, ligamentous, vascular, and neurological tissue interactions.

Due to a combination of imaging and analysis limitations, along with unexpected results, the original aim of the project was subsequently modified. It was originally intended that a full ontogenetic documentation of trabecular architecture and cortical morphology would be undertaken. However, this was restricted to include analysis of only the fetal and neonatal developmental period for two distinct reasons. The first of these was due to the limitations of the imaging system and associated analysis software which were unable to produce sufficient spatial resolution for accurate

quantification of structural parameters in specimens older than the neonate due to increasing specimen size. Secondly, analysis was confined to the fetal and neonatal age range, due to the unexpected results obtained from the early developmental sample which required further investigation. As results from trabecular and cortical analysis deviated from the initial hypothesis, it was deemed appropriate to focus the aim of the project towards explaining the organised early bone patterning. This was conducted through extensive analysis and discussion of this isolated developmental period and complimented the inability to extend analysis beyond this developmental period due to technical limitations.

CHAPTER 2 – Anatomy and Biomechanics of the Pelvis

2.1 Anatomical structure of the adult pelvic girdle

The pelvic complex, in its skeletal and soft tissue form, is the anatomical component which links the entirety of the upper body to the lower limbs. The soft tissue structures of the pelvis are supported and protected by the bones of the pelvic girdle which confer both stability and the potential for mobility to the trunk and lower limbs. The joints at which stability and movement must be regulated are: the hip joints, linking the lower limb to the pelvic girdle via the acetabulum; the sacroiliac joints, which unite the girdle to the axial skeleton posteriorly, and the pubic symphysis which completes the osteo-articular ring anteriorly.

Soft tissue structures associated with the pelvic complex are considered to influence its morphological characteristics through form:function relationships. These soft tissue interactions involve muscular, ligamentous, vascular and neural structures which are associated with the innominate bones at defined sites, aiding to sculpt its morphological form. Muscular interactions are major determinants of pelvic morphology, responsible from the fetal period for initiating periosteal ossification (Delaere *et al*, 1992), to the effects on the maturing bone in defining its various characteristic landmarks. Additionally, ligamentous tissues are considered to induce a significant remodeling response within the skeleton dependant upon their anatomical location and associated functional role. The pelvic complex is also host to other soft tissue structures which, although not attaching directly to the bony skeleton, are considered to have an influence on skeletal morphology. Soft tissue structures of this nature housed within the complex include the fasciae, vessels, nerves and viscera of the pelvis. Other than sexual differences related to the internal genital viscera, the basic soft

tissue anatomy of the pelvis between the two sexes is fundamentally the same (Rosse and Gaddum-Rosse, 1997).

In the most simplistic terms, sexual differences reflected in the morphology of the pelvic complex, post-puberty, are controlled by the influence of a biochemical system that has either a higher level of testosterone or oestrogen, resulting in the human pelvic complex being described as the most sexually dimorphic skeletal component in the human body (Krogman and Isçan, 1986). Sexual dimorphism results from the response of tissues to either a surge in testosterone or oestrogen at puberty. In the female, it is largely the presence of oestrogen receptors that result in the growth changes that relate to female alteration in shape. The relative proportions of the female pelvis give it a more spacious cavity, wider apertures, and a lighter skeletal frame compared to the male (Rosse and Gaddum-Rosse, 1997; Leong, 2006) (Figure 2.1). Adaptations of the female pelvic complex to parturition are also reflected widely in the pelvic skeletal landmarks and overall morphology (Correia *et al*, 2005), features which are essential for safe and successful passage of the fetal head through the pelvic inlet and outlet.

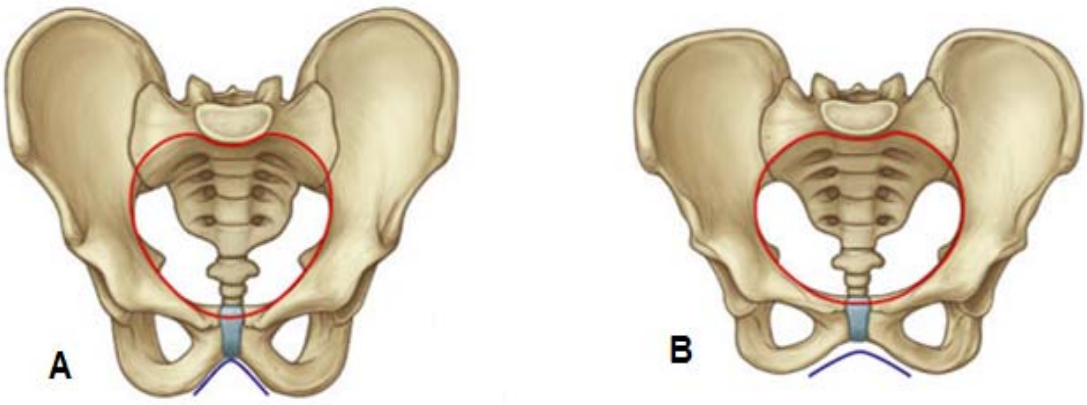

Figure 2.1. The sexually dimorphic features in the male (A) and female (B) pelvic complex. The female has a wider pubic arch, oval pelvic inlet and more laterally positioned ischial tuberosities than the male. Modified from Drake *et al*, 2005.

Sexual differences in hormone levels are present from the early fetal period, which has resulted in studies aimed at identifying sexual differences in pre-pubertal morphology (Thomson, 1899; Weaver, 1980; Schutkowski, 1993). However, it is widely considered that these levels are insufficient in quantity to allow dimorphism to be measured. Whilst bone remodeling occurs throughout life those changes instigated at puberty tend to be retained into adulthood, however, levels of dimorphism in the elderly have not been investigated in any detail. The sexually dependant differences observed in the pelvis are intimately linked with its adaptive functions (Leong, 2006), and are most likely to be directly related to the differing temporal events of development and the pathway along which weight is directed. A description of skeletal and soft tissue structural composition will follow to provide an overall brief account of pelvic osteology and anatomy.

2.1.1 Pelvic skeleton

The pelvic complex is composed of the two innominates and the sacrum which articulate posteriorly at the sacroiliac joints and anteriorly at the pubic symphsis (Figure 2.2). The primary function of the pelvic complex is the transmission of forces between the axial skeleton and the lower limbs (Dalstra and Huiskes, 1995; Rosse and Gaddum-Rosse, 1997). In acting as the segmental link between the upper body and lower extremity, its structure must be robust and confer strength as well as being relatively light weight (Jacob *et al*, 1976), particularly in an animal that habitually walks on two legs. Taken in isolation, the innominate, or os coxae, is a large, flattened, irregularly shaped bone, unique from any other in the human skeleton (Figure 2.3). It and its symmetrical partner are involved in constituting the bony pelvic complex, each forming a respective lateral boundary of what is often described as a basin-like structure.

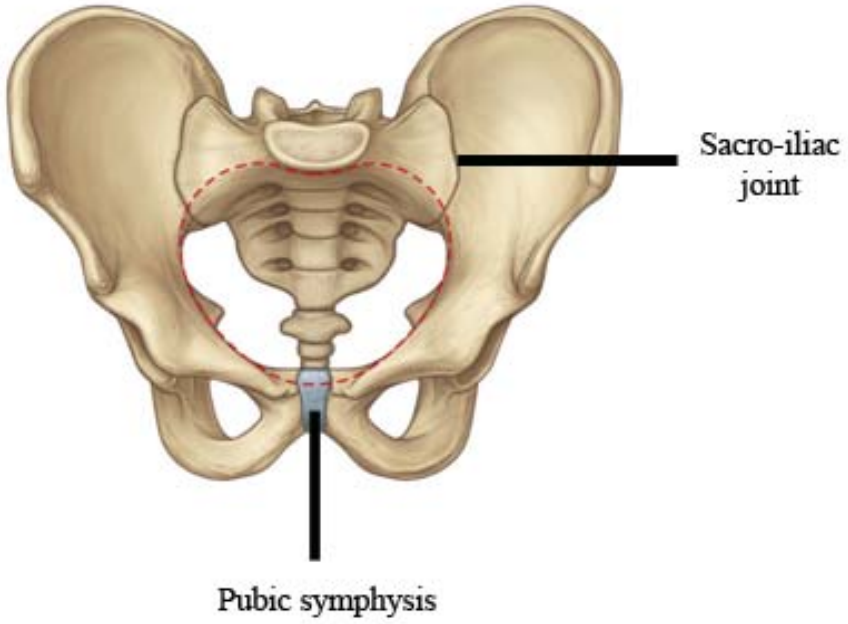

Figure 2.2. Pelvic complex composed of two innominates and sacrum articulating at the sacro-iliac joints posteriorly and pubic symphysis anteriorly. Modified from Drake *et al*, 2005.

The pelvis is often referred to in this manner as the word pelvis can be translated to basin and is a term which is used for referring to both the skeletal structure of the pelvis and the pelvic cavity as a whole when introducing soft tissue structures. The adult innominate is formed by the fused orientation of the ilium, ischium and pubis which diverge in different directions from the focus of the acetabulum (Figure 2.3). The ilium is the upper most extensive part of the innominate forming the large superiorly directed iliac blade and the superior 2/5 of the acetabulum (Scheuer and Black, 2000). The ischium forms the posteroinferior directed portion of the innominate forming the large ischial tuberosity posteriorly and the posterior 2/5 of the acetabulum. Finally, the pubis forms the anteromedially directed portion of the innominate and contributes to the anterior 1/5 of the acetabulum. The ischium and pubis are also connected via the ossified ischio-pubic ramus (Williams *et al*, 1989; Scheuer and Black, 2000).

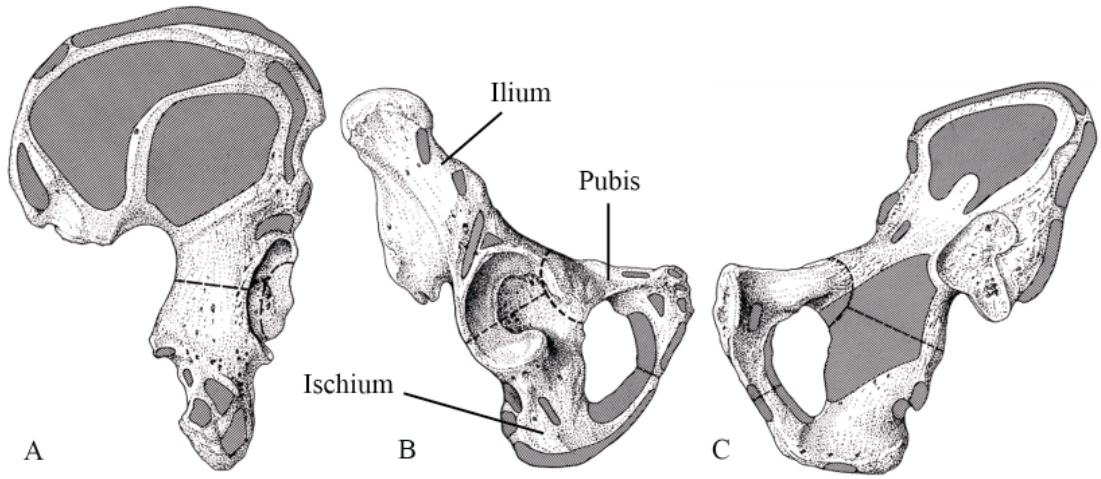

Figure 2.3. Right innominate viewed from gluteal (A), acetabular (B) and sacro-pelvic (C) surfaces. Shaded regions represent areas of muscle attachment. Dashed line represents the division between the ilium above, ischium below and posterior, and pubis below and anterior. Modified from Scheuer and Black, 2000.

On the lateral aspect of the innominate there is a deep cup shaped depression known as the acetabulum which is defined as facing laterally, downwards and forwards (Rosse and Gaddum-Rosse, 1997). Around most of the acetabular perimeter, a bony lip causes a dense incomplete rim of bone which is open inferiorly manifesting as the acetabular notch leading into the acetabular fossa in the central aspect of the acetabulum. The centre of the fossa is characterised by a roughened non-articular appearance, which is surrounded by the articular portion of the joint presenting as a smooth lunate surface.

Within the innominate there is a large, oval foramen termed the obturator foramen which lies below the acetabulum and is bounded by the pubis and ischium (Figure 2.3). This is a large foramen when compared to the structures which pass through it and in the living this opening is closed by the obturator membrane and only a small portion remains patent to allow a conduit for relevant neurovascular bundles to enter the medial aspect of the thigh. Observed in its whole form, the pelvic complex

resembles a funnel, with an inferiorly directed narrow aperture (pelvic outlet) and a superiorly positioned broad aperture (the pelvic inlet), which is the link between the abdominal and pelvic cavities (Rosse and Gaddum-Rosse, 1997).

The remaining features of the innominate are best described in connection with the individual bones in which they manifest. Therefore, the ilium, ischium and pubis and their associated features will be described in isolation.

Ilium

The ilium is a large flattened area of bone which projects superiorly from its acetabular portion into a large wing like expanse termed the ala or blade. The medial (pelvic) surface of the iliac ala flanks the abdominal cavity and forms the iliac fossa. The lateral (gluteal) surface of the ala forms a large surface area for the attachment of the gluteal musculature. Superiorly, the terminal border of the ala is thickened and forms the iliac crest which is S-shaped terminating anteriorly in the anterior superior iliac spine, and posteriorly in the posterior superior iliac spine. Located below the anterior superior iliac spine on the anterior border of the bone, is the anterior inferior iliac spine. Likewise, the posterior inferior iliac spine is located below the posterior superior iliac spine on the posterior border of the bone. It is at the point of the posterior inferior iliac spine that the greater sciatic notch commences and it is defined by a concavity along the inferior margin of the ilium allowing for the passage of important anatomical structures including the sciatic nerve, piriformis muscle and several neurovascular bundles.

The portion of the ilium superior to the greater sciatic notch is thickened and presents the sacropelvic surface, which faces medially. On the lower part of this surface is the auricular surface, which is covered with articular cartilage, and articulates with

the sacrum forming the sacroiliac joint. The rest of the sacropelvic surface, superior and posterior to the auricular surface, is occupied by a rough protuberance, the iliac tuberosity. Attached to the tuberosity are the strong sacroiliac ligaments, of major importance for assuring a stable union between the pelvic girdle and the sacrum. A smooth ridge, the arcuate line, begins at the anterior border of the auricular surface and extends forwards and downwards, separating the iliac fossa from the medial surface of the body of the ilium.

Ischium

The ischium is composed of a body and a ramus forming the posteroinferior directed portion of the innominate. The body contributes to forming the acetabulum and the lateral wall of the pelvic cavity, with its posterior margin bordering the greater sciatic notch. The ramus extends inferiorly from the body then curves anteriorly to form the posteroinferior boundary of the obturator foramen. The junction of the ramus and the body is marked on the posterior margin of the ischium by a bony prominence, termed the ischial spine. On the posteroinferior margin of the ramus a large bony protuberance is evident and is termed the ischial tuberosity. The concavity of the posterior margin of the ramus between the ischial spine and tuberosity forms the lesser sciatic notch.

Pubis

The pubis forms the ventral component of the pelvic girdle and consists of a body and two rami. The body is a flat, somewhat triangular piece of bone that forms the narrow anterior wall of the pelvic cavity. Its pelvic surface faces upwards and posteriorly, and its perineal surface downwards and anteriorly. Medially, the body

presents a rough and narrow symphseal surface with which it is firmly bounded, in the median plane, to the contralateral pubis. The anterosuperior margin of the body is thickened and forms the pubic crest which terminates laterally as the prominent pubic tubercle. The two rami of the pubis diverge from the body into superior and inferior divisions. The superior ramus passes laterally and superiorly to fuse with the ilium and ischium in the acetabulum. Conversely, the inferior ramus passes inferiorly and fuses with the ramus of the ischium forming the inferior boundary of the obturator foramen.

2.1.2 Pelvic soft tissue anatomy

The pelvic skeleton is approximated with several anatomical structures, some of which are considered to contribute to its developing and ultimate adult morphological form. These anatomical interactions are considered to have a specific effect on the ultimate phenotype of the growing complex due to their close association with the skeleton and the potential strains/influences they may confer to the approximated skeletal components. Specific details of anatomical interactions will be restricted to the ilium for the purposes of this communication.

Initial consideration is given to the muscles which attach to the iliac cortex on both the pelvic and gluteal surfaces. The iliac ala, due to its large and superiorly fanning expanse is well suited for the large degree of muscle attachment which it must support (Figure 2.4). Indeed, it may also be argued that the ilium adopts this morphology in response to the muscle mass it must accommodate. On the gluteal surface of the iliac blade there are several muscular attachments which can be subdivided into regional compartments. Muscular interactions described here will follow those documented for the adult but reflect the same, albeit reduced mass of the muscle tissue, in the developing child.

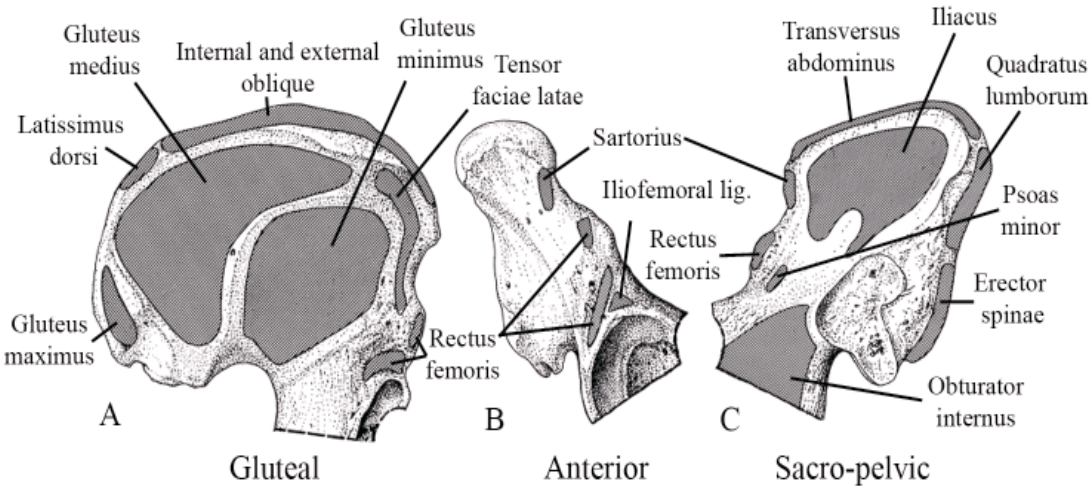

Figure 2.4. Muscular attachment sites on the A: gluteal, B: anterior, and C: sacro-pelvic surfaces of the adult ilium. Modified from Scheuer and Black, 2000.

The large muscles of the buttocks take their origin from the ala of the gluteal surface (Figure 2.4). These include the gluteus maximus, gluteus medius, gluteus minimus and the tensor fasciae latae muscle. Along the iliac crest there is a strong muscular interaction from the latissimus dorsi, internal and external abdominal oblique muscles. At the anterior superior iliac spine the attachment of sartorius, the inguinal ligament and the external oblique is responsible for the bony protuberance which defines this landmark. Inferior to this at the anterior inferior iliac spine, the attachment of the straight head of the rectus femoris is evident, the reflected head of rectus femoris is observed on the acetabular component of the gluteal surface just superior to the acetabulum.

On the ala of the pelvic surface of the ilium the large and expansive iliacus muscle takes attachment to the majority of the iliac fossa, further to this the psoas minor is observed to attach to the acetabular component of the pelvic cortex at a position superior to the acetabulum (Figure 2.4). Along the iliac crest on the pelvic surface, transversus abdominus, quadratus lumborum and erector spinae muscles take

attachment and contribute, along with gluteal crest musculature, to producing largely superiorly directed tensile forces (Figure 2.4).

Ligamentous interactions are also considered to have a dominant influence on the morphology of the skeletal elements with which they are associated. On the gluteal surface the ligamentous attachments are few and are considered to have a limited impact on the overall morphology of the ilium and instead are considered to influence only isolated landmarks. Predominant ligamentous interaction on the gluteal surface comes from the ligamentous hip joint capsule (Figure 2.5). Although this capsule surrounds the entirety of the acetabulum which involves all three bones of the innominate, only the most superior portion of the capsule and the iliofemoral ligament are associated with the ilium.

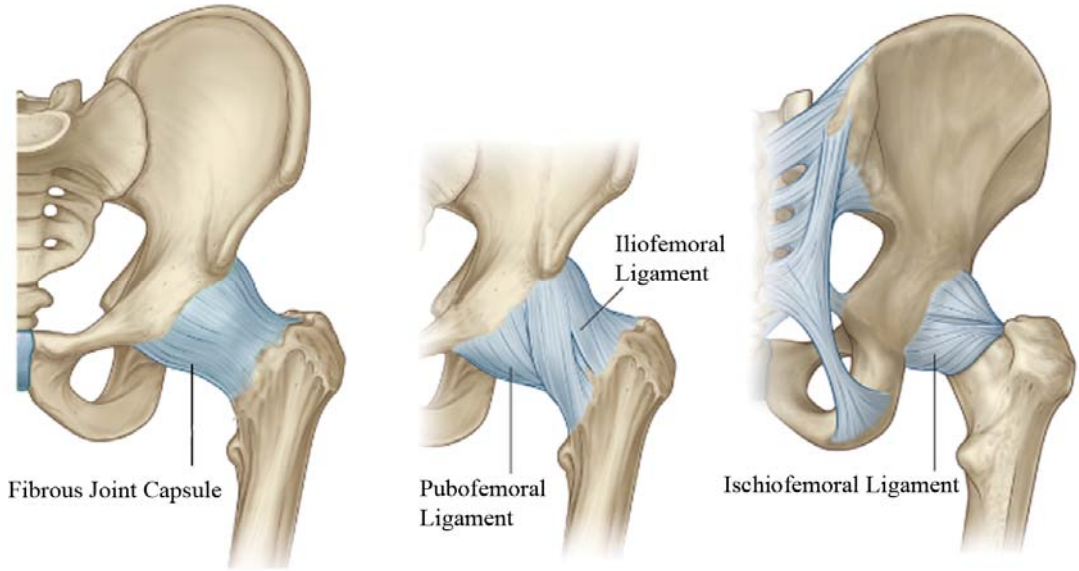

Figure 2.5. Ligamentous joint capsule. Modified from Drake *et al*, 2005.

On the sacropelvic surface of the ala, much larger ligamentous attachments manifest due to the necessity to stabilise the union between the sacrum and the innominate in the joint that is the sacroiliac joint. These ligaments are present as the iliolumbar ligament,

dorsal and interosseous sacroiliac ligaments, and the ventral sacroiliac ligament (Figure 2.6). These intricate ligaments are more extensive dorsally, functioning as a connecting band between the sacrum and ilia (Bowen and Cassidy, 1981). This ligamentous interaction is particularly evident in the posterior auricular region where ligamentous association causes the bony attachment site to become extremely pronounced and robust. The main function of this ligamentous system is to limit motion in all planes of movement. However, in the female pelvis these ligaments are weakened during the final stages of pregnancy, to facilitate the mobility necessary for parturition.

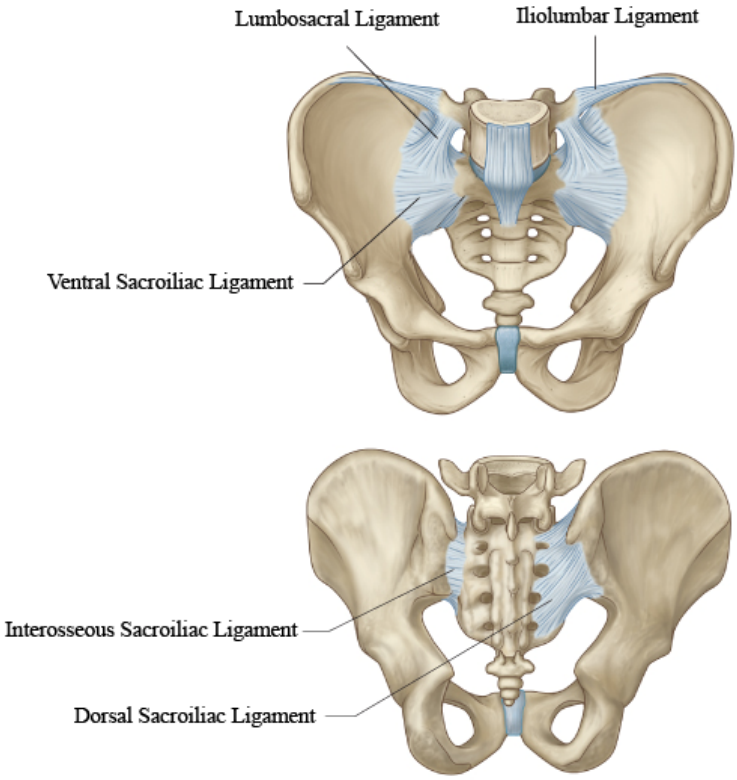

Figure 2.6. Ligaments of the sacroiliac joint. Modified from Drake *et al*, 2005.

Consideration must also be given to the influence that neurovascular structures have on the developing structure of the pelvis and its ultimate adult morphology. The common iliac artery and vein are the primary vessels which supply and drain all the

pelvic structures (Figures 2.7 and 2.8). The vessels which branch from, and form tributaries to, the common iliac vessels may have an impact on bone morphology. The main branches of the common iliac artery are the internal and external iliac arteries. Branches of the internal iliac artery take their course within the pelvis to supply the walls of the pelvis, the pelvic viscera and the gluteal region and medial thigh. The larger external iliac artery exits the pelvic complex under the inguinal ligament to become the femoral artery, supplying the lower limb (Figure 2.7). The venous drainage in this region adopts similar positioning and nomenclature to the arterial structures (Figure 2.8). In addition to the dominant arteries discussed, small vessels pierce the cortex of the ilium invading the trabecular architecture as dominant nutrient arteries (Brookes, 1971; Crock, 1996).

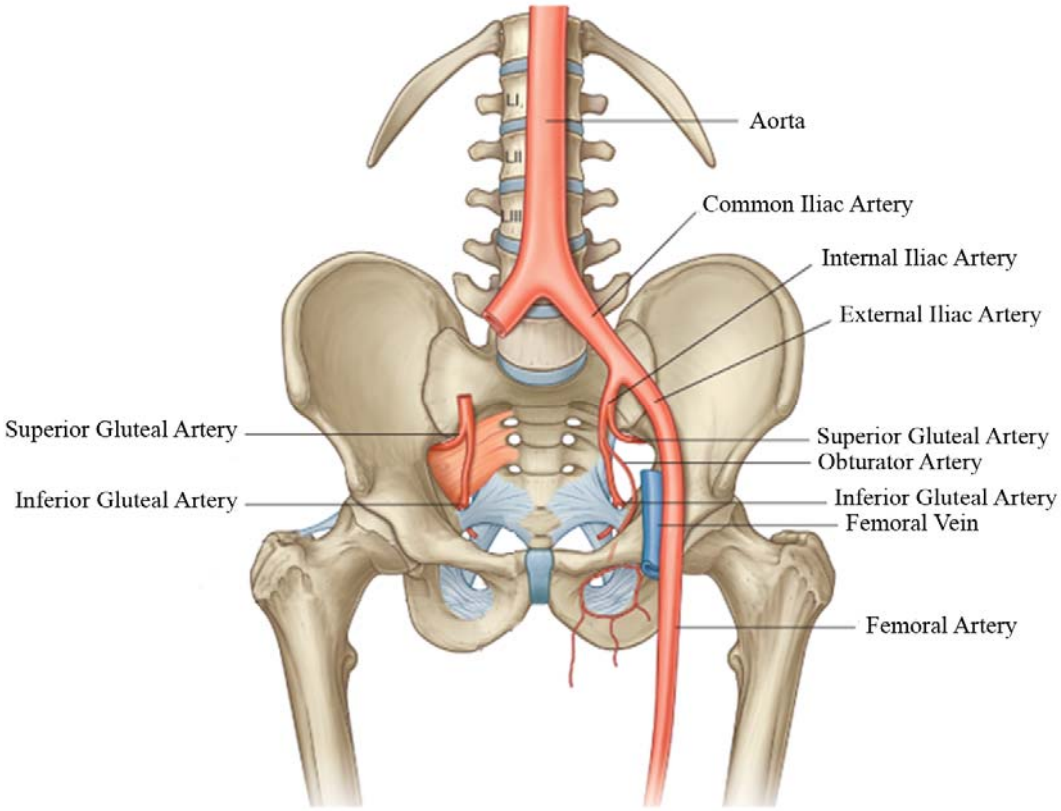

Figure 2.7. Arteries associated with the pelvic complex. Modified from Drake *et al*, 2005.

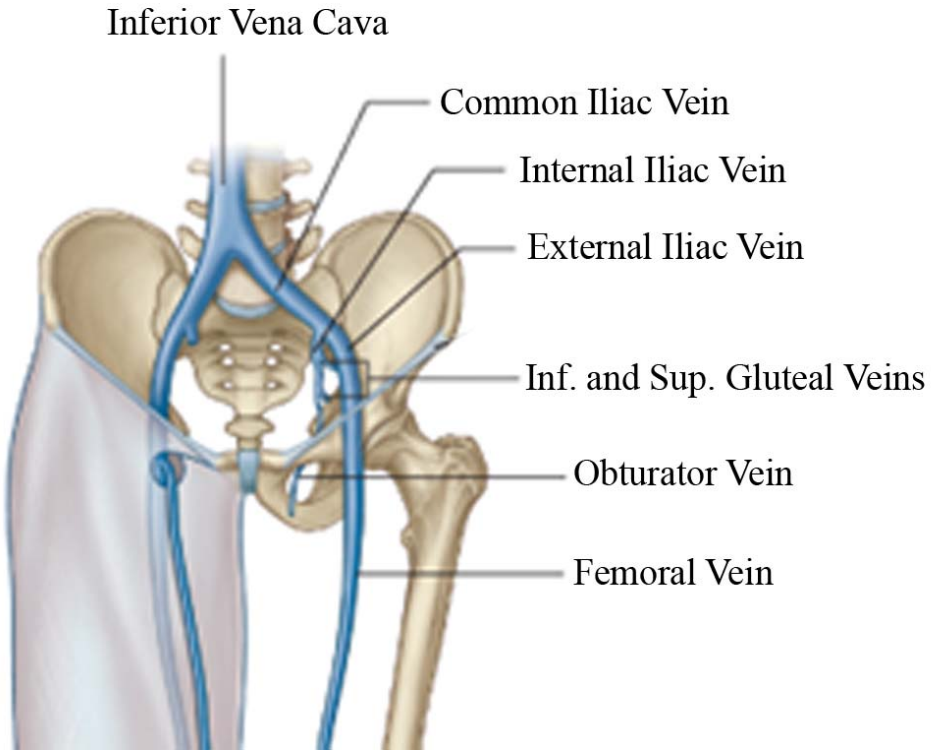

Figure 2.8 Veins associated with the pelvic complex. Modified from Drake *et al*, 2005.

Further to vascular influences, several nerves enter the pelvis in the form of the lumbosacral plexus and have various associations with the soft tissues and more importantly, proximity to the skeletal tissues (Figure 2.9). Nerves enter the pelvis through the superior pelvic aperture or through the sacral foramina. They leave the pelvis by passing over the brim of the pelvic diaphragm, through the urogenital hiatus or by ascending back out of the superior pelvic aperture. The main branch of the sacral plexus which may have implications for the developing form of the ilium is the sciatic nerve. The sciatic nerve passes in close proximity to the greater sciatic notch. This structural association is considered to influence the form of the developing external and internal structure due to the physical positioning of this large nerve in relation to the bone and also due to potential neurogenic signalling which may alter the way in which bone remodels (Laurenson, 1963; 1964a).

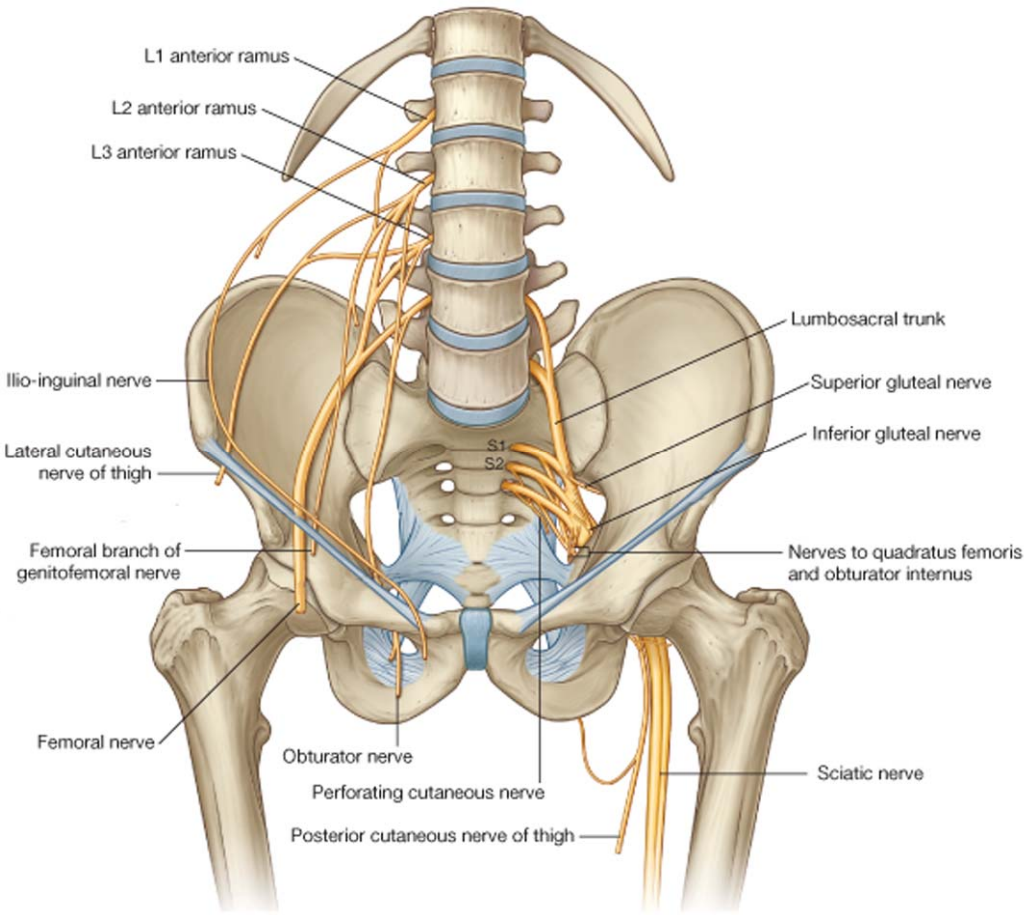

Figure 2.9. Nerves associated with the pelvic complex. Modified from Drake *et al*, 2005.

Finally, the pelvic viscera must be considered due to their proximity to the pelvic skeleton. The pelvic viscera which present and develop equally in both sexes are the rectum, urinary bladder, and the ureters. However, sexual differences in the internal genitalia are evident and the reasons for these differences can be attributed to the fact that the descent of the female gonad is arrested in the pelvis whereas that of the male gonad proceeds to the outside of the body (Rosse and Gaddum-Rosse, 1997). The interactions the pelvic viscera have on the skeletal form of the pelvic complex are of particular importance around the time of visceral descent (3-5 years), when the viscera move from their abdominal origin downwards into the pelvic cavity (Scheuer and Black, 2000).

2.2 Biomechanics of the pelvic girdle

When considered from a mechanical perspective, the human musculoskeletal system is a poorly adapted structure in terms of its characteristic upright posture. This is primarily due to its multisegmented structure, its inefficiently positioned centre of mass, and its small base of support. However, the skeleton's multi-joint design allows balance to be maintained in a variety of body configurations, as well as during movement. Therefore, despite the mechanical complexity of the body's anatomical composition, it is surprisingly stable, and the central nervous system has the ability to coordinate posture and movement by combining mobility with stability (Hodges *et al*, 2002). This is particularly relevant to the pelvic complex which is viewed as a mechanically complex intersection from a biomechanical perspective, in terms of the range of movements it must accommodate, the loads it transmits and the structures it protects. During normal bipedal walking, the joints of the pelvic complex, namely the sacro-iliac joint and hip joint, are required to be sufficiently mobile to accommodate required movements whilst at the same time remaining suitably stable to prevent inefficiency or collapse of the structure.

2.2.1 Hip joint

The hip joint, sometimes referred to as the acetabulofemoral joint is the multiaxial synovial joint situated between the acetabulum of the innominate and the head of the femur that connects the lower limb to the pelvic girdle. The primary function of the hip joint is to support the weight of the body in both static and dynamic postures whilst facilitating movement. The joint is surrounded by a thickened fibrous capsule and associated ligaments which confer strength and combined mobility allowing for a stabilised yet highly moveable joint with a large range of movement. Yet

despite this wide range of movement, the joint remains capable of accommodating the weight of the trunk, head and upper limbs. The primary ligamentous associations which act to stabilise and reinforce the joint are the iliofemoral, pubofemoral, ischiofemoral ligaments and ligamentous orbicularis (Torry *et al*, 2006). These ligaments act to resist excessive extension, abduction and medial or lateral rotation of the joint, reinforcing the anterior, inferior and posterior aspects of the joint capsule respectively. Specifically, the iliofemoral ligament, considered to be the strongest ligament in the body, is involved in the efficient counterbalance of gravitational forces during relaxed standing (Aspden *et al*, 2006).

Movements of the hip joint are an essential element of normal gait activities. Due to the ball and socket like nature of the joint the movements permitted include; flexion-extension, abduction-adduction, lateral and medial rotation and circumduction (Rosse and Gaddum-Rosse, 1997). Flexion and extension are produced by the spin of the femoral head within the acetabulum around a mechanical axis that passes through the femoral neck. Abduction, adduction, and medial and lateral rotation are the result of swing and slide of the femoral head and neck.

The muscles that allow for mobility of the hip joint as well as conferring inherent stability can be divided into five groups according to their orientation around the hip joint. Firstly, the extensor muscle group includes gluteus maximus, quadriceps femoris and the hamstrings. The lateral rotator muscle group includes obturator and the gemellus muscles as well as quadratus femoris and piriformis. The adductor muscle group includes pectineus and adductors brevis, longus and magnus. The flexor muscle group includes iliopsoas, rectus femoris, tensor facia lata and sartorius. Finally, the abductor muscle group includes tensor faciae latae, gluteus medius and gluteus

minimus. Many of these muscles are responsible for more than one type of movement in the hip, as different areas of the muscle act on tendons in different ways.

2.2.2 Sacro-iliac joint

The largest axial joint in the skeleton is the sacro-iliac (SI) joint (Bernard and Cassidy, 1991) and is the joint which connects the sacrum to the ilium via respective auricular surfaces. This joint is extremely variable in its morphology between individuals and often between contralateral sides of the same individual. It has irregularly shaped articular surfaces which permit only minimal movement in the form of gliding (translation) and rotation. The sacro-iliac joint is not considered to display any significant sexual dimorphism due to the fact that the SI joint does not transmit forces from the upper body across the joint surfaces (Last, 1973; Scheuer and Black, 2000), instead, weight is transferred through the strong ligamentous material which encapsulates the joint (Bowen and Cassidy, 1981; Vleeming *et al*, 1990). The joint is regularly characterised as a diarthrodial synovial joint, however, only the anterior aspect of the joint surface is synovial, with the remainder comprised of predominantly strong ligamentous association (Bowen and Cassidy, 1981; Vleeming *et al*, 1990; Cohen, 2005). The primary function of the large ligamentous component is to limit motion of the joint in all planes of movement (Cohen, 2005), conferring overall strength to the joint. However, this strength is compromised in the female to allow for necessary mobility during parturition. In addition to supporting ligaments, strength is also conferred to the joint capsule by a network of muscles which are functionally connected to the SI joint ligaments (Walker, 1992), contributing to joint mobility (Cohen, 2005). These muscular interactions are considered to increase the compressive force between the ilium and sacrum, protecting the ligamentous system and assisting in the distribution

of force from the trunk to the lower extremity (Pel *et al*, 2008). Although, the anatomical arrangement of the joint allows a degree of mobility, the primary function is that of stability, by limiting x-axis rotation, and specifically for the transmission and dissipation of forces from the upper body to the lower extremities (Cohen, 2005).

In younger individuals, rotational displacements and translational movements occur normally during locomotion. However, the joint is prevented from significant displacement due to the interlocking of the sacral and iliac auricular surfaces when a load is transferred across the joint. As a result of this load transmission and the interlocking of the joint surfaces, the sacrum effectively becomes wedged between the ilia. In normal movement of the joint, loads transmitted to the first sacral vertebra tend to force the sacrum downwards and forwards, causing its lower end to rotate upward and backwards. The sacrotuberous and sacrospinous ligaments anchor the lower end of the sacrum and resist rotation of the sacrum between the innominate bones. This movement of the sacrum puts tension on the interosseous sacroiliac ligaments which, in turn, tend to draw the two ilia closer together (Rosse and Gaddum Rosse, 1997).

Therefore, the sacrum combined with the two innominates act as a single biomechanically secure functional unit. Nevertheless, slight movements are possible between the pelvic girdle and the sacrum prior to potential obliteration of the joints with advancing age in males. These potential biomechanical movements of the joint occur about all three axis, however, movements are very small and notoriously difficult to measure (Walker, 1992). Various studies have been undertaken to investigate this degree of movement, aimed at explaining load-displacement and rotation in the joint (Miller *et al* 1987). Further studies using cadaveric material have investigated the range of motion within the joint during flexion and extension, concluding that movement is in fact minimal (Sturesson *et al*, 1989; Vleeming *et al*, 1992). Further to this, studies

investigating sex differences in the movement observed at the SI joint revealed that the main motion in males tends to be translation, whereas in females it is rotation (Brunner *et al*, 1991). Based on these studies of normal joint motion it has been postulated that when rotation is more than 6 degrees and translation more than 2 mm there is pathological sacroiliac joint movement (Kissling and Jacob, 1996).

2.2.3 Pubic symphysis

The final joint constituting the pelvic complex is the pubic symphysis which is a secondary cartilaginous joint formed by the midline association of the symphyseal surfaces of right and left innominates. This joint is stabilised by strong ligaments which traverse the joint both superiorly and inferiorly attaching to the pubis. The superior pubic ligament connects the superior aspect of the pubic bodies, extending along their superior border and attaching to the pubic tubercles. The inferior pubic ligament connects the inferior borders of the joint forming the superior border of the pubic arch (Moore and Dalley, 1999). The primary function of the pubic symphysis is the absorption of forces which are generated within the complex during bipedal gait (Dalstra and Huiskes, 1995).

2.2.4 Gait

The interaction of each of the joints and anatomical structures discussed, results in the ability for controlled movement manifesting predominantly in obligate ambulation. Therefore, the development of mature gait is a particularly significant biomechanical milestone involving well coordinated relationships between inborn reflexes, the musculoskeletal system and neuromotor systems (Keen, 1993). The documentation of gait, from a biomechanical and developmental point of view, is

particularly important as humans are characterised by the fact that at the age of around one year a bipedal stance is adopted and developed throughout subsequent years until adoption of a fully mature gait pattern (Bril and Brenière, 1992; Kubo and Ulrich, 2006). The adoption of a bipedal stance is an important developmental event due to the fundamental nature of the skill for human functioning and for understanding the process of developmental change (Adolph, 2002). It is now generally considered that the development of obligate bipedal locomotion was one of the most significant adaptations to occur within the hominin lineage (Harcourt-Smith and Aiello, 2004). Locomotion is required for a large number of activities, from simple walking, through to more complex demands such as running, support against gravity and reciprocating motions (Rose and Gamble, 1994). It is for these reasons, as well as many others, that a comprehensive understanding of gait is fundamental to the interpretation of biomechanical alteration within the skeleton. In response to this, much work has been carried out to investigate normal and abnormal gait mechanisms. Analysis has ranged from basic recordings taken from footprint impressions to the more advanced and sensitive force plate equipment currently applied (Li *et al*, 1996; MacWilliams *et al*, 2003). These studies have demonstrated that it is possible to visualise and understand a very detailed pattern of walking which enables a clear representation of what is clinically accepted as normal. With the ability to define a normal gait pattern, the template can then be applied to the diagnosis of abnormal gait and lead to the planning and application of corrective procedures. The application of gait analysis is widely used in many fields, including medicine for predictive purposes, e.g. in determining if a muscle compartment is fully functional and for preventative purposes, e.g. in preventing ulceration of the diabetic foot (Rajput *et al*, 2008). Gait analysis has also been used in the forensic context when trying to establish an individual's identity (Barker and Scheuer, 1998). It is therefore

clear that normal gait and the ability to analyse it, is essential for many different purposes.

Mature gait can be defined by five specific determinants including; duration of single limb support, walking velocity, cadence, step length and ratio of pelvic span to ankle spread (Sutherland *et al*, 1980). Once gait maturity is reached, and each of the determinants has been fulfilled, normal gait then remains constant throughout life unless a gait anomaly occurs, such as those most frequently observed with advancing age (Sudarsky, 1990) and in gait pathologies (Saunders *et al*, 1953; Perry, 1992). Normal walking can be defined as 'a method of locomotion involving the use of the two legs, alternately, to provide both support and propulsion' (Whittle, 2002). Usually when describing elements of gait, only one leg is taken into account as the opposing leg is performing the same actions only a little out of phase. When describing the actions of the single limb, the first contact of the foot with the ground is termed first heel strike, simply because the heel is the first structure which comes in contact with the ground. This event is followed by the main events summarising single leg actions which are; foot flat, mid stance, heel off, toe off and mid swing before returning to second heel strike when the cycle starts again. Each stage is illustrated well by its given term. These events are grouped into different stages of the gait cycle, namely stride time, stance phase and swing phase. Stride time is the time taken from the first heel strike until the second heel strike of the same foot. Stride time is then further divided into stance phase and swing phase. Stance phase is defined as the time from heel contact to toe off , when the foot is in contact with the ground, whereas swing phase is defined as the period from toe off to second heel strike, when the foot is not in contact with the ground (Whittle, 1991). The timing of the gait cycle, documenting the movement of each individual leg with respect to the other can be well illustrated in a simple diagram where periods of

double support, when both feet touch the ground, and single support can be seen in between strides (Figure 2.10).

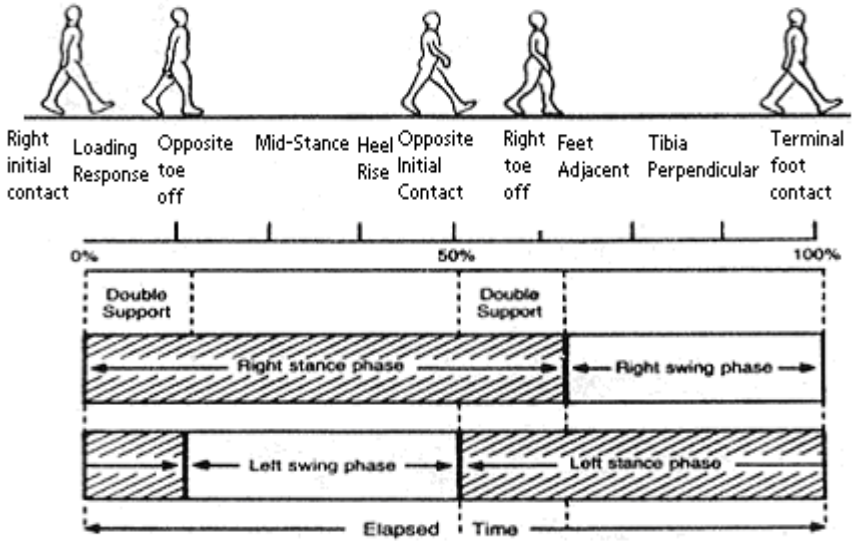

Figure 2.10.Gait cycle. Modified from: Sudarsky, 1990

Prior to normal mature gait being observed or analysed, the ontogeny of gait must first be fully understood. This is optimally traced from the earliest developmental periods, throughout embryonic life, into fetal life and through to birth when the means for walking is developed. Developmental events include the formation of the nervous system followed by mesenchymal derivatives such as bone and muscle within the limb bud at around four weeks of gestation (Rose and Gamble, 1994). The harmony of each system and process is essential for the future viability of the fetus as well as the early childhood ability to walk. During the fetal period the primary forces which act on the pelvis are considered to arise from early limb movements induced by muscular action (Walker, 1991, Thelen *et al*, 2002). It has long been held that this movement is a pivotal factor in the development of the locomotor apparatus (Pitsillides, 2006), and ossification in general. Considerable evidence exists to support the hypothesis that mechanical

forces have an essential role in embryonic skeletal development (Nowlan *et al*, 2007). Such evidence has suggested that defined periods of embryonic movement may impact upon the future adaptability of individual components of the musculoskeletal system to mechanically derived stimuli (Pitsillides, 2006).

At the time of birth, the child has the means for walking but has yet to develop and learn to master the co-ordination of its limbs in order to develop a bipedal stance. The process of learning to stand and then walk is different in humans than in other animals as the ability to walk is not an inborn reflex, and instead mastering of an erect bipedal stance is a prolonged learning process (Inman *et a*l, 1981). Once a child has learned to stand upright at approximately one year, there are a number of characteristic gait phases which occur sequentially. These include the ability to run at around 2 years, climbing stairs to varying ability between 2 and 4 years, as well as more developed characteristics such as hopping and skipping between 4-5 years (Keen, 1993). These developmental milestones culminate in a single major definable stage which is when the characteristic 'mature' patterns of walking, seen in the adult, are observed. The exact time frame for the emergence of this mature pattern is debated in the literature, presumably due to the criteria used for this conclusion. It has been reported that a mature gait is developed as early as three years of age (Sutherland *et al*, 1980; Sutherland, 1997), however, several other reports state that mature gait is not reached until seven to nine years of age (Popova, 1935; Inman *et al*, 1981; Li *et al*, 1996; Keen, 1993; Verhulst, 2003; Kubo and Ulrich, 2006). These observations have been made, based upon the many variables thought to be accountable for the maturation of gait, each influencing the developmental potential. These variables include neurological changes and the resultant effect on muscle action, with the maturation of the central nervous system from the second week of gestation through the second year of life being

of premier importance (Rose and Gamble, 1994). Other variables include psychological changes associated with motor learning, biomechanical influences observed in gross changes in skeletal structure and the effect of environmental influences, including the amount of handling and opportunities the child has had to walk (Sutherland *et al*, 1980).

2.3 Ontogenetic development of the pelvis

With a knowledge of the anatomy and biomechanics of the adult pelvic form, it is appropriate to consider the development of the complex from an ontogenetic perspective. The growth of the pelvic complex is achieved through skeletogenesis, a complicated, dynamic and generally co-ordinated process (Guldberg *et al*, 2004), involving strategically monitored temporal events which ultimately lead to the fully functional mature bony pelvis. The first appearance of the pelvic form is observed early in the embryonic period at around Carnegie stage IX (Bardeen, 1905), when the mesenchymal primordium extends in the form of three processes: a superior iliac, an inferior posterior ischial and an inferior anterior pubic (Fazekas and Kosa, 1978). At this time the pelvic scleroblastema of the embryo undergoes rapid development, with the iliac portion extending dorsally towards the sacral region (Bardeen, 1905; Fazekas and Kosa, 1978), and anteriorly towards the abdominal musculature (Bardeen, 1905). While the blastemal ilium is becoming differentiated, both the pubic and ischial processes of the pelvic blastema extend rapidly forward and ventral to the obturator nerve ultimately becoming joined by a tissue condensation, forming the obturator foramen of the blastemal pelvis. Finally, the pubic mesenchymal primordia meet in the midline and fuse at the site of the future pubic symphysis (Scheuer and Black, 2000).

As the blastemal pelvis matures and differentiates, the formation of cartilage in the ilium, ischium and pubis proceeds, extending rapidly from the centres of

chondrification, which appear at around 44 days, Carnegie stage XVIII (Bardeen, 1905; O'Rahilly and Gardner, 1975). The process of chondrification has been documented to include five phases of development:

- phase one, characterised by the presence of intercellular material enclosing cells emerging from the skeletal blastema.
- phase two, by the slender shape of the cell.
- phases three and four, by the cuboidal shape of the cells as well as increasing cell size and vacuolisation of the cytoplasm.
- phase five, characterised by the extensive disintegration of the cell (Streeter, 1949).

During chondrification the cartilage model grows as a result of proliferation of fibroblasts in the mesenchyme surrounding the cartilage primordium and their transformation into young cartilage cells (Laurenson, 1964b). The first area of chondrification in the pelvis is observed at five weeks, in the ilium, situated cephalad to the greater sciatic notch (Laurenson, 1964b), and is present as a flattened rod of cartilage with anterior and posterior surfaces (Bardeen, 1905). The ischial and pubic chondrification centres first appear at around 7-8 weeks (Gardner and O'Rahilly, 1972), as rounded masses of tissue lying within the central portion of their respective blastemal processes (Bardeen, 1905). At this stage in the pelvic development, at the interface between blastemal pelvis and chondrification, the acetabular region is composed mainly of blastemal tissue with the exception of the iliac and ischial cartilages, which form part of its floor (Bardeen, 1905). Chondrification events which follow in succession are:

- The meeting of the cartilaginous pubic masses by the end of the second month (Adair, 1918).

- Definition of anatomical landmarks including the anterior superior iliac spine, ischial tuberosity and ischial spine (Bardeen, 1905).

At the beginning of the third intra-uterine month the cartilaginous pelvis is well developed and approaching completion (Bardeen, 1905; Adair, 1918).

Upon establishment of the cartilaginous pelvic template, ossification is observed to proceed. Ossification of the pelvic complex is first observed between the end of the second and beginning of the third intra-uterine month (Bardeen, 1905; Adair, 1918; Noback, 1944; Gardner and Gray, 1950; Noback and Robertson, 1951; O'Rahilly and Gardner, 1975; Birkner, 1978). The site of primary ossification is observed in a similar region to where each centre of chondrification was first observed, specifically in the perichondrium, superior to the greater sciatic notch (Laurenson, 1964a). Ossification in the ilium proceeds in a cranial direction into the iliac blades on both the gluteal and pelvic surfaces, without invading the underlying cartilage (Birkner, 1978; Delaere *et al*, 1992). Intramembranous ossification of the iliac shells is considered to commence in response to the development of the alar musculature (Laurenson, 1964a; Delaere *et al*, 1992; Scheuer and Black, 2000). This initial mode of bone formation is termed intramembranous appositional ossification, which is the more primitive of the two modes of ossification which will ultimately ensue (Scheuer and Black, 2000).

Intramembranous ossification is defined as the direct mineralization of a highly vascular connective tissue membrane and commences via the process of *de novo* mineralization. This process involves structures known as matrix vesicles (MVs), which are double membrane bound extracellular structures of approximately 100 nm in diameter (Anderson, 1995). These membrane-invested particles are selectively located at sites of initial calcification in cartilage, bone, predentin (Anderson and Pandy, 2003), and generally within connective tissue, often in clusters between collagen fibrils

(Bonucci, 1967). The first crystals of apatitic bone mineral are formed within the MVs close to the inner surface of their investing membrane (Anderson and Pandy, 2003). Matrix vesicle biogenesis occurs by polarized budding and pinching-off of vesicles from specific regions of the outer plasma membranes of differentiating growth plate chondrocytes and osteoblasts. Polarized release of MVs into selected areas of developing osteoid matrix determines the non-random distribution of calcification. Initiation of the first mineral crystals, within MVs, is augmented by the activity of MV phosphatases in addition to calcium-binding molecules, all of which are concentrated in or near the MV membrane. The next phase of biologic mineralization begins with crystal release through the MV membrane, exposing preformed hydroxyapatite crystals to the extracellular fluid which normally contains sufficient Ca_2^+ and $PO_4^{(3-)}$ to support continuous crystal proliferation. The preformed crystals then serve as template nuclei for the formation of new crystals by a process of epitactic nucleation (Anderson and Pandy, 2003). The mineral deposits which result from this process are observed as bone nodules within the mesenchymal matrix which subsequently fuse to form seams of woven bone. As the matrix becomes increasingly mineralised the matrix vesicles are fragmented and destroyed as they serve no further purpose (Bonucci, 1967; Scheuer and Black, 2000). At this time there is evidence of vascular invasion, with the proliferating centre of ossification concentrating around a capillary network. The initial signs of early intramembranous bone are the appearance of fine trabeculae between adjacent differentiating mesenchymal cells, gradually expanding into a diffuse network of bony spicules, which thickens with the laying down of osteoid on their surfaces. Once this process has laid down a bony shell over the iliac cartilage, endochondral ossification proceeds.

Endochondral ossification is defined by the replacement of hyaline cartilage with true bony tissue involving the deposition of chondrocytes in the cartilage matrix followed by secondary absorption and replacement by bone. Specifically, chondrocytes proliferate and deposit matrix until a cartilage model of future bone is formed. Subsequently, the cartilage cells grow and the matrix calcifies. Unresorbed calcified cartilage cores form the substrate in which osteoblasts appose woven bone to form the primary spongiosa. The bony spicules of the primary spongiosa are composed of calcified cores surrounded by woven bone tissue. This primary woven bone growth is later lost, to be replaced either by bone marrow or with a lamellar trabecular hemiosteon or an osteon, representative of the adult secondary spongiosa. Endochondral ossification forms the bulk of the future trabecular bone within the ilium, ischium and pubis as well as other bones of the skeleton. In the ilium, endochondral ossification is observed first in the ilium at 10-11 weeks when pores develop in the ossified external shell allowing invading osteoblasts and vascular elements to enter the internal disintegrating cartilage matrix, attracted by resultant angiogenic factors (Alini *et al*, 1996). This process of nutrient invasion is considered to bring about initial endochondral ossification (Trueta, 1963; Laurenson, 1964a; Brandi and Collin-Osdoby, 2006; Eriksen *et al*, 2007). Several periosteal vessels enter the cartilaginous anlage, with a single vessel becoming the dominant nutrient artery (Scheuer and Black, 2000). The principal nutrient vessels are first observed in late embryonic life when a localised vascular irruption occurs at right angles to the cartilaginous primordium (Brookes, 1971). These nutrient vessels carry with them osteoprogenitor cells which differentiate to form osteoblasts. Osteoblasts utilise the calcified matrix of the remaining chondrocyte columns as a scaffold upon which to secrete osteoid which eventually forms the primary bony trabeculae once mineralised (Erlebacher *et al*, 1995).

The endochondral ossification of the ischium and pubis follow next in this respective order, with the ischial centre first appearing at around 4 intrauterine months, and that of the pubis slightly later, between 4 and 5 intrauterine months (Bardeen, 1905; Gardner and Gray, 1950; Noback and Robertson, 1951). At this stage in the development of the pelvis, many definable landmarks begin to be observed including the presence of the greater sciatic notch, as well as anterior and posterior superior iliac spines (Fazekas and Kosa, 1978). At birth, the pelvic girdle is composed of three distinct and separate bones, the ilium, ischium and pubis, all of which are held together by a Y-shaped cartilage, conferring early structural continuity to the innominate (Laurenson, 1963; Scheuer and Black, 2000; Lee and Eberson, 2006). At this time, each of the bones of the innominate are readily identifiable in isolation (Scheuer and Black, 2000).

In the first months after birth, the bones of the innominate exhibit rapid growth until 2-3 years of age when this slows until the time of puberty (Scheuer and Black, 2000). These three bones remain relatively unchanged until fusion of the ischio-pubic ramus at around 5-8 years of age and then until the age of puberty when the ossification of the triradiate cartilage converts the three bones into a single innominate bone or *os coxae* (Scheuer and Black, 2000; Rissech *et al*, 2001). The area of fusion between these bones presents as a large cup shaped depression called the acetabulum, on the outer gluteal surface, which is directed laterally to articulate with the head of the femur. Medially, on the inner pelvic surface, fusion occurs at the triradiate unit. From the time of puberty there are several secondary centres of ossification which ossify in the form of epiphyses, contributing to formation of the complete mature pelvis. These secondary centres are present on each of the innominate bones at their proximal and distal ends.

The secondary centres of ossification arise in the ilium due to the retained cartilage in the epiphyseal plates, located on what would be described on a long bone as a metaphysis, the area between the diaphysis and the epiphysis. Ossification of the ilium is often said to be similar to that of a long bone, possessing three cartilaginous epiphyses and one cartilaginous process (Delaere *et al*, 1992). These areas of cartilage are known as secondary centres of ossification, where transformation into bony trabeculae occurs as modelled by endochondral ossification. Ultimately as growth progresses, the replacement of cartilage by bone results in the obliteration of the epiphyseal growth plate, termed epiphyseal closure. These secondary centres of ossification in the ilium appear proximally at the iliac crest and distally at the acetabulum. Accessory centres are also known to be present although these tend to be more variable and are poorly documented, for example that of the anterior inferior iliac spine (Scheuer and Black, 2000). Inherent to secondary ossification of the ilium and indeed the ischium and pubis are the centres associated with the maturation of the acetabulum. Acetabular formation is a complicated process requiring co-ordination of many events involving all three bones. The ilium is involved in this union and contributes to the area of fusion located between the ilium and pubis and between the ilium and ischium. Following the fusion of the acetabular centres, at around 11-15 years in females and 14-17 years in males (Scheuer and Black, 2000), the remaining secondary centres of ossification tend to fuse in a general pattern. In the ilium the iliac crest epiphysis begins fusing first, followed by fusion of the anterior inferior iliac spine (Scheuer and Black, 2000).

The thin, long, spiral iliac crest epiphysis ossifies from two separate centres (Scheuer and Black, 2004), one anterior and one posterior which radiate towards one another and unite at the centre of the crest to form a conjoined iliac crest epiphysis. The

anterior iliac crest epiphysis forms the anterior superior iliac spine and the anterior half of the iliac crest whereas the posterior iliac crest epiphysis forms the posterior superior iliac spine and the posterior half of the iliac crest (Frazer, 1948). Ossification of the crest has been said to commence around the age of 12 in girls and 14 in boys (Scheuer and Black, 2004), with the anterior iliac crest epiphysis preceding the formation of the posterior iliac crest epiphysis. It has been shown that the timing of epiphyseal fusion is extremely variable for the iliac crest. Complete fusion of the iliac crest is said to occur within the range of 15-22 years of age (Webb and Suchey, 1985).

The location of ossification in the anterior inferior iliac spine has been indicated to be an extension of the superior acetabular epiphysis, however little data is available on the variability of this centre. Scheuer and Black (2000) noted that the anterior inferior iliac spine and lower aspect of the anterior border of the ilium may form from an extension of the superior acetabular epiphysis. Additionally an extra flake-like epiphysis can occasionally be seen developing on the upper aspect of the anterior inferior iliac spine in some individuals. The mature pelvic complex is complete when each of these secondary ossification centres has completed its growth and fused with the existing osseous pelvis which will occur by around 22 years of age.

2.4 Temporal forces acting on the pelvis throughout ontogeny

The pelvic complex is an area of the skeleton which accommodates a significant degree of forces which vary throughout development. These forces are present and evident in resultant skeletal form, from the early embryonic modeling period through to the homeostatically remodelled adult morphology. Although the pelvis is subjected to continuous modeling and remodeling forces throughout life, these forces change in magnitude and directionality depending on developmental requirements. The resultant

changes to the internal architecture and external morphology of the complex may be closely associated with key developmental milestones.

Much of the very early work in the area of developmental biomechanics has concentrated on the study of locomotion, with the promise of relating changing motor activities to the maturation of neural structures (Burnside, 1927; Shirley, 1931; McGraw, 1945). With this extensive research, different investigators have defined the development and maturation of the locomotor apparatus, and in doing so, have divided the developmental timeline into several unique milestones (Table 2.1). These studies and conclusions have ranged from the intricately subdivided maturation sequence of crawling to the strategic developmental series involved in the adoption of a bipedal gait. These studies have added significant and detailed knowledge to the field of locomotor development, demonstrated by the characterisation of 22 stages in the development of crawling (Gesell and Thompson, 1938), and 7 stages in the development of walking (McGraw, 1945). These stages range from independent head control at 2 months, to the movements of arms and legs during crawling and finally development of independent walking at the end of the first year (Adolph, 1997). During the first year, infants progress from behaviour that is stereotyped and reflexive to increasingly goal-directed and skillful movement (Thelen *et al*, 1984; 2002). Therefore, when considering the natural progressive stages of development it is appropriate to begin with the earliest developmental period and work towards maturity. The major developmental milestones which have the potential to influence pelvic form are outlined in Table 2.1.

Motor Milestone	Average Age of Attainment
Head control	2 months
Rolls to spine	4months
Maintains sitting	6-7 months
Rolls to prone	7 months
Creeps on all fours	10 months
Stands momentarily	10 months
Cruises (walks without support)	10 months
Walks independently	12-14 months
Begins to run	2 years
Walks up and down stairs	2 years
Runs well	3 years
Walks up stairs alternating feet	3 years
Walks down stairs alternating feet	4 years
Hops on one foot	4 years
Skips	5 years
Walks with mature adult gait	7-9 years

Table 2.1. Developmental milestones. Taken from: Keen, M. (1993). Early development and attainment of normal mature gait. *Journal of Prosthetics and Orthotics*. **5**:35-38.

The fetal period is the developmental window which is considered to form the natural baseline for subsequent ontogenetic development. During intrauterine growth and development the spinal column is positioned in a single primary curvature with the limbs adopting a flexed and internally rotated posture (Keen, 1993; Thelen *et al*, 2002). As a result of this intrauterine crowding, the fetus has a limited range of movement and infants are born with mild joint contractures and curves in the long bones which resolve soon after birth (Keen, 1993). In the fetus, the pelvic complex is considered to represents the baseline template that is free from direct stance related load bearing influences.

The subsequent window of biomechanical alteration in response to changing forces is considered to occur during the neonatal period and when the child reaches the age of six months, prior to the adoption of a sitting posture. During this period the child is predominantly placed in the supine position. Therefore, similar to the fetal period, the newborn is not expected to display any significant internal architectural changes

associated with the influences of stance related locomotion. The only biomechanical changes which may be observed could result from the effects of gravity and body weight transmission from lying in the supine position and the advanced development of soft tissue interactions. Specifically, the muscular attachments to the ilium will have increased in mass and have an increased force inducing capacity resulting in potential remodeling and changed morphology. This muscle mass also serves to enable the infant to adopt a supine kicking movement which is maintained throughout the infant's first year (Thelen, 1981), and may serve to induce a force component which passes into the ilium. Likewise when a child is held in the upright position, stabilised underarm, they display a stepping reflex which is present for the first months of life then disappears before returning prior to independent bipedalism (Forssberg, 1985; Adolph, 2002; Thelen *et al*, 1984; 2002). These primitive reflexes are naturally present in the newborn and infant younger than six months (Keen, 1993). Indeed, in the neonatal ilium the iliac crest is flattened in appearance and adopts its adult-like curvature as the muscular influences on the gluteal and pelvic surfaces become more pronounced.

The next temporal developmental window in which changes to the internal and external pelvic form are expected to be observed is when the child is between six months and one year of age. During this developmental period the child normally adopts a sitting posture (Robson, 1984; Carruth and Skinner, 2002). The postural responses which bring about this positioning gradually appear as primitive reflexes, cease, and are then incorporated naturally into movement and locomotion (Keen, 1993). At this time, when the child begins to sit up, weight is transferred, from its initial concentration on the first sacral vertebra, through the sacro-iliac joints and ischial tuberosities for the first time. Due to the establishment of this weight transfer pathway through the pelvis the presence of a definable sacro-ischial trajectory is reported to

develop (Aiello and Dean, 1990). At this stage of development the sacro-ischial trajectory pathway should be rather primitive in its form and trabecular volume, but will be maintained and modified in both its position and volume throughout life as this is a posture which is maintained throughout ontogeny. At the later stages of the sitting phase, at around eight months, the child usually begins to crawl on all fours (Carruth and Skiner, 2002) which will again significantly change the centre of gravity of the whole complex and induce new biomechanical alterations.

Further to this milestone, a significant developmental event occurs at around one year of age when an independent bipedal stance is normally adopted (Sutherland *et al*, 1980; Forssberg, 1985; Keen, 1993), representing the culmination of developing motor skills throughout infancy (Adolph, 2002). At this stage in the child's pelvic development the adoption of a bipedal stance and the locomotor influences of altered weight transfer along with a shift in the centre of gravity should translate into alterations of both internal and external modeling and remodeling. During this phase of development, the changes which occur should account for the development of a further two weight trajectory pathways. The first should result in increased trabecular volume in the direction from the sacro-iliac joint into the ilium, passing out of the superior part of the acetabulum (Aiello and Dean, 1990). This pathway in the adult has been termed the superior auriculo-acetabular or sacro-femoral trajectory pathway and is thought to be dominant during standing. The second pathway developed at this stage should show a similar pattern of increased trabecular volume passing from the sacro-iliac joint into the ilium, through the inferior part of the acetabulum and then into the femur (Aiello and Dean, 1990). In the adult this pathway has been termed the inferior auriculo-acetabular trajectory pathway, and is primarily thought to be associated with walking (Freund, 1868; 1878 cited in Wolff, 1986).

Other than developmental milestones associated with attainment of gait, a major temporal event which influences the pelvic complex and specifically the ilium occurs between the age of four and five years. This developmental window is significant to understanding the external morphology and internal architecture of the ilium as it is the time frame within which the pelvic complex has continued to grow in size, and as such, is sufficiently capacious to receive the abdominal viscera that will now descend into the cavity. Visceral descent has major implications for the dynamics of the pelvic complex in that the centre of gravity is altered significantly due to a reduction of the lumbar lordosis which was caused by the viscera residing in the abdominal region resulting in vertebral column compensation (Scheuer and Black, 2000). Also, the presence of additional structures within the pelvic cavity is thought to have a consequential impact on both the internal and external architecture. Immaturity of gait during this stage is also considered to impact on the skeletal form. Primary features of gait during this period include a greater knee flexion wave during stance and slightly increased pelvic rotation, hip joint rotation and hip abduction. However, despite this, children have achieved an adult pattern of joint angles throughout the gait cycle by this stage (Keen, 1993).

At a more advanced developmental stage, between the ages of five to eight years, the pelvic complex undergoes further dynamic alterations. During this period, the pelvis undergoes various structural modifications which have the potential to change the external appearance of the complex and alter its internal structure. It is within this time frame that fusion occurs between the ischium and pubis forming the rigid ischio-pubic ramus (Scheuer and Black, 2000). This fusion will result in a reduced pliability of the complex as a whole, which may affect the dynamics of the pelvis or conversely may have a limited impact by simply representing the end product of the change requirements for descent of the pelvic viscera. Further to this, as has previously been

discussed, it has been reported that mature gait is achieved within this time frame. As such, the way in which weight is distributed throughout the complex is expected to alter, resulting in both external and internal changes in trabecular volume and patterning.

Subsequently, the appearance of secondary sexual characteristics is considered to have a profound influence on the external form of the pelvis and resultant transfer of forces through the complex. Secondary sexual characteristics generally start to become evident around ten years in females and twelve years in males (Scheuer and Black, 2000), although there is much variability within and between sexes (Papadimitriou and Chrousos, 2005; Slyper, 2006). At the onset of puberty, the female pelvis enters a phase of rapid and extensive alteration in response to the hormones associated with pubertal change. At this time, particularly in the female, there will be extensive external structural and presumably substantial internal trabecular changes in preparation of the structure as a birth canal. Also during this period, several other significant developmental events occur, including the commencement of fusion at the acetabulum, with a proposed significant degree of external and internal structural upheaval, as well as the fusion of other pelvic epiphyses. Other than the known morphological outcomes that give rise to the sexually dimorphic elements of the pelvic complex, there is no information pertaining to the alterations within the internal architecture of the complex. Additionally, there is no information regarding the manner with which the bones grow relative to each other to maintain the structural integrity of the pelvis, ensuring that whilst it grows and responds, it maintains internal and therefore external functional viability.

Once the adolescent period is complete, the pelvic complex reaches its adult morphology which is maintained and remodelled depending on prevailing functional

influences. In the normal adult, the trabecular architecture is expected to represent the resultant ontogenetic development with established weight trajectory pathways and regions of increased trabecular volume. These regions are representative of the mode by which load is transferred from the upper body through the pelvic complex to the lower extremities as well as the forces incurred from ground reaction forces. This adult morphology and architecture undergoes a final significant period of alteration in the elderly, in response to age related degeneration and pathologies. In the elderly adult it is considered that only vital trajectories are maintained when bone resorption outweighs bone formation and maintenance. In this period, significant bone resorption will have taken place, particularly if osteoporosis or other degenerative bone disorders are present, leaving only the fundamental trajectory pathways which are required for the maintenance of the complex. This is supported by the extremely rare occurrence of pelvic skeletal failure with age (Lüthje *et al*, 1995).

CHAPTER 3 –Bone Modeling, Remodeling and Bone Biomechanics

3.1 Bone Structural Composition

Postcranial bone in human and other mammalian skeletons is generally classified into two macroscopically distinct types; compact bone and trabecular bone. Although these types are similar in their histology and basic biology, they differ quite markedly in their gross morphology, anatomical distribution and mechanical behaviour (Swartz *et al*, 1998). The ilium is composed of an external compact bone shell with a central core of trabecular bone. These two bone types, as they are arranged in the ilium, allow the bone to develop its characteristic morphology and respond appropriately to biomechanical influences. The ilium is purported to consist of mainly low density trabecular bone covered by inner and outer layers of thin cortical bone forming a strong, low-weight structure that is well suited to accommodate high loads and is commonly referred to as a 'sandwich construction' by engineers (Dalstra and Huiskes, 1995). The compact arrangement of the cortex allows for a large surface area for muscle attachment and for the efficient distribution of principal strains through its relatively unique structure (Dalstra and Huiskes, 1995). Conversely, the trabecular bone, also often referred to as cancellous or spongy bone, minimises the weight of the structure due to its porous low density arrangement while maintaining the structural requirements for optimal load transfer (Huiskes *et al*, 2000). This lightweight, mechanically robust structural conformation is optimal for the functional requirement of the pelvis as a central loaded component of the locomotor apparatus, allowing for efficient locomotor ability (Turner, 1998, Preuschoft, 2004).

The term trabecula derives from the Latin for 'a little beam' and is the general anatomical term given to a supporting or anchoring strand of connective tissue which is

usually interconnected with other similar strands. Trabecular bone characterises this definition as it is composed of a three-dimensional lattice work of interconnecting struts. These struts can present in various distinct forms, either rod-like, plate-like or an intermediary between these two extremes. This structural appearance, often referred to as the structural model of trabecular bone, constantly changes throughout life and is different between sites within a single bone, reflective of the spatially distributed and temporally changing forces experienced by that bone. Conversely, cortical bone is of a dense composition and predominantly forms the external surface of bones. It is a hard and robust tissue which is formed by multiple stacked layers. Its main function is to support the body, protect organs, and combined with trabecular bone, store minerals.

The microscopic structure of trabecular and compact bone is composed of a network of proteins and collagen fibres impregnated with mineral salts, principally calcium hydroxyapatite [$Ca_{10}(PO4)_6(OH)_2$], which gives the structure inherent density and strength as well as a degree of flexibility (Cowin, 2001). The strength of cortical and trabecular bone, coupled with its pliability, is the optimal structural composition for its primary biomechanical role in the distribution of forces within the ilium. This is emphasised by the mechanical requirement of the trabecular bone latticework to transfer loads to and from cortices without undue deformation or fracture (Swartz *et al*, 1998). As well as its biomechanical role, bone is also important in mineral homeostasis (Swartz *et al*, 1998; Bronner and Worrell, 1999), acting as a reservoir for calcium, phosphorus, sodium, magnesium and carbonate (Pearson and Lieberman, 2004). Due to its high turnover rate, bone has the potential to release these inherent minerals through osteoclastic action (Cowin, 2001). The role of bone and in particular its biomechanical function and the way in which it remodels throughout development are topics of great importance and have been investigated extensively from the early studies of the

nineteenth century to the current day research which applies modern technology to elucidate the function of this dynamic structure.

3.2 Historical overview of bone biomechanics

The earliest documented work on bone adaptation in the biomechanical literature was from Bourgery (1832), illustrated in early artworks (Wolff, 1986). Bourgery was the first investigator to raise questions on the relationship between the internal architectural form and the mechanical function of bone (Wolff, 1986; Roesler, 1987), a theory with associated questions which are, to this day, still being investigated. His postulations were based on observations in the proximal femur where he stated that cancellous trabeculae appear dense and strong along compression lines and conversely they appear in a lighter, less dense pattern outside compression lines. In his work he described principles which are reminiscent of the maximum-minimum principle (Fung, 1981), not adopted until some years later by Roux (1881), which proposes that the maximum strength of bone is achieved with a minimum of constructional material. This theory of strength versus minimal structural composition was also inadvertently mentioned in a communication by Bell in 1834 (cited in Roesler, 1987) when he remarked that “in natures work, strength is given with the least expense of materials”. Bourgery’s research remained fundamentally solitary until the publications of Ward (1838), who produced some pioneering work for the time likening the architecture of the proximal femur to that of an old type bracket crane with three trabecular orientations representing (i) the support column of the crane, (ii) the principal support arm of the crane and (iii) and a cross bracing arm. His observations and comparisons contributed to the theory that different stress trajectories exist within a bone dependent upon the stresses and strains which act upon and pass through it. As such, he described that:

> "in the lower extremity of the bone [femur] there are numerous slender columns of bone which spring on all sides from the interior surface of the compact cylinder, and descend converging towards each other so as to form a series of inverted arches, adapted, by their pointed form, to sustain concussion or pressure transmitted from below" (Ward, 1838).

Ward's work was expanded upon with the next advance in the field from Wyman (1857), who presented a paper on the arrangement of the trabecuale, using sections of vertebrae, talus and calcaneus as well as a more accurate description of the internal architecture of the proximal femur than his predecessor (Evans, 1957). Following Ward, he described three trajectory systems, but now these introduced the idea of tension, compression and connective trabeculae systems. He described the compression trabeculae as studs, and the tension trabeculae, which resist the tension and pressure forces impinging upon the bone, as braces (Wyman 1857; Evans, 1957). Engel (1851) was the next investigator in this period to present his work and was the first person to describe and draw the general architecture of trabecular bone with accuracy representative of more modern findings. In his communication he wrote:

> "the bony trabeculae interlock each other with surprising regularity and similarity during the building of the skeleton in such a way, for instance that the bones of the skull present a very delicate appearance soon after their formation. Longitudinal or transverse cross sections through adult bones, through the medullary cavity or through the cortex, show fine and regular architecture which leaves nothing to be desired" (Engel, 1851)

Although Engel's research was relatively generalised it laid down the foundation that was followed by Humphry (1858), whose work on the mechanical arrangement of the internal architecture of bone led him to propose that the ends of trabeculae are positioned at right angles to the articular surfaces of joints. The importance of his observations were not fully understood until much later when they played an important role in the mathematical analysis of the functional significance of trabecular orientation (Evans, 1957). Up until this point the majority of work on bone biomechanics and the internal architecture of bone had been carried out on long bones with a resultant increasing knowledge of cancellous patterning and trabecular trajectory pathways.

The first work to be carried out on the pelvis appeared subsequently in the history of investigation with the work of Freund (1868, 1878). Freund commented on the characteristics of the trabecular arrangements found in the pelvis and began to describe the reasons behind their presence. He noted that the load of the trunk was exerted in the vicinity of the oblique process of the first sacral vertebrae and transmitted partly to the superior acetabulum and partly to the ischial tuberosity. In summary, he stated that two bony arches run from the proximal sacral vertebrae, to the distal acetabulum and ischial tuberosity and are characterised by their strength. He elaborated by suggesting that these trabecular arches are protected from crushing by proximal widening, and from shear rupture by ligamentous attachment. Further to this he suggested form:function relationships related to the structural modifications inherent in bipedal posture and sitting. This work on the bone biomechanics of the pelvis subsequently remained relatively neglected and any further work on bone architecture from this period concentrated, again, back to that of the femur and other long bones.

A significant addition to the knowledge of trabecular architecture came from Von Meyer (1867), when he described the trajectories of the cancellous architecture of several bones of the human skeleton (Figure 3.1) and discussed their origins (Evans, 1957; Wolff, 1986; Roesler, 1987). Von Meyer continued to contribute to the work of the principal investigators before him and made significant progress in contributing to understanding in the biomechanical field. His advances came when he likened the mechanics of the Fairbairn crane, an engineering construction designed by Karl Culmann, to the trabecular trajectories present in the proximal end of the femur (Figure 3.1). He went on to demonstrate that the trabeculae of the proximal femur showed an architectural pattern closely connected with the statics and mechanics of bone tissue and directly correlated the mathematical projections of the crane with these biological patterns. According to this theory, both compressive and tensile trabeculae align along trajectories of maximum internal stress, crossing one another at right angles and arise perpendicularly from the surface of the bone or articular cartilage (Evans, 1957). The collaboration between Von Meyer and Culmann was the first cooperation in the field of biomechanics between an anatomist and an engineer (Roesler, 1987), and was at the time thought to prove sufficiently that the structure of cancellous bone was determined by the direction of principal stresses. It was also a major milestone in the understanding of bone behaviour and was to set the hypothesis and pose new questions for subsequent research in the field.

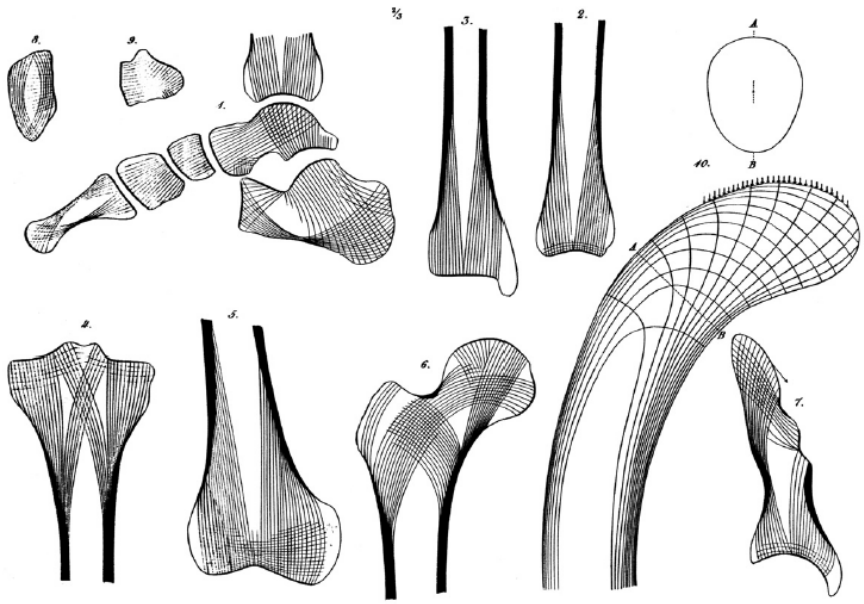

Figure 3.1. Composite illustration likening the mechanics of the Fairbairn crane to the trabecular trajectories present in the proximal end of the femur. Also, sections through several human bones showing trabecular patterning. Taken from: Skedros, J.G. and Baucom, S.L. (2007). Mathematical analysis of trabecular 'trajectories' in apparent trajectorial structures: The unfortunate historical emphasis on the human proximal femur. *Journal of Theoretical Biology*. **244**:15-45.

It was within the following years that the literature and knowledge on bone biomechanics was set to grow significantly with the introduction of Julius Wolff to the field in 1869. At this point Wolff commandeered the subject with his ideas and subsequent publications which attempted to link the structure of cancellous bone in the proximal femur to the trajectories of the Culmann crane through mathematical formulae (Figure 3.2). It was the culmination of his work with contributions from his predecessors that led to his famous monograph about the law of bone remodeling (Wolff, 1892). In his monologue Wolff disseminated his law which stated:

> "the law of bone remodeling is the law according to which alterations of the internal architecture clearly observed and following mathematical rules, as well as secondary alterations of the external form

of the bones following the same mathematical rules, occur as a consequence of primary changes in the shape and stressing of the bones" (Wolff, 1986).

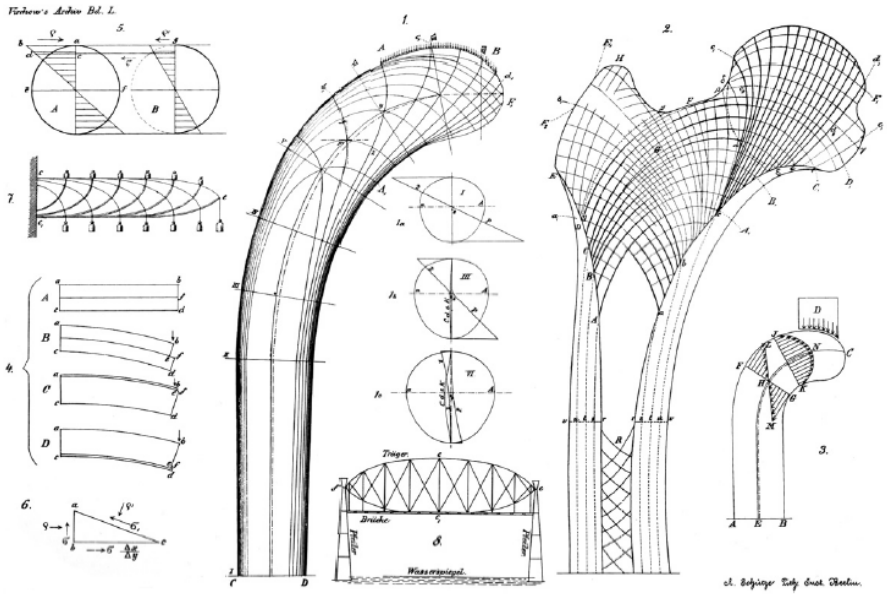

Figure 3.2. Wolff's composite diagram which includes the Culmann crane, cantilevered beam and hypothesised force trajectories in the proximal femur. Taken from: Skedros, J.G. and Baucom, S.L. (2007). Mathematical analysis of trabecular 'trajectories' in apparent trajectorial structures: The unfortunate historical emphasis on the human proximal femur. *Journal of Theoretical Biology.* **244**:15-45.

The foundations of Wolff's law are based on the interpretations made in compact and cancellous bone where a high density of trajectories signified that stresses and strains were passing through the bone and consequently necessitating the requirement for compact bone support. Conversely, low density trajectories signified that less stress was passing through a particular region and as such resulted in trabecular bone. Finally no density inferred a medullary cavity where there were no stresses acting (Wolff, 1986). Wolff's theories generated great debate among fellow researchers, with some endorsing his doctrine and others fiercely criticising it (Koch, 1917, Evans, 1957). Many investigators studied the mathematical trajectorial hypothesis postulated by Wolff

resulting in a barrage of fierce objections and theories which deviate from the original proposal (Koch, 1917; Janssen, 1920; Carey, 1929; Murray, 1936). Wolff's work was shown to falter primarily in its adoption of strict mathematical hypotheses which were seen as untenable from a mechanical and elastomechanical point of view (Roesler, 1987). However, Wolff's misconceptions regarding the biological and physiological growth of bone also shrouded his doctrine with great criticism. He contended that bone grew by interstitial growth (Prendergast and Huiskes, 1995), however, this concept is fundamentally flawed as it is known that bone grows by the addition of matrix at the bone's surfaces, appositional growth and remodeling.

Modern interpretations of Wolff's law involve the works of Roux (1881), which were brought to light during this period but were never fully explored. Roux proposed a new principle of functional adaptation and required a biological system upon which to test his hypotheses, this happened to be bone. He hypothesised that a quantitative self-regulating mechanism which was controlled by a functional stimulus could affect biological tissues (Lee and Taylor, 1999). This new hypothesis complicated the works of Wolff as his theory of bone remodeling was inextricably linked to his mathematically defined doctrine. Rather than challenge this theory, Wolff responded by accepting it and used it as support for his continuing work. As such, Wolff's law as we know it today is a culmination of the work from three nineteenth century anatomists; Wolff's trajectorial hypothesis (Wolff, 1892, 1986), the theory of functional adaptation postulated by Roux (1881) and the maximum-minimum principle originated in the earliest days of biomechanical investigation by Bourgery (1832) (Pearson and Lieberman, 2004). Summarised, this culmination of theories proposes that bone is deposited and resorbed to achieve an optimum balance between strength and weight and that trabeculae in cancellous bone tend to line up with the directions of principal stresses to which they

are exposed. Both these phenomena occur through self-regulating mechanisms that respond to mechanical forces acting upon bone tissues (Martin *et al*, 1998). The reason that Wolff's law still remains as named today, although interpreted very differently from the original proposal, is due to its repeated use in the literature and in research (Roesler, 1987). Some researchers have suggested that 'Wolff's law' be replaced with 'Roux's law' as it more accurately considers bone remodeling through the process of bone functional adaptation. However, this has never been widely accepted and instead the adoption of the term 'bone functional adaptation' as a substitute to Wolff's law is now commonly recognised (Cowin, 2001; Pearson and Lieberman, 2004; Ruff *et al*, 2006). It is clear to today's investigators that Wolff's conclusions of direct mathematical links to the way in which bone models and remodels are unreliable, severely flawed and inadequate. Wolff's law is a concept that has at times been misrepresented in both the anatomical and anthropological literature. His analysis appears to be fundamentally based on misinterpreted mechanical data and a rejection of the relevance of bone resorption (Lee and Taylor, 1999).

3.3 Recent investigations of bone biomechanics

Much recent work has been conducted on the theories and problems proposed by Wolff's law which apply advanced modern and informative techniques to gain a more insightful perspective of bone form and function. This has resulted in the knowledge of bone biomechanics and the specialised micro anatomy of trabecular characteristics expanding exponentially, with studies addressing the continuous modification and alteration of external and internal bone structure.

Current knowledge has been advanced by the application of several investigative techniques and various experimental scenarios, each with the aim of elucidating the

fundamental principles of bone biomechanics. The most predominant contemporary investigations have included strain gauge techniques, finite element analyses, and non-invasive imaging protocols. These techniques have been aimed at investigating the material properties of cortical and trabecular bone, the theoretical stress distributions throughout specific bones and the skeletal morphology in relation to functional influences.

There has been a noticeable and steady shift in the biomechanical and morphological literature towards more widely used and accepted imaging modalities which are specifically designed to assess three dimensional microstructure at high resolution and have the benefit of being non-destructive (Genant *et al*, 2000; Jones *et al*, 2007). This high degree of spatial resolution coupled with the possibility to observe the internal structure of bone non-destructively has made it possible to investigate previously inaccessible rare skeletal material, where destructive analysis is discouraged due to the uniqueness and value of the material involved. These studies are beginning to replace previous histomorphometric investigations which required destructive histological sectioning techniques and physical incision of the bone in order to investigate trabecular patterning in relation to stress (Holm, 1980). The most significant information in the recent literature has originated from imaging techniques such as radiography, micro-magnetic resonance imaging (microMRI) and micro-computed tomography (microCT).

Radiographic studies have elucidated that trabecular patterns of individual bones vary depending upon bone density and that the relationship between fine and coarse trabeculae are influenced by biomechanical forces and changes in the body's internal environment (Siffert and Levy, 1981). These studies have also concluded that fine trabeculae may exist as either cross-bracing struts between the coarse major weight

bearing trabeculae or relatively homogenously tightly packed at sites subjected to constant changing dynamic forces (Siffert and Levy, 1981).

Further to conventional radiographic techniques, micro-imaging modalities are emerging techniques for the non-destructive assessment and evaluation of the three dimensional trabecular bone architecture (Müller and Ruegsegger, 1997; Qin *et al*, 2007). These imaging modalities can visualise the internal structure of intact bones with a high degree of spatial resolution and provide an efficient and reliable means by which 3D architecture can be quantified (Cooper *et al*. 2003). The introduction of three-dimensional measuring techniques and associated software in bone research has been instrumental in the development of knowledge into the microenvironment of trabecular architecture. These techniques have also made it possible to capture the actual architecture of trabecular bone without assumptions of the trabecular structure type (Hildebrand *et al*, 1999). A full account of the available modern non-destructive three-dimensional imaging modalities and associated quantification software which can be applied to bone analysis is documented in Chapter 4.

As well as direct structural analysis, data sets obtained from three-dimensional imaging studies can also be investigated in a predictive mechanical sense using finite element modeling. Finite element analysis as applied to the investigation of bone biomechanics is a numerical technique employed to calculate the mechanical properties of bone as they relate to its microstructure (Van Rietbergen, 2001). Recent applications of this method have allowed the determination of trabecular bone mechanical behaviour under specific conditions (Van Rietbergen *et al*, 1996), the assessment of the physiological bone tissue loading (Van Rietbergen *et al*, 1995), and the analysis of trabecular bone mechanical properties *in vivo* (Ulrich *et al*, 1999a). Further to this, particular emphasis in the recent literature has focused on obtaining the biomechanical

signal which drives the adaptation process in bone, suggesting that the signal is associated with either, microdamage in the bone or strain in the mineralised tissue (Lanyon, 1993; Mullender and Huiskes, 1995; Prendergast and Huiskes, 1995). Other studies have concentrated on obtaining a clearer insight into the mechanical properties of pelvic trabecular bone showing that bone densities within the pelvis vary dependant upon anatomical position (Dalstra *et al*, 1993). It has also been established that remodeling is responsible for creating nearly all of the new bone tissue in the human skeleton (Kobayashi *et al*, 2003) with recent research supporting the hypothesis proposed by Frost (1990a) that minimodeling is persistent and perpetual throughout life (Kobayashi *et al*, 2003).

Although there has been an increasing and accelerated trend in the investigation of pelvic bone biomechanics, no study has fully investigated the human ontogenetic pattern and as such, there is a significant deficit in our fundamental understanding of how the pelvic complex changes architecturally, both internally and externally throughout its development. Likewise, although the potential is now available for such studies, the paucity of provenanced juvenile material remains restrictive to the advancement of this fundamental area of skeletal biology and as a result a significant portion of research remains directed to phylogenetic variation in primates (Fajardo and Müller, 2001; Fajardo *et al*, 2002; Ryan and Ketcham, 2002; Ryan and van Rietbergen, 2005).

3.4 Bone mechanics

The skeleton is a metabolically active structure which undergoes continuous modeling and remodeling throughout life from early embryonic developmental modeling to the constantly changing structural morphology of the adult skeleton

(Hadjidakis and Androulakis, 2006; Robling *et al*, 2006). This changing structural skeletal morphology always tends towards homeostasis, due to the fact that bone is a plastic material which is highly responsive to functional forces. Functional forces are inherent to the skeleton's role as a protective structure, fundamental to movement and indeed to weight transfer throughout development. These forces can manifest in everyday loading regimes, such as bipedal gait, or can be initiated by isolated temporal events, such as pathologies, which may act to remodel the skeleton into a biomechanically optimal form, under given conditions. This is reflected in the ability of bone to accommodate and remodel into an optimal structural configuration in response to changing stresses (Martinon-Torres, 2003). This is fundamental to skeletal function as trabecular architecture has a significant role to play in bone strength and in determining biomechanical properties (Majumdar *et al*, 1998; Ulrich *et al*, 1999b; Müller, 2005; Bevill *et al*, 2006). One of the most fundamentally simplistic views of bone functional adaptation and the way in which bone is modelled and remodelled is represented by a simple feedback model (Lanyon, 1982) (Figure 3.3). This is based on the principle that modeling and remodeling stimuli are influenced by strain, the actual physical deformation of bone tissue, and not stress, the applied force or system of forces that tends to deform a body. The premise of bone functional adaptation is based upon this feed-back loop where increased strain leads to the deposition of more bone tissue, which then reduces strain to the original optimum strain level. Conversely, decreased strain leads to the resorption of bone tissue which again restores the original strain levels (Ruff *et al*, 2006). This is emphasised in the bone's highly responsive reaction to stresses and strains in that it is laid down and remodelled at sites of increased and decreased mechanical force or microdamage (Evans, 1957; Turner, 1998; Raisz, 1999; Huiskes *et al*, 2000).

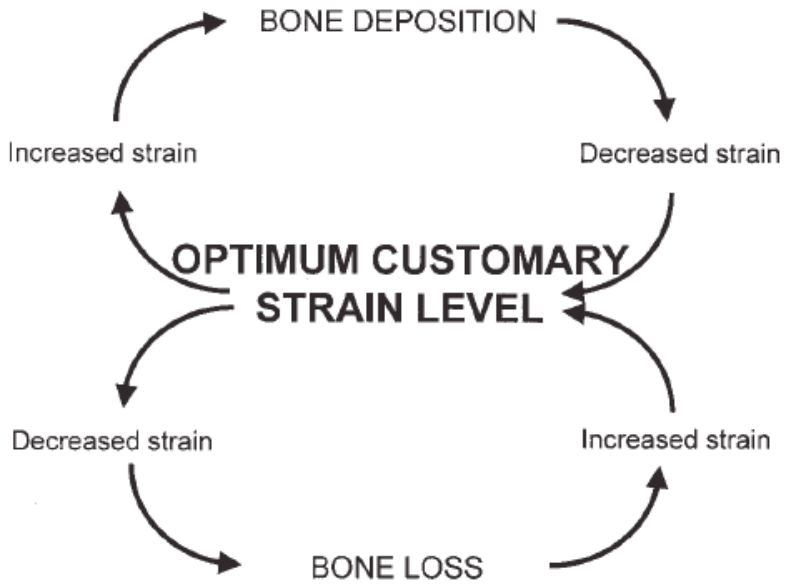

Figure 3.3. Feedback model of bone functional adaptation (from Lanyon, 1982).

Both cortical bone and trabecular bone are acted upon during development and in adulthood in order to model and remodel their respective structures into an optimally placed architectural configuration which is suited to accommodating prevailing functional requirements including growth. The attainment of a bone's mature morphology during growth is accomplished through cell-based processes called 'modeling' (Frost, 1990a). Whereas in maturity, local bone resorption and subsequent formation is achieved via a process called 'remodeling' which continually renews and balances the structure (Frost, 1990b).

3.4.1 Bone Modeling

Much recent experimental and modeling work has expanded our understanding and knowledge of the mechanisms of bone modeling (Huiskes *et al*, 2000; Sommerfeldt and Rubin, 2001). It is now relatively well established that the local bone modeling

processes are governed by mechanical feedback and that growth and modeling are continuous (Cowin, 2001; Baron 1999). Local influences modulate growth to produce a functionally and mechanically optimal architecture. Bone modeling is defined as a continuous process by which a bone is altered in size and shape during its growth by resorption and formation of bone at different developmentally determined sites and rates (Raisz, 1999). These resorption and formation mechanisms remove or add bone over wide regions of the bone surface. During growth, formation tends to predominate over resorption. Bone modeling is the apposition of bone tissue brought about by the disequilibrium of bone laying down (modeling) and bone resorption processes at different sites, where bone modeling predominates. This apposition of bone tissue through bone modeling has been suggested to be most predominantly active in the early developmental years and tends to subside after skeletal maturity (Frost, 1990a). Initial modeling fits a growing bone's architecture to the mechanical demands of typical physical activities, body weight, and neuromotor function (Frost, 1990a). In acting in this manner, modeling controls the growth, shape, size, strength, and anatomy of bones and joints (Jee, 2001). Collectively, modeling increases the outside cortex and marrow cavity diameters, shapes the ends of long bones, and produces trabecular and cortical drift, the relative shift in the deposition of these bone types across a bone. Modeling not only allows the development of normal architecture during growth, but also modulates this architecture and mass when mechanical conditions change.

3.4.2 Bone Remodeling

Bone remodeling is the central process of coupled resorption and deposition of bone at the same site (Frost, 1990b). It is the process by which old bone is continually replaced by new tissue and is a complex process which requires the interaction of

different cell types and is regulated by a variety of biochemical and mechanical factors (Hadjidakis and Androulakis, 2006). Our understanding of this process has expanded as science elucidates more in-depth perspectives as to the biology of bone remodeling.

At the cellular level, bone modeling and remodeling are indistinguishable as they are both based on the individual actions of bone resorbing osteoclasts and bone forming osteoblasts (Ruimerman, 2005). Clear distinctions between the two processes are summarised in Table 3.1. Remodeling is the process of growth, reinforcement and resorption which living bone is constantly undergoing. The remodeling process begins at a quiescent bone surface with the appearance of large multinucleated osteoclasts which form by fusion of mononuclear progenitors of the monocyte/macrophage family (Väänanen & Horton, 1995; Teitelbaum, 2000; Pearson and Lieberman, 2004). The newly formed osteocytes attach to the bone matrix creating an isolated microenvironment upon which resorption of the organic and inorganic matrices of bone are initiated by acidic secretions (Raisz, 1999; Teitelbaum, 2000; Väänanen *et al*, 2000). Once this resorptive process has taken place and eventually ceases, the newly degraded surface is invaded by osteoblasts.

Osteoblasts are derived from undifferentiated mesenchymal stem cells (Ducy *et al*, 2000; Pearson and Lieberman, 2004), found in the bone marrow, periosteum and other soft tissues. Osteoblasts work by depositing osteoid onto a bone surface (mineralising it), resulting in the formation of new bone. As a result of this deposition and mineralisation process, some of the osteoblasts become trapped within their own deposits becoming encapsulated in the osteoid matrix and as a result of this, they undergo a differentiation process into osteocytes. Remaining osteoblasts continue to synthesise bone until they eventually transform to quiescent lining cells that cover the newly formed bone surface. These lining cells are highly interconnected with the

osteocytes in the bone matrix through a network of canaliculi (Klein-Nulend *et al*, 2003).

	Remodeling	Modeling
Location	Spatially related	Different surfaces
Coupling	A-R-F	A-F; A-R
Timing	Cyclical	Continuous
Extent	Small (<20%)*	Large (>90%)
Apposition Rate	Slow (0.3-1.0μm/day)	Fast (2-10 μm/day)
Cement Line	Scalloped	Smooth
Balance	No change of net loss	Net gain
Occurrence	Throughout life span	Prominent during growth; ineffective in adults
MES Threshold^	<200 microstrain	>1500 microstrain

*: of available surface
^: MES = minimum effective strain
A = activation; R = resorption; F = formation

Table 3.1. Comparison of modeling and remodeling (extract from Bone Mechanics Handbook; edited by Cowin, 2001)

Remodeling allows for the maintenance of a particular bone's shape, the quality of the bone, and the overall size of the skeleton (Hadjidakis and Androulakis, 2006). This maintenance is accomplished through the repairing of micro fractures and the modification of structures in response to stresses impinging upon the skeleton, such as biomechanical forces in the form of compression, tension, and torsion, as well as biochemical stresses inherent to bone remodeling. The processes of formation and resorption on the bone surface during bone remodeling, alternate with periods of inactivity throughout life for both cortical and trabecular bone. The rate of cortical bone

remodeling, which is as high as 50% per year in the mid-shaft of the femur during the first two years of life, gradually declines to a rate of 2 to 5% per year in the elderly (Simon, 1994). In contrast to this, the rate of trabecular bone remodeling is proportionately higher throughout life and is normally five to ten times higher than that of cortical bone in adults (Simon, 1994; Lee and Einhorn, 2001).

3.4.3 Bone Remodeling Unit (BRU)

The specialised group of bone cells that orchestrate the bone turnover process, involving the removal and replacement of pre-existing bone with a new structural unit (the osteon in cortical bone, or hemiosteon in trabecular bone), is referred to as a bone remodeling unit (BRU) or basic multicellular unit (BMU). Osteoclasts and osteoblasts closely collaborate in the remodeling process indicating that a coupling mechanism must exist between formation and resorption (Frost, 1964), although the exact mechanism of this coupling mechanism is yet to be fully understood (Ruimerman, 2005). The life cycle of the BMU includes sequential steps which are highly regulated including: resting, activation, resorption, reversal (coupling), formation, and mineralisation (Raisz, 1999; Cowin, 2001). Each stage will be described to permit an understanding of this process.

In humans, a large proportion of bone surfaces are in the resting state with about 80% of the cancellous and cortical bone surfaces (periosteal and endosteal) and about 95% of the intracortical surface being inactive with respect to bone modeling activity at any given time (Cowin, 2001). These inactive surfaces are covered by osteogenic precursor cells, known as bone lining cells, and a thin unmineralised endosteal connective tissue membrane. These quiescent surfaces are subsequently converted, by activation, to a resorptive state. It is believed that this transition from resting to

activation is brought about by initiation of factors activated in response to local structural, biochemical and biomechanical requirements (Raisz, 1999; Cowin, 2001). The process of remodeling requires the recruitment of osteoclasts and a means for them to gain access to the bone surface. This is considered to be achieved by bone lining cells which digest the endosteal membrane resulting in the exposure of the mineralised bone surface which is chemotactic for osteoclastic precursor cells (Ruimerman, 2005). Once the osteoclasts are in approximation with the bone surface they begin digesting the underlying bone, forming small cavities called Howship's lacunae. The period between completion of the resorption phase and the initiation of the formation stage has been termed the reversal period of bone turnover. This reversal stage has also been termed the coupling stage due to the physiological coupling of bone formation and bone resorption, before bone formation predominates.

Bone formation is observed to occur in two stages, the first of which is matrix synthesis, followed secondly by extracellular mineralisation. Firstly, a layer of cement substance is laid down upon which new bone matrix is subsequently deposited by osteoblasts. This new layer of bone matrix is termed the osteoid seam. The cement line acts as the boundary between a newly formed osteon and the surrounding older bone. Subsequently, complete mineralisation takes about 3 to 6 months in both cortical and trabecular bone (Cowin, 2001).

In cortical bone the remodeling process proceeds by the formation of a cylindrical canal within the existing bone by the BMU. The cortical BMU is regarded as an osteon. Conversely in trabecular bone, remodeling is predominantly a surface event and as a function of the increased surface area of the trabecular bone it is much more actively remodelled than cortical bone (Ruimerman, 2005). The trabecular BMU can be regarded as half a cortical BMU. The resulting structure that is formed is called a

trabecular osteon or hemi-osteon. This is the main morphological difference between cortical and trabecular bone BMU action.

3.4.4 Remodeling initiation - Mechanotransduction

Mechanical forces are known to have a profound effect on bone modeling and remodeling processes in both trabecular and cortical bone. This effect is evident in the altered morphology observed when bone tissue is subjected to increased or decreased forces. The mechanism by which mechanical loading is transduced into cellular signals of bone adaptation has generated much debate in the field of mechanobiology and has been ascribed the term mechanotransduction of bone tissue. Mechanotransduction refers to the mechanisms by which cells convert mechanical stimuli into electrical or biochemical activity (Turner, 1998). In bone, this process is considered to be complex and the way by which mechanical forces are expressed in osteoclast and osteoblast activity is currently one of the main unresolved issues in bone mechanobiology (Ruimerman, 2005), although it is thought to be mediated by several mechanisms (Pearson and Lieberman, 2004). The three dimensional network of osteocytes and bone lining cells within bone substance are considered to provide the cellular basis for mechanotransduction in bone and resultant adaptive bone remodeling (Klein-Nulend *et al*, 1995). Osteocytes are known to play an important role in mechanotransduction in that they respond to mechanical stimulation (Klein-Nulend *et al*, 1995). Together with bone lining cells they form a network that is well equipped for signal transduction (Cowin *et al*, 1991). To further understand the role of these cells in mechanotransduction it is important to understand the microanatomy of the osteocyte which possesses long processes located within canaliculi which radiate from the cell

body allowing for communication with other osteocytes (Cowin *et al*, 1991; Knothe Tate *et al*, 2004; Pearson and Lieberman, 2004).

Osteocytes and their associated processes form a complex connected cellular network (CCN) throughout a bone. The CCN allows communication between the osteocytes and bone lining cells. The manner in which the CCN senses mechanical loading is not fully understood, however there are several viable hypotheses for this action. One hypothesis is that osteocytes sense shear stress through a process known as the canalicular fluid flow. This hypothesis proposes that when mechanical loading is induced, interstitial fluid flows through the canalicular systems within bone and is thought to act as the stimulus for osteocyte mechanosensing (Weinbaum *et al*, 1994). Further to this hypothesised mode of action, other theories have been considered. These include the proposal that osteoblasts and osteocytes sense strains which may induce stretch-activated ion channels in their plasma membranes, promoting calcium influx which in turn initiates other intracellular responses (Guggino *et al*, 1989; Davidson *et al*, 1996). Also, strain induced fluid flow within the bone matrix itself has been proposed to generate small electrical potentials which are detected directly by the osteocytes (Cowin, 2001).

3.5 Factors influencing bone biomechanics

The relationship between bone form and function is well understood and has been investigated extensively from the early studies in the nineteenth century (Ward, 1838; Von Mayer, 1867; Wolff, 1892; Evans, 1957; Wolff, 1986), the seminal work in the past decades (Evans, 1973; Lanyon, 1974; Carter and Hayes, 1977; Gibson, 1985; Goldstein, 1987; Frost, 1990a; Biewener *et al*, 1996), and finally the recent application of current approaches (Ciarelli *et al*, 1991; Keaveny *et al*, 2001; Jee, 2005; Liu *et al*,

2006). However, the knowledge of bone biomechanics and the specialised micro anatomy of trabecular characteristics have expanded exponentially over the past two decades with complex studies continually adding to the knowledge of the constantly changing internal structure of bone. With this expansion in knowledge there has been a much greater understanding of the trabecular changes which occur in response to mechanical force or microdamage (Evans, 1957; Turner, 1998; Raisz, 1999; Huiskes *et al*, 2000), development (Nuzzo *et al*, 2003; Ryan and Krovitz, 2006), genetics (Bertram and Swartz, 1991; Huiskes, 2000; Huiskes *et al*, 2000; Lovejoy *et al*, 2002; Pearson and Lieberman, 2004; Ruff *et al*, 2006), ageing (Macho *et al*, 2005; Müller, 2005; Stauber and Müller, 2006, Nagaraja *et al*, 2007), systemic and local regulation (Raisz, 1999; Ripamonti, 2006) and therapeutic intervention (Ding *et al*, 2003; Pierroz *et al*, 2006).

3.5.1 Mechanical loading and bone remodeling

Trabecular bone structural organisation is considered to be predominantly influenced by localised temporal forces which act to maintain and remodel the trabecular architecture into a biomechanically optimal configuration. In particular, trabecular architecture is known to respond to its mechanical loading environment (Lanyon, 1974; 1984; Turner, 1998; Ehrlich and Lanyon, 2002). This response is characterised when a bone either experiences an increased or decreased strain-related stimulus. When an increased strain-related stimulus is encountered, remodeling occurs, resulting in a net increase in bone formation (Hsieh *et al*, 2001). Conversely, where there is a reduction in strain-related stimulus, a net reduction in bone mass tends to occur.

In order to explain these phenomena, a ‘bone mechanostat theory’ was proposed which aids in the explanation of strain-adaptive remodeling. This theory suggests that

when normal loading conditions are present, normal bone turnover in response to everyday loading is evident and conversely when loading outwith normal physiological limits occurs, adaptive remodeling to accommodate the new strain magnitudes occurs (Frost, 1987). However, although this theory holds true in essence, the adaptive remodeling ability of bone has been shown to be more complex with an increased emphasis on strain-related stimulus rather than strain magnitude (Lanyon and Rubin, 1984; Ehrlich and Lanyon, 2002). In response to this, an updated account of bone's mechanostat has been proposed (Frost, 2003), which takes into account recent findings and the bearing they have on the mechanical function of bone's remodeling processes.

Many experimental models have been used to investigate the mechanical loading of bone and the associated biomechanical response. These studies have predominated as animal experimental models (Hert *et al*, 1969; Liskova and Hert, 1971; Lanyon *et al*, 1982; Lanyon and Rubin, 1984) and human exercise models (Nilsson and Westlin, 1971). However, although these techniques demonstrated that there was a substantial influence on bone's developmental form in response to mechanical loading, they contained inherent flaws in their experimental design (Bertram and Swartz, 1991). Therfore, revised animal models were developed to exclude these flaws (Turner *et al*, 1991; Torrance *et al*, 1994), and these have been adopted in several modern studies aimed at understanding bone modeling and remodeling in response to altered mechanical loading (Hsieh *et al*, 2001; Burr *et al*, 2002; Robling *et al*, 2002).

Studies assessing the effect of mechanical loading on bone adaptation have demonstrated that a clear relationship exists between mechanical usage and bone architectural arrangement (Lanyon, 1996). This is evident in the fact that strenuous exercise increases bone mass (Courteix *et al*, 1998) and conversely disuse through inactivity or microgravity reduces bone mass (Collet *et al*, 1997; Zerwekh *et al*, 1998).

Further investigations on individual human bones have shown that trabecular patterning in the calcaneus is controlled by principal stress flows through the bone which are characteristic of the standing posture (Gefen and Seliktar, 2004). Furthermore, trabecular microarchitecture and bone mineral density have been shown to exhibit regional adaptation responses under the influences of habitual weight-bearing loading (Lai *et al*, 2005). Similarly, studies in cortical bone have demonstrated remodeling at site-specific regions of increased stress and strain (Drapeau and Streeter, 2006). However, although these studies have tended to concentrate on extreme mechanical loading which brings about a change in bone morphology through remodeling, normal everyday loading and the resultant effect on bone, must also be considered. As such, it has been proposed that bone can accommodate normal loading environments, those which do not significantly change the functional environment, without the need for remodeling. This is considered to be a critical aspect of bone tissue's ability to adapt to mechanical stimuli and is mediated by the ability of the osteocyte to normalise the mechanical environment (Rubin *et al*, 2002).

The effects of loading on cortical and trabecular remodeling during growth and development have also been investigated. The development of cortical bone has also been shown to be mechanically driven (Tanck *et al*, 2006). Furthermore, studies have suggested that trabecular bone density is adapted to external mechanical loads from the early phase of growth whereas trabecular orientation is adapted to principal loading direction later in development to produce an efficient architectural arrangement (Tanck *et al*, 2001).

3.5.2 Genetic influences on bone remodeling

Both genetics and environmental influences have a profound effect on the morphology of the skeleton. Therefore, an understanding of the gene-environment interface is critical to understanding morphological variation in bone (Ruff *et al*, 2006). The relative influences of mechanical and genetic factors are still a question of great debate with the full contribution of genetic influences to bone development not fully understood (Bertram and Swartz, 1991; Huiskes, 2000; Huiskes *et al*, 2000; Lovejoy *et al*, 2002; Pearson and Lieberman, 2004; Ruff *et al*, 2006). However, the role of genetic and epigenetic influences on bone development have been increasingly investigated in recent years through the application of experimental models which aim to provide an interpretation of genetic bone patterning in isolation from functional influences (Hall and Herring, 1990; Hosseini and Hogg, 1991; Germiller and Goldstein, 1997; Bobroff *et al*, 1999; Henderson *et al*, 2005). These studies have strongly suggested that bone form and internal structure are, in part, genetically determined as although skeletal growth is reduced in the absence of functional forces (Hall and Herring, 1990) bone structure is not significantly altered (Hall and Herring, 1990; Hosseini and Hogg, 1991; Germiller and Goldstein, 1997; Gilbert *et al*, 2004; Henderson *et al*, 2005; Sawamura *et al*, 2006). This principle was discussed by Lanyon and Skerry (2001) who proposed that although genetic influences may affect mechanically adaptive processes they cannot substitute for them, summarising that appropriate mechanical loading in conjunction with genetic processes is required for normal skeletal development. Further to this, Ruff *et al* (2006) in their discussion on genetic determination of bone morphology summarised that the major evolutionary features of skeletal morphology may be genetically determined in principle but the features that differentiate one individual skeleton from another is likely to be the combined effect of both environmental and genetic influences. It is therefore

suggested that, coupled with genetic influences, mechanical stimuli *in utero* and in later development may serve to reinforce bone shape and structure (Ruff *et al*, 2006; Skedros *et al*, 2007). The evidence that the final structure of bone results from a combination of genetic, epigenetic, and extragenetic factors is now widely accepted (Skedros *et al*, 2007).

3.5.3 Systemic and local regulation of bone remodeling

Bone remodeling is a complex process which is regulated tightly by systemic hormones and local growth factors (Canalis *et al*, 1988). This remodeling is necessary both to maintain the structural integrity of the skeleton and to subserve its metabolic functions (Raisz, 1999). The responses to changes in mechanical force and repair of microfractures, as well as the maintenance of the remodeling cycle, are determined locally by cytokines, prostaglandins and growth factors (Raisz, 1999). The metabolic regulation of resorption and formation of bone is controlled largely by the systemic calcium regulating hormones, parathyroid hormone (PTH) and vitamin D (Raisz, 1999; Hercz, 2001). However, a further hormone, calcitonin, is also considered to be important in skeletal development along with other systemic factors. Documentation of the major systemic factors involved in the regulation of bone remodeling is summarised in Table 3.2.

	Bone resorption	Bone formation
PTH	↑ [a]	↑ (↓) [b]
1,25(OH)$_2$ Vitamin D	↑	↑ (↓) [b]
Calcitonin	↓	?
Estrogen	↓	(↓) [c]
Androgen	?	↑
Growth hormone/IGF	↑	↑
Thyroid hormone	↑	↑
Glucocorticoids	↑ [d]	↓

[a] ↑, increase; ↓, decrease; ?, not known.
[b] PTH and vitamin D decrease collagen synthesis in high doses.
[c] Estrogen decreases bone formation by decreasing remodeling, but formation is decreased less than resorption and bone mass increases.
[d] Glucocorticoids may increase resorption indirectly by inhibiting intestinal calcium absorption and sex hormone production.

Table 3.2. Systemic regulation of bone remodeling. Taken from: Raisz, L.G. (1999). Physiology and pathophysiology of bone remodeling. *Clinical Chemistry*. **45**(8B):1353-1358.

PTH is a potent stimulator of bone resorption and can both increase and decrease bone formation (Raisz, 1999). It is secreted by the parathyroid glands and acts to regulate the serum calcium concentration in the blood. PTH enhances the release of calcium from the large reservoir contained in bone. This release is initiated via bone resorption by osteoclasts, which are indirectly stimulated by PTH. Osteoclasts are not directly stimulated by PTH as they do not posses the parathyroid hormone receptor, therefore their activation is indirect through the binding of PTH to osteoblasts, which do possess the parathyroid hormone receptor. Binding stimulates osteoblasts to increase their expression of RANK-L or osteoprotegerin ligand, which can bind to osteoclast precursors containing RANK, a receptor for RANK-L. These two cell surface proteins, RANK expressed on osteoclast precursor cells and its partner RANK-L expressed on osteoblasts, are the key regulators of osteoclast formation and function. The binding of RANK-L to RANK stimulates these precursors to fuse, forming new osteoclasts which ultimately enhance the resorption of bone. Plasma PTH tends to increase with age, and

this may produce an increase in bone turnover and a loss of bone mass, particularly of cortical bone (Raisz, 1999).

Vitamin D regulates the calcium and phosphorus levels in the blood by promoting their absorption in the intestines and by promoting re-absorption of calcium in the kidneys, enabling normal mineralisation of bone. Vitamin D is responsible for the recruitment of osteoclasts and plays a crucial role in the mineralisation of bone matrix. Although vitamin D has its greatest effect on interstitial calcium and phosphate absorption, it is also considered to have direct effects on bone and other tissues (Li *et al*, 1998). It has an important role in the differentiation of both osteoblasts and osteoclasts and can stimulate both bone resorption and formation (Molina, 2006).

Calcitonin is an important systemic factor in skeletal development due to its role as a potent inhibitor of bone resorption and its osteoclastic sensitivity (Manolagas and Olefsky, 1988; Wallach *et al*, 1999; Zaidi *et al*, 2002). The main physiologic function of calcitonin is to decrease calcium and phosphate concentrations, mainly by decreasing bone resorption. Calcitonin acts directly on osteoclasts to inhibit bone resorption by inhibiting osteoclast motility, preventing osteoclast differentiation, and causing a loss of osteoclast functionality and number (Molina, 2006).

In addition to these systemic regulators of bone remodeling, many other factors play an important role in bone homeostasis. A further systemic hormone which is important in regulating the normal physiology of skeletal growth is growth hormone (GH) which acts directly in a systemic manner and locally through insulin-like growth factor (IGF) production, ultimately stimulating bone formation and resorption (Rosen and Donahue, 1998, Molina, 2006). GH stimulates longitudinal growth by increasing the formation of new bone and cartilage. Before the epiphyses in long bones have fused, it has been proposed that GH stimulates longitudinal bone growth directly by

stimulating prechondrocytes in the growth plate. This is followed by a clonal expansion of differentiating chondrocytes caused both by the GH-induced local production of insulin-like growth factor I (IGF-I) and by a GH-induced increase in circulating levels of IGF-I (Ohlsson *et al*, 1998).

In summary, skeletal growth is stimulated directly through the interaction of GH with its receptor on osteoblasts and indirectly through stimulation of the synthesis of IGF-I, which mediates the growth effects of GH (Molina, 2006). Further to this, glucocorticoids also have an important role in the regulation of bone remodeling as they are necessary for bone cell differentiation during development and cause profound effects on bone cell replication, differentiation, and function. Glucocorticoids increase bone resorption by stimulating osteoclastogenesis by increasing the expression of RANK ligand and decreasing the expression of its decoy receptor, osteoprotegrin (OPG) (Canalis and Delany, 2002). However, their greatest potential effect is to inhibit bone formation by decreasing the number of osteoblasts and their function (Advani *et al*, 1997; Canalis and Delany, 2002). This is the major pathogenetic mechanism in glucocorticoid-induced osteoporosis (Canalis, 1996). In contrast to this, the indirect effects of glucocorticoids on calcium absorption and sex hormone production may increase bone resorption (Raisz, 1999).

Further systemic factors which act to regulate bone remodeling are thyroid hormones which are crucial for normal bone maturation. They stimulate growth and development, via bone resorption and formation, through activation of osteoclast and osteoblast activities and are critical for maintenance of normal bone remodeling (Kawaguchi *et al*, 1994). However, excessive presence of thyroid hormone as in hyperthyroidism causes accelerated bone turnover (Mosekilde *et al*, 1990) and a shortening of the normal bone remodeling cycle (Eriksen, 1986) leading to increased

bone loss (Greenspan and Greenspan, 1999). Thyroid hormone is considered to have a more detrimental effect on cortical bone than it does on trabecular bone (Ross, 1994).

The most important systemic hormone involved in maintaining normal bone turnover, especially during puberty, is considered to be oestrogen (Pacifici, 1998). Oestrogen is known to promote the closure of the growth plate leading to the maturation of bone structure. Further to this, it acts to maintain bone mass by suppressing bone turnover and maintaining homeostasis between bone formation and bone resorption. Oestrogen affects the generation, life span, and functional activity of both osteoclasts and osteoblasts by decreasing osteoclast formation and activity and increasing osteoclast apoptosis. (Molina, 2006). Considerable evidence exists to suggest that oestrogen prevents bone loss by blocking the production of proinflammatory cytokines by bone marrow and bone cells (Pacifici, 1996; Manolagas and Jilka, 1995). The main consequence of increased cytokine production in the bone microenvironment is a significant increase in osteoclast formation leading to an expansion of the osteoclastic pool (Roodman, 1996). In addition, enhanced cytokine production results in increased activity of mature osteoclasts and in increased osteoblastic activity. Conversely, oestrogen deficiency is known to lead to an increase in bone remodeling in which bone resorption exceeds bone formation and results in a net decrease in bone mass. This can be observed not only in women, but also in men with defects either in the oestrogen receptor or in the synthesis of oestrogen from testosterone (Bilezikian *et al*, 1998; Khosla, 2008).

Further to systemic remodeling factors, local factors also act to maintain the bone environment. Local factors which act on the skeleton are summarised in Table 3.3.

- Cytokines that may cause bone loss: IL-1, TNF,[a] IL-6, IL-11, and ODF
- Cytokines that may prevent bone loss: IL-4, IL-13, IL-18, IFN, OPG, and IL-1ra
- Colony-stimulating factors: M-CSF and GM-CSF
- Prostaglandins, leukotrienes, and nitric oxide
- Growth factors: IGF, TGFβ, FGF, PDGF, and PTHrP

[a] TNF, tumor necrosis factor; ODF, osteoclast differentiation factor; IFN, interferon; M-CSF, macrophage colony-stimulating factor; GM-CSF, granulocyte-macrophage colony-stimulating factor; TGFβ, transforming growth factor-β; FGF, fibroblast growth factor; PDGF, platelet-derived growth factor; PTHrP, PTH-related protein.

Table 3.3. Local factors acting on the skeleton. Taken from: Raisz, L.G. (1999). Physiology and pathophysiology of bone remodeling. *Clinical Chemistry*. **45**(8B):1353-1358.

Cytokines were the first local regulators of bone remodeling to be discovered (Raisz, 1999). Many cytokines present in the extracellular matrix or locally synthesised by bone cells have been shown to be involved in bone remodeling (Amling *et al*, 2000). Cytokines are produced by cells which are present in the osteoclast microenvironment and can affect osteoclast formation and osteoclast activity. Cytokines have been shown to have very different actions on bone depending on which factor is acting, with some stimulating the formation and bone resorbing capacity of osteoclasts and others actively inhibiting osteoclast formation and activity (Roodman, 1992).

A large number of cytokines and growth factors that can affect bone cell functions have now been identified, including some proteins that are responsible for the interaction between cells of the osteoblastic and osteoclastic lineage. Recent work has culminated in the cloning of osteoprotegrin (OPG), which is a protein secreted by osteoblasts that contributes to the regulation of bone resorption by inhibiting osteoclast differentiation, and RANK-L, which is an osteoclast differentiation factor (Lacey *et al*, 1998). These two cytokines play important roles during osteoclast differentiation and can act via paracrine mechanisms (Lacey *et al*, 1998; Amling *et al*, 2000). Specifically,

OPG can be produced by cells of the osteoblast lineage, but it can also be produced by other cells in the marrow. OPG acts as a soluble decoy receptor that binds to RANKL, preventing it from binding to RANK and thereby effectively inhibiting RANK-Lmediated osteoclast maturation. PTH and glucocorticoids decrease the production of osteoprotegerin, whereas oestrogens increase its expression (Raisz, 1999; Molina, 2006).

Local growth factors are present in large numbers within bone, each with their specific action on development and remodeling of the skeleton. Of these growth factors the most abundant is considered to be the insulin-like growth factors (IGFs) (Raisz, 1999). IGF-I increases replication of cells of the osteoblastic lineage, enhances osteoblastic collagen synthesis and matrix apposition rates. IGF-I is also thought to stimulate bone resorption by enhanced osteoclastic recruitment, thus acting on both bone formation and resorption and possibly coupling the two processes (Molina, 2006). Transforming growth factor beta (TGFβ) and the related family of bone morphogenetic proteins (BMPs) are also important in the remodeling and regulation of skeletal form, having originally been identified as stimulators of bone formation but are now also recognised as being important regulators in skeletal development (Van Der Eerden *et al*, 2003). Vascular endothelial growth factors are important as chemoattractants essential for attracting vascular elements to the hypertrophying chondrocytes during the initial stage of ossification, as well as for terminal differentiation of chondrocytes during the end stages of endochondral ossification (Van Der Eerden *et al*, 2003). Several other growth factors involved in skeletal development and remodeling include; platelet-derived growth factor which plays a significant role in angiogenesis, PTH-related protein which is responsible for the regulation of chondrocyte differentiation, and fibroblast growth factor which is a regulator of embryonic bone development. Each

of these growth factors has its own individual and important actions on the development and remodeling of the skeleton.

3.5.4 Effects of bone age on remodeling

During the juvenile developmental period of human skeletal growth, mechanical loading primarily influences the skeletal form (Bertram and Swartz, 1991). However, although age specific differences in bone's response to mechanical loading are evident, sensitivity to mechanical loading does not cease at the end of the juvenile growth period (Ruff *et al*, 2006). Instead, mechanical loading produces greatly decreased modeling and remodeling responses in skeletally mature individuals (Lieberman *et al*, 2003). Many models have been proposed and applied in the investigation of bone response to mechanical loading throughout ontogeny and enhance our understanding of age related biological responses (Pearson and Lieberman, 2004). In a recent review, Pearson and Lieberman (2004) outlined the major details and assumptions of the models used for examining the effects of age on bone modeling and remodeling. These included descriptive models, equilibrium models and optimisation models. Descriptive models have been applied to make interpretations of variations in cross-sectional geometry between juveniles and adults under loading conditions (Ruff *et al*, 1994). Equilibrium models have been developed to aid the explanation of structural variations that maintain bone stiffness and strength within some threshold range at specific sites (Rubin and Lanyon, 1984; Carter and Beaupre, 2001; Frost, 1987, 1990a). Finally, optimisation models make explicit predictions which account for the variation between bones, between ontogenetic stages and between species in both strain magnitudes and osteogenic responses to loading (Lieberman and Pearson 2001; Lieberman *et al*, 2003).

The results of these studies have confirmed that in juvenile bones the response to mechanical loading is more marked than in the adult.

CHAPTER 4 – Preliminary Investigative Techniques

4.1 Introduction

The introduction of three-dimensional imaging modalities has created the potential for reliable and repeatable non-destructive analysis of bone. Therefore, a large part of this study involved the identification and optimisation of appropriate imaging and analysis techniques for application to the study sample, in order to achieve a comprehensive perspective of three dimensional structural composition within the ilium. A number of three-dimensional imaging techniques were trialled throughout the duration of this study, including micro-magnetic resonance imaging, clinical computed tomography and micro-computed tomography, each yielding a varying degree of resolution and resultant structural interpretation. In addition to this, multiple software applications, for the calculation of various histomorphometric indices, were also trialled to determine the most appropriate method for structural analysis.

Although imaging techniques have become the analysis method of choice for the structural investigation of protected skeletal samples, there are several inherent limitations which have an impact on subsequent quantification. Additionally, analysis software as applied to image stacks also possesses inherent limitations which may further weaken the true assessment of bone structural morphology. Acknowledgment of these limitations is essential for the accurate assessment of trabecular and cortical results and is necessary for producing informed conclusions regarding bone form. It is therefore appropriate that this aspect of the project is thoroughly discussed in the context of the sample studied and the results obtained.

At the outset of this project it was intended that a full ontogenetic documentation of developing trabecular and cortical structure be undertaken, however, this was

ultimately restricted to the fetal and neonatal age cohort due to inherent and unavoidable imaging and analysis limitations. These limitations are important in the context of studies which apply image analysis to the quantification of microstructures in whole bone analysis and their implications must be fully addressed.

Therefore, prior to documentation and discussion of the qualitative and quantitative results obtained in this study, it is the purpose of this chapter to outline the imaging and analysis methods trialled, providing a discussion of the limitations associated with each. This will provide justification for the analysis approaches finally adopted. This aspect is discussed here to enhance the clarity of the principal results discussion in later chapters.

4.2 Imaging Modalities

Traditionally, histomorphometric techniques performed on two dimensional sections were recognised as the gold standard for the assessment and calculation of trabecular characteristics (Saparin *et al*, 2006) with occasional extrapolation to the third spatial dimension using various model assumptions of trabecular bone (Parfitt *et al*, 1987). These histomorphometric techniques were based on the use of optical microscopy and the principles of quantitative histology and stereology (Dalle Carbonare *et al*, 2005). However, the introduction of three-dimensional imaging techniques and associated software, which have the capabilities to handle large data sets and calculate complex trabecular characteristics, have been instrumental in the development of knowledge into the microenvironment of trabecular architecture. Indeed, many imaging techniques are now optimised for analysis of specific tissue types and these include magnetic resonance imaging (MRI) and computed tomography (CT).

Although these modern imaging techniques have the ability to resolve structural elements down to the sub-micron level and can be applied to a variety of biological structures for the purposes of quantification, the system specifications often documented by imaging manufacturers regularly fail to clearly acknowledge that several factors have to be considered and optimised prior to achieving such high spatial resolutions. These factors are numerous and range from biological parameters including specimen size and tissue type under investigation, to the technical specification of the imaging system including scanning time and gantry size. These specifications are particularly relevant to this study as a novel whole bone approach has resulted in the inability to optimise the parameters necessary for high resolution imaging of larger iliac specimens. This has led to a number of limitations which reduce the ability of certain imaging systems to quantify accurately the structural composition of the ilium.

Each of the imaging techniques applied during this study involved inherent limitations which, to a greater or lesser extent, influenced the results obtained. Each of the imaging techniques applied are discussed in terms of associated limitations and the impact of these on image quality and subsequent quantification. Ultimately, the imaging technique chosen for full sample analysis was the technique which minimised limitations and provided the most reliable account of structural morphology.

4.2.1 Micro-magnetic resonance imaging (μMRI)

Micro-magnetic resonance imaging was the initial imaging modality applied in this study for the visualisation of internal bone structure. Magnetic resonance imaging is a complex imaging technique which is based on the application of high magnetic fields, the transmission of radiofrequency waves and the detection of radiofrequency signals from excited hydrogen protons (Genant *et al*, 1999; Jiang *et al*, 2000). These principles

can be specifically applied to the visualisation and analysis of trabecular bone architecture (Genant and Jiang, 2006). Micro-MRI has been well documented in the literature with regards to assessment of osteoporosis (Genant *et al*, 1999), with its use in this regard being particularly aimed towards animal models. Studies of this kind have demonstrated trabecular bone loss in ovariectomised rats which are comparable to those obtained through histological assessment (Jiang *et al*, 200). Additionally, this technique has been used to document developing elements of the skeletal system in the chick (Li *et al*, 2007). However, its application has also been widely used in determining bone strength in humans by assessment of trabecular parameters (Wehrli *et al*, 1998), as well as providing a means for structural and functional assessment of both trabecular and cortical bone (Wehrli, 2007). Unfortunately, this technique is only suited to studies where there is the presence of both bone and surrounding soft tissues. This is due to the fact that bone mineral lacks free photons, which generates a limited MR signal. This results in a dark image when contrasted against soft tissues and marrow which produce a strong MR signal resulting in a white image. In dry bone there is no significant contrast against soft tissues therefore resulting in a poor representation of bone structure.

Despite the expected limitations of applying μMRI to dry bone, an initial pilot study was conducted with the use of a small pelvic specimen. μMRI was conducted within the Division of Biological Chemistry and Drug Discovery, College of Life Sciences, University of Dundee. MicroMRI data were acquired on a Bruker AVANCE FT NMR spectrometer with a wide bore 7.1 Tesla magnet resonating at 300.15 MHz for ^{1}H. The spectrometer was fitted with Bruker micro-imaging magnetic field gradients. Micro-magnetic resonance imaging required the specimen to be submerged in water for 24 hours prior to imaging. After submersion, excess water was dried and imaging could

proceed. The diffusion of water into the tissues allowed for an improved image contrast to be obtained. The sample was placed into a 30mm glass tube and fixed in place using a combination of glass rods and plastic tubing to achieve a tight, non-obstructive specimen orientation. The glass tube was then entered into a birdcage radio-frequency (RF) resonator with an internal diameter of 30 mm and subsequently placed into the magnet. Spin echo MRI experiments, from the Bruker Paravision® library, were performed. The RF resonator was tuned and the magnet shimmed for each sample. Typically four to twelve acquisition sequences were collected and averaged to improve the signal-to-noise ratio and reduce artefacts. Three dimensional 256 x 256 x 256 data sets were acquired. Spin-echo imaging experiments were carried out to observe the bone architecture of the specimen. All acquisitions were made at 19^{o} C. The MRI pulse sequence used was: T_R/T_E = 1000/40 ms and T_R/T_E = 1000/6 ms spin-echo image (Matrix size = 256 x 256 x 256, field of view = 25 mm x 25 mm x 25 mm, voxel dimensions = 97 μm x 97 μm x 97 μm).

This study highlighted that the contrast between bone and non-bone regions was insufficient for analysis of trabecular parameters and cortical thickness (Figure 4.1). Also, the obtainable resolution for this size of specimen was outwith the limits for accurate quantification of trabecular architecture. As certain individual trabecular elements in early developmental specimens are below 100μm in thickness, the resolution used for μMRI imaging resulted in distortion of the true structural composition. Additionally, the small size of the MRI resonator was a limiting factor as the available equipment only allowed the imaging of specimens below 30mm^3. As a result of these limiting factors μMRI was not applied to the full sample and instead alternative imaging modalities were sought.

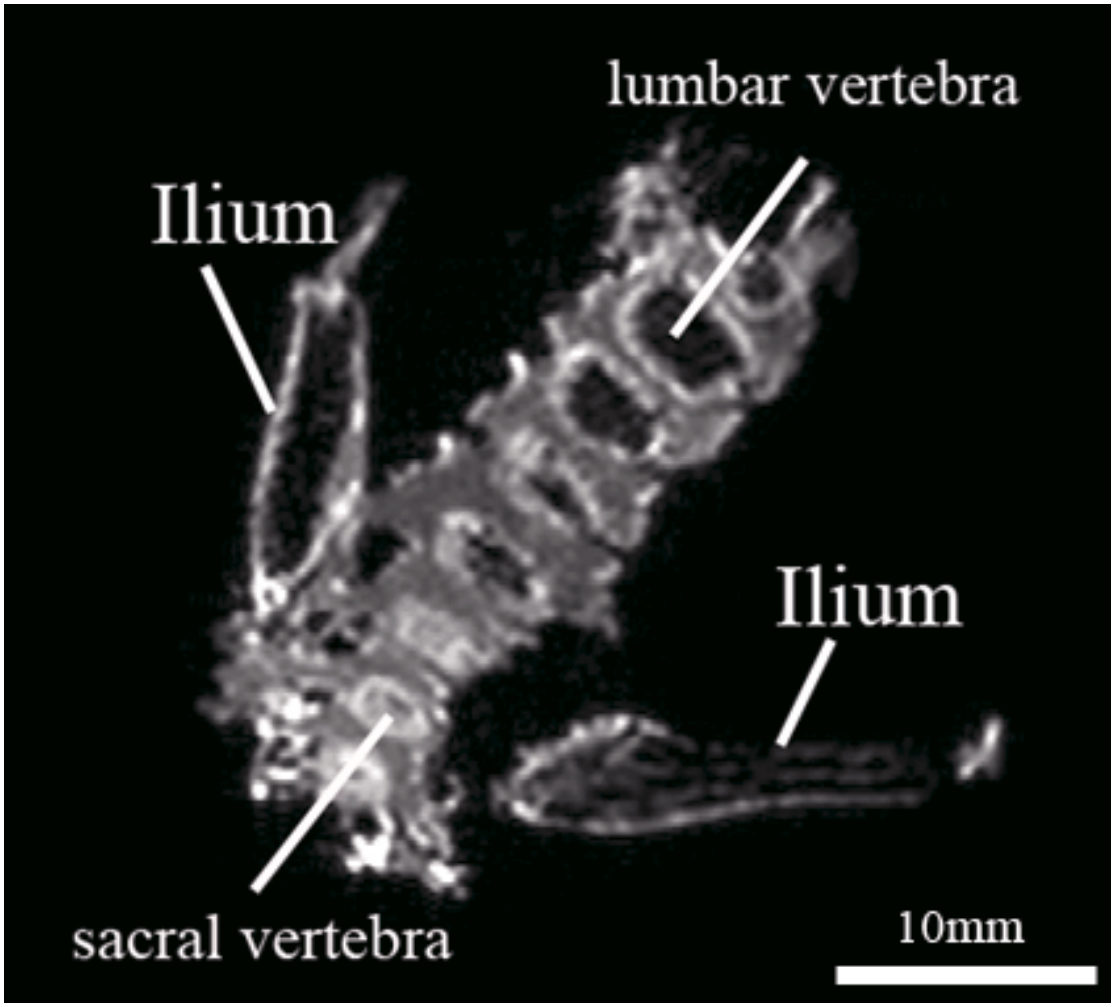

Figure 4.1. 2D coronal μMRI slice through fetal pelvis displaying right and left iliac blades as well as lumbar and sacral vertebrae. Note the poor definition of trabeculae within the ilium and vertebral bodies.

4.2.2 Clinical computed tomography (CT)

Clinical computed tomography was the subsequent imaging modality applied to the study sample for visualisation of internal bone structure. Computed tomography (CT) is a non-invasive medical imaging technique which has revolutionised clinical diagnostic practice since its introduction in the early 1970s (Hounsfield, 1973). It can be summarised as an imaging method which employs tomography, the process of imaging an object by sections. Subsequent reconstruction of these image sections enables the generation of a three-dimensional image. There are various types of clinical CT scanner currently in use, including conventional, spiral and multi-slice tomographic scanners

(Garvey and Hanlon, 2002). Each of these CT applications can produce a volume of data which can be manipulated, through a process known as windowing, which differentiates between structures dependant on their x-ray attenuation. Computed tomography has several advantages over the use of conventional 2D radiography, the main advantage being that it eliminates the superimposition of structures within an image as well as providing a good differentiation between different tissue types. Additionally, CT data can be viewed in the axial, coronal and sagittal planes, referred to as multiplanar reconstruction, which provides the opportunity to visualise structures from different perspectives instead of the conventional single 2D interpretation provided by plain plate radiography.

During computed tomography scanning, CT slice data are generated by the interaction between an x-ray source and x-ray detectors, which are arranged opposite one another in a rotating ring around the object being scanned. The x-ray detectors are scintillation systems based on photo diodes which convert x-rays into light and then into electrical signals (Jackson and Thomas, 2004). Slice data are progressively produced as the specimen being scanned is passed through the rotating ring containing the x-ray source and detectors. Each data slice produced is then combined by tomographic reconstruction. Subsequently, data are arranged in a matrix in memory, and each data point is convolved with its neighbours according to a seed algorithm using Fast Fourier Transform techniques. This dramatically increases the resolution of each voxel (volume element). Then a process known as “back projection” essentially reverses the acquisition geometry and stores the result in another memory array (Jackson and Thomas, 2004). This data can then be displayed, or used as input for further processing, such as multiplanar reconstruction. Helical multi-slice CT systems integrate the data of the moving individual slices to generate 3D volumetric information.

Pixels in a slice image obtained by CT scanning are displayed in terms of relative radiodensity. The pixel itself is displayed according to the mean attenuation of the tissue that it corresponds to on a scale from “most attenuating” to “least attenuating” on the Hounsfield scale, a quantitative scale for describing radiodensity. A pixel is a two dimensional unit based on the matrix size and the field of view selected. When CT slice thickness is also factored in, the unit becomes a three-dimensional voxel.

Manipulation of the produced CT volume is achieved through the process of windowing which utilises the calculated Hounsfield units (HU) (Spoor *et al*, 1993). A typical display device can resolve 256 shades of gray which are distributed over a wide range of HU values providing an overview of structures that attenuate the beam. Alternatively, these shades of gray can be distributed over a narrow range of HU values centered over the average HU value of a particular structure to be evaluated, such as bone. In this way, subtle variations in the internal makeup of a structure can be discerned.

Several studies have applied clinical CT to the assessment of bone quality, including the calculation and assessment of cortical structure and trabecular microarchitecture (Sandor *et al*, 1992; Louis *et al*, 1993; Silva *et al*, 1994; Link *et al*, 1998; Ito *et al*, 2005). Several recent studies have also compared CT assessment of bone to other more resolute methods of analysis and reported the correlation in values of bone structure (Link *et al*, 2003; Diederichs *et al*, 2009). These studies have indicated that it is feasible to investigate trabecular indices using modern clinical CT apparatus to gain an insight into bone structure.

In this study, clinical computed tomography was initially undertaken due to its availability and because of the large gantry size which was deemed suitable for accommodating the entire ontogenetic series of pelvic specimens. The large gantry size

of a clinical CT scanner makes reproducible specimen positioning particularly simple. This combined with an extremely fast scan and reconstruction time, in the order of minutes, made clinical CT a particularly attractive choice for full sample imaging. Additionally, the use of clinical CT in the literature for the purposes of cortical thickness assessment and simple finite element mesh production encouraged its initial application for the documentation of structural composition in this study.

Each specimen was scanned at Ninewells Hospital and Medical School, University of Dundee under the supervision of a qualified radiographer. A GE (General Electric) Lightspeed Plus. 4 slice helical multislice CT scanner using the following protocol was used to obtain data: 1sec rotation, 140kVp, 100mA, 0.7mm focal spot size, table speed 3.75mm/s, 32cm field of view, 1.25mm slice thickness with 0.25mm increment, 4X 1.25mm Helical Acquisition, Pitch = 0.75:1, 512 x 512 Matrix. The radiation dose applied to the specimens imaged in this study was optimised by considering the volume of the scan and the desired resolution required. Specimens were scanned individually and positioned in a consistent and reproducible way to aid subsequent analysis. The surface of the iliac blade was positioned perpendicular to the x-ray beam and detectors, with the iliac crest positioned superiorly and the acetabular component positioned inferiorly against the scanner bed. Scan data was produced in the DICOM format and automatically transferred to the in-house picture archiving and communication system (PACS). PACS enabled images to be stored electronically and to be viewed on screens. This storage system was accessed and datasets were downloaded onto removable storage devices for future reference and analysis. A typical clinical CT slice from an iliac specimen is presented in Figure 4.2. An additional source of clinical CT data was also sourced from the Victoria Institute of Forensic Medicine (VIFM), Melbourne, Victoria using a Toshiba1 Aquilion 16 MDCT. All cadavers

entering the VIFM are subjected to a post-mortem CT which produces a data set of approximately 1500–2000 images of 1–2 mm slice thickness. Pelvic scans from this data collection was made available for the purposes of this research.

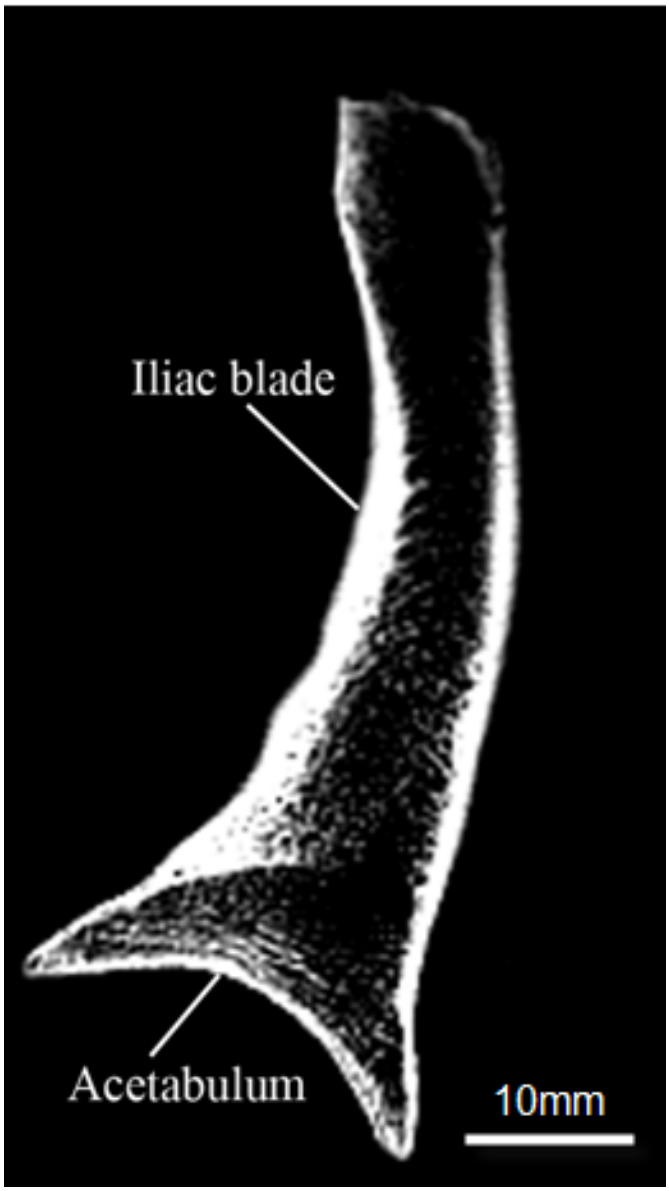

Figure 4.2. Clinical CT coronal slice through the iliac blade and acetabular roof of a juvenile specimen.

Upon initial application of this imaging technique it became apparent that there were significant inherent limitations which had a direct impact on the quality of the image produced, resulting in the rejection of clinical computed tomography as a

potential imaging technique for application to the entire sample. The main limitation presented was the insufficiency of spatial resolution to resolve individual trabecular elements and cortical thicknesses. Although gross internal architecture could be visualised between the iliac cortices (Figure 4.2), resolution was not sufficiently high to characterise individual trabecular struts and the thinnest regions of the cortex. This is an inherent limitation with all clinical CT systems, as even the most modern high resolution multislice scanners are only capable of reaching resolutions of around 300 microns, which is insufficient to resolve the smallest human trabeculae (Patel *et al*, 2005; Petersson *et al*, 2006). A further limitation observed during clinical imaging was the presence of scan artefacts which resulted in a distortion of the true scan representation. The most common artefact encountered during clinical CT scanning was an aliasing artefact which presented as dark lines passing through the bone radiating from defined anatomical protuberances such as the iliac spines. Further artefacts, such as the partial volume effect, were also evident however, due to its significance in both clinical and micro- CT imaging it will be further discussed later in isolation (see section 4.3). An additional limitation included the identification and selection of a suitable imaging algorithm and associated imaging parameters. As clinical CT scanners are intended for patient use, all algorithms are pre-set for specific anatomical regions of interest. Each of these algorithms is designed to attenuate both soft and hard tissues as they present in the living patient. However, specimens from the Scheuer collection possessed no soft tissues resulting in difficulty identifying an appropriate imaging algorithm. Ultimately, a best scenario was applied where a musculoskeletal algorithm was used to optimally visualise bone. Unfortunately, this was not ideal and resulted in poor definition of bone in certain areas. Therefore, specimens were surrounded by a soft-tissue substitute to reduce edge artefacts which distorted the internal trabecular

structure. Soft tissues were simulated using rolls of paper towelling held in place using surgical tape which substantially reduced image artefacts and enabled the simulation of a soft tissue to hard tissue boundary. The use of soft tissue substitutes including rice has been used in previous studies for this purpose (Mays *et al*, 1998) enabling an improved signal to noise ratio. A further consideration, which was taken into account when using clinical CT during this research project, was scanner availability. As the scanner was predominantly used for diagnostic imaging in a hospital setting, any research scanning had to be conducted when the scanner was not being used for clinical purposes. The available time was often limited and resulted in significant delays in obtaining core data. Additionally, cost implications were a significant consideration in terms of scanning time and personnel costs. As scanning necessitated the presence and instruction of a qualified radiographer, significant planning was required to enable optimal time management during scanning sessions. A final unexpected limitation encountered whilst applying a clinical CT scanner for the purposes of research involved issues relating to removal of scan data for subsequent analysis. This became a problem as the PACS system used to store all CT scan data obtained during project scanning was a common drive which also contained patient scan data. As a result, ethical restrictions prevented the bulk download of research scans, to reduce the risk of any inadvertent removal or copying of patient data. This restricted the ease of access to raw data however, to overcome this, data extraction was conducted in small single scan cohorts with permission from hospital medical records.

4.2.3 Micro-computed tomography (µCT)

The final imaging technique applied in this study was micro-computed tomography (micro-CT). Micro-CT is a technique which was first introduced by

Feldkamp *et al* (1989) and revolutionised the ability to visualise the internal structural components of many previously inaccessible materials. This technique uses a micro-focus x-ray tube as an x-ray source, an image intensifier as a 2D detector, and a cone-beam reconstruction to create a three-dimensional image. Although the principles and components are similar to the image collection method applied in clinical CT, the process involved in micro-computed tomography imaging differs in certain aspects. In clinical CT, the x-ray source and detectors rotate around the object being imaged, whereas in micro-CT imaging the scanned object rotates around its own axis with the x-ray source and detector being fixed (Figure 4.3). X-rays are partially attenuated by a specimen as it rotates in equal steps through 360^{o} about a single axis. At each rotational position, the surviving x-ray photons are detected by a planar 2D array. Finally, a 3D reconstruction array is created directly in place of a series of 2D slices (Jiang *et al*, 2000). From this 3D reconstruction, an image stack can be created and exported for analysis. The introduction of this technique allowed for early non-destructive analyses of trabecular bone architecture (Kuhn *et al*, 1990) and examination of standard histomorphometric parameters (Goulet *et al*, 1994). Indeed, it was the study of bone architecture and density that drove the initial early development of microCT imaging (Genant *et al*, 1999; Holdsworth and Thornton, 2002). Micro-CT is now regarded as the primary imaging technique for trabecular bone analysis (Qin *et al*, 2007), attributed loosely to its ability to visualise the internal structure of intact bones with a high degree of spatial resolution and provide an efficient and reliable means by which 3D architecture can be quantified (Cooper *et al*. 2003).

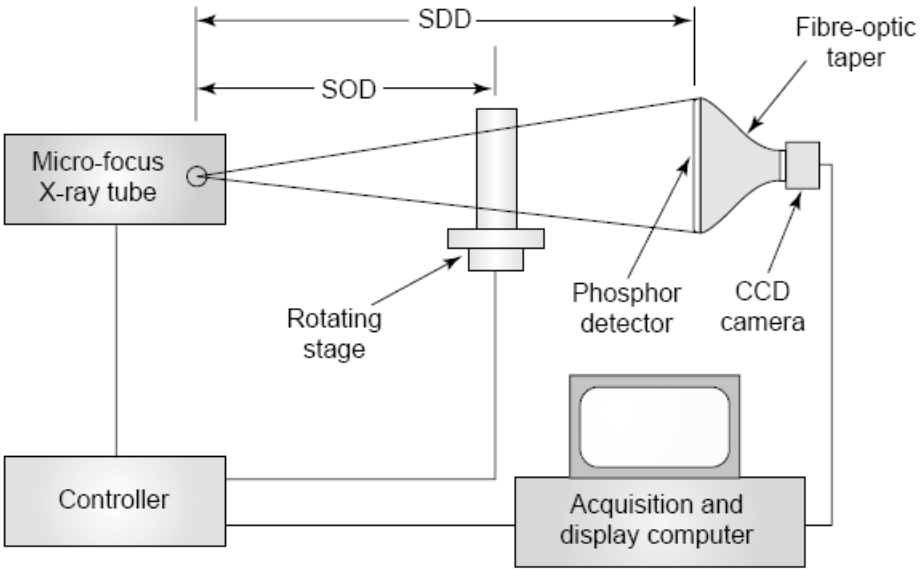

Figure 4.3. Typical components from an *in vitro* micro-computed tomography (micro-CT) scanner. A specimen mounted on a rotating stage, is positioned between an X-ray source and detector. The source to object distance (SOD) and source to detector distance (SDD) are selected to provide the appropriate amount of geometric magnification. Typically, the SDD is ~20cm and the SOD ranges between 7 and 18cm. X-ray projections are acquired by a phosphor detector, coupled to a CCD camera by a fiber-optic taper, which reduces the size of the image. During acquisition, the computer controls the X-ray tube and specimen stage, obtaining X-ray projections at hundreds of angular positions. (Taken from Holdsworth and Thornton, 2002).

MicroCT is particularly well suited to the evaluation of bone density and the quantitative assessment of 3D structural architecture due to the high signal contrast between bone and soft tissue (Genant *et al*, 1999). It is now widely used for the non-destructive evaluation of trabecular bone microarchitecture in both *in vitro* and *in vivo* studies (Müller and Ruegsegger, 1997; Ito *et al*, 1998; Laib *et al*, 2001; Beaupied *et al*, 2006; Boyd *et al*, 2006). More recently, the application of micro-computed tomography to the analysis of trabecular bone architecture has been commonly used for investigating ontogenetic development of human skeletal collections (Ding and Hvid, 2000; Ryan and Krovitz, 2005; McColl *et al*, 2006; Ryan and Krovitz, 2006; Ryan *et al*, 2007; Volpato, 2008; Gosman and Ketcham, 2009). The increased use of non-destructive microCT imaging for the analysis of bone microstructure can be attributed to the close correlation

between trabecular values obtained from computed analysis and those from traditional histomorphometric investigation and therefore increasing confidence in the veracity of the data (Uchiyama *et al*, 1997; Müller *et al*, 1998; Cendre *et al*, 1999; Fajardo *et al*, 2002; Chappard *et al*, 2005; Thomsen *et al*, 2005). As such, more information regarding the arrangement and appearance of trabecular characteristics within a variety of bones is now possible. Application of this three-dimensional imaging technique allows for structural interpretation of the trabecular architecture through quantification of several structural indices. Each of these indices yields important information regarding the structural composition of the trabecular environment (Parfitt *et al*, 1987).

In the current study, micro-computed tomography was chosen for full sample application due to the high spatial resolution which was obtainable and could be applied to the early developmental spectrum. This high spatial resolution was well suited to visualising bone trabeculae in the earliest of developmental periods and allowed for accurate and reliable quantification of trabecular parameters. Additionally, micro-CT provided a good contrast between bone and non-bone regions when dry bone was analysed. Furthermore, the large gantry size was the largest currently available for a micro-imaging modality and was deemed optimal for whole bone analysis. However, in addition to each of the advantages outlined it must also be borne in mind that there are several inherent limitations associated with micro-CT each of which were carefully considered in the context of the results obtained in this study.

The primary limitation of high resolution imaging of whole bones via micro-CT is the restricted gantry size of the scanner. As a result of this, studies have generally been confined to animal models of skeletal form due to the capability of the imaging systems to comfortably accommodate small bones. This has prompted many studies to investigate trabecular architecture using rodent models and in particular the detailed

knowledge of bone disease, such as osteoporosis, has increased considerably. Investigators can manually control variables such as endocrine influences (Laib *et al*, 2001; Boyd *et al*, 2006) or induced stresses (Nakano *et al*, 2003) thereby assessing changing structural parameters in a longitudinal study. Scanner size limitations have restricted studies of this kind in the human to clinical and post-mortem trephined bone samples taken from various anatomical sites including the vertebrae, iliac crest and calcaneus (Moore *et al*, 1989; Chappard *et al*, 1999; Hildebrand *et al*, 1999; Glorieux *et al*, 2000; Thomsen *et al*, 2002). This is restrictive as only limited anatomical regions can be accessed and an assessment of overall trabecular bone structure cannot be gained. Only recently have technological advances in microcomputed tomography apparatus allowed for scanners to be produced with gantry sizes capable of accommodating much larger sample sizes coupled with a maintained high spatial resolution (Müller *et al*, 1998**,** Ritman, 2004; Stauber and Müller, 2008)**,** in the range required for trabecular visualisation (Whitehouse, 1974; Chappard *et al*, 1999; Byers *et al*, 2000).

An additional technical limitation involved the fact that CT reconstruction normally requires the acquisition of an x-ray projection of the entire object being scanned, not only a truncated volume of interest (Cho *et al*, 1996). Scanning a full iliac specimen requires the use of large fields of view with a resulting large number of x-ray detectors. With an increased field of view, which is inherent to whole bone analysis, there is a resultant and directly related decrease in image resolution (Kim *et al*, 2004). Attempting to scan isolated volumes of interest within the full specimen would most likely result in image distortion and artefact production (Holdsworth and Thornton, 2002). Furthermore, as described for clinical CT imaging there are inherent artefacts associated with micro-CT imaging which can influence the results of quantitative

analysis (Davis and Elliott, 2006). Some of these artefacts, particularly those which influence image resolution, will be discussed separately (see section 4.3).

Despite the outlined limitations, micro-computed tomography imaging was considered to be the preferred imaging technique for resolving both cortical and trabecular bone at levels required for quantification. Micro-CT was also chosen due to its relatively fast acquisition time compared to previous time-consuming histomorphometric sectioning. Additionally, the extensive use of micro-CT for the quantification of cortical and trabecular architecture, as reflected in the literature, was a significant supporting factor for its dominant use in producing the primary data source in this study (Qin *et al*, 2007). Furthermore, data sets produced using micro-CT could be fully manipulated through different imaging planes via multiplanar reconstruction enabling an advanced interpretation of architectural arrangement. The image stack produced from micro-CT imaging could then be analysed using model-independent software for the calculation of primary indices associated with trabecular integrity.

A full account of the micro-CT apparatus and imaging parameters used in this study for full sample analysis are outlined in Chapter 6.

4.3 Spatial Resolution

The resolution of a scanning system is fundamentally important to the visualisation of trabecular bone structure and must be carefully considered for the bone specimen under investigation. In computed tomography, this resolution is determined through a combination of “scanning voxel size” and “reconstruction voxel size”. Scanning voxel size is defined as a measure of the raw data image quality and determines the best level of detail that can be resolved in the image. The raw data can then be reconstructed appropriately to any voxel size that is larger than or equal to the

scanning voxel size. Reconstruction voxel size is the actual voxel size chosen for 3D image reconstruction (Kim *et al*, 2004). If the scanning and reconstruction voxel size is insufficient to visualise the smallest of trabecular elements then certain architectural parameters will be inaccurately represented upon quantification. Unfortunately, the use of larger scanning and reconstruction voxel sizes is an inherent limitation when imaging whole bone elements (Kim *et al*, 2004), which can result in partial volume averaging. Additionally, the use of lower resolutions is often unavoidable due to field of view limitations and because of the large computational cost involved when a high resolution is applied to a large sample.

Partial volume averaging (also known as the partial volume effect) occurs when the structure being imaged, for example a trabecular strut, is only partially contained within a 2D pixel or 3D voxel. This results in the averaging of structural densities of adjacent or surrounding structures in the pixel or voxel. As a result, erroneous pixel or voxel signal values result, leading to potential misinterpretations of structural parameters. A schematic representation of partial volume averaging is given in Figure 4.4. Only a pixel contained completely within the trabecular strut (between thickened black lines) will have a true pixel value (green), other pixels (blue) will contain an area or volume weighted average of the density of the structure together with that of the surrounding non-bone structures.

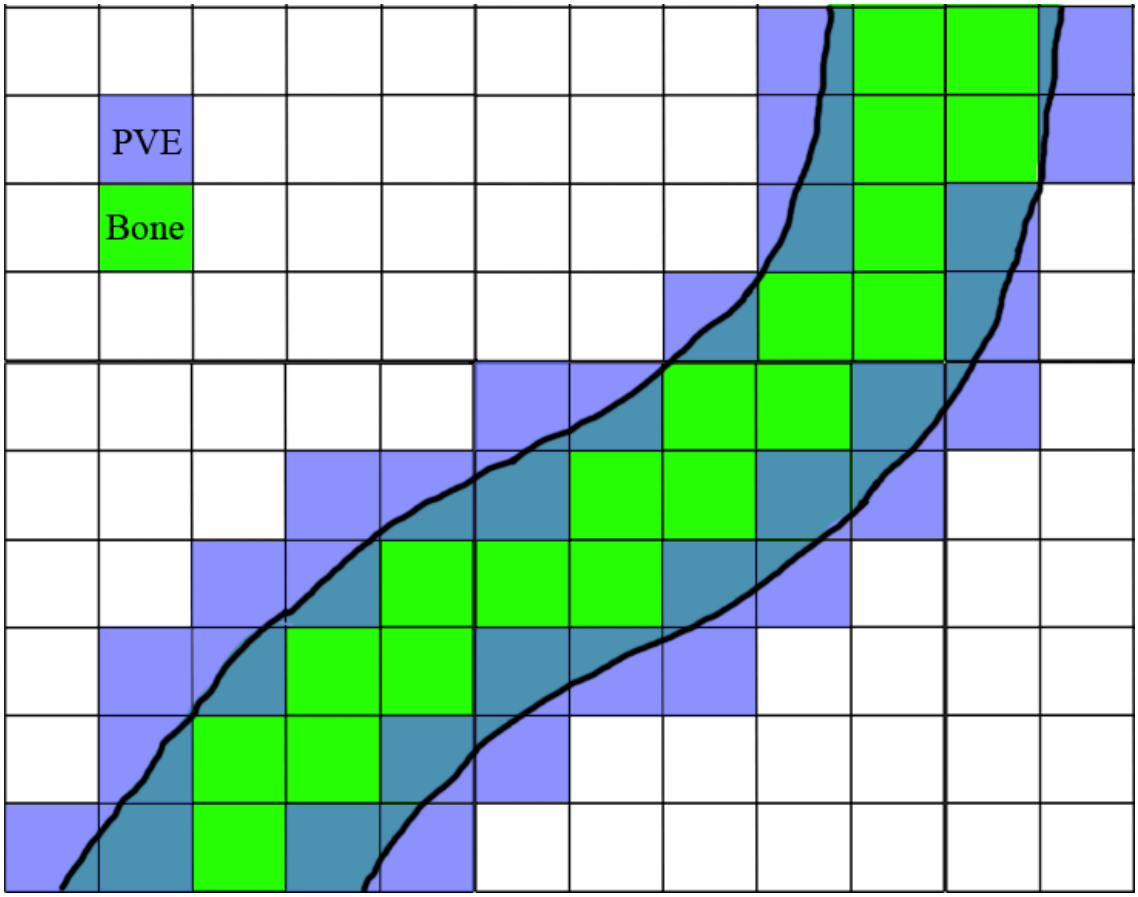

Figure 4.4. Schematic of partial volume averaging (PVE). Each square is representative of a single pixel. A trabecular strut is delineated by the strong black lines. Green shading represents a pixel contained completely within the trabecular strut and possessing a true pixel value representative of bone. Blue shading represents pixels which only partially contain the trabecular strut and are partly composed of non-bone regions resulting in the partial volume effect where the pixel density is an average.

To investigate the effects of partial volume averaging, several *in vitro* studies of trabecular architecture have applied various resolutions which have ranged from voxel sizes of a single micron up to and in excess of 120µm. Each of these studies have documented varying results (Majumdar *et al*, 1996; Kothari *et al*, 1998; Kim *et al*, 2004). Although the predominant reason for the application of micro-CT is the achievement of high resolution, this is often compromised when scanning large specimens, such as whole bones, which require spatial resolutions which are in excess of 100µm (Engelke *et al*, 1993). As these resolutions are in the order of typical

trabecular thickness for certain human bones, errors in calculation of trabecular morphology will become evident due to the partial volume effect (Kothari *et al*, 1998).

More specifically, studies have investigated the effects of differing resolution on the accuracy of some common indices of trabecular architecture. Magnitudes of stereological parameters of trabecular bone have been shown to be dependant on voxel size when voxels are larger than 100μm (Ding and Hvid, 2000). Kim *et al*, (2004) applied three different scanning and reconstruction voxel sizes to examine the effects of image resolution on stereological measures of trabecular bone. The results of this study indicated that certain trabecular parameters displayed errors of up to 102% compared to the gold standard imaging resolution when a low resolution of 110μm was used for human vertebral body trabecular analysis. This study concluded that caution should be exercised when evaluating trabecular morphological parameters at low resolutions. Further to this, Kothari *et al*, (1998) documented a strong resolution dependency of certain histomorphological parameters such as trabecular thickness and structural anisotropy. When a lower resolution was used to image the trabecular architecture, thickening of vertical trabeculae and loss of horizontal trabeculae was predominantly observed. This in turn resulted in an apparent decrease in trabecular number and increase in bone volume fraction. However, taken in isolation, trabecular number and trabecular separation were shown to display a weak resolution dependency. These findings have reinforced previous work which suggested that parameters such as trabecular thickness are increasingly overestimated with lowered resolution (Majumdar *et al*, 1996) and that parameters such as trabecular number and spacing may be accurately maintained up to resolutions of around 175μm (Müller *et al*, 1996).

4.4 Analysis software

Stereology is the study of three-dimensional objects through the interpretation of two-dimensional images. This is useful not only because it enables the study of gross structural morphology within tissues based on thin sections, but also because it enables structural quantification. Modern analysis of two-dimensional slice images produced from imaging modalities is performed by automated computed analysis which applies either model dependent or model-independent stereology. As a result, the analysis methods for characterising three dimensional trabecular parameters are becoming increasingly automated with the application of varying techniques to the calculation of important structural indices. In this study, assessment of trabecular and cortical morphology was carried out via computed analysis through the application of three-dimensional model-independent analysis.

There are many commercially and freely available software applications for the analysis and calculation of trabecular and cortical bone parameters. This variety presents a challenging and often confusing situation when selection of the optimal analysis package for a particular data set or a specific research question is not always intuitive. Many of the available packages are integral components of micro-imaging systems allowing for the efficient throughput of data, from initial scanning and data production to final data analysis. However, most of these packages are also available for isolated use and can be purchased in this capacity allowing for a comparison of analysis ability between software packages. Additionally, certain software packages are also available as freeware applications which can be freely downloaded and distributed for analysis of data which has been produced from a variety of micro-CT systems. Each of the available software applications has its own advantages and disadvantages in terms of cost efficiency, analysis methodology, and system requirements and each must be

considered in the context of the research questions being addressed. In this study, three software applications were trialled prior to the identification of the final software application utilised for full sample analysis. Each of these software applications will be documented in terms of analysis methodology and trabecular parameters measured.

4.4.1 VGStudioMax

An initial analysis programme which was trialled during the early stages of this study was VGStudioMax. VGStudioMax is a software application for the analysis of voxel data by providing advanced volume visualisation capabilities. This software offers a bone structure analysis tool to process CT voxel data from bone samples in order to determine structural parameters. This tool allows for full three-dimensional analysis for the determination of values of bone volume fraction (BV/TV), trabecular thickness (Tb.Th), number (Tb.N) and separation (Tb.Sp). This programme has the ability to deal with large data volumes and can import many files types, including HDF, binary, ASCII, AVS Field, AVS Volume Data, bitmap, JPEG, BMP, PPM, TIFF and DICOM. Once imported, data can be rendered as three-dimensional images that can be manipulated in several ways.

This software was applied to the data on a trial basis to determine its suitability for calculating various trabecular and cortical bone indices. This trial determined that VGStudioMax was not optimised for the purposes of this study. This was due to the main application of the software being aimed towards engineering principles rather than quantification of microstructures and as a result only a small add-on module for this purpose was available. Furthermore, the procedure for trabecular bone calculation was laborious and complex and assumed that the trabecular structure was plate like and therefore based all calculations around a model-dependent method. Additionally, the

trabecular parameters which could be potentially measured were limited and did not provide a full account of structural morphology. Finally, the software licence fee and conditions of use would have placed an unnecessary constraint on project resources.

4.4.2 Microview

A further analysis programme trialled was MicoView. MicroView 3D volume viewer and analysis tool is a visualisation and quantification application provided by General Electric Health Care. It can be applied to two-dimensional and three-dimensional data. It compliments micro-CT systems by offering a number of visualisation and analysis tools for micro-CT data. MicroView is an open source programme, written in the C++ and python-based programming language VTK based on a number of open source software packages. The MicroView application may be opened either using a Microsoft windows computer with a maximum file size capability of 846MB, or using an Apple Macintosh, with no maximum file size restriction, enabling analysis of data files in excess of 1GB in size. The system requirements for running MicroView were:

- Apple Macintosh: G3 computer, MAC OS X 10.3.4, optional X11 components installed, RAM: 32MB, a 3D accelerated video card with 64MB of texture memory.
- Windows operating system: Windows 98, NT 4.0, 2000, XP, a minimum Pentium III, 450MHz processor, with 256MB RAM and a 55MB hard drive, a 3D accelerated video card with 64MB of texture memory was also required.

The system specification used in this study was a Dual 2GHz Power PC G5 Apple Mac, running Mac OS X 10.3.9, with 2.5Gb DDR SDRAM memory and a hard drive space of 120MB. 3D accelerated video card with 64MB of texture memory.

The MicroView display consisted of an application tool bar and a central 3D image viewport. In the image viewport an image stack can be constructed and viewed in 3D or in the 2D X, Y and Z planes using the accessory 2D viewports. The default display contains several application tools including window and level adjustment sliders for optimisation of the image and a progress indicator. The image import function allows a TIFF image stack to be imported. Scan and image parameters including voxel dimensions of the reconstructed volume, matrix size and number of image slices can then be manually entered. Completing this information enables the programme to load the raw data set producing a 3D reconstruction which is displayed in the 3D viewport and in the respective 2D viewports.

Initially a low resolution full bone isosurface reconstruction was performed in order to confirm orientation and siding of the specimen. This was carried out by selecting a large volume of interest (VOI) which fully covered the slice images in all planes. An auto threshold was then performed using the bone analysis module to define a binary value which could differentiate between bone and non-bone. From this information, an isosurface, with a low surface quality factor was produced. Once the orientation and siding of the isosurface was confirmed, the reconstruction could be cleared and further steps for analysis could begin.

Several VOIs within each bone were analysed as outlined in Chapter 6. To identify and select a VOI within a particular bony component, a rectangular volume was selected and placed in the appropriate position using pre-defined anatomical landmarks. The VOI could be subsequently adjusted in terms of position and size using numerically scaled adjustment sliders. Once the VOI was in an appropriate position the analysis of bone parameters could be initiated by selecting ‘bone analysis’ from the application toolbar. Once the bone analysis tool was initialised an auto threshold of the VOI was

performed in order to determine bone from non-bone for binarisation. Subsequently, before the bone analysis could be completed, an isosurface of the VOI was created with a high surface quality factor to confirm that the VOI only contained trabecular bone and that there was no involvement of cortical bone. Finally, an output file was created and coded against the bone which was being examined. The analysis was then run and saved to this location. This procedure was carried out for every chosen VOI within a bone.

Trabecular parameters calculated by MicroView were obtained using automated model-dependant stereology. The following parameters were calculated assuming parallel plate morphology:

- BV/TV = Bone Volume (mm^3) / Tissue Volume (mm^3) = %
- BS/BV = Bone Surface (mm^2) / Tissue Volume (mm^3) = mm^{-1}
- Tb.Th = Trabecular Thickness = 2/(BS/BV) = mm
- Tb.N = Trabecular (connection) Number = (BV/TV)/Tb.Th = mm^{-1}
- Tb.Sp = Trabecular (spacing) Separation = (1/Tb.N)-Tb.Th = mm

Initially, MicroView was selected as the analysis package of choice due to its easily accessible freeware availability, its ability to characterise several important trabecular indices and its intuitive user interface. This choice resulted in a lengthy data collection period, during which a large proportion of the study sample was analysed in terms of trabecular morphology. This data collection was undertaken using MicroView before a final quantification package was identified. Once a significant proportion of data had been collected and analysed, a decision was made to discontinue using MicroView, disregarding collected data, and to identify an alternative software package. This decision was made because limitations were identified in the calculation potential

of the software which was considered to reduce the reliability of the results. The primary limitations identified included the application of model-dependant calculation of trabecular bone indices and the inability of the freeware edition to calculate structural model index and degree of anisotropy. This software relied on the assumption that trabecular structure was composed of trabecular plates which were aligned parallel to one another. From this model type assumption each trabecular index was calculated on a model-dependant basis resulting in potentially biased results. Additionally, the inability to independently calculate structural model independently, or degree of anisotropy within a trabecular bone region, was deemed a significant limitation due to the importance of these indices in determining bone strength (Odgaard, 1997). A solution to this limitation was found by the identification of an advanced bone analysis module which could be added onto the existing MicroView freeware application to allow for more advanced calculation. However, the advanced bone analysis module was not applied due to the significant licence fee required and due to poor communications with software providers GEHealthcare, highlighting that the availability of the software was not in keeping with the timeframe of the project. As a result, alternative software was sought which would fulfil the requirement for comprehensive and independent trabecular bone analysis.

4.4.3 SkyScan CTAn

SkyScan CTAnalyser was subsequently identified as a software application which had the potential to fulfil the requirements for model-independent analysis of trabecular indices and the ability to make linear measurements of cortical thickness. The ability of this software to calculate all required trabecular indices regardless of structural model was the primary reason for its selection and application to analysis. Additionally,

CTAn was chosen due to the favourable cost implications, which were minimised by collaboration with the University of Aberdeen who were in possession of an educational licence for the software. Agreement with SkyScan and the University of Aberdeen allowed full use of this licence between institutions.

SkyScan CTAn has been widely used for the calculation of trabecular characteristics in both animal and human bone. Due to the size restrictions inherent to many of the available micro-CT scanners most studies have investigated the trabecular architecture of mouse bones (MacRae *et al*, 2008). However, this software has recently been applied to the investigation of trabecular bone structure in humans taken from biopsies of the femora and iliac crest (Chappard *et al*, 2005; Beaupied *et al*, 2006), as well as more recent whole bone analysis of metacarpals (Lazenby *et al*, 2008).

As Skyscan CTAn was the analysis software selected for full sample analysis in this study, a full account of its analysis protocol and application to the data set is provided in Chapter 6.

4.5 Software considerations

When selecting analysis software for quantification of bone architecture several factors must be given serious consideration. These factors include the methods of structural quantification, thresholding and binarisation protocols, the structural parameters available, analysis field selection and cost implications. Therefore, a full discussion of each of these points will be given along with a summary of the interim solutions applied in this study, where a limitation in an aspect of software design and implementation was identified.

4.5.1 Model dependant/independent calculation

The appearance of trabecular bone architecture is different between various skeletal elements and between sites within a single bone (Hildebrand *et al*, 1999; Müller, 2003). Additionally, during aging and in certain diseases the structural model of the trabecular architecture can shift between the extremes of plate and rod morphology in response to bone remodeling. Therefore, traditional histomorphometric techniques, which are based upon model-dependant assumptions of trabecular structure for the quantification of architectural parameters, tend to lead to questionable results (Hildebrand *et al*, 1999). Much literature based on the calculation of trabecular bone parameters from imaging studies have traditionally applied model-dependant calculation. While parameters like bone volume density and bone surface density can be obtained directly from two dimensional images, a range of important indices including trabecular thickness, spacing and number are indirectly derived assuming a fixed structural model. Although model-dependant calculations are available for ideal plate-like and rod-like structures it is typically the parallel plate model for trabecular bone assessment which is commonly employed (Parfitt *et al*, 1987; Simmons and Hipp, 1997; Hildebrand *et al*, 1999; Day *et al*, 2000). In a study comparing model dependant and independent calculation of various trabecular indices, Hildebrand *et al,* (1999) found that model independent trabecular thickness is systematically higher than trabecular thickness assessed using the parallel plate model. They summarised that this was due to a deviation of the trabecular structure from an ideal plate-like model. This is evidenced in the current study where values of structural model index lie above a true value of plate-like architecture. Hildebrand *et al*, (1999) concluded that model-independent assessment of trabecular bone was "closer to reality" than model-dependant assessment. Furthermore a study by Day *et al*, (2000) indicated that the parallel plate model of

trabecular assessment produced a volume-dependant bias for measures of trabecular thickness and spacing. This study recommended that direct thickness measures be used when three-dimensional data sets are available.

Due to the inherent limitations involved with the application of model-dependant analysis, the results of this study are based on the use of model-independent analysis software for the calculation of trabecular architectural parameters and cortical thicknesses. It was concluded that model-independent calculation of the required bone indices would provide the most accurate assessment of structural composition in the ilium. The introduction of three-dimensional model-independent measurement techniques have made it possible to gain an insight into the actual trabecular architecture within bones without the assumption of structural model type (Odgaard *et al*, 1990; Odgaard, 1997; Hildebrand and Ruegsegger, 1997a, 1997b; Ding *et al*, 1999). These methods make direct use of the 3D data and allow direct quantification of bone architecture. Direct model-independent assessment methods have been applied in a number of recent studies for the evaluation of trabecular structure with encouraging results (Fajardo and Muller, 2001; Fajardo *et al*, 2007).

4.5.2 Image thresholding

Although micro-CT is a powerful tool for the non-destructive evaluation of trabecular bone structure, one of its most severe limitations is the inability to differentiate between materials of similar anatomical density (Shen *et al*, 2004). The differentiation of image contrast between different materials is determined by the attenuation of x-rays by the materials. Materials which have different attenuation properties will have different greyscale intensities upon image production. However, if there are insufficient differences in material attenuation properties, for two optically

distinct materials, there will be a negligible difference in greyscale intensities and the two materials will appear as one in a reconstructed micro-CT cross-section. It is also often observed that even when materials have attenuation properties which are marginally different and distinguishable by visual interpretation, difficulties can still arise when attempting to determine a greyscale threshold value between the materials for quantification purposes (Shen *et al*, 2004).

Image thresholding can be defined as a method of segmentation for partitioning a digital image into sets of pixels. In greyscale images, thresholding is used to create binary images for subsequent quantitative analysis. This is an important step in the process of bone analysis from micro-CT scans and must be undertaken prior to 3D visualisation and quantification. In a conventional approach to image thresholding, a greyscale threshold range is selected using a combination of visual interpretation and the application of a greyscale distribution histogram for an image. The histogram distribution presents a series of peaks and troughs which are representative of areas of high attenuation (bone) and low attenuation (marrow and air space) respectively. Individual pixels in the image are then determined as being 'bone' pixels if their value lies within the pre-determined greyscale distribution of the peak and as 'non-bone' if their value lies outwith the chosen greyscale distribution. Typically, a bone pixel is assigned a value of 1, while a non-bone pixel is assigned a value of 0 (Feldkamp *et al*, 1989; Shapiro and Stockman, 2002). The resultant binary image is produced dependant on the pixel labelling and coloured black for 0 and white for 1. In the scans used for this study the histogram only presented a single dominant peak with a trough on either side, this was because the dry bone had no other soft tissues associated with it, therefore, only two material phases were represented, either bone or non-bone. This eliminated the common problem encountered when a structure is composed of multiple materials

which have threshold ranges which overlap resulting in difficult separation of materials from greyscale values (Hoa and Hutmacher, 2006).

A significant limitation when applying image thresholding is the fact that only greyscale intensity is considered, and not the relationship between individual pixels. For example, it cannot be assumed that all pixels defined by thresholding are contiguous, some extraneous pixels not representative of bone may be included and conversely pixels which do contribute to bone may be eliminated. This is a particularly significant issue at bone/non-bone boundaries where pixel resolution may not allow for a clear definition between the two phases (Spoor *et al*, 1993).

When applying global thresholding to an image, a single greyscale range representative of bone for the entire image is used. However, the attenuation properties of the trabecular structure may differ between regions within the image resulting in different greyscale ranges (Kuhn *et al*, 1990). Therefore, using a global threshold may result in over or under estimation of trabecular structure in certain aspects of a single image (Feldkamp *et al*, 1989). As a result, it is more appropriate to use local thresholds. This involves producing a greyscale distribution histogram for individual volumes of interest within the image and defining the bone/non-bone grey value distribution locally for each individual region under investigation.

Information regarding the influences of threshold variation on the quantification of various measures of trabecular architecture is extremely important for determining which parameters can be analysed reliably and which must be treated with caution (Hara *et al*, 2002). A study by Hara *et al*, (2002), investigating the influence of micro-CT threshold variations on the assessment of structural and mechanical trabecular bone properties, suggested that threshold selection was extremely important for the accurate determination of bone volume fraction and mechanical properties of bone. This study

showed that trabecular thickness, bone volume fraction and structural model index were all influenced by marginal alterations in threshold values. Trabecular thickness was shown to increase upon application of a low threshold and become disconnected upon application of a high threshold. Bone volume fraction decreased linearly with increasing threshold and structural model index increased marginally with increased threshold values. Conversely, trabecular number and morphological anisotropy demonstrated negligible effects in response to altered thresholds. Hara *et al's* study reiterated the conclusions of Ding *et al*, (1999), that care must be exercised when applying thresholds in generating 3D data.

4.5.3 VOI/ROI placement

The selection of volumes (VOI) and regions of interest (ROI) when undertaking bone structural analysis is an extremely important aspect of the analysis methodology when quantifying overall bone morphology. This pre-processing stage has been regarded as the 'most delicate' task when quantitatively analysing bone architecture (Martin-Badosa *et al*, 2003), and is often performed manually as is the case in the current study. The main limitations involved in volume and region of interest selection are the definition of anatomical reference points for initial placement of analysis fields, the reproducibility of these points and fields throughout a sample and the time consuming nature of manual placement when using multiple VOI's and ROI's per specimen.

The definition of suitable anatomical reference points is often the most predominant limitation in studies which seek to analyse similar volumes of interest between specimens. This can prove to be a problem both within developmental cohorts and to a greater degree between developmental cohorts. Ryan and Krovitz, (2006),

documented the ontogenetic trabecular morphology of the human proximal femur by analysing standardised volumes of interest between specimens defined by anatomical landmarks. They noted that due to the significant morphological alterations observed with advancing age it was not possible to definitively select anatomically or developmentally homologous VOIs across all age groups. A further study by Gosman and Ketcham, (2009), investigated the ontogenetic development of trabecular architecture in the proximal tibia through the application of VOI placement. This study used a systematic selection strategy for reproducible VOI placement across individuals of differing size and maturity which tracked the leading edge of ossification (Fajardo and Müller, 2001). These studies have reinforced that the confidence in reproducible analysis field placement is not guaranteed and instead follows a best practice methodology for this type of developmental study. Additional studies have sometimes referred to region of interest selection as being 'roughly' positioned (Mulder *et al*, 2005), without acknowledging the potential limitations of inconsistent positioning. Recent studies in the human ilium have applied methods of simple VOI placement using external morphologic landmarks. The first such study attempted to identify eight areas of interest which were scaled to the size of the specimen. The areas of interest selected were placed using a horizontal antero-posterior axis between the superior iliac spines and a vertical axis which was perpendicular and midway along the former (Abel, 2006). A further study investigated seven regions of interest which appeared to be randomly placed across the iliac blade. This study did not provide a clear description of ROI placement for reproducibility purposes and only stated that the size of each ROI was calibrated according to the maximum width of the specimen (Volpato, 2008).

Further to limitations involved with volume and region of interest positioning and reproducibility, it is pertinent to note the time consuming nature of manual multiple

analysis field positioning. Previous studies of this nature have restricted their VOI and ROI selection to between 2 and 8 (Mulder *et al*, 2005; Abel, 2006; Ryan and Krovitz, 2006; Volpato, 2008; Gosman and Ketcham, 2009).

4.5.4 Structural parameters

A further significant consideration when selecting an analysis package for bone structural analysis is the structural parameters that the analysis package is capable of calculating. This is important as a greater number of histomorphometric indices provides a more comprehensive account of bone structural composition. The number of structural parameters available is a good indication of the quality of analysis package available. In this study, the initial model-dependant software packages applied calculated only basic histomorphometrics and failed to provide information on important indices such as structural anisotropy and structural model. Although basic histomorphometrics provided a good insight into the structural architecture of the ilium, an incomplete assessment of structural composition was not satisfactory due to the importance of absent trabecular indices to bone strength (Odgaard, 1997). The failure to provide a full account of architectural composition due to the inability of software to calculate a full range of bone parameters is inherent to several studies. As a result, these studies have tended to investigate isolated trabecular indices and their influence on the mechanics of a bone rather than providing a full account of trabecular morphology. More recently, with the advanced computational powers of analysis software and a more standardised method of calculation, studies have been able to fully document trabecular morphology as a matter of routine (Chappard *et al*, 2005; Beaupied *et al*, 2006; Lazenby *et al*, 2008; MacRae *et al*, 2008). A full account of the trabecular characteristics analysed in this study using Skyscan CTAn is presented in Chapter 6.

4.5.5 Costs

Finally, the cost of software procurement is an important part of a research project's design and must be taken into consideration in the context of individual research project aims during the planning stages. Analysis packages vary greatly in their licence fees and licence terms which can significantly impact upon project resources. Some software applications possess a very high licence fee which must be justified in terms of financial suitability and the alternative suitable software packages available. Often the costs of software implementation may exceed certain project budgets and therefore alternative analysis means must be identified and justified. This is a particularly significant point which is often overlooked and is rarely discussed in the literature. Furthermore, certain software packages are restricted in their distribution and licence period resulting in the licence being restricted to a single computer and having to be replaced annually. This can result in further financial and logistical constraints on project progression.

CHAPTER 5 - Qualitative Radiographic Analysis of Early Bone Development

5.1 Introduction

Prior to application of three dimensional imaging and quantification procedures, an initial qualitative study was conducted to investigate gross bone patterning within fetal and neonatal ilia. This preliminary qualitative analysis was undertaken using plain plate macroradiography to investigate the overall gross morphology of early developmental bone patterning and was considered to be the optimal baseline for future quantitative studies. The primary aim of this investigation was to document previously unknown internal structural characteristics of the fetal and neonatal ilium and relate these to relevant temporal functional influences and developmental milestones. The lack of previous research in this area required the development of an appropriate analysis methodology which could be applied to the smallest of iliac specimens and be subsequently applied to specimens with advanced developmental status. Previous qualitative research of this kind in the ilium has been restricted to studies of the early fetal period resulting in loosely descriptive data with greater emphasis on external morphological features (Laurenson, 1963; Gardner and O'Rahilly, 1972; O'Rahilly and Gardner, 1975). Additional radiographic documentation of human bone has often been aimed at several other areas of the skeleton (Ogden *et al*, 1979; Ogden and Phillips, 1983), however, the pelvic complex and in particular the ilium has remained largely neglected.

The most predominant information on the radiographic structural composition of the ilium, although still sparse, is from studies which have attempted to document the adult iliac morphology in relation to locomotor stresses and strains (Latarjet and Gallois, 1910; Correnti, 1955; Macchiarelli *et al*, 1999; Rook *et al*, 1999; Martinon-

Torres, 2003). This has been supplemented to some degree with hypothesised information on the proposed internal trabecular arrangement of the pelvis from the introductory sections of certain textbooks (Kapandji, 1987; Aiello and Dean, 1990; Scheuer and Black, 2000). These studies and theories on the adult pattern have predominantly considered the stresses and strains accommodated by the complex in response to bipedalism. As such, the existing information on the internal architecture of the adult human ilium is summarised here to permit an understanding of the patterns evidenced in the younger individuals in this study.

Pelvic trabeculae are reported to be predominantly plate-like and oriented perpendicular to the cortical shell affording the trabecular structure an optimal mechanical orientation for accommodating predominantly shear-loading modes (Gibson, 1985; Dalstra *et al*, 1993). In the adult ilium (Fig. 5.1), the most strongly represented cortical/trabecular pattern is located posteriorly in what is commonly referred to as a compressive posterior trajectory (pt) which is directed antero-inferiorly from the sacroiliac region towards the upper area of the acetabulum. A further structural ray is located anteriorly and is represented by a well defined and reported tensile anterior trajectory (at) which passes postero-inferiorly from the anterior superior region towards the upper area of the acetabulum. These two trajectories are believed to absorb and distribute loads that are generated during a striding gait and converge upon a structurally significant central region, termed the trabecular chiasma (tc) which is located in the widest region of the bone (Macchiarelli *et al*, 1999; Rook *et al*, 1999). The trabecular trajectories form the boundaries of a poorly represented structural region supero-medially (sm) which is clearly defined in all normal adult ilia and represents an area of the iliac blade where the gluteal (outer) and pelvic (inner) shells of compact bone may fuse without any intervening cancellous bone. Surprisingly, Dalstra and

Huiskes (1995), suggest that this is an area of maximum stress distribution within the trabecular bone, however, the significant reduction or absence of trabecular bone in this region makes this observation questionable. Posteriorly in the regions of the greater sciatic notch (sn) and the acetabular roof (ar) there are additional areas of dense structural organisation. Each of these regions labelled in Figure 5.1 has been explained by various authors as reflecting the interaction of biomechanical forces acting on the pelvic complex during a bipedal stance and bipedal locomotion (Kapandji, 1987; Aiello and Dean, 1990; Macchiarelli *et al*, 1999; Rook *et al*, 1999; Scheuer and Black, 2000).

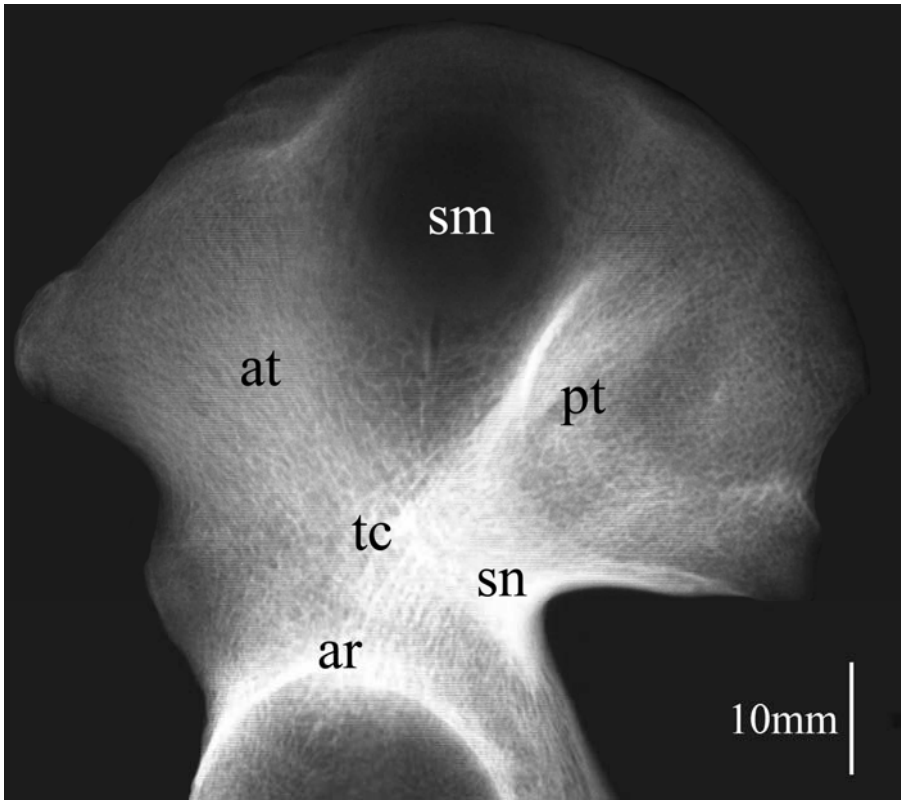

Figure 5.1. Conventional radiograph of an adult ilium. Principal features are labelled; posterior trajectory (pt), anterior trajectory (at), superior medial region (sm), trabecular chiasma region (tc), greater sciatic notch region (sn) and acetabular roof (ar).

As one of the primary tasks of the pelvis is to support the weight of the upper body and transfer it to the lower extremities (Dalstra and Huiskes, 1995), distinct function related density representations are alleged to be produced. Kapandji (1987)

proposed that there are three principal trabecular pathways within the pelvis:- two arising from the auricular region that extend towards the acetabulum for weight transfer to the lower limb during bipedal locomotion and one passing to the ischium for weight transfer in sitting (Aiello and Dean, 1990) (Figure 5.2). This architectural representation is said to be produced by the site-specific magnitude and direction of the locomotion-related peak strains imposed on the growing bone (Gibson, 1985; Rook *et al*, 1999).

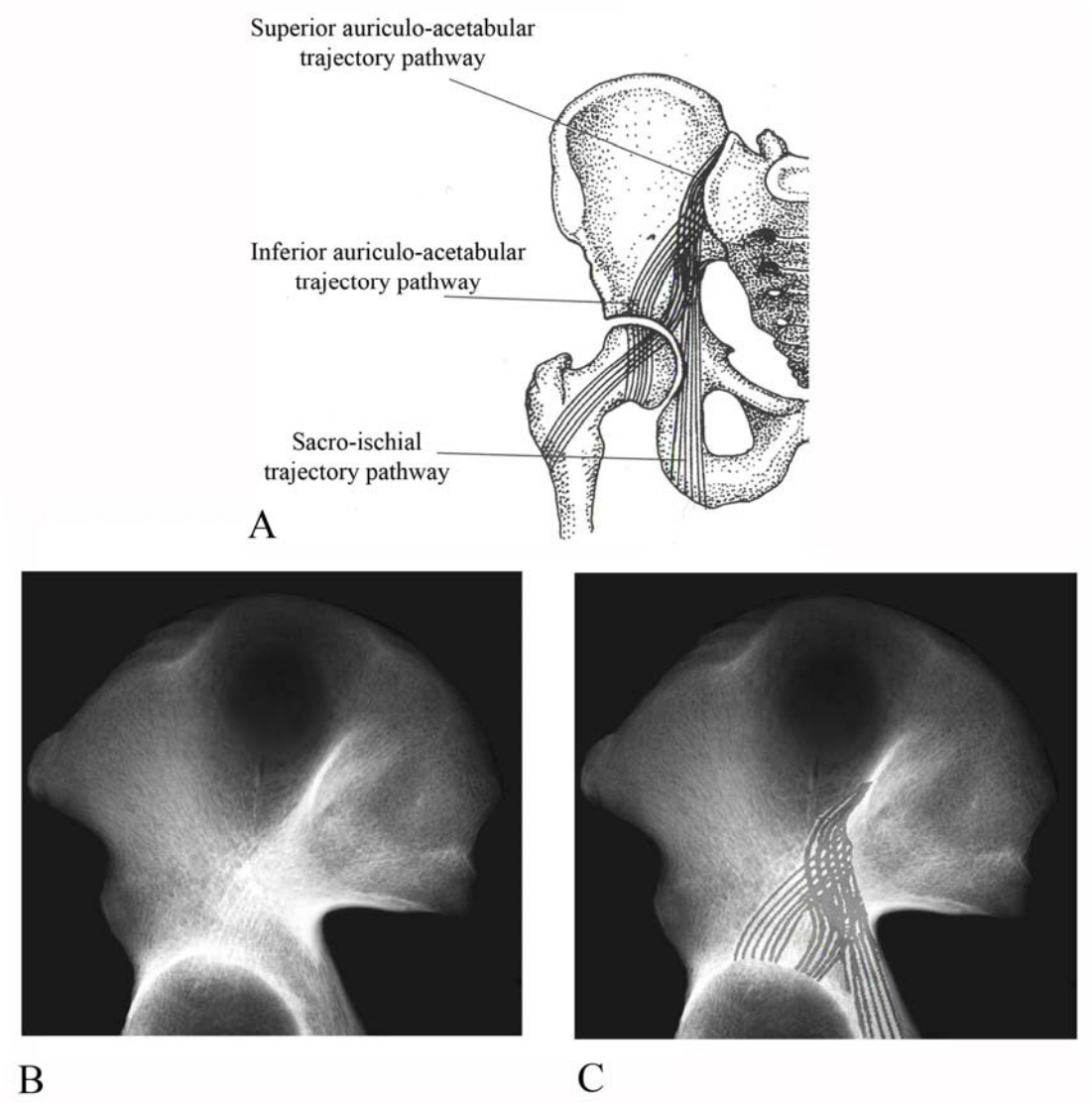

Figure 5.2. A: Schematic displaying hypothesised weight trajectory pathways within the pelvis modified from Scheuer and Black, 2000. B: Conventional radiograph of an adult ilium displaying areas of defined density. C: Conventional radiograph with superimposed hypothesised trajectory pathways.

During growth, bone structure responds to loading and in particular the trabecular architecture is reported to respond to the magnitude and direction of loading reflected in the relative densities and structural organisation of trabecular pathways. These pathways or trajectories are observed to be of high density in regions of higher stress and of conversely low density in regions of lower stress (Lanyon, 1974; Currey, 1986; Turner, 1992). Therefore, the forces involved in bipedal locomotion are reported to be reflected in the pattern of trabecular trajectories observed in the adult human innominate (Macchiarelli *et al*, 1999). The density representation in the ilium has been further investigated radiographically with trabecular patterning being documented in both the human and non-human primate (Latarjet and Gallois, 1910; Macchiarelli *et al*, 1999; Rook *et al*, 1999; Martinon-Torres, 2003). Studies have confirmed characteristic features of gait-related trabecular systems in the human ilium, with the presence of distinctive trabecular bundles which intersect at the well-defined trabecular chiasma (Macchiarelli *et al*, 1999). Macchiarelli *et al* (1999) applied a system of terminology to the trabecular features observed in the human ilium which can be paralleled with the terminology used in this study (Figure 5.3; Table 5.1). In the ilium, they identified a sacropubic trabecular bundle, an ilioischial bundle, an iliocotyloid bundle, a pericotyloid bundle and a trabecular chiasm region, each of which parallels respectively with the posterior trajectory, anterior trajectory, greater sciatic notch density, acetabular roof and trabecular chiasma of this study. In addition, Macchiarelli *et al*, (1999) also highlighted further accessory gait related trabecular characteristics at the iliac crest, anterior inferior iliac spine, superior acetabular margin and posteriorly extending towards the ischium.

To date, there appears to be no single study that has investigated the full human ontogenetic spectrum of the development of the internal and external architecture of the

pelvis, encompassing all locomotive stages of development which may influence the overall trabecular and cortical morphology. The lack of information may be attributed to the paucity of appropriate samples upon which to base such an investigation and the complex morphology of the pelvis (Majumder *et al*, 2004). This part of the study examines the overall gross architecture of the fetal and neonatal ilium through the application of radiographic procedures to establish the pattern of early stage trabecular maturation prior to load bearing locomotive influences.

At the commencement of this part of the study a null hypothesis was adopted which proposed that the pattern of fetal and neonatal iliac trabecular organisation would be one of random distribution between the gluteal and pelvic cortical shells acting only as a rudimentary spacer for subsequent ontogenetic remodeling. These results form the first part of the overall study that will seek to examine the specific internal trabecular architecture and external cortical structure during the earliest stages of development. Therefore, it is the aim of this study to document the qualitative, gross cortical and trabecular bone organisation present in the earliest developmental ranges of the human ilium and compare these to the well established, although perhaps ill understood, adult pattern described in the literature.

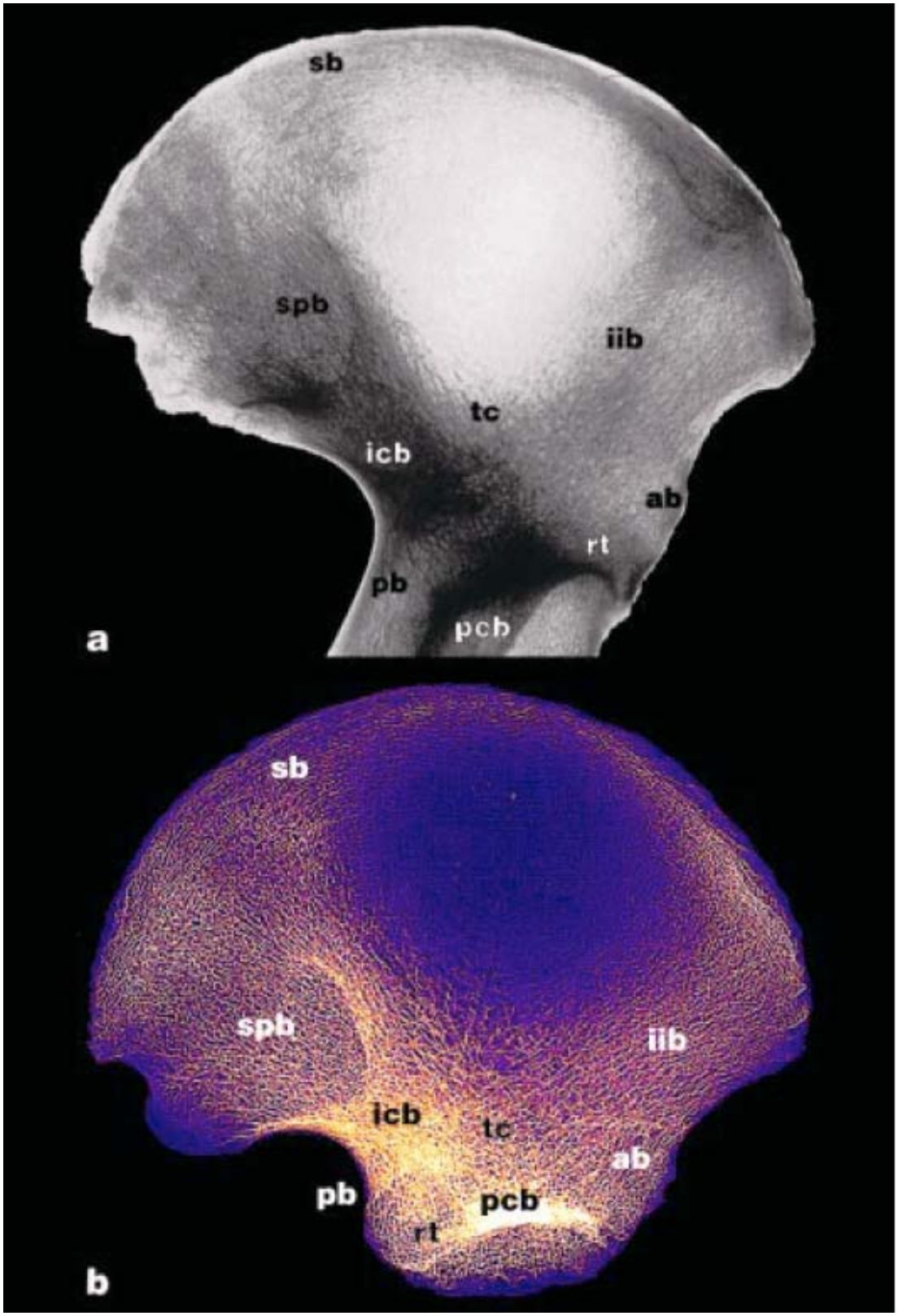

Figure 5.3. Trabecular architecture of the human ilium. a: adult; b: juvenile (~9 years). Inverted unprocessed radiographic images. ab: anterior bundle; icb: iliocotyloid bundle; iib: ilioischial bundle; pcb: pericotyloid bundle; pb: posterior bundle; rt: radial trabeculae; sb: superior bundle; spb: sacropubic bundle; tc: trabecular chiasma. See Table 5.1 for descriptions of architectural features. Taken from Macchiarelli *et al*, 1999.

Trabecular systems[1]	Sections	Main structures	Description
Osteomeric	Pericotyloid	Pericotyloid bundle (pcb)	Concentrically surrounds the acetabulum
		Radial trabeculae (rt)	Radially surrounds the acetabulum
	Periopic	Periopic bundle	Surrounds the margin of the obturator foramen
Idiobatismatic	Marginal (ectochoric)	Superior bundle (sb)	Runs along the superior margin of the ilium
		Anterior bundle (ab)	Runs along the anterior margin of the hip bone (ilium and pubis)
		Inferior bundle	Runs along the inferior margin of the hip bone (pubis and ischium)
		Posterior bundle (pb)	Runs along the posterior margin of the hip bone (ischium and ilium)
	Arcuate (endochoric)	Ischiocotyloid bundle	Derived from trabeculae of the inferior and posterior marginal bundles, runs upwards between the posterior and the anterior external aspects of the ischial tuberosity towards the *facies lunata*
		Sacropubic bundle (spb)	From the auricular surface and the posterior superior and inferior iliac spines runs diagonally downwards and forwards along the iliopectinal line as far as the pubic symphysis
		Iliocotyloid bundle (icb)	Slightly differentiated from the sacropubic bundle, this thinner fan-shaped bundle runs diagonally downwards and forwards as far as the acetabulum crossing the ilioischial bundle
		Ilioischial bundle (iib)	From the region of the tubercle of the iliac crest, posterior to the anterior spines, runs diagonally downwards and backwards with arcuate trajectory as far as the ischial tuberosity
		Trabecular chiasma (tc)	High-density trabecular net transversely located at the level of the sciatic notch, defined by a distinct saltire-shaped crossing over the acetabulum between the sacropubic and the ilioischial bundles

Table 5.1. Human innominate bone trabecular architecture. Descriptions are relevant to figure 5.3. Osteomeric relates to circumscribed portions of the bone; Idiobatismatic relates to gait related trabecular systems. Modified from Macchiarelli *et al*, 1999, after Correnti, 1955.

5.2 Materials and Methods

Fifty three ilia representing the entirety of the perinatal component of the Scheuer collection (25 fetal and 28 neonatal), were analysed (Table 5.2). There was no indication that there were any pathological conditions associated with these specimens that might have affected either the external or internal architecture. Each specimen was subjected to plain plate radiography, computed radiography and macroradiography. Resulting radiographic images were then subjected to a gradient analysis to enhance the greyscale representation and allow for improved visual interpretation. Each stage of specimen preparation, imaging methodology and subsequent analysis are documented below.

5.2.1 Specimen Preparation

A complete catalogue of the early developmental iliac specimens contained within the Scheuer collection was produced. This inventory documented the siding, known or assigned age, known sex, and any visible ante-mortem/post-mortem damage/pathology for each specimen. Specimens which contained any damage to the cortical bone resulting in an altered external morphology or exposure of the underlying trabecular bone were recorded and if extensive, excluded. These details were then taken into account when documenting the radiographic morphology so that any artificial density patterns caused by damage could be discarded. Subsequently, each specimen was radiographed in a consistent and repeatable orientation with the gluteal surface orientated towards the radiographic plate and the pelvic surface orientated towards the x-ray source to ensure reliable comparison between radiographs. Each specimen was labelled and scaled using lead numerals and a calibration ruler. At the time of radiography each specimen was photographed in a position consistent with the produced

radiographic image to aid comparison between external and internal morphological features (Figure 5.5). For this study, if the age of the specimen was not known, it was assigned following the metric evaluations described by Fazekas and Kosa (1978). Ilium width (maximum distance between anterior and posterior superior iliac spines) and ilium length (maximum distance between the mid point of the iliac crest and the convexity of the acetabular extremity) were measured. Subsequently, specimens were then assigned to one of four age groups (Table 5.2).

	n		
Age (fetal weeks)	**Right**	**Left**	**Total**
18-22	**3**	**3**	**6**
23-30	**4**	**5**	**9**
31-39	**5**	**5**	**10**
40+ (term)	**15**	**13**	**28**
Total	**27**	**26**	**53**

Table 5.2. Scheuer collection fetal and neonatal specimen age ranges and numbers used for radiographic documentation

5.2.1.1 Specimen Maceration and Preservation

During cataloguing, certain fetal specimens were observed to possess varying amounts of mummified connective tissue therefore retaining the ilia, ischia, pubes and sacral vertebrae in their anatomical approximation. The presence of this connective tissue obscured the external visualisation of the specimens and also presented problems when radiography was applied. Upon radiography the remaining connective tissue presented as radio-opaque regions which superimposed and made the differentiation of specific areas of bone density somewhat ambiguous. Additionally, positional orientation

of the ilium perpendicular to the radiographic plate was not possible due to the presence of constituent pelvic parts. As a result, A pilot study was conducted in order to dissect these specimens into constituent parts to allow for more resolute imaging. Endeavours were made to macerate and dissect a single test specimen whose constituent parts were held together by connective tissue. This was conducted in order to determine the feasibility and justifiability of macerating all specimens which were held together by connective tissue. A specimen representative of all other specimens containing desiccated soft tissue (Figure 5.4) was subjected to several cycles of bathing in a water bath at 80ºC which contained a standard biological detergent.

Figure 5.4. Fetal pelvic specimen. Constituent pelvic elements connected by soft tissue interactions.

This technique was successful in softening mummified tissue so that dissection could separate constituent pelvic parts into iliac, ischial, pubic and sacral elements. However, damage was sustained to the thin peripheral cortical bone which exposed the underlying trabecular bone in certain places. It was therefore deemed that due to the irreplaceable

nature of the collection, further maceration would not be conducted. All remaining connected specimens were imaged following the intended protocol as closely as was practically possible. Imaging of connected specimens resulted in superimposition of constituent parts and a reduced visualisation of ilia. As such, results from such specimens were treated with caution as being loosely representative of the overall pattern evidenced in older neonatal individuals.

5.2.2 Radiography

Application of plain plate macroradiographs for the visualisation of gross external and internal structural composition was regarded as the natural starting point for non-destructive analysis. This technique allowed for a general overview of structural density and highlighted areas of significant architectural arrangement which could be further analysed using subsequent analysis techniques in later parts of the study. In making a preliminary radiographic record of the youngest specimens in this study it was possible to make parallels between existing data on the adult structure before complex three-dimensional applications were introduced.

Each iliac specimen was positioned onto an appropriately sized radiographic plate and was radiographed using predetermined exposure factors. Three forms of plain plate radiography were used in this study: conventional radiography, macroradiography and computerised radiography. Radiographs were conducted within the radiography department at Ninewells Hospital and Medical School, Dundee, under the instruction of a qualified radiographer. Each specimen was initially subjected to a conventional plain plate radiograph using a Siemens Multix Tube and Table CPH. The exposure factors used were 47Kv, 2mAs (fine focus). The images were exposed onto a film screen combination of Agfa Curix, Ortho Medium, Curix HT1.00l Plus. Hard copies were

retained and digitised using an Epson flatbed scanner with a superiorly mounted radiographic lamp. Images were scanned at a consistently high resolution with a maintained dpi of around 1200. Digitisation of radiographs was conducted to allow for application of image analysis and enhancement packages for qualitative assessment procedures.

Once conventional radiographic images had been obtained, macroradiographs of each specimen were taken. Bone positioning for macroradiography was identical to that described for the conventional procedure. Macroradiography is a radiographic imaging technique used to increase the size of the image relative to the object. It is based upon increasing the object-film distance in relation to a fixed focal-film distance (Clark *et al*, 1984; Davidson and Bowman, 2002). It has been described to consistently show greater detail than conventional radiography when examining both small and large bones (Sundaram *et al*, 1978). It is for this reason that macroradiography was implemented in this study to enhance any trabecular or gross density patterns which were present in the ilium. This method involved the use of a Siemens Mutix Tube and table CPH. The exposure factors used were 47Kv, 2mAs, Fine Focus, with an Agfa film screen combination. A focus film distance (F.F.D) of 140cm and an object film distance (O.F.D) of 30cm were applied. The increased O.F.D is responsible for the increased magnification. As macroradiographs were produced as hard copies, they also had to be converted into a digitised format to facilitate manipulation (Figure 5.5). Digitisation was conducted using the same method as described for conventional radiography, again the scan resolution was set to 1200 dpi which optimised visualisation and file size. Each image was subsequently saved as a TIFF file without compression and was comprised of a standard 256 grey levels.

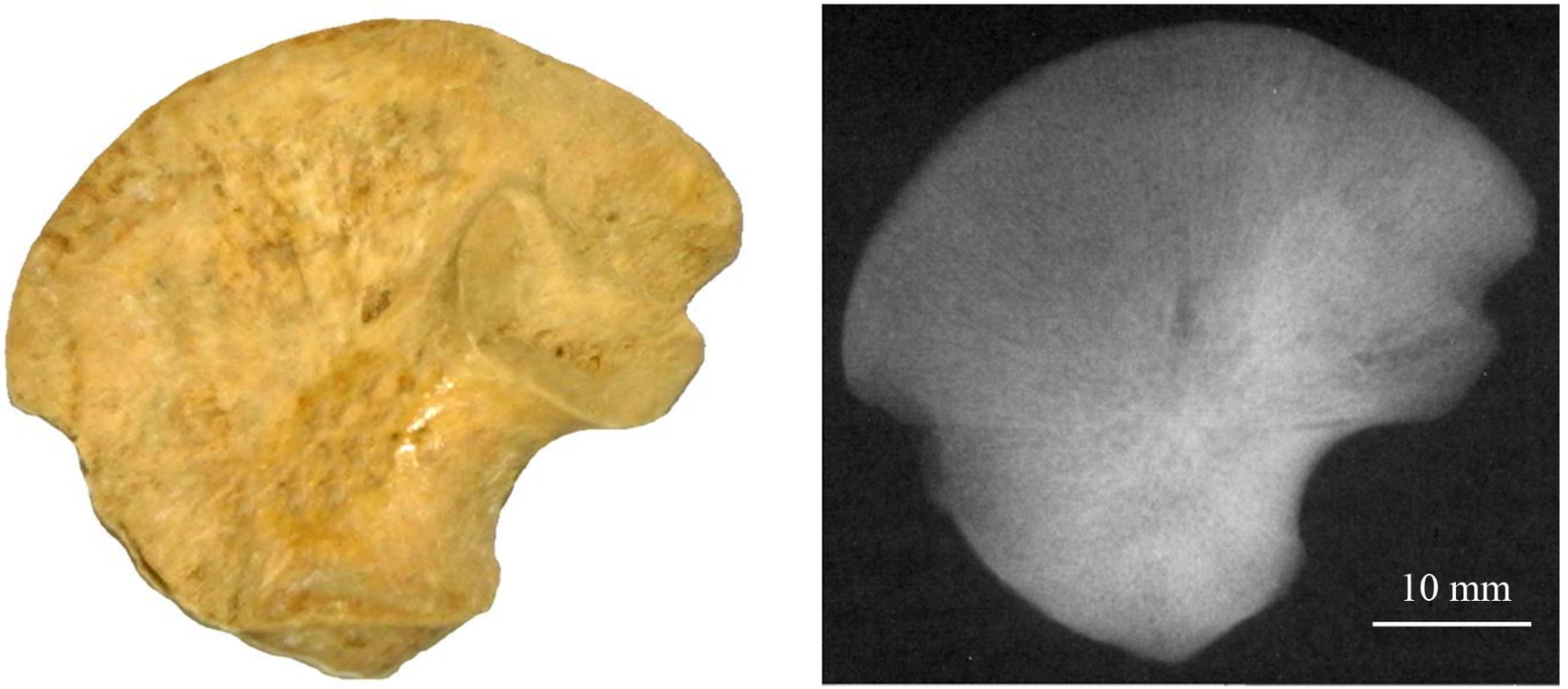

Figure 5.5. Photograph and macroradiograph of a neonatal ilium.

Finally, computed radiography (CR) was applied to the sample to enable assessment of its quality against previous conventional and macroradiographic procedures. Computed radiography, scientifically known as photostimulable phosphor radiography, is a digital technology for the acquisition of radiographic images (Sonoda *et al*, 1983; Samei *et al*, 2001; Schaetzing, 2003). CR uses very similar equipment to conventional radiography except that in place of a film, an imaging plate is used. Therefore, instead of taking a film into a darkroom for developing in chemical trays, the imaging plate is processed by a computer scanner which reads and digitizes the image. The image can then be viewed and enhanced using software that has functions very similar to conventional image-processing software. The technology uses conventional radiographic acquisition geometry to deposit x-ray energy in a photostimulable phosphor screen with delayed luminescence properties. After irradiation, the screen is stimulated by a scanning laser beam, to release the deposited energy in the form of visible light. The released photostimulated light is captured by a light detector, converted to digital signals, and registered with the location on the screen from which it has been released. The digital data are then post processed for appropriate presentation, and are sent to a hard copy printer or soft copy display monitor for evaluation. Computerised radiography of the pelvic specimens in this study was carried out using an Agfa CR system and a Philips generator and x-ray tube. The exposure factors used were 50Kv, 1.6mAs.

Although each of the three radiographic imaging techniques applied to the bone specimens produced interpretable greyscale images, the results of this study are based upon the digitised macroradiographic representation which produced the most resolute representation of iliac density patterning. Additionally the magnified size of the image allowed for an improved structural interpretation of the density pattern observed.

Images produced using conventional radiography were not used for analysis as they provided insufficient magnification for visualisation of the smallest fetal specimens. Likewise, CR images were not used for analysis as images were of reduced quality. CR is primarily applied to chest radiography in the clinical environment and is best suited for larger structures in which visualisation is not influenced by lower resolutions.

5.2.2.1 Limitations of plain plate radiography

Although plain plate radiography served its initial purpose by providing an overview of gross bone density it is appropriate to discuss the limitations of this method and the impact these may have on the results. The radiographic factors used in this study were systematically calibrated in order to obtain the optimum exposure for early developmental specimens. These were finalised through the application of set point literature values and adjustment to the final values applied through multiple trial and optimisation procedures. However, specimens differ in their thickness distribution throughout the developmental spectrum analysed and also individual bones differ in thickness topographically across the ilium. As it was not possible to calibrate exposure factors for each specimen individually, due to limited availability of equipment, a generic exposure factor was applied to the fetal and neonatal sample. Although these exposure factors were deemed to be optimal for appropriate visualisation of this developmental cohort it must be considered that a minimal amount of either under exposure or overexposure may have occurred. It must be emphasised, however, that any degree of under and over exposure would be very minimal and is unlikely to have influenced the final density pattern observed in any substantial manner. A further limitation of this part of the study is the fact that a radiographic image is a two-dimensional representation of a three-dimensional structure. This results in the

superimposition of structures and can obscure the appearance of true anatomical morphology. In the case of the ilium the pelvic and gluteal shells as well as the internal trabecular bone are superimposed to produce an overall density representation. It is for this reason that gradient images were only visually inspected from a qualitative perspective and no quantification of density patterns from grey scale values was attempted. This limitation will be overcome in the next part of the study where cortical structure and internal trabecular architecture will be assessed independently using three-dimensional imaging techniques.

5.2.3 Analysis of specimens and radiographs

Each specimen and macroradiograph was visually inspected and recorded. Plain plate macroradiographs were analysed and all significant radiographic features were documented. However the greyscale representation produced by macroradiography was difficult to interpret due to the subtle grading of greyscale values within the image (Figure 5.5). Therefore, an enhanced methodology was developed in order to improve visualisation of the density patterns present.

5.2.4 Radiographic enhancement and gradient analysis

The analysis of bone density patterning was enhanced by transferring the digitised macroradiographic images into a software package capable of differential mapping of grey levels. Radiographic scans were opened in the Adobe PhotoShop CS2 application and auto coloured, relative to their grey levels, using the gradient map tool. The “gradient map” command, maps the equivalent greyscale range of an image to the colours of a specified gradient fill. A four-colour gradient fill was selected to assist in the evaluation of gross trabecular organisation. Grey values in the image were mapped

to one of the endpoint colours of the gradient fill, dependant on their predefined percentage value. This technique employs a colour look-up table (CLUT) function, a tool which converts the logical colour numbers stored in each pixel into physical colours. In using this software application, a representation of the two-dimensional radiographic structural organisation can be obtained and depicted in colour. This process was repeated for each grey level range ultimately producing a colour coded map of graded structural ‘densities’ (Figure 5.6).

5.2.5 Definition of gross regions of apparent density

Macroradiographic gradient analysis divided the ilia into a colour map composed of three colours representing differing apparent ‘densities’ to aid the simple interpretation of absolute greyscale values (Fig. 5.6B). The colours selected were:

- Blue representing the highest density regions of 71-100% opacity.
- Orange representing densities of 51-70% opacity.
- Magenta representing densities of 31-50% opacity.
- Yellow representing the lowest density regions of 0-30% opacity, which exclusively represented background levels of film exposure.

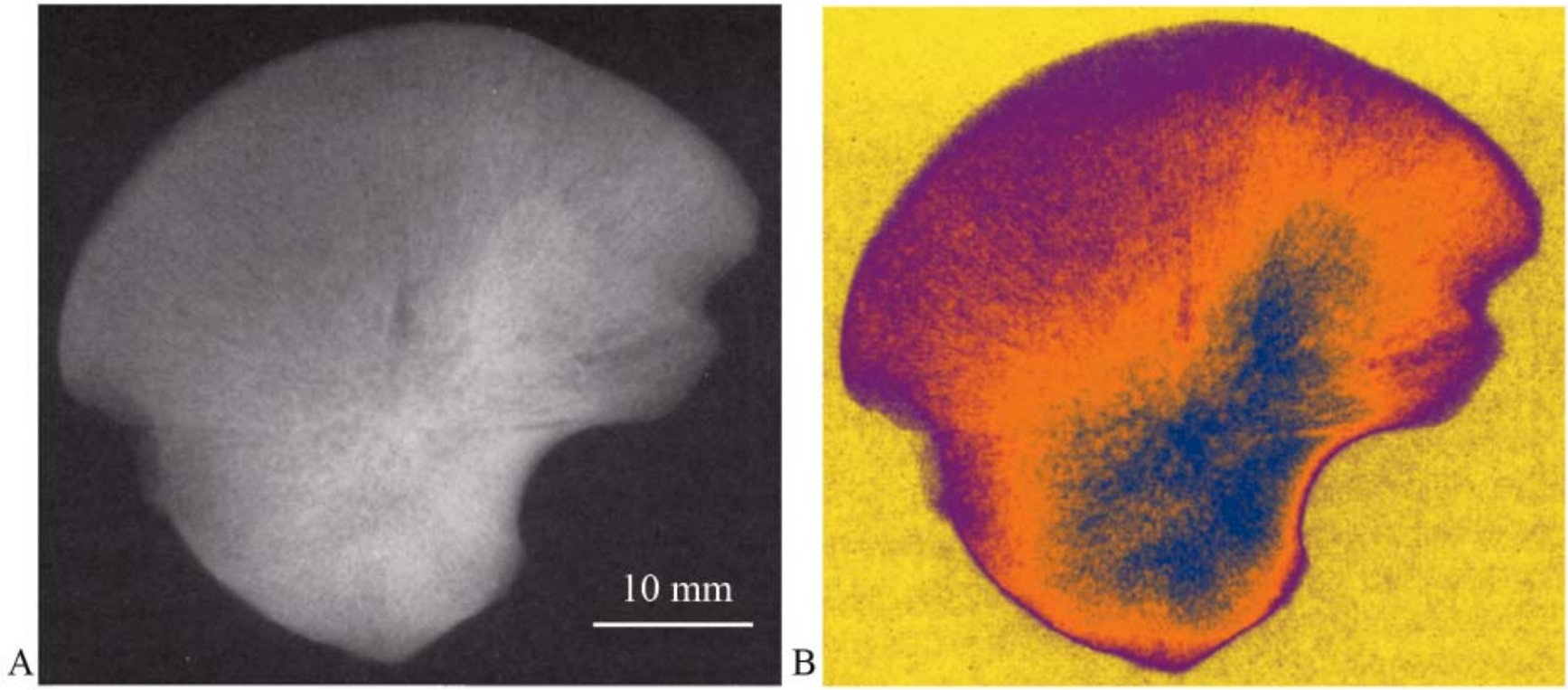

Figure 5.6. Macroradiograph (A) and gradient map (B) of the same right neonatal ilium. Three distinct grades of differing ‘density’ are observed within the ilium as represented by the three colours; magenta, orange and blue. Background exposure is represented by yellow colouring.

5.3 Results

This study initially considered the external morphological appearance of each specimen followed by an account of structural 'density' based on macroradiographic analysis. Therefore, a comprehensive description of the gross external morphological and structural composition of the ilium is provided.

5.3.1 External morphological appearance of specimens

Each of the specimens included in this part of the study were visually examined and external morphological features were documented. It was apparent that a similar but progressive external morphology was evident from the early fetal period through to the neonatal period. In the earliest age range of the fetal period, between 18-22 weeks (Fig 5.7a), few qualitative observations could be made regarding the external morphology of the ilium. This restriction was imposed by the presence of mummified tissue and the association of the ischium and pubis which served to obscure a full interpretation of external morphological features. However, morphologically the ilium was distinctive in its shape and was identifiable in isolation. Important features which could be visualised were the well defined dominant nutrient foramen on the pelvic surface of the ilium, the posteriorly located greater sciatic notch and the iliac crest. In the subsequent developmental cohort of fetal pelves, at around 23-30 weeks (Fig 5.7c), ilia were again distinctive in their external morphology and could easily be identified in isolation. The position of the dominant nutrient foremen was maintained and the separation of the ilia from the sacrum allowed for the definition of the dorso-caudally orientated auricular surface on the pelvic surface of the ilium. Additionally, the greater sciatic notch was well defined posteriorly as was the acetabular surface inferiorly. Specimens occupying the more advanced period of fetal development, at around 31-39 weeks, (Fig 5.7e)

demonstrated a further progressive pattern of external morphology which included advanced definition of the auricular surface and the progressive curving of the iliac crest with a thickening of the crest anteriorly and posteriorly. Finally, in the neonatal age range (Fig 5.7g), radiographs were more resolute which improved visualisation of external morphological features. This was primarily due to the size increase of the specimens within this developmental period. Neonatal specimens had a very characteristic shape with a well defined greater sciatic notch, auricular surface, centrally located nutrient foramen and a blade curvature which were all progressive to the previous developmental cohort.

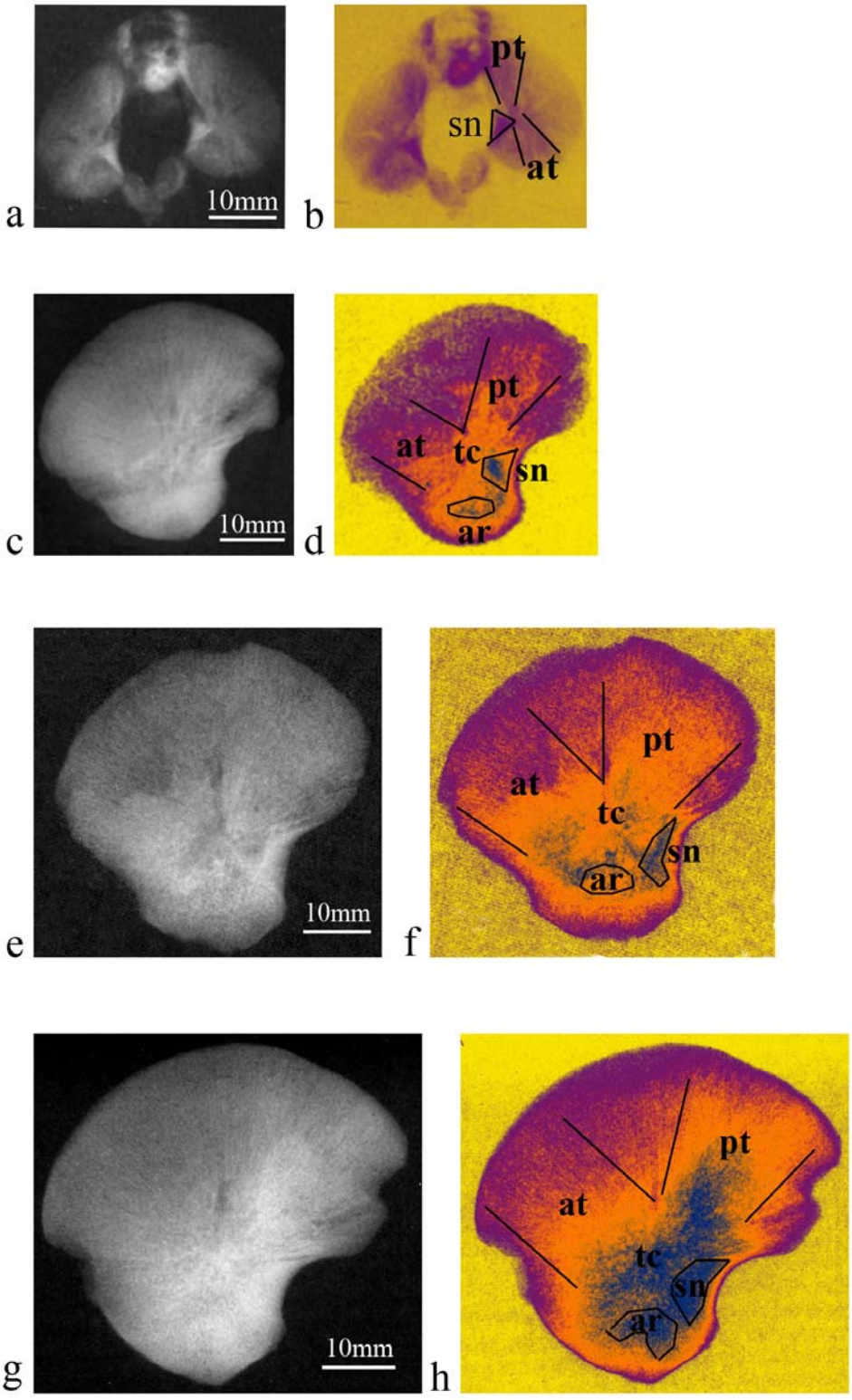

Figure 5.7. Macroradiograph (a) and gradient map (b) of fetal specimen (18-22 weeks). Macroradiograph (c), and gradient map (d) of fetal specimen (23-30 weeks). Macroradiograph (e), and gradient map (f) of fetal specimen (31-39 weeks). Macroradiograph (g), and gradient map (h) of neonatal specimen (40+ weeks). Areas outlined include density regions associated with the greater sciatic notch (sn), acetabular roof (ar), anterior (at) and posterior (pt) trajectories and the trabecular chiasma (tc).

5.3.2 Morphology from macroradiographic density gradients

An incremental and progressive pattern of developing internal bone architecture was observed between each of the developmental groups. Within each age cohort the extent of structural maturity was ranked from least to most mature so that the progressive pattern of structural maturation could be examined and any variability in the pattern could be highlighted. Passing from left to right, Figure 5.8 illustrates the least, average and most mature specimens within each of the age cohorts except the earliest fetal group, where only the least and most mature specimens are illustrated.

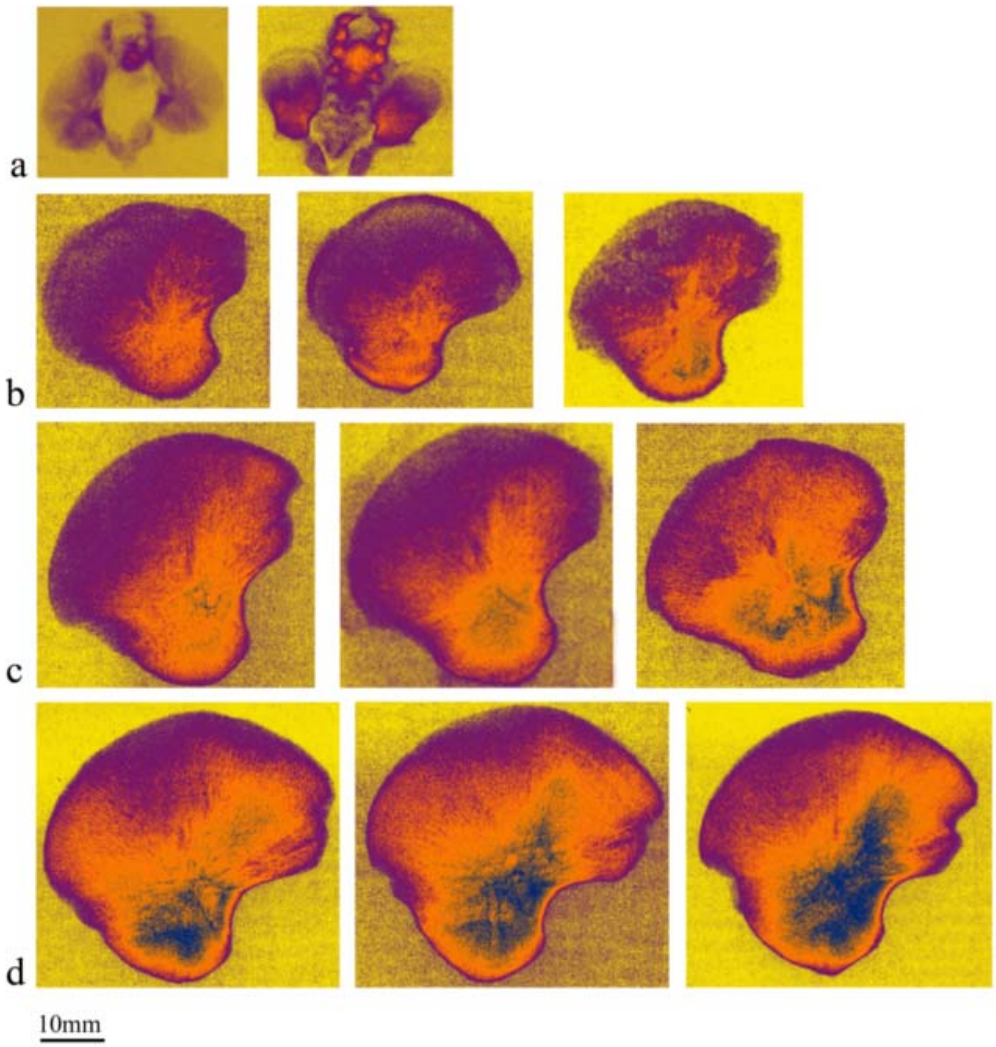

Figure 5.8. Gradient maps of multiple specimens within each developmental group. Those to the left represent the least mature within each age group and those to the right are the most mature whilst those in the middle represent the modal appearance of specimens in each age group. (a) 18-22 weeks. (b) 23-30 weeks. (c) 31-39 weeks. (d) 40+ weeks. The scale bar provided is relevant to each image.

18-22 weeks (n=6)

In the youngest fetal specimens (Figs 5.7a-b; 5.8a), radiographs were difficult to analyse due to the small dimensions of the pelvic complex and the low level of mineralisation. The resultant image, even when macroradiographed, yielded very limited information. The radiographic representation was obscured as specimens possessed a small degree of retained but mummified soft tissue. This resulted in the ilium, ischium and pubis being conjoined in an orientation which prevented optimal flat plate radiographic imaging. Due to the importance of the Scheuer collection, specimens could not be macerated as this would result in irreversible damage to this irreplaceable material. Although the gradient representation was somewhat obscured, a basic pattern of internal architecture could be observed. Due to the obscured representation, interpretations from this age group were treated with caution as being loosely supportive of the more mature pattern witnessed in the older age groups. The most pronounced radiographic feature observed during this developmental period is a central radio-opaque region which corresponded well to the position of the dominant nutrient foramen in the trabecular chiasma (tc). Radiating from this central area of increased density were flanges of increased and decreased radio-opacity which extended towards the periphery of the bone. The more radio-opaque trajectories which fan from the central locus appear to be directed (i) towards the posterior ilium in the direction of the externally defined auricular surface (pt) and (ii) towards the anterior ilium in the direction of the anterior superior iliac spine (at). The less radio-opaque flanges are interspersed between the former and appear to be directed (i) centrally towards the midpoint of the iliac crest (sm) and (ii) towards the anterior part of the ilium inferior to the anterior superior iliac spine. Finally, a further area of significant radio-opacity is associated with the perimeter of the greater sciatic notch (sn).

23-30 weeks (n=9)

In the subsequent developmental cohort at 23-30 intrauterine weeks, a consistent pattern was observed in each specimen (Figs 5.7c-d; 5.8b) that was progressive to the primitive pattern identified in the 18-22 week group. The most significant differences were observed in the region of the greater sciatic notch (sn), which was represented by a more clearly defined region of increased density. The anterior (at) and posterior (pt) trabecular trajectories were also more clearly delineated and could clearly be seen emanating from the area of the trabecular chiasma (tc). An area of markedly increased density was also observed in the region of the acetabular roof (ar).

31-39 weeks (n=10)

The specimens from this more mature period of fetal development (Figs. 5.7e-f; 5.8c), displayed a further progressive pattern to the previous age cohort. More refined details relating to both the external and internal characteristics were observed. This was due primarily to the increased size of the ilia, which facilitated greater macroradiographic resolution. Trajectory lines were clearly visible passing in rays from the well-defined trabecular chiasma (tc) to both the posterior area of the ilium (pt) and the anterior superior iliac spine region (at). These trajectories were observed to form the boundaries of a well-defined area of low density radiolucency in the body of the iliac blade (sm). There was also more clearly defined radio-opaque regions at the greater sciatic notch (sn) and the acetabular roof (ar).

40+ weeks (n=28)

In the neonatal age range (40 weeks +) (Fig. 5.7g-h; 5.8d), radiographs presented markedly improved visual representation with greater definition and delineation of all internal structures that had been identified in the younger age cohorts. As the neonatal pattern appears to be an advanced progression of earlier developmental patterning, discussion will be based upon the pattern evidenced in this developmental period.

Regions of highest structural 'density', depicted in blue (Figure 5.9) presented in three distinct areas of interest:

1. Trabecular chiasma (tc) - represented by the intersection of two dense flanges, the first passing antero-inferior to postero-superior (pt), and another passing postero-inferior to antero-superior (at).
2. Acetabular region – represented in the area of the future acetabular roof.
3. Sciatic notch – represented as a wedge of well-defined dense bone associated with the position of the greater sciatic notch.

Areas of intermediate density, represented in orange (Figure 5.9), were characterised by areas of significant but not high bone 'density'. This category was represented by several defined regions of particular significance. The first of these, located in the sacro-iliac region, was well defined as a continuation and advanced radiation of the posteriorly directed flange of high density. It was observed to extend to a significant posterior extent and completely surround and cover the auricular surface. A further region of second level density, located anteriorly, again appeared to be a less dense extension of the anterior directed flange of higher density. Its extent was observed over a wide anterior area from the anterior superior iliac spine region extending towards the posterior region of second level density surrounding the auricular surface. As well as

having a large anterior-posterior spread, it extended superiorly terminating gradually leaving an area of reduced density along the perimeter of the crest. Another area of second level density was observed antero-inferiorly extending towards the region of the anterior inferior iliac spine. The final region of intermediate density was observed in the inferior acetabular region and was represented along the inferior border of the ilia inferior to the trabecular chiasma region of highest density.

Finally, tertiary areas of density, represented in magenta (Figure 5.9) were characteristic of areas of comparatively low bone ‘density’ throughout the ilium. Two regions of particular significance were noted. The first of these has been termed the “perimeter region” and was represented around the entire perimeter of the ilium in a continuous band. The perimeter area was particularly pronounced in the regions corresponding to the anterior superior and anterior inferior iliac spines as well as the most posterior aspect of the ilium at the posterior superior and posterior inferior iliac spines. A further region of tertiary ‘density’, termed the superior medial region (sm), was characteristic in each of the specimens observed. It was present as a wedge of low ‘density’ located along the iliac crest converging towards the central point of the iliac body resulting in a well defined region of low density in the central band located between the anterior and posterior trajectories of increased density.

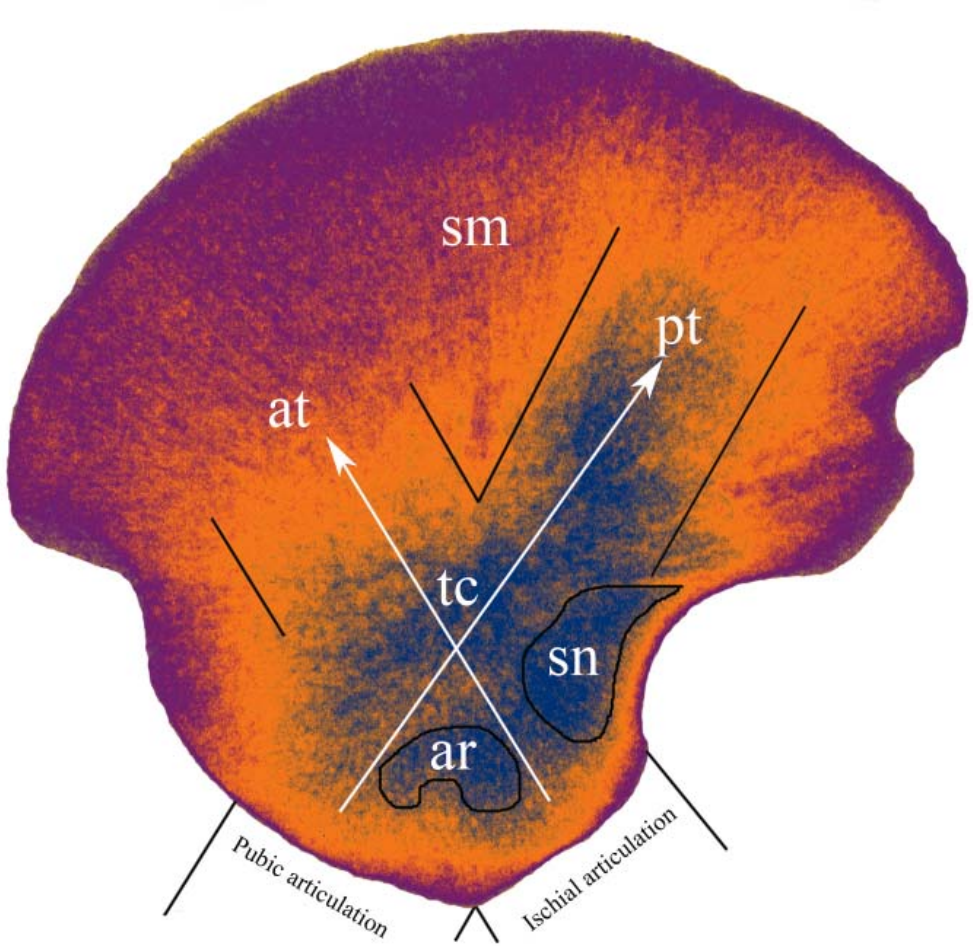

Figure 5.9. Gradient map of a neonatal ilium illustrating regions of density. Acetabular roof (ar). Anterior (at) and posterior (pt) trajectories with central trabecular chiasma (tc). Greater sciatic notch region (sn). Superior medial region (sm).

5.4 Discussion

The radiographic representation of all specimens in this study, demonstrated a progressive but consistent pattern of trabecular alignment that was comparable with the template identified in more developmentally mature individuals. Density patterns, which have previously been attributed to locomotive response in the adult, were observed in both the fetal and neonatal samples prior to the possibility of any significant weight bearing locomotive influences (Figure 5.10).

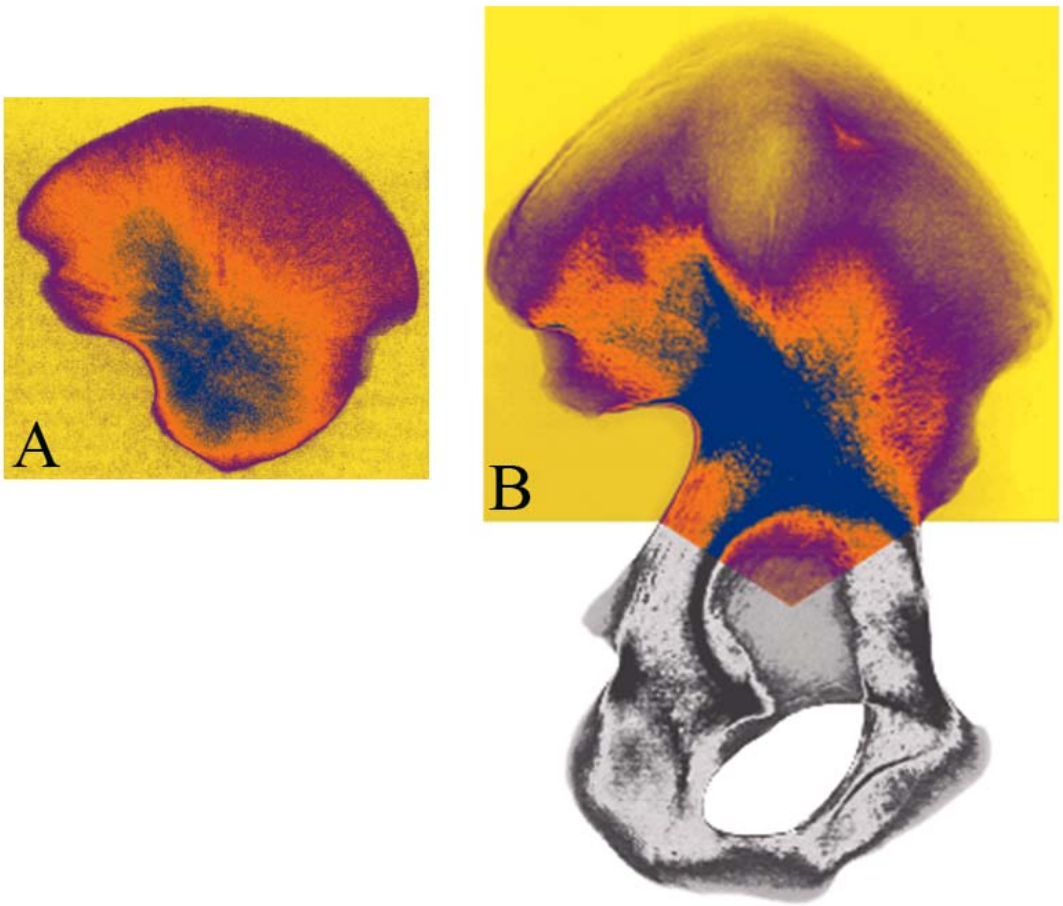

Figure 5.10. Comparison of gradient map of neonate (A) and mature specimen (B) illustrating similarities between density representations. Not to scale.

Specific areas of internal architectural interest have been identified in the adult human ilium and previous literature has suggested a strong relationship with locomotion and bipedal gait (Thomason, 1985; Carter *et al*, 1989; Galichon and Thackeray, 1997; Macchiarelli *et al*, 1999; Rook *et al*, 1999; Fajardo and Müller, 2001; MacLatchy and Muller, 2002; Ryan and Ketcham, 2002; Lai *et al*, 2005; Ryan and Krovitz, 2006; Fajardo *et al*, 2007). The primary areas of functional interest in the adult include two distinct flanges of structural significance present within the anterior and posterior portions of the ilium. The first and most pronounced of these is a structural ray which is located in the posterior aspect of the ilium. Some previous literature has attributed this to biomechanical compressive forces passing from the sacro-iliac joint through the body

of the ilium towards either the acetabulum in a bipedal stance, or towards the ischium in a sitting posture (Kapandji, 1987; Aiello and Dean, 1990; Scheuer and Black, 2000). The second consistent structural ray is located anteriorly within the ilium and has often been attributed to the tensile forces which are set up in this region to act as a counter balance to the compressive forces from the posterior flange to prevent buckling of the bone under the pressures of bipedal locomotion (Macchiarelli *et al*, 1999). These two defined rays of structural significance, previously attributed solely to forces associated with bipedal locomotor abilities, converge upon a structurally distinct region within the ilium termed the trabecular chiasma. This structural chiasma has been described in terms of bipedal gait as being the locus where loads derived from the sacro-iliac joint and those arising from the acetabulum are distributed and absorbed (Macchiarelli *et al*, 1999; Rook *et al*, 1999). Furthermore, it has been suggested that the well developed arcuate bundles in the posterior and anterior flanges which intersect into the high density trabecular chiasma are related to striding gait (Correnti, 1957; Dalstra and Huiskes, 1995; Rook *et al*, 1999).

Further areas of internal architectural interest have been identified in the acetabular roof and greater sciatic notch of the ilium. Previous literature has emphasised that these density representations are also gait related with a maintained emphasis on the forces which pass through the sacrum into the ilium via the sacro-iliac joint (Dalstra and Huiskes, 1995). These forces are reported to set up distinct trabecular bundles which pass posteriorly in a sacro-ischial trajectory contributing to the sciatic notch density representation and through the acetabulum in the superior and inferior auriculo-acetabular trajectories, contributing to the density representation observed in the acetabular component of the ilium (Kapandji, 1987; Aiello and Dean, 1990; Rook *et al*, 1999). Additionally, the iliac part of the acetabulum has been noted to be particularly

robust in the adult, due to alterations in bony trabeculation caused by buttressing in the weight bearing line of the pelvis (Johnstone *et al*, 1982). Finally, the superior medial region of the ilium is observed to be structurally redundant in the adult due to the approximation of the gluteal and pelvic cortices and the absence of any significant intervening trabecular structure. Surprisingly, this observation of maintained structural redundancy is in contrast to observations by Dalstra and Huiskes (1995) who suggested that this region was an area of maximal stress distribution within the trabecular bone. This suggestion is confusing as it might be expected that trabecular regions experiencing high stresses would adapt to a structural conformation capable of accommodating the prevailing stresses rather than simply regressing and in some individuals disappearing completely.

5.4.1 Density patterns observed

Each of the internal architectural regions of interest described have been well documented for mature individuals and have been explained in terms of locomotion and bipedal gait. However, in this study, the distinct structural regions of the adult representation have been unequivocally identified in the fetus and neonate which cannot be influenced by direct stance related weight transfer as the pelvis is not weight bearing *in utero* (Walker, 1991). Therefore, an alternative suite of forces and influences must be considered during the earliest stages of development of the ilium to cause and influence the maintenance of this distinctive pattern.

Consideration has been given to potential genetic influences on the bone structure and resultant density representation present in the earliest of developmental stages. The relative influences of mechanical and genetic factors are still a question of great debate with the full contribution of genetic influences to bone development not

fully understood (Bertram and Swartz, 1991; Huiskes, 2000; Huiskes *et al*, 2000; Lovejoy *et al*, 2002; Pearson and Lieberman, 2004; Ruff *et al*, 2006). However, the role of genetic and epigenetic influences on bone development have been investigated extensively in recent years by employing experimental models where paralysis has been artificially induced or is inherent in congenital conditions such as cerebral palsy (Hall and Herring, 1990; Hosseini and Hogg, 1991; Germiller and Goldstein, 1997; Bobroff *et al*, 1999; Henderson *et al*, 2005). In using such models, the influences of muscular contraction on bone development can effectively be eliminated allowing for a greater insight into genetic contributions to skeletal form. These studies have strongly suggested that bone form and internal structure are in part genetically determined as although skeletal growth is reduced (Hall and Herring, 1990) bone structure is not significantly altered in the paralysed state (Hall and Herring, 1990; Hosseini and Hogg, 1991; Germiller and Goldstein, 1997; Gilbert *et al*, 2004; Henderson *et al*, 2005; Sawamura *et al*, 2006).

It is further suggested that, coupled with genetic influences, mechanical stimuli *in utero* and in later development may serve to reinforce bone shape and structure (Ruff *et al*, 2006; Skedros *et al*, 2007). The evidence that the final structure of bone results from a combination of genetic, epigenetic, and extragenetic factors is now widely accepted (Skedros *et al*, 2007). In the case of the developing ilium the regions of increased density may well represent initial genetic patterning upon which subsequent *in utero* loading may then direct the remodeling of this primary structure into the form observed in this study.

During fetal development the primary forces acting on the ilium may include those induced by primitive reflex muscular action (Mulder *et al*, 2007). These reflex contractions are believed to be responsible for initiating intramembranous ossification

of the ilium (Laurenson, 1964; Delaere *et al*, 1992) and recent studies have shown that early limb movements induced by random neurological firing are pivotal to the normal development of the locomotor apparatus (Pitsillides, 2006).

As a function of muscular attachment, movement induced by limb musculature will have an influence on all three components of the innominate (ilium, ischium and pubis) as the ilium maintains cartilaginous continuity with both the ischium and the pubis via the acetabulum from its earliest embryological formation (Laurenson, 1963; Scheuer and Black, 2000; Lee and Eberson, 2006). Therefore, it is highly likely that any forces acting on these developing bones both independently and in unison may be transferred across the primitive acetabulum into the ilium. As bone is highly responsive to biomechanical forces (Lanyon, 1974; Currey, 1986; Linde *et al*, 1991; Turner, 1992; Huiskes *et al*, 2000), the patterns which are observed passing in well defined trajectories through the ilium may represent some element of force distribution from these sources. The posterior trajectory passes in a direct line from the acetabular site of articulation between the ilium and the pubis whilst the anterior trajectory passes in a direct line from the acetabular articulation between the ilium and the ischium. It is possible that forces instigated by early reflexive limb movement, which originate through muscle attachment to both the ischial and pubic components of the developing pelvis might be transferred across the cartilaginous acetabular complex to manifest in the ilium i.e. in the opposite direction to the explanation given for the adult form. It is acknowledged that as cartilage is different in its tissue properties to bone, the degree of force transmittance may be influenced, however it is suggested that the continuity of the acetabular anlage with the three innominate bones will allow the potential for a degree of force transference. Cartilage is described as being viscoelastic in that it acts as a cushioning material for dampening dynamic loads, however, it also has significant

tensile and compressive strength which enables the transference of forces (Currey, 2002). The concept of ossification and bone induction by early reflexive movement of musculature has been discussed in other areas of the skeleton including neural arch ossification in response to the gasp reflex (Bagnall *et al*, 1977). This reinforces the possibility that the early internal architecture of the human ilium could mirror the final adult pattern as both reflect a form of force transfer across the acetabulum in relation to the lower limb movement. Furthermore, the posterior trajectory may be considered as a common site for not only pubis-ilium force transference but also early sacro-iliac force transference. It is possible that primitive forces are established at this joint arising from reflexive vertebral movement and associated anatomical interactions which may act to reinforce the posterior density pattern. This multifactorial hypothesis may aid in explaining why the posterior trajectory is more pronounced than that of the anterior trajectory.

Anatomical proximity has also been considered to contribute to the early developmental form of the ilium. Laurenson (1964) indicated that the position of the nutrient foramen, which lies over the region of the trabecular chiasma, is the first region of the ilium to commence ossification and there is evidence in the literature to suggest that areas of intersection of differential stress patterns can act as an initiator for bone deposition and as an angiogenic attractant (Carter and Beaupre, 2001). It is proposed that the presence of the dominant nutrient artery at its point of invasion leads to a more mature pattern of bone formation reflected in a higher density representation at the trabecular chiasma region. Additionally, whilst it is reported that the compact shells of the ilium ossify through intramembranous ossification resulting from the attachment of the iliacus muscle on the inner surface and the gluteal muscles on the pelvic surface (Scheuer and Black, 2000) the maintenance and development of the internal architecture

could also be influenced by forces generated through muscle contraction and limb movement associated with muscular groups attaching to the ischium (hamstrings) and pubis (adductors).

A further significant density representation is also observed at the acetabular roof component of the ilium. This region is considered to be dominantly represented due to its increased three dimensional thickness when compared to other areas of the ilium. Superimposition of the increased volume of underlying trabecular bone and the overlay of the acetabular metaphyseal component produces a two dimensional radiographic representation of increased bone density in this region. In its early developmental form, the well represented acetabular component has previously been attributed to metaphyseal bone growth at the acetabular margin (Ponseti, 1978) and interstitial growth of the acetabular roof cartilage (Ippolito *et al*, 1984). Therefore the density representation in this region may simply be a function of the increased thickness of the acetabular component.

A further region of high density is present as a persistent and dense triangular wedge located along the perimeter of the greater sciatic notch extending towards the chiasma region. This is consistently the most densely represented area and is present in the earliest fetal specimens. The presence of density in this region may be attributed to the neurogenic influences from the closely positioned sciatic nerve. Proximity of peripheral nervous tissue has been shown to initiate ossification at the greater sciatic notch as well as in other skeletal areas (Laurenson, 1964). Therefore, an increased bone density in this region may be attributed to a protective mechanism for the large approximated sciatic nerve.

In the sacro-iliac region of the ilium, the posterior flange of greatest density is continued and represented by a distinct area of secondary structural density. This region

is particularly well represented around the borders and surface of the auricular surface. Due to the significant anatomical proximity of ligamentous tissue in this region, soft tissue association is considered to be primarily responsible for the pattern observed. These ligamentous associations which envelope the joint (Bowen and Cassidy, 1981; Vleeming *et al*, 1990) are proposed to be well established, having been recognisable covering the articular surfaces from 20 intrauterine weeks (Salsabili and Hogg, 1991). These ligaments may have the potential to induce various forces around the joint capsule causing the bone to respond by laying down an increased bone density at the regions of stress. Further adding to this theory of ligamentous interaction is the fact that the sacro-iliac joint is not weight bearing across its joint surfaces, instead, weight is largely transferred through the ligamentous material which encapsulates the joint (Last, 1973; Scheuer and Black, 2000). The specific areas of density represented in this posterior region follow the anatomical borders presented by ligamentous attachment very closely. In the anterior region of the ilium there is again a continuation of the previously described high density anterior flange. It is suggested that this density region may be explained simply as an extension of the antero-superiorly directed trajectory of highest density, possibly produced in response to early reflex limb movements. The final region of secondary density, represented in the inferior acetabular region, may be produced by the sloped acetabular roof component. The slope in this region results in a natural grading of apparent density. The reduction in three-dimensional volume reduces the resultant radio-opacity of the radiographic representation giving the impression of an apparent reduction in bone density. It is therefore suggested that this region is a superimposition artefact.

Finally, the most widespread regions of tertiary density were observed around the entire perimeter of the ilium. This perimeter region was represented as having

relatively low structural density compared to other regions within the bone. Firstly, this low density perimeter region may be considered as an artefact of 'visual fall-off' at the boundary between bone and non-bone edge regions where there is a tapering of the bone which leads to a reduced density representation. However, this explanation is only plausible at the terminal perimeter of the ilium. As the low density region is observed in a wide band in most perimeter regions an additional theory may explain this visual presentation. Therefore, the low density regions have been further explained in terms of continuous growth through modeling processes at perimeter regions. This continued modeling during the developmental period results in the continuous renewal of perimeter cortical and trabecular bone allowing the bone to increase in size. As a result of this continuous modeling, newly ossified bone at perimeter regions is considered to present as a low density representation. This theory of continuous modeling contributing to perimeter form will be discussed further when dealing with quantitative data in Chapter 6. A further region of low density was observed in a superiorly located central band, this region of the ilium was extremely under-represented when paralleled with neighbouring anterior and posterior regions. This area of poor structural representation is considered to be a structurally redundant by-product of the well represented anterior and posterior trajectories which form the primary structural support within the ilium. This representation of structural redundancy has been demonstrated in other bones including the proximal femur, as Ward's triangle, bounded by the compressive and tensile regions of increased structural integrity (Evans, 1957).

This study has contradicted the null hypothesis of random distribution of rudimentary trabeculae by highlighting that the iliac cortical and trabecular architecture is organised in well defined and regular patterns from a very early stage of fetal development. This precocious development mirrors the more mature pattern, seen in the

adult, which has been attributed to biomechanical forces associated with direct stance load bearing and bipedalism. As the fetal and neonatal representation is free from direct stance related load transfer, further investigation is required to elucidate the origins and progression of structured bone patterning in the ilium. It is proposed that the structural observations made in this study in non-load bearing fetal and neonatal pelves may be a preliminary response to early limb movement perhaps augmenting a pre-existing genetic template. If there is indeed a basic genetic internal and external form to the ilium then it is possible that the patterns of internal architecture seen in this study may represent a maintenance and reinforcement of that preliminary genetic scaffold by the forces instigated by *in utero,* reflexive limb movement. Therefore, the structural form of the ilium is considered to be a multi-factorial end product rather than the outcome of a single influencing factor as has been the current mode of thinking with regards to bipedalism.

In summary, it is clear that the internal construction of the perinatal ilium develops in a complex manner that cannot be simply attributed to locomotor requirements. It is likely that it is influenced by multifunctional components that may include: genetic blueprints, muscular and joint activity, neurogenic influences and vascular proximity. The subsequent part of this study will now examine the three dimensional pattern of the trabecular system of the neonatal ilium via micro-computed tomography imaging. This will aid the evaluation of changes that occur to this primitive pattern during the neonatal developmental period.

CHAPTER 6 - Quantitative Analysis of Neonatal Trabecular & Cortical Structure

6.1 Introduction

In this part of the study, the initial radiographic investigation was expanded by application of three-dimensional imaging to twenty eight neonatal ilia from the Scheuer collection. The neonatal cohort was chosen for full analysis and investigation as it was considered to be the most mature and progressive pattern of early bone formation which would provide optimal resolute structural interpretation and be suitably representative of the early developmental period. Following three-dimensional micro-computed tomographic imaging of the sample, reconstructed data sets were subjected to computerised histomorphometric analysis to determine various measures of trabecular structure and cortical thickness. This chapter deals with the data collection method, the quantitative data obtained from the neonatal trabecular and cortical structural analysis and a discussion of these results to aid an understanding of trabecular and cortical variation across the ilium within this developmental period.

6.2 Micro-computed tomography (µCT)

Each specimen was scanned at the University of Hull, Centre for Medical and Engineering Technology (CMET) using an X-Tek HMX 160 micro-computed tomography scanner (µCT) (X-Tek Systems Ltd, Tring, UK) at voltage (84 kV), current (17 µA) with an aperture setting of 50%. The µCT system consists of an X-ray generating gun which generates a continuous beam of x-rays from a 5-micron spot and fires them through the sample mounted on a turntable. These x-rays are then collected by a photodetector and cast an x-ray shadow onto the intensifier window. The intensifier converts the x-ray shadow into a visible image, which is recorded by a video

camera and displayed on a monitor. The number of X-rays reaching the detector at any point depends on the energy of the X-rays and the absorption rate of the different parts of the sample through which they pass, which is proportional to the material's thickness and density. The result is a 2D digitised greyscale X-ray image. The magnification of the sample depends on its position between the X-ray source and intensifier. Moving the sample towards the x-ray source enlarges the X-ray shadow and shows greater detail.

In preparation for scanning, each specimen was positioned in a vertically upright position within the μCT system with the iliac crest positioned superiorly and the acetabular component positioned inferiorly resting on the gantry turntable. During the scanning process the sample was rotated through 360° in typically 1300 steps, with a 2D image collected at each step. Extraneous noise in the images was minimised by taking 16 images at each scanning step and averaging the results. Image reconstruction, whereby the digitised 2D X-ray images were converted into a 3D volumetric structure, was performed using NGI CT Control software (X-Tek, Tring, UK). From this volume an image stack was created for which the resultant slice pixel size ranged between, 34.5μm and 44μm dependent on sample size. After completion of the scanning process and image reconstruction, 2D μCT slice images were exported as a stack of 16-bit tiff (Tagged Image File Format) images (Figure 6.1).

The scanning resolutions applied in this study were always set to the operating system maximum for any individual specimen, this resulted in scanning resolutions which were directly related to the size of the specimen under investigation.

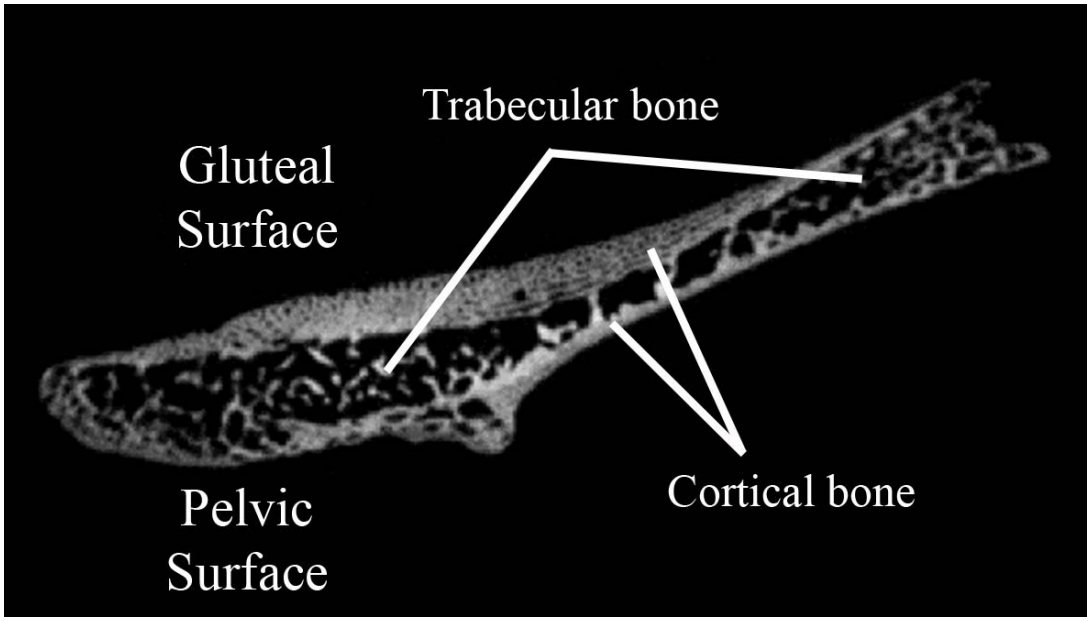

Figure 6.1. 2D μCT slice through a neonatal iliac blade in transverse plane.

6.3 Data Handling

The volume of data produced from a single micro-CT scan is extremely large, with routine volumetric images containing greater than 10^9 voxels equating to several gigabytes of data (Holdsworth and Thornton, 2002). In this study, each scan was in excess of 1 Gb in size. These large data sets place a substantial burden on the computer systems which produce, output, store and compute the data. As a result the computer system which dealt with the initial data production was an integrated part of the micro-CT system and was of a high specification to allow for optimal processing. A powerful industrial computer was responsible for running the X-Tek Inspect-X image processing, control and acquisition software. Further to this, the large data set imposed an additional constraint on the handling system dealing with the initial storage of the raw data. As a result, a storage device with a large memory capacity (320 Gb) was used to store and backup all scan data collected during this study. This data was backed up on a weekly basis onto an accessory mirrored drive to minimise the likelihood of significant data loss. A subsequent problem posed by the large data sets was the ability of a

computer system to handle the data in terms of image analysis and manipulation. Data sets were therefore viewed and analysed on a computer with a large amount of random-access memory (RAM), a fast processor and a dedicated graphics card to allow for efficient data interpretation. Subsequently, specialised stereological analysis software was applied to the data to gain quantifiable trabecular parameters from the high resolution data.

6.4 SkyScan CTAn

The software package applied to the sample data was SkyScan CT-Analyser. CT-analyser (CTAn) is a software application provided by SkyScan which can be applied to micro-CT data to obtain quantitative parameters from bone microarchitecture and construct visual models from scanned datasets. This software programme was operated on a Viglen standard desktop Intel(R), Pentium(R) 4 CPU, 3.00GHz and 1.00 Gb RAM. The procedural application of SkyScan CTAn to the data set will be outlined.

6.4.1 Volume and region of interest selection

Prior to analysis of data produced from μCT using CTAn software, specific volumes and regions of interest for analysis were selected. Volumes of interest were applied for the analysis of a trabecular volume and regions of interest were applied for selection of cortical thickness sampling sites. For trabecular volume analysis, twenty three volumes of interest (VOI 1-23) were selected within the ilium based on a uniform grid which was superimposed onto the iliac surface using specific anatomical points of reference (Figure 6.2).

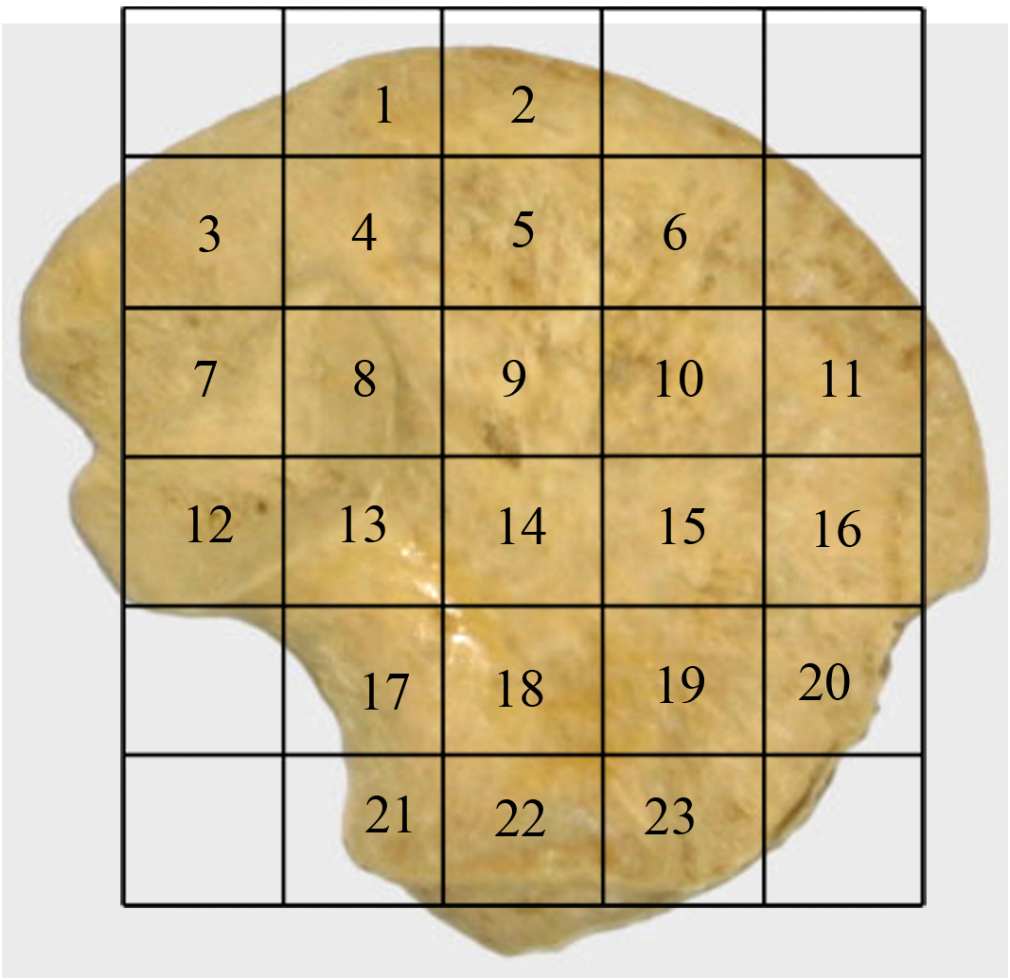

Figure 6.2. Image of a human neonatal ilium illustrating position of volumes of interest (VOI) for trabecular analysis and comparable regions of interest (ROI) for cortical analysis.

The grid was positioned so that in the horizontal plane, VOI 12 was located at the posterior inferior iliac spine and VOI 16 at the anterior superior iliac spine. In the vertical plane, VOI 2 was positioned at the mid point of the iliac crest and VOI 22 at the mid point of the acetabular surface. From these set-point landmarks all other VOI's adopted a standardised position allowing a uniformity of grid placement for each bone to be achieved with minimal difficulty. Similar anatomical points and VOI positioning have been used in previous studies investigating the bone architecture of the ilium (Abel, 2006; Volpato, 2008). To identify and select the field for analysis within a particular VOI, an elliptic volume was selected and placed in the appropriate grid

position within a biphasic (bone/non-bone) region and interpolated throughout the 3D data set for each grid square. Individual VOI's ranged from 50-200 mm^3 depending on the volume under investigation, due to the topological variation in potential trabecular volume between the cortices across the ilium. For example the volume of trabecular bone within a VOI for the acetabular region was much larger than the volume within the central body where the two cortices were in close approximation. Once the VOI was in an appropriate position, bone parameters were calculated. The VOIs and ROI's analysed are defined in Figure 6.2 and their regional descriptions shown in Figure 6.3.

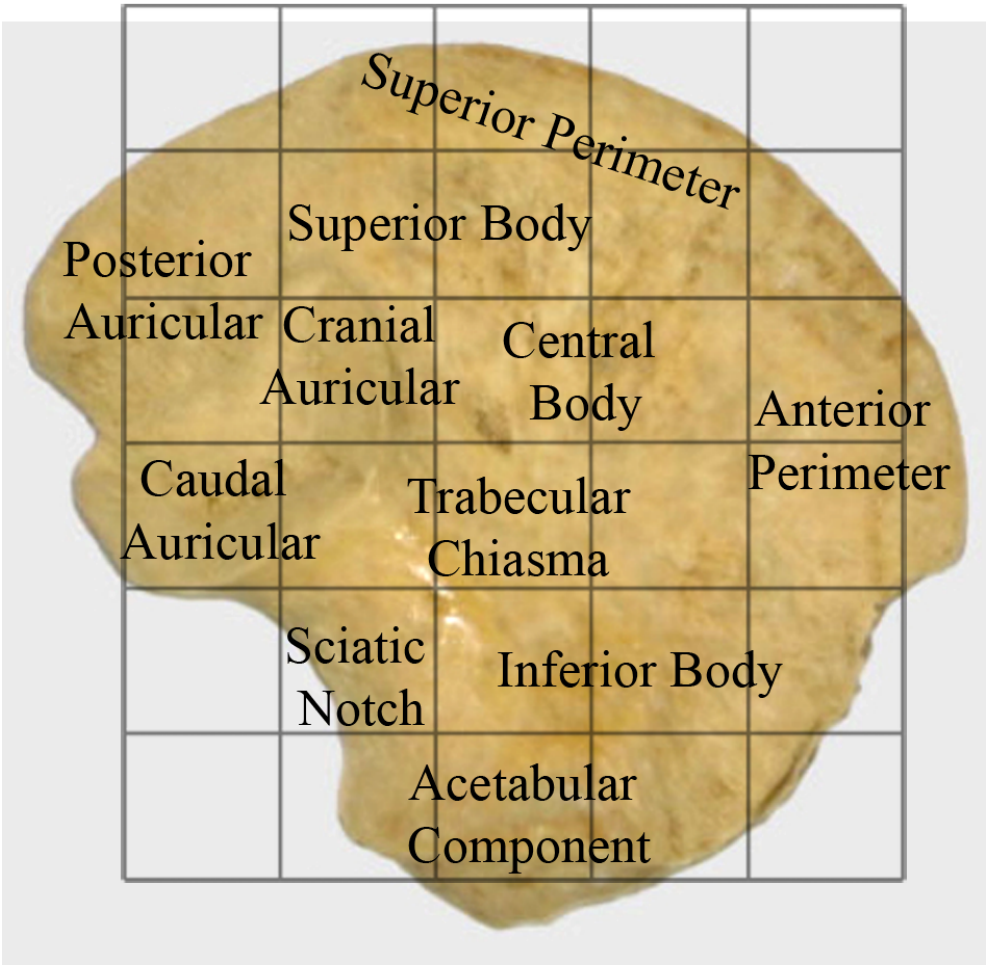

Figure 6.3. Image of a neonatal ilium documenting descriptive terminology in relation to volumes (regions) of interest.

Cortical analysis involved placement of the same grid using the same anatomical landmarks, e.g. VOI 6 directly equates to ROI 6. This grid was positioned onto the pelvic and gluteal surfaces of the ilium and contained the same twenty three regions of interest (ROI 1-23) which allowed for comprehensive coverage of the cortical shells on respective surfaces of the ilium (Figure 6.4).

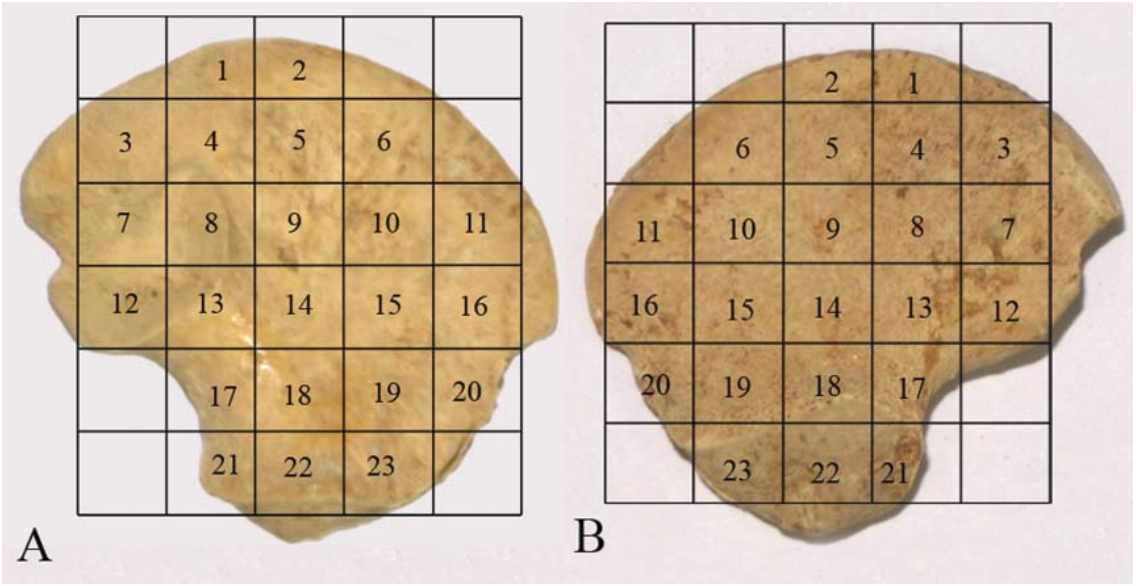

Figure 6.4. Placement of grid and resultant ROIs on both pelvic (A) and gluteal (B) cortices.

Although providing a comprehensive analysis of iliac trabecular and cortical morphology, this computational volume requires a significant amount of preparation and intricate positioning prior to any quantification and analysis. Best efforts were made to position the grid so that comparable volumes of interest could be analysed between specimens. As developmental homology could not be assumed it is acknowledged that there may be some degree of variation between individuals. However, it is suggested that this variation is minimal due to all ilia occupying the same developmental group and having very similar size and shape. Furthermore, uniformity of volume of interest size may not always be directly comparable between analysis fields due to the changing

morphology of the bone. This limitation is unavoidable but can be justified as all trabecular indices calculated are presented as an average of the trabecular volume analysed.

The decision to include 23 volumes and regions of interest for analysis was taken to ensure that extensive coverage of the cortical shell and underlying trabecular structure was achieved. By selecting this number of analysis fields, rather than additional or reduced fields, a balance was struck between excessive data processing per specimen and the ability to obtain sufficient detail to provide a reliable interpretation of regional cortical and trabecular patterning.

6.4.2 Image import and calibration

Once volumes of interest were identified, micro-CT data sets were imported into CTAn as animated image stacks so that each scan could be viewed sequentially to ensure that the slice data were in the correct order without any missing or erroneous files. Once the image stack was imported, a mid section slice was chosen and a colour look-up table (CLUT) was applied to improve visual representation. Using the CLUT palette, the greyscale option was selected and window levels were adjusted to improve contrast within the image (Figure 6.5). The CLUT values applied to the mid section slice were then interpolated through all other slices. At this point the data set was calibrated for future measurement and this was achieved by accessing the image properties menu and opening the voxel size window. Voxel values could then be entered manually and were obtained from the raw data header produced during scanning which accompanied each specimen scan. Once calibration was completed several options became available in a control toolbar, these included original image

view, region of interest selection, binary conversion, and finally image analysis. Each of these steps will now be described sequentially.

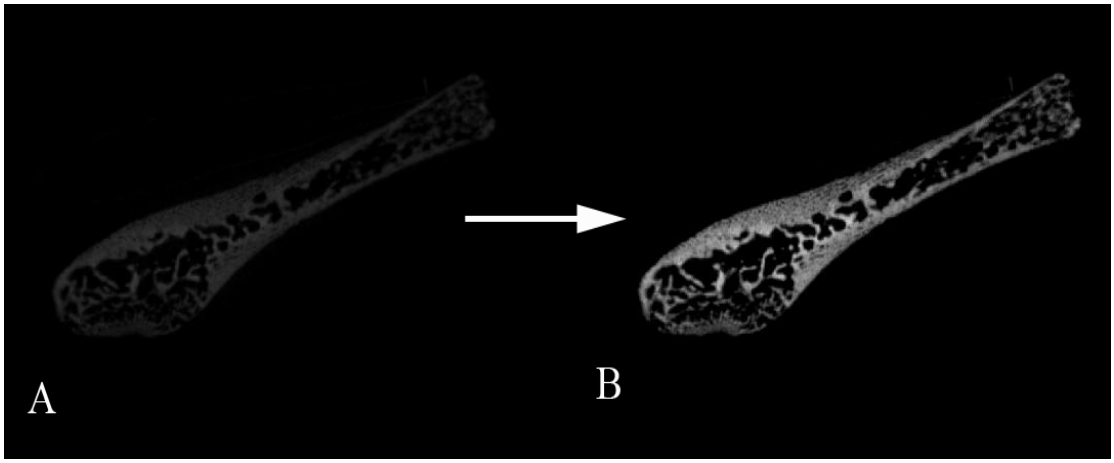

Figure 6.5. Illustration of improved contrast through application of CLUT palette. A: original image import. B: application of CLUT palette values.

6.4.3 Original image view

In the initial data view it was possible to truncate the number of data slices which would be subjected to analysis. This was the first step in isolating individual inter-slice regions of the ilium before subsequent intra-slice region of interest selection. Using vertical panning sliders it was possible to locate specific areas of the scan and isolate these using the anatomical landmarks which divided the ilium into the different selected volumes of interest. When selecting volume of interest 1 (VOI 1) for example, the iliac crest was identified and marked as 'top of selection' so that no slice above this would be analysed, then a calculated number of slices below this selection (approximately $1/6^{th}$ of the slices composing the entire ilium) was marked as 'bottom of selection'. This was representative of the bottom of VOI 1, so that no slice below this selection would be analysed. This in essence defined a gross region within the ilium which could be further isolated by applying subsequent region of interest selection.

6.4.4 Application of volume and region of interest to data

When selecting a volume of interest within the previously truncated dataset it was first necessary to select the generic "volume of interest" tool to outline a gross volume of interest within a single slice. This single slice selection would subsequently be interpolated through all previously selected slices. To further refine the region of interest selection, a number of pre-calibrated shapes were available from the main toolbar menu. An elliptical volume of interest was used for region of interest selection in this study due to its ability to be optimally altered in response to the topographical changes in the iliac morphology. The ellipse could be altered in size by clicking on its perimeter and dragging until the desired dimensions were achieved. Once the final single slice region of interest was selected, this was interpolated through all slices to produce an analysis volume of interest. Each individual slice within the analysis selection was then checked to ensure its region of interest was maintained within a biphasic (bone/non bone) region and that no cortical bone contributed to the selected volume. Additionally, a check was made to ensure that VOI's within each slice lay within the limits of the trabecular volume being analysed and did not cross into another volumes analysis field.

6.4.5 Binary conversion

Once a volume of interest had been identified, the contained slice data was binarised prior to analysis. Binary selection was initiated by selecting the "convert to binary images" tab. Prior to final binary selection an image threshold was determined. This was achieved by creating a histogram which displayed the distribution of grey level values for a selected VOI. From this histogram, upper and lower global thresholds could be selected to determine bone from non-bone regions. Local thresholding for each

VOI was initially conducted using the automated thresholding tool, however, further fine-tuning of image thresholding was conducted by eye to ensure that only trabecular bone was being calculated in the absence of any cortical bone and non-bone marrow space. The white part of the binary images represented solid objects (trabecular bone) for subsequent analysis and the black part of the binary images represented non-bone (Figure 6.6).

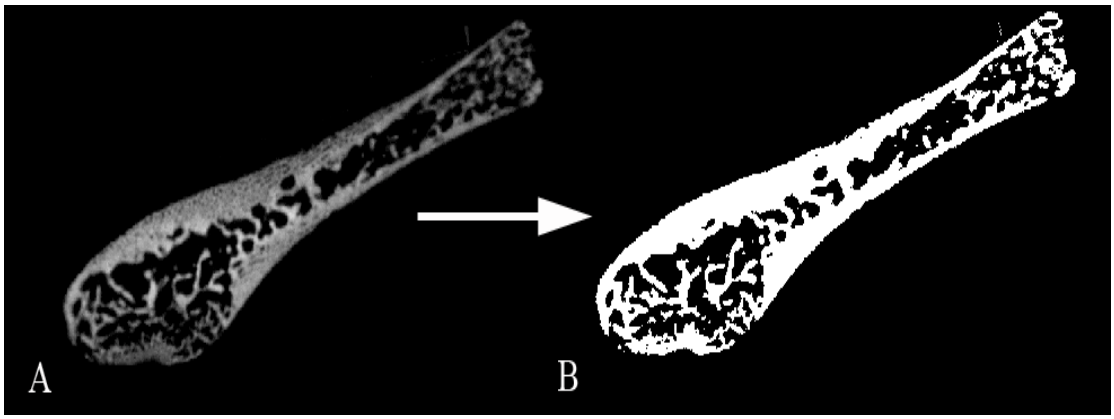

Figure 6.6. Binary conversion. A: CLUT adjusted image. B: binarised image.

6.4.6 Image analysis

Image analysis of the binarised volume of interest was the final analysis step undertaken. This was completed by selecting the "3D analysis" tab and subsequently selecting the trabecular parameters to be investigated. Automated trabecular calculation was then undertaken by the software programme. This process was repeated for each volume of interest within each specimen. Data was saved as a tabular line-by line file, an appended comma-delineated file and as a hard copy printout.

Skyscan was chosen as the analysis software for application to the full study sample due to its model-independent calculation potential, the multiple indices which could be calculated and its intuitive user interface. As Skyscan CTAn was the image

analysis method of choice, specific details regarding trabecular parameters and their method of calculation are presented separately.

6.5 Quantifying Trabecular Architecture using CTAn

Volumes of interest were selected based upon the defined grid template as outlined in section 6.4.1. Once each volume of interest was correctly positioned, analysis was initiated by applying the standard CTAn protocol. The trabecular indices calculated included; bone volume fraction (BV/TV), trabecular thickness (Tb.Th), trabecular separation (Tb.Sp), trabecular number (Tb.N), structural model index (SMI), and degree of anisotropy (DA).

6.5.1 Bone volume fraction (BV/TV)

Bone volume fraction is a measure of the trabecular bone volume to the total reference volume represented as a percentage. It is considered to be the single most important parameter for quantifying the trabecular architecture of bone and is routinely obtained from reconstructed microCT data (Ruegsegger *et al*, 1996; Odgaard, 1997; Ding *et al* 1999; Cowin, 2001). It is highly associated with the mechanical competence of trabecular bone (Fernández-Seara *et al*, 2001; Pothuaud *et al*, 2002) and has been shown to reflect environmental influences earlier in development than other trabecular characteristics (Tanck *et al*, 2001). Therefore, BV/TV is a particularly relevant and useful index for understanding structural changes during early development. When applied in isolation, BV/TV can be used to explain 64% of a bone's strength, however, when applied in combination with other structural parameters it can explain up to 94% of a bone's strength (Hildebrand *et al*, 1999). This parameter is only relevant if studied

within a biphasic region of solid and space such as a trabecular bone region, but it must not include any region of solid cortical bone.

6.5.2 Trabecular Thickness (Tb.Th)

Trabecular thickness is a primary morphometric parameter used when analysing and describing trabecular bone architecture (Ding and Hvid, 2000). This value may be used to determine the degree of modeling and remodeling which has occurred, as more advanced regions of ossification and growth are proposed to present with increased values of trabecular thickness. Trabecular thickness can be measured independently of model assumptions, with three-dimensional image analysis applied to micro-computed tomography data. Trabecular thickness was determined as an average of the local thickness at each voxel representing bone as defined by binarisation (Ulrich *et al*, 1999b). Local thickness for a point in solid is defined by Hildebrand and Ruegsegger (1997a) as the diameter of a sphere which fulfils two conditions: (i) the sphere encloses the point (but the point is not necessarily the centre of the sphere); (ii) the sphere is entirely bounded within the solid surface (Figure 6.7). Histomorphometrists typically measure a single mean value of bone trabecular thickness from a particular volume of interest. The values for trabecular thickness are represented in mm.

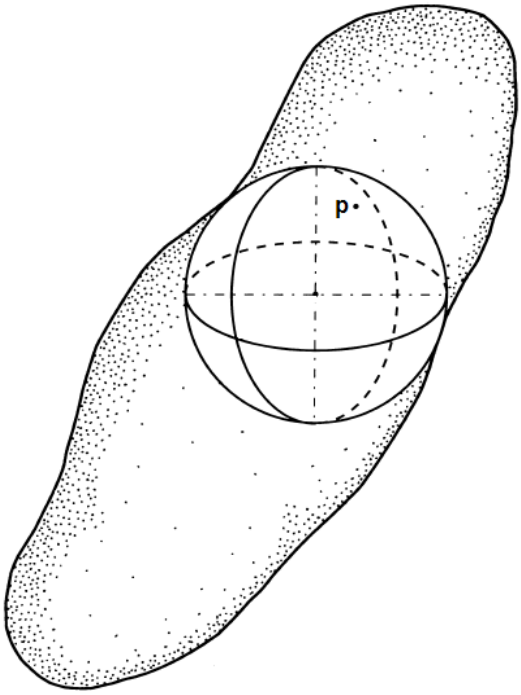

Figure 6.7. Local thickness of a structure determined by fitting maximal spheres. The maximal local thickness is equivalent to the diameter of the largest sphere that completely fits inside the structure and encloses a defined point (p). Modified from Hildebrand and Ruegsegger, (1997a).

6.5.3 Trabecular Separation (Tb.Sp)

Trabecular separation is a particularly important parameter for further explaining the mechanical properties of trabecular bone in conjunction with other histomorphometrics (Ulrich *et al*, 1999b). The implications of trabecular separation are often applied to the investigation of osteoporosis as increased trabecular separation may have significant biomechanical consequences (Kang *et al*, 1999). Trabecular separation is essentially a measure of the thickness of space between trabecular struts as defined by binarisation within the volume of interest. Trabecular separation is calculated independently in three-dimensions using the same method outlined for measurement of trabecular thickness (Figure 6.8). The values for trabecular separation are expressed in mm.

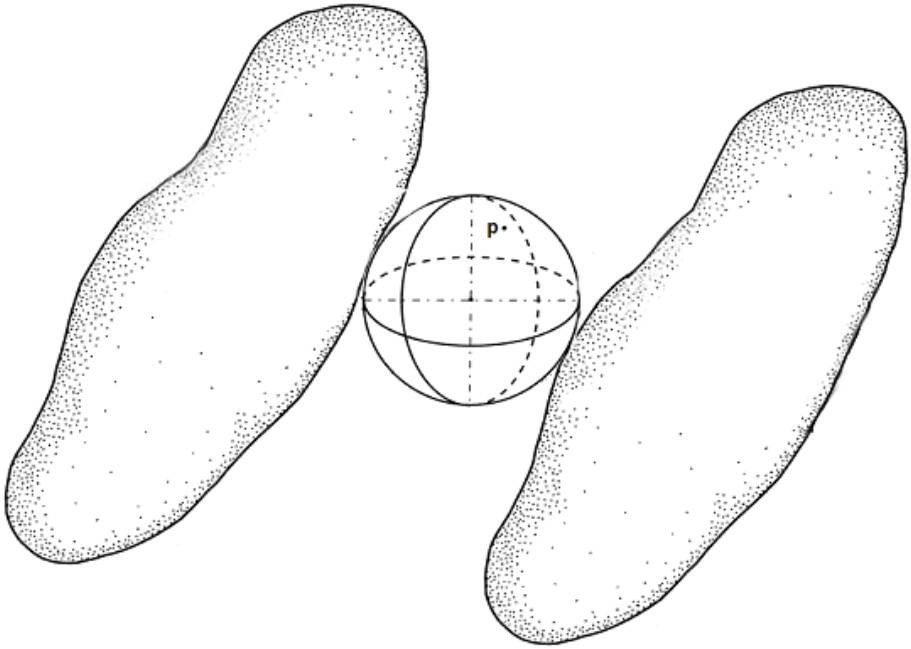

Figure 6.8. Local thickness between structures determined by fitting maximal spheres. The maximal local thickness is equivalent to the diameter of the largest sphere that completely fits between the structures and encloses a defined point (p). Modified from Hildebrand and Ruegsegger, (1997a).

6.5.4 Trabecular Number (Tb.N)

Trabecular number is a further important stereological measure of trabecular bone morphology used in conjunction with other histomorphometric indices as a measure of biomechanical competency (Ulrich *et al*, 1999b). Trabecular number is a measure of the number of traversals across a trabecular or solid structure made per unit length (mm) on a linear path through a trabecular bone region. The complexities of model dependence are eliminated by the true three-dimensional calculation of Tb.N from μCT images. Trabecular number is measured by the application of the following equation for a parallel plate model of trabecular structure.

$$Tb.N = (BV/TV)/Tb.Th$$

The values for trabecular number are expressed in mm^{-1}.

6.5.5 Structural model index (SMI)

Structural model index is a morphometric parameter first introduced by Hildebrand and Ruegsegger (1997b). This structural index allows for quantification of the characteristic form of a 3D trabecular volume by indicating the relative prevalence of rods and plates in a three-dimensional structure (Jiang *et al*, 2000). An ideal plate, cylinder (rod) and sphere have structural model index values of 0, 3 and 4 respectively. For a structure with both plates and rods of equal thickness the value lies between 0 and 3, depending on the volume ratio of rods to plates. The calculation of SMI is based on dilation of the 3D voxel model by artificially adding one voxel thickness to all binarised object surfaces. SMI is derived as follows:

$$SMI = 6\times(S'\times V/S^2)$$

Where S is the object surface area before dilation and S' is the change in surface area caused by dilation. V is the initial undilated object volume.

6.5.6 Degree of anisotropy (DA)

Isotropy is the measure of three-dimensional symmetry or the presence or absence of preferential alignment of structures along a particular directional axis. After bone volume fraction, DA is regarded as the most important determinant of mechanical strength (Odgaard, 1997). The degree of anisotropy of trabecular bone has also been observed to correlate highly with an increased risk of hip fracture (Ciarelli *et al*, 2000). Mean intercept length (MIL) and Eigen analysis are used to calculate DA. A single parameter measuring anisotropy, the degree of anisotropy (DA), is traditionally expressed as the maximum eigenvalue divided by the minimum eigenvalue. Values for

DA calculated in this way vary from 1 (fully isotropic) to infinity (fully anisotropic). Mathematically this is a cumbersome scale therefore, a more convenient mathematical index of anisotropy is calculated by the following equation.

DA = (1-[min eigenvalue/max eigenvalue])

Application of this formula delimits DA as 0 for total isotropy and 1 for total anisotropy. Total isotropy can be defined as uniformity of trabeculae in all directions (trabecular organisation) whereas total anisotropy can be defined as a difference in the physical properties of the trabecular structure when measured along different axes (trabecular disorganisation).

6.6 Quantifying Cortical Thickness

As well as the investigation of trabecular bone architecture, a study of the cortical thickness of the ilium was also undertaken. Cortical thicknesses from defined regions of interest (ROI) of both pelvic and gluteal shells of the neonatal ilium were measured to provide an insight into early developmental cortical thickness and to relate this to the underlying trabecular structure. A greater appreciation of the contribution cortical bone offers to bone strength and fracture risk is being realised (Mosekilde and Mosekilde, 1989; Spadaro *et al*, 1994; Augat *et al*, 1998; Jarvinen *et al*, 2005). Advanced imaging technologies have begun to address a previous deficit in this area of bone structural composition, thereby permitting analysis of independent and co-dependent interactions within various bones (Sandor *et al*, 1992; Louis *et al*, 1993; Silva *et al*, 1994; Hangartner and Gilsanz, 1996). However, even with the recent advances in imaging capabilities, spatial resolution has remained a limiting factor for

reliable cortical measurement when the cortex of a bone is below a certain threshold thickness of around 1.1mm (Cody *et al*, 1989; Spoor *et al*, 1993; Newman *et al*, 1998; Silva *et al* 1994; Hangartner and Gilsanz, 1996). The application of micro-computed tomography however, has enabled detailed information to be gained regarding cortical structure in animal models (Laib *et al*, 2001; Bagi *et al*, 2006) and it is now being applied to human bone (Wachter *et al*, 2001; Dempster *et al*, 2001).

6.6.1 In-plane orientation

When recording cortical thickness measurements, it was important that the scanning plane and positioning of the specimen in the scanner was known, in order to make reliable linear measurements. Therefore, concerted efforts were made to position each specimen into the scanner in a consistent orientation using reproducible landmarks and procedures. Each specimen was placed into the scanner with the mid-point of the iliac crest positioned superiorly and the inferior acetabular component positioned inferiorly on the turntable. This ensured that the iliac blade was positioned perpendicular to the turntable (Figure 6.9). The positioning of each scan was confirmed in the CTAn application using the profile tool and if discrepancies in orientation were identified, the data were re-sampled using the 'reslice model' application. Thickness measurements were made in the transverse plane of the ilium.

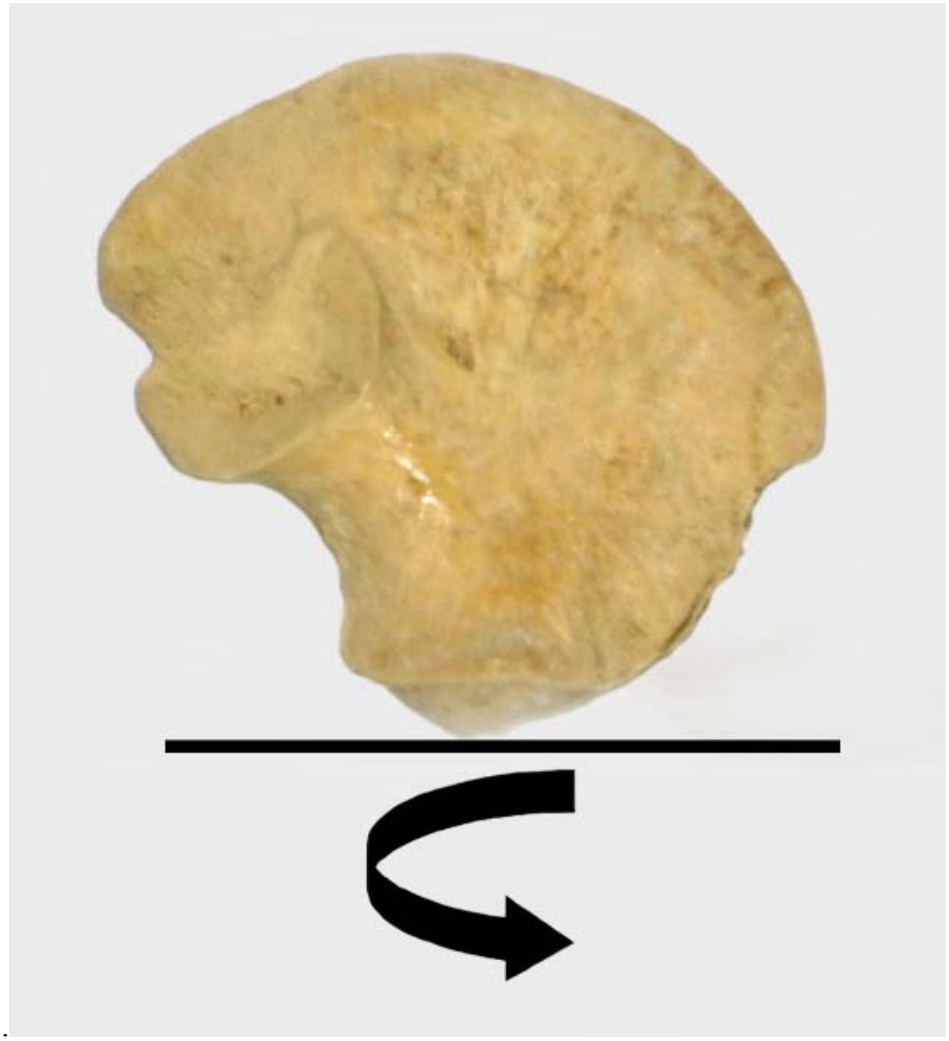

Figure 6.9. Orientation of the ilium perpendicular to the scanner turntable. The iliac crest was positioned superiorly and the acetabular component positioned inferiorly. The turntable is represented by the black line and the arrow represents the clockwise direction of the turntable rotation within the scanner.

6.6.2 Linear Measurement

Cortical measurements were defined from a point on the endosteal surface where no trabecular struts were observed to anchor, extending to a parallel point on the periosteal surface for both pelvic and gluteal cortices (Figure 6.10). This measurement was made by zooming in on the region of interest under investigation, as defined by the previously described grid system, and identifying corresponding periosteal and endosteal points with a mouse click. From this, CTAn displayed the linear distance measurement between the two points. For each ROI, measurements were made four

times at random points across the ROI to provide a mean value of cortical thickness representative of that ROI.

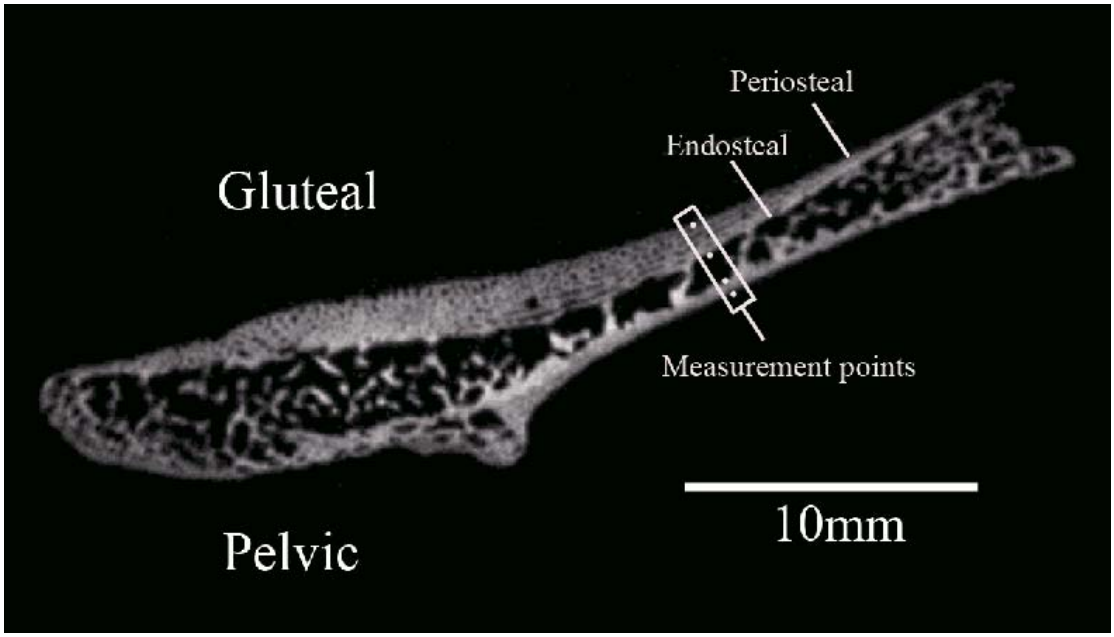

Figure 6.10. Transverse microCT slice through the neonatal ilium at the level of ROI's 7-11. Measurements were recorded between regions of the endosteal cortex which had no associated trabecular struts and the associated parallel periosteal surface for both pelvic and gluteal cortical shells.

6.7 Statistical Testing

A method of statistical analysis was identified to compare the data produced between volumes of interest for trabecular characteristics and between ROI's for cortical thicknesses. The statistical method identified displayed the significance of differences observed between defined volumes and regions, in a manner which could be easily interpreted for the large volume of data produced. SigmaStat was identified as the optimal statistical package for this kind of analysis and was used to perform an analysis of variance (ANOVA) test between all VOI's and ROI's for each structural parameter to determine overall statistical significance. Further to this, multiple pairwise

comparison procedures were subsequently carried out to specifically identify which VOI's displayed statistical differences for trabecular parameters.

6.7.1 ANOVA and Pairwise Multiple Comparison Procedures

Analysis of variance (ANOVA) was applied to the results of both trabecular and cortical quantification. This analysis was undertaken to investigate relationships between volumes and regions of interest across the trabecular and cortical structure of the ilium. Data sets either presented with parametric or non-parametric distribution to which a parametric ANOVA test or Kruskal-Wallis ANOVA on Ranks test was applied respectively.

Parametric data

One way analysis of variance is a parametric test that assumes that all samples are drawn from normally distributed populations with equal variance. The null hypothesis for a parametric ANOVA is that there is no significant difference between the populations from which the samples were drawn. Parametric ANOVA summarises the sample sizes n, number of missing values, mean, standard deviation, differences of the means and standard deviations and standard error of the means. Additionally, parametric ANOVA produces a report describing the source of variation within the groups. This report displays the sum of squares, a measure of variability of the average differences of the sample groups; degrees of freedom, the number of groups and sample size which affects the sensitivity of the ANOVA; and mean squares of the groups, which provides two estimates of the population variances. In addition, the F statistic and the corresponding p value are presented and are the most important statistics relating to statistical significance.

If the F ratio approaches 1, it can be concluded that there are no significant differences between groups (i.e., the data groups are consistent with the null hypothesis that all the samples were drawn from the same population). However, if the F statistic is large, it can be concluded that at least one of the samples was drawn from a different population (i.e., the variability is larger than what is expected from random variability in the population).

The p value is the probability of being incorrect in concluding that there is a true difference between the groups (i.e., the probability of falsely rejecting the null hypothesis). The smaller the p value, the greater the probability that samples are drawn from different populations. Traditionally, it is concluded that there are statistically significant differences when $p < 0.05$. To determine exactly which groups were different, multiple comparison procedures were subsequently applied.

Parametric multiple comparison procedure

Multiple comparison procedures isolate differences between individual VOIs. Multiple comparisons produced comparisons between group pairs which were used to determine which were statistically different and the corresponding size of these differences.

Pairwise comparison results listed comparisons of all possible combinations of group pairs. For parametric data the Holm-Sidak method was applied as it is recommended as the primary procedure used for pairwise comparison testing. When performing the test, the p values of all comparisons are computed and ordered from smallest to largest. Each p value was then compared to a critical level that depends upon the significance level of the test, the rank of the p value and the total number of comparisons made. A p value less than the critical level ($p<0.05$) indicates that there is a significant difference between the corresponding groups.

If a group is found not to be significantly different from another group, all groups with p ranks in between the p ranks of the two groups that are not different are also assumed not to be significantly different and a result of DNT (Do Not Test) is assigned for those comparisons.

Non-parametric data

The Kruskal-Wallis ANOVA on Ranks is a non-parametric test that does not require the assumption that all the samples were drawn from normally distributed populations with equal variances. It compares several different experimental groups that receive different treatments. The null hypothesis is that there is no difference in the distribution of values between the different groups. The ANOVA on Ranks report displays the H statistic and the corresponding p value for H.

ANOVA on Ranks summarises the medians, the percentiles, sample sizes (n) and missing values. The ANOVA on Ranks test statistic, (H), is computed by ranking all observations from smallest to largest. The average value of the ranks for each treatment group are computed and compared. If H is small, the average ranks observed in each treatment group are approximately the same and it can be concluded that the data is consistent with the null hypothesis that all the samples were drawn from the same population. If H is a large number, the variability among the average ranks is larger than expected from random variability in the population and it can be concluded that the samples were drawn from different populations (i.e., the differences between the groups are statistically significant).

The p value is the probability of being wrong in concluding that there is a true difference in the groups (i.e., the probability of falsely rejecting the null hypothesis). The smaller the p value, the greater the probability that the samples are significantly

different. Traditionally, it can be concluded that there are significant differences when $p<0.05$.

Multiple Comparisons

If a difference is found among the groups, multiple comparison procedures can be performed which compares group pairs. Multiple comparison results were used to determine exactly which groups were different.

Pairwise comparison results listed comparisons of all possible combinations of group pairs. In this study, Dunn's Test was used to compare all groups. Dunn's test lists the difference of rank means, computes the Q test statistic and displays whether $p < 0.05$ for each group pair.

Large values of Q indicate that the difference between the two groups being compared is statistically significant. If the p value for the comparison is less than 0.05, the likelihood of being incorrect in concluding that there is a significant difference is less than 5%. If it is greater than 0.05, one cannot conclude confidently that there is a difference.

If a group is found to not be significantly different than another group, all groups with ranks in between the rank sums of the two groups that are not different are also assumed not to be significantly different, and a result of DNT (Do Not Test) is generated for those comparisons.

6.8 Neonatal trabecular results

Initially, pelvic specimens possessing both right and left ilia were subjected to a Mann-Whitney Rank Sum Test to test for a difference between right and left trabecular parameters which may be greater than what could be attributed to random sampling

variation. All trabecular parameters for right and left ilia from a single individual displayed no statistically significant differences (Table 6.1). Therefore, all ilia regardless of siding were grouped into a single cohort for overall trabecular analysis.

Specimen Pair	BV/TV	Tb.Th	Tb.Sp	Tb.N	SMI	DA
LTH/E	0.066	0.865	0.418	0.166	0.502	0.868
LTH/F	0.758	0.538	0.758	0.613	0.263	0.727
NP1	0.198	0.119	0.860	0.913	0.145	0.792
NP2	0.998	0.474	0.742	0.826	0.567	0.463
P1	0.989	0.455	0.843	0.764	0.860	0.810
SA/B	0.643	0.875	0.539	0.764	0.764	0.123
SA/E	0.653	0.334	0.143	0.568	0.626	0.929
SA/F	0.238	0.416	0.381	0.613	0.608	0.789
SA/J	0.184	0.830	0.558	0.294	0.070	0.514
SS3	0.719	0.991	0.913	0.739	0.051	0.998
STHB1	0.816	0.947	0.553	0.775	0.379	0.626
STHB2	0.551	0.725	0.913	0.613	0.203	0.947

Table 6.1. Statistical comparison of single specimen right/left pairs using Mann-Whitney Rank Sum Test. p values are displayed for each specimen pair and associated trabecular parameter. A statistically significant difference can be confirmed when $p < 0.05$. No statistically significant differences are observed between right/left specimen pairs.

Subsequently, an analysis of variance (ANOVA) test was performed between each VOI within a histomorphometric parameter grouping. For parametric data a parametric ANOVA test was used and for non-parametric data a Kruskal-Wallis one way analysis of variance on ranks test was used. These tests were used to determine overall significance between VOIs. Subsequently, pairwise multiple comparison procedures were performed to determine significance between individual VOIs within a parameter grouping. For parametric data the Holm-Sidak method was used. When performing this test, the p values of all comparisons were computed and ordered from smallest to largest. Each p value was then compared to a critical level that depends upon the significance level of the test ($P<0.05$), the rank of the p value, and the total number of comparisons made. A p value less than the critical level indicates there is a

significant difference between the corresponding two groups. For non-parametric data Dunn's method was used. Dunn's test lists the difference of rank means, computes the Q test statistic, and displays whether $p < 0.05$, for each group pair. This statistical test is aimed at determining statistically significant differences between selected volumes of interest.

The descriptive statistics, graphed data, summarised statistical significance and illustrated representation of each individual trabecular parameter analysed is presented. A full documentation of structural parameters for each individual specimen included in the neonatal cohort is presented in Appendix 1. Analysis of variance highlighted an overall significant difference between VOIs for each structural parameter (Table 6.2). Pairwise multiple comparisons further investigated relationships between individual regions. Summarised statistical significance is presented for each trabecular parameter measured. For full statistical significance between each VOI see Appendix 2. Descriptions of trabecular morphology will be based upon the regional terminology shown in Figure 6.3. Descriptions of regional trabecular morphology have been divided into groups with statistically similar values to aid understanding.

It is acknowledged that certain volumes of interest contributing to a single regional grouping may well be of a value which produces some ambiguity as to which grouping it should be attributed. However, for ease of interpretation, the regional grouping with which such an ambiguous VOI trabecular index is most akin, in terms of mean value, was chosen. This results in some volumes of interest not being statistically different, in certain trabecular characteristics, to a neighbouring regional grouping, see below for an example. However, a majority of VOIs for a particular grouping being statistically different to the majority of VOIs from a neighbouring regional grouping

was considered to be substantive evidence of trabecular patterning within the trabecular volume.

Trabecular Parameter	Statistic	Degrees of Freedom	p	Significance
BV/TV	H	22	<0.001	***
Tb.Th	H	22	<0.001	***
Tb.Sp	H	22	<0.001	***
Tb.N	H	22	<0.001	***
SMI	F	22	<0.001	***
DA	H	22	<0.001	***

Table 6.2: One way analysis of variance of between volume measurements. (see text for details) N.B: H=Kruskal-Wallis One-way ANOVA on Ranks for non parametric data F=parametric ANOVA. *** = very highly significant.

Bone Volume Fraction (BV/TV)

Table 6.3 displays the descriptive statistics for neonatal bone volume fraction (BV/TV) at each volume of interest. BV/TV for the neonatal ilium has been divided into three distinct regional groupings based on the percentage bone volume observed within volumes of interest (Figures 6.11 - 6.13). Volumes of interest contributing to a group generally display no statistical difference between each other, although as mentioned above there were some exceptions (VOIs 7v23; 14v19; 15v19) (Figure 6.12). The regional grouping which displayed higher BV/TV (34.866 – 43.475 %) comprised volumes corresponding to the superior perimeter (VOIs 1, 2&6), posterior auricular (VOIs 3&7), anterior perimeter (VOIs 11&16) and acetabular regions (VOIs 21-23). A decrease in BV/TV (30.857 – 34.415 %) was observed in the superior body of the ilium (VOIs 4&5), anterior central body (VOI 10) and at the caudal limb of the auricular surface (VOIs 12&13). A further decrease in BV/TV (18.909 – 30.021 %) was observed in the cranial auricular surface (VOI 8), central body of the ilium (VOI 9), the

trabecular chiasma region (VOIs 14&15), greater sciatic notch region (VOI 17), and inferior body (VOIs 18-20).

Differentiation of certain VOIs into a particular grouping for BV/TV is somewhat ambiguous whereby arguments can be made for inclusion of a single VOI in more than one regional grouping. This required that a defining value be chosen to which values above and below this value could be defined into separate groupings. This problem arose when placing VOIs 5 and 7 into different groupings based on their statistical significance to other VOI's in their respective groupings. As VOIs 5 and 7 have very similar values, a BV/TV of 34.50% was chosen as a discriminating arbitrary value upon which VOIs greater than this value were defined within the higher BV/TV grouping and VOIs below this value were defined as the intermediate BV/TV grouping.

Inter-specimen variation was assessed by the application of the coefficient of variation (CV) which is a useful statistic for indicating the variation of values within a sample. Coefficient of variation for BV/TV highlighted that the inter-specimen variation was low for all volumes of interest. However, although an overall low value of CV was observed, certain volumes displayed marginally higher values for CV, these included the central body, trabecular chiasma and inferior body regions.

	BV/TV (%)				
	MEAN	RANGE		SD (±)	CV (%)
VOI		MIN	MAX		
1	36.891	30.311	44.028	3.639	9.864
2	40.377	32.627	48.771	3.865	9.572
3	37.820	29.547	46.753	4.776	12.628
4	33.460	24.089	41.969	5.105	15.257
5	34.415	26.686	43.553	4.179	12.143
6	35.655	22.034	42.434	4.245	11.906
7	34.866	27.779	43.941	3.897	11.177
8	26.734	21.265	33.818	3.034	11.349
9	21.710	15.622	32.254	3.898	17.955
10	30.857	18.007	40.114	5.224	16.930
11	37.655	27.868	46.781	4.950	13.146
12	33.022	26.700	38.583	3.031	9.179
13	31.953	21.347	39.865	4.206	13.163
14	18.909	12.836	26.186	2.927	15.479
15	19.013	13.209	26.909	3.600	18.934
16	41.044	32.671	47.810	3.813	9.290
17	25.998	18.022	31.385	3.660	14.078
18	29.126	21.621	41.165	4.695	16.120
19	30.021	20.831	40.399	5.536	18.440
20	25.659	15.879	32.713	4.440	17.304
21	42.751	24.727	56.272	6.326	14.797
22	39.374	29.094	46.394	5.208	13.227
23	43.475	33.248	51.127	4.268	9.817

Table 6.3. Descriptive statistics (mean, range, standard deviation and coefficient of variation) for neonatal bone volume fraction (BV/TV) at each volume of interest (VOI). Data for individual specimens can be found in Appendix 1.

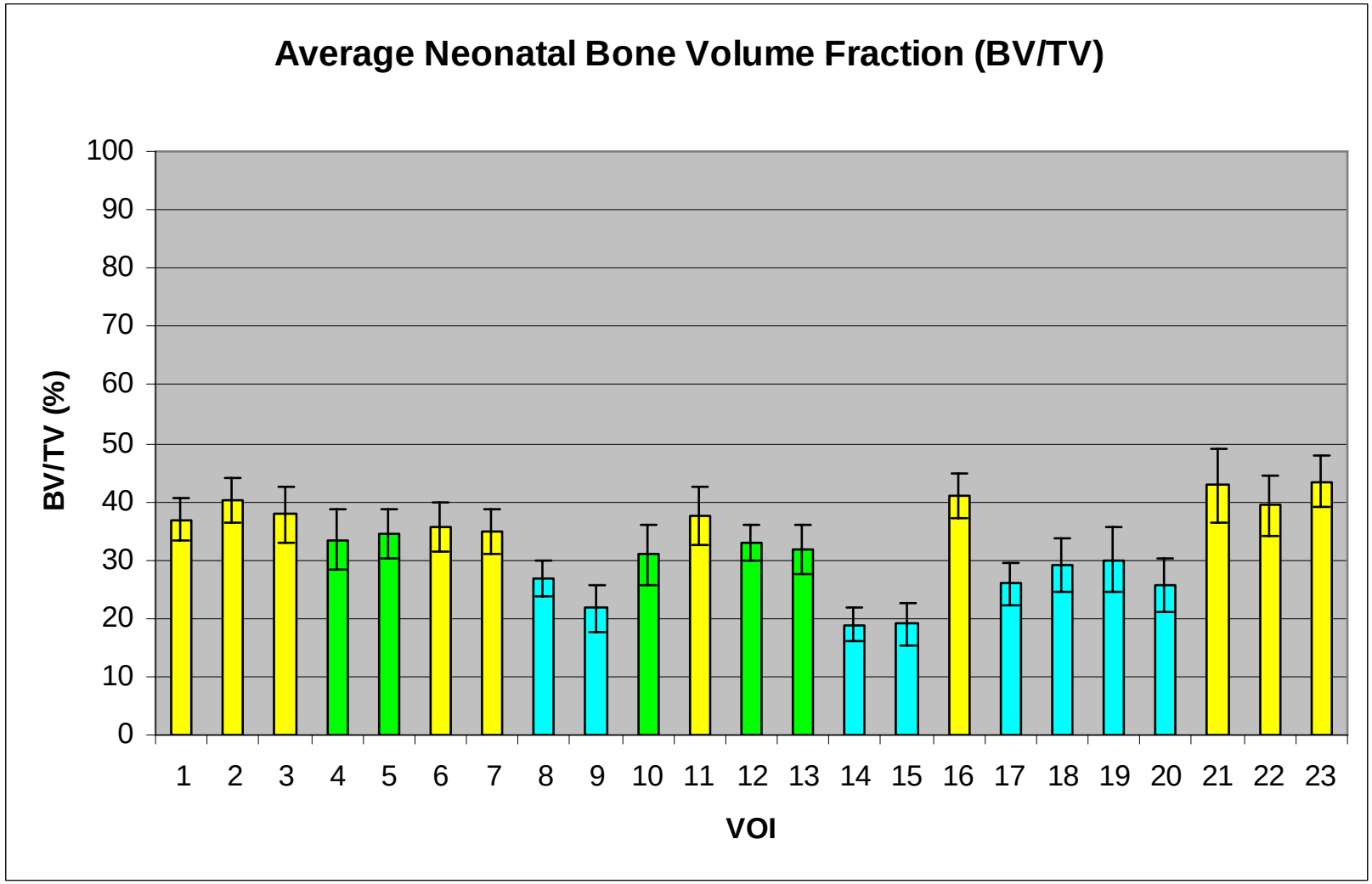

Figure 6.11. Graphic representation of mean (± SD) bone volume fraction at each volume of interest. High (yellow), medium (green) and low (blue) bone volume fraction.

BV/TV																						
2	N																					
3	N	N																				
4	N	N	N																			
5	N	N	N	N																		
6	N	N	N	N	N																	
7	N	N	N	N	N	N																
8	Y	Y	Y	N	Y	Y	Y															
9	Y	Y	Y	Y	Y	Y	Y	N														
10	N	Y	N	N	N	N	N	N	N													
11	N	N	N	N	N	N	N	Y	Y	N												
12	N	Y	N	N	N	N	N	N	Y	N	N											
13	N	Y	N	N	N	N	N	N	Y	N	N	N										
14	Y	Y	Y	Y	Y	Y	Y	N	N	Y	Y	Y	Y									
15	Y	Y	Y	Y	Y	Y	Y	N	N	Y	Y	Y	Y	N								
16	N	N	N	Y	N	N	N	Y	Y	Y	N	Y	Y	Y	Y							
17	Y	Y	Y	N	Y	Y	Y	N	N	N	Y	N	N	N	N	Y						
18	Y	Y	Y	N	N	N	N	N	N	N	Y	N	N	N	N	Y	N					
19	N	Y	Y	N	N	N	N	N	N	N	Y	N	N	Y	Y	Y	N	N				
20	Y	Y	Y	N	Y	Y	Y	N	N	N	Y	N	N	N	N	Y	N	N	N			
21	N	N	N	Y	N	N	N	Y	Y	Y	N	Y	Y	Y	Y	N	Y	Y	Y	Y		
22	N	N	N	N	N	N	N	Y	Y	Y	N	N	Y	Y	Y	N	Y	Y	Y	Y	N	
23	N	N	N	Y	Y	N	Y	Y	Y	Y	N	Y	Y	Y	Y	N	Y	Y	Y	Y	N	N
VOI	1	2	3	4	5	6	7	8	9	10	11	12	13	14	15	16	17	18	19	20	21	22

Figure 6.12: Pairwise multiple comparison of parameters between individual volumes. Non-parametric data was produced using Dunn's test. Statistical output has been summarised to illustrate which volumes are statistically similar. Y=significant difference; N=no significant difference. VOI groupings have been coloured to aid interpretation. High (yellow), medium (green), low (blue) bone volume fraction (BV/TV). Full statistical data can be found in Appendix 2.

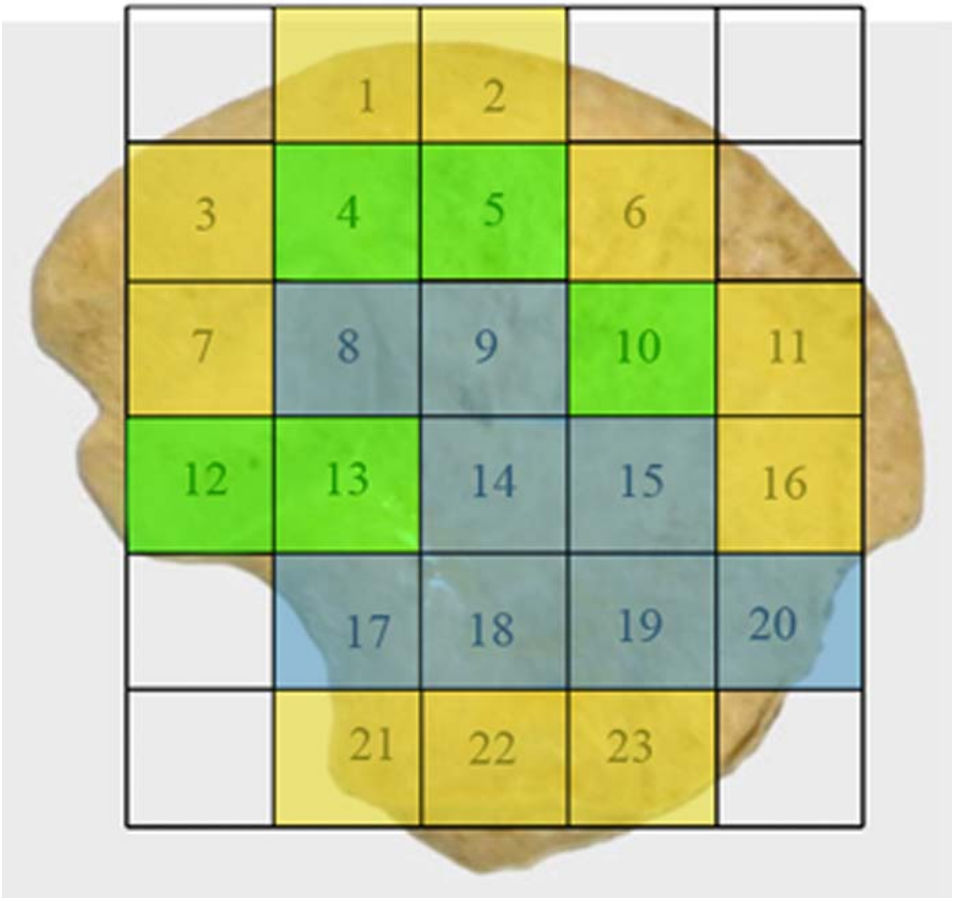

Figure 6.13. Coloured map representing regional groupings with statistically similar trabecular characteristics taken from Table 6.3. High (yellow), medium (green) and low (blue) bone volume fraction (BV/TV).

Trabecular Thickness (Tb.Th)

Table 6.4 displays the descriptive statistics for neonatal trabecular thickness (Tb.Th) at each volume of interest (VOI). Tb.Th within the neonatal ilium can be defined by three different groupings (Figures 6.14 - 6.16). There is no statistical difference between volumes of interest that contribute to a single group (Figure 6.15). The first of these regional groupings with the lowest values for Tb.Th (0.146 – 0.162 mm) is observed in the superior perimeter (VOIs 1, 2&6), posterior auricular region (VOI 3), superior and central body (VOIs 5, 9&10), anterior perimeter (VOIs 11&16), and the acetabular component (VOIs 21-23). Increased trabecular thickness volumes (0.165 – 0.175 mm)

are located in the cranial limb of the auricular surface (VOI 4&8), posterior auricular aspects of the ilium (VOI 7), and the inferior body (VOIs 18-20). The thickest trabeculae (0.186 – 0.223 mm) are located at the caudal auricular volume (VOI 12&13), trabecular chiasma (VOIs 14&15), and greater sciatic notch (VOI 17).

As described for BV/TV, differentiation of certain VOI's into a particular grouping was ambiguous for Tb.Th, where a single VOI may be included in more than one regional grouping. This occurred when differentiating VOIs 3 and 19 based upon their statistical significance to other VOIs in their respective groupings. As VOIs 3 and 19 have similar values, a Tb.Th of 0.165 was chosen as an arbitrary discriminatory value upon which VOIs lower than this were placed in the lowest Tb.Th grouping and VOIs higher than this were placed in the intermediate Tb.Th grouping.

The coefficient of variation for trabecular thickness, as a measure of inter-specimen variation, was observed to be a maintained low value representing minimal variation within the sample for each volume of interest.

	Tb.Th (mm)				
	MEAN	RANGE		SD (±)	CV (%)
VOI		MIN	MAX		
1	0.146	0.122	0.187	0.014	9.589
2	0.148	0.126	0.170	0.012	8.108
3	0.162	0.145	0.178	0.009	5.556
4	0.169	0.151	0.193	0.012	7.101
5	0.148	0.123	0.171	0.010	6.757
6	0.145	0.120	0.180	0.013	8.966
7	0.174	0.149	0.197	0.012	6.897
8	0.175	0.156	0.200	0.009	5.143
9	0.156	0.123	0.186	0.016	10.256
10	0.148	0.121	0.184	0.012	8.108
11	0.150	0.133	0.163	0.009	6.000
12	0.223	0.191	0.262	0.021	9.417
13	0.220	0.192	0.250	0.016	7.273
14	0.209	0.169	0.266	0.021	10.048
15	0.186	0.142	0.223	0.024	12.903
16	0.157	0.139	0.178	0.011	7.006
17	0.204	0.168	0.243	0.019	9.314
18	0.166	0.134	0.193	0.012	7.229
19	0.165	0.142	0.190	0.011	6.667
20	0.168	0.147	0.233	0.021	12.500
21	0.151	0.131	0.177	0.013	8.609
22	0.153	0.131	0.178	0.012	7.843
23	0.157	0.136	0.184	0.011	7.006

Table 6.4. Descriptive statistics (mean, range, standard deviation and coefficient of variation) for neonatal trabecular thickness (Tb.Th) at each volume of interest (VOI). Data for individual specimens can be found in Appendix 1.

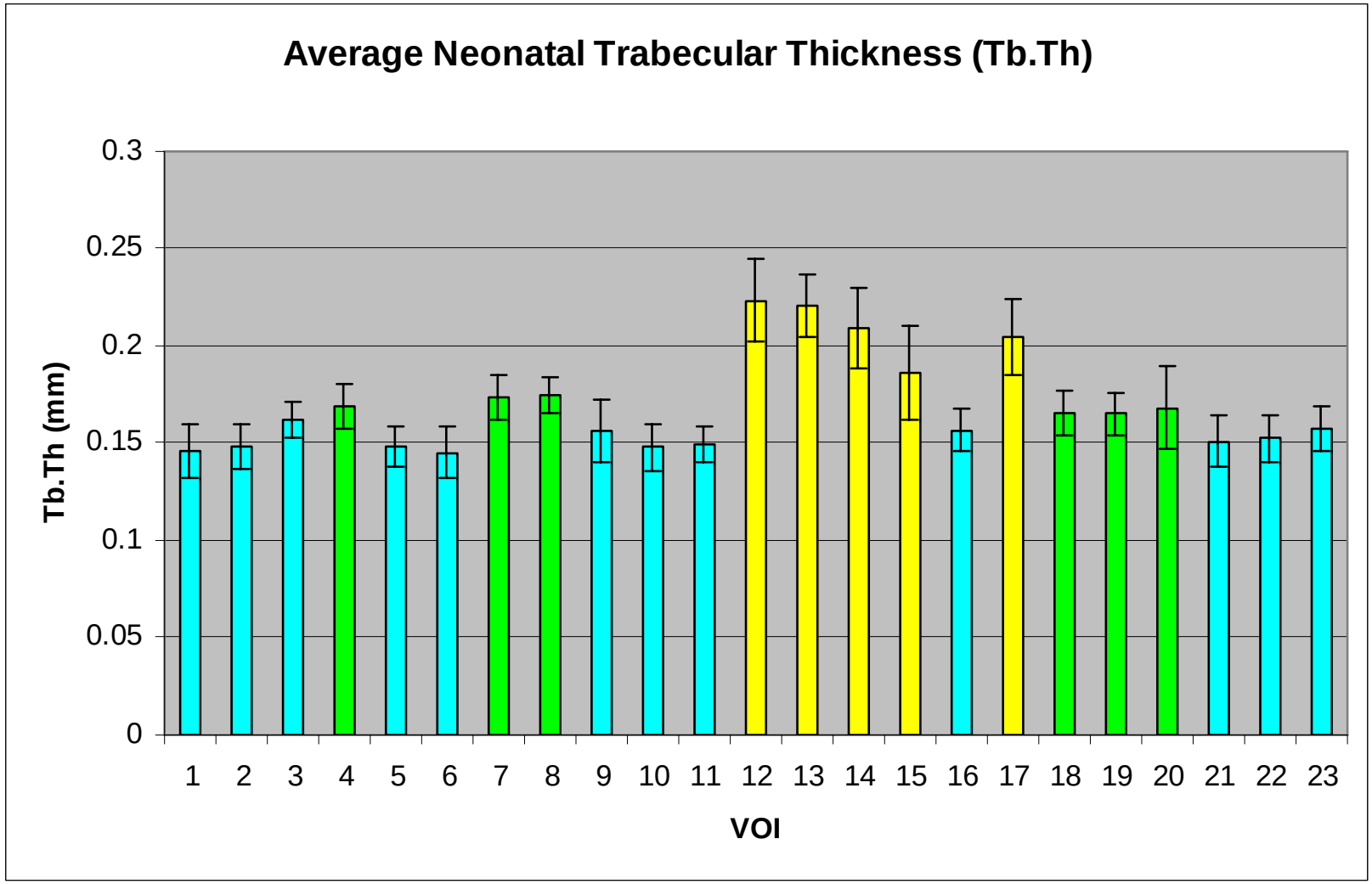

Figure 6.14. Graphic representation of mean (± SD) trabecular thickness at each volume of interest. High (yellow), medium (green) and low (blue) trabecular thickness.

Tb.Th																						
2	N																					
3	N	N																				
4	Y	Y	N																			
5	N	N	N	Y																		
6	N	N	N	Y	N																	
7	Y	Y	N	N	Y	Y																
8	Y	Y	N	N	Y	Y	N															
9	N	N	N	N	N	N	N	N														
10	N	N	N	Y	N	N	Y	Y	N													
11	N	N	N	Y	N	N	Y	Y	N	N												
12	Y	Y	Y	Y	Y	Y	N	N	Y	Y	Y											
13	Y	Y	Y	Y	Y	Y	N	N	Y	Y	Y	N										
14	Y	Y	Y	N	Y	Y	N	N	Y	Y	Y	N	N									
15	Y	Y	N	N	Y	Y	N	N	Y	Y	Y	N	N	N								
16	N	N	N	N	N	N	N	N	N	N	N	Y	Y	Y	Y							
17	Y	Y	Y	N	Y	Y	N	N	Y	Y	Y	N	N	N	N	Y						
18	Y	N	N	N	Y	Y	N	N	N	Y	N	Y	Y	Y	N	N	Y					
19	Y	N	N	N	N	Y	N	N	N	N	N	Y	Y	Y	N	N	Y	N				
20	Y	N	N	N	N	Y	N	N	N	N	N	Y	Y	Y	N	N	Y	N	N			
21	N	N	N	Y	N	N	Y	Y	N	N	N	Y	Y	Y	Y	N	Y	N	N	N		
22	N	N	N	N	N	N	Y	Y	N	N	N	Y	Y	Y	Y	N	Y	N	N	N	N	
23	N	N	N	N	N	N	N	N	N	N	N	Y	Y	Y	Y	N	Y	N	N	N	N	N
VOI	1	2	3	4	5	6	7	8	9	10	11	12	13	14	15	16	17	18	19	20	21	22

Figure 6.15: Pairwise multiple comparison of parameters between individual volumes. Non-parametric data was produced using Dunn's test. Statistical output has been summarised to illustrate which volumes are statistically similar. Y=significant difference; N=no significant difference. VOI groupings have been coloured to aid interpretation. High (yellow), medium (green), low (blue) trabecular thickness (Tb.Th). Full statistical data can be found in Appendix 2.

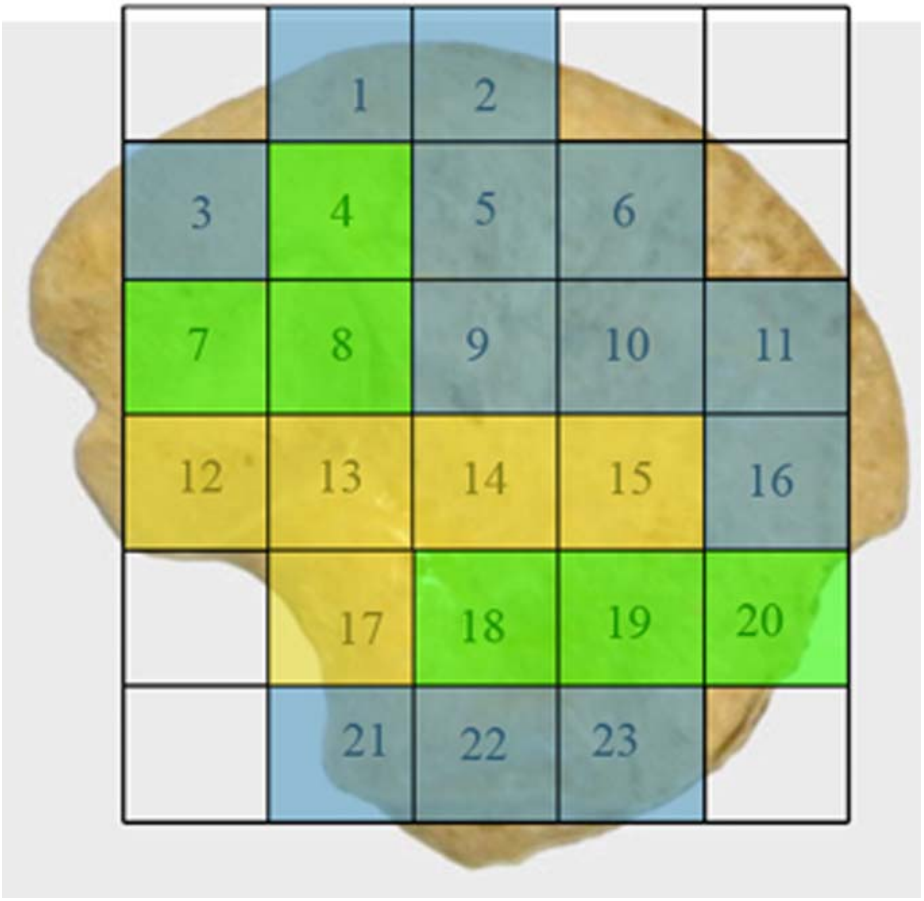

Figure 6.16. Coloured map representing regional groupings with statistically similar trabecular characteristics taken from Table 6.4. High (yellow), medium (green), low (blue) trabecular thickness (Tb.Th).

Trabecular Separation (Tb.Sp)

Table 6.5 displays the descriptive statistics for trabecular separation (Tb.Sp) at each volume of interest (VOI). Tb.Sp within the neonatal ilium can be defined by three different groupings (Figure 6.17 - 6.19). Volumes of interest that contribute to a single group display no statistical difference between values except (VOI 2v10) (Figure 6.18). Values are lowest (0.210 – 0.270 mm) in the superior perimeter (VOI 1, 2&6), posterior auricular (VOI 3), superior and central body (VOIs 5&10), anterior perimeter (VOI 11&16), and the acetabular component of the ilium (VOIs 21-23). Increased values of Tb.Sp (0.291 – 0.359 mm) are observed in the cranial limb of the auricular surface and surrounding volumes (VOI 4,7&8), central body (VOI 9), and in the inferior body

(VOIs 18-20). The final and largest value of average Tb.Sp (0.414 – 0.548 mm) is observed to be located in the caudal limb of the auricular surface (VOIs 12&13), the trabecular chiasma region (VOIs 14&15), and the sciatic notch region (VOI 17).

Coefficient of variation for trabecular separation again presented as a relatively low value across all volumes of interest. Those volumes which displayed a marginally increased value for coefficient of variation, reflective of increased inter-specimen variation, included the cranial auricular, central body, trabecular chiasma and anterior inferior body regions.

	Tb.Sp (mm)				
	MEAN	RANGE		SD (±)	CV (%)
VOI		MIN	MAX		
1	0.226	0.180	0.305	0.026	11.504
2	0.21	0.172	0.246	0.018	8.571
3	0.244	0.201	0.298	0.025	10.246
4	0.304	0.232	0.447	0.053	17.434
5	0.252	0.196	0.325	0.035	13.889
6	0.23	0.199	0.265	0.018	7.826
7	0.291	0.210	0.337	0.032	10.997
8	0.38	0.265	0.480	0.058	15.263
9	0.359	0.251	0.482	0.067	18.663
10	0.27	0.221	0.331	0.036	13.333
11	0.225	0.193	0.265	0.024	10.667
12	0.414	0.320	0.537	0.063	15.217
13	0.433	0.303	0.635	0.072	16.628
14	0.548	0.391	0.800	0.112	20.438
15	0.509	0.332	0.699	0.097	19.057
16	0.225	0.181	0.295	0.031	13.778
17	0.455	0.350	0.582	0.07	15.385
18	0.328	0.234	0.404	0.051	15.549
19	0.317	0.215	0.420	0.048	15.142
20	0.341	0.268	0.547	0.057	16.716
21	0.218	0.167	0.254	0.025	11.468
22	0.239	0.195	0.305	0.025	10.460
23	0.22	0.180	0.306	0.026	11.818

Table 6.5. Descriptive statistics (mean, range, standard deviation and coefficient of variation) for neonatal trabecular separation (Tb.Sp) at each volume of interest (VOI). Data for individual specimens can be found in Appendix 1.

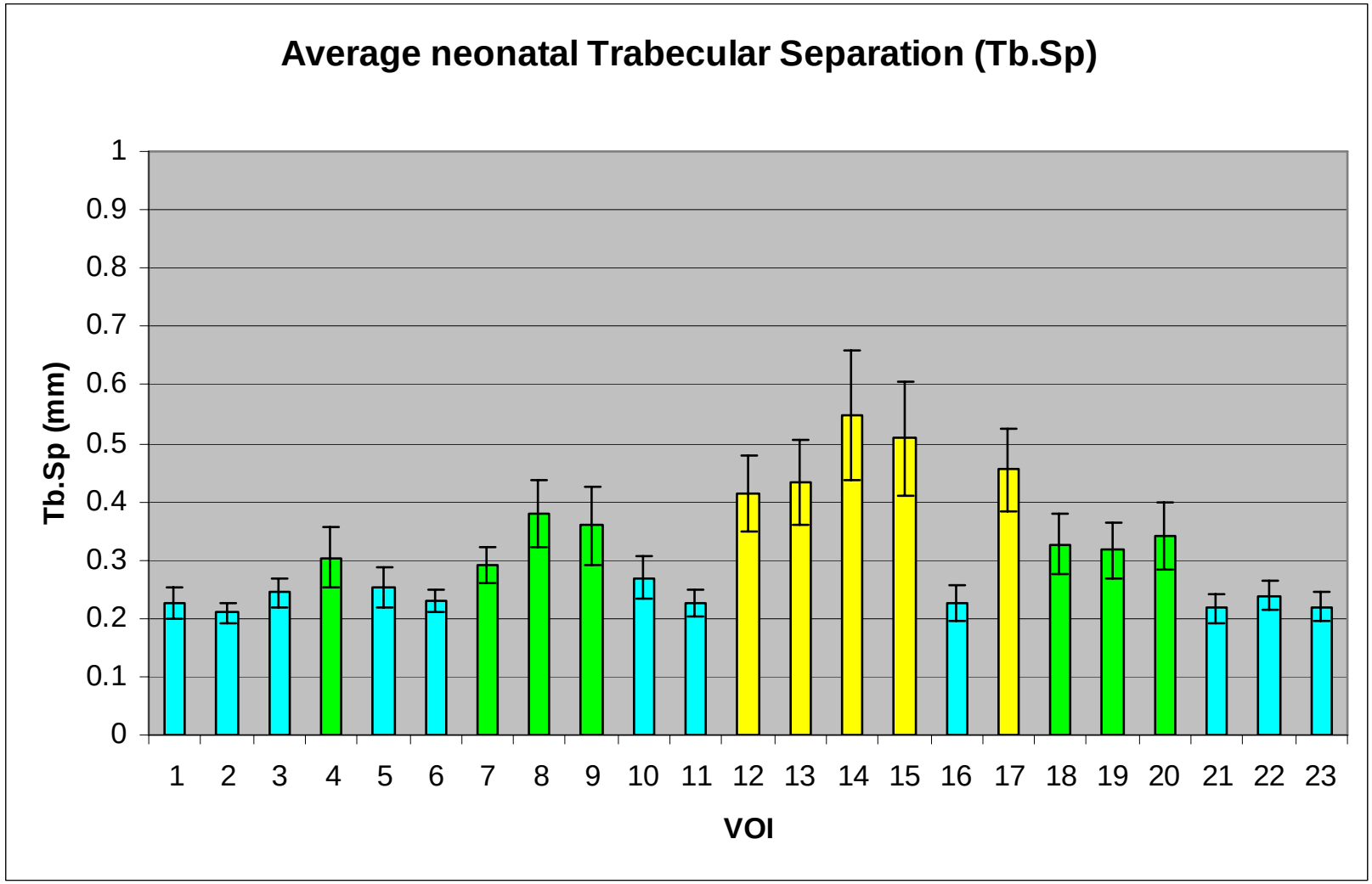

Figure 6.17. Graphic representation of mean (± SD) trabecular separation at each volume of interest. High (yellow), medium (green) and low (blue) trabecular separation.

Tb.Sp																						
2	N																					
3	N	N																				
4	Y	Y	N																			
5	N	N	N	N																		
6	N	N	N	Y	N																	
7	Y	Y	N	N	N	N																
8	Y	Y	Y	N	Y	Y	N															
9	Y	Y	Y	N	Y	Y	N	N														
10	N	Y	N	N	N	N	N	Y	N													
11	N	N	N	Y	N	N	Y	Y	Y	N												
12	Y	Y	Y	N	Y	Y	N	N	N	Y	Y											
13	Y	Y	Y	N	Y	Y	Y	N	N	Y	Y	N										
14	Y	Y	Y	Y	Y	Y	Y	N	N	Y	Y	N	N									
15	Y	Y	Y	Y	Y	Y	Y	N	N	Y	Y	N	N	N								
16	N	N	N	Y	N	N	Y	Y	Y	N	N	Y	Y	Y	Y							
17	Y	Y	Y	Y	Y	Y	Y	N	N	Y	Y	N	N	N	N	Y						
18	Y	Y	Y	N	N	Y	N	N	N	N	Y	N	N	Y	N	Y	N					
19	Y	Y	N	N	N	Y	N	N	N	N	Y	N	N	Y	Y	Y	N	N				
20	Y	Y	Y	N	Y	Y	N	N	N	N	Y	N	N	N	N	Y	N	N	N			
21	N	N	N	Y	N	N	Y	Y	Y	N	N	Y	Y	Y	Y	N	Y	Y	Y	Y		
22	N	N	N	N	N	N	N	Y	Y	N	N	Y	Y	Y	Y	N	Y	Y	Y	Y	N	
23	N	N	N	Y	N	N	Y	Y	Y	N	N	Y	Y	Y	Y	N	Y	Y	Y	Y	N	N
VOI	1	2	3	4	5	6	7	8	9	10	11	12	13	14	15	16	17	18	19	20	21	22

Figure 6.18. Pairwise multiple comparison of parameters between individual volumes. Non-parametric data was produced using Dunn's test. Statistical output has been summarised to illustrate which volumes are statistically similar. Y=significant difference; N=no significant difference. VOI groupings have been coloured to aid interpretation. High (yellow), medium (green), low (blue) trabecular separation (Tb.Sp). Full statistical data can be found in Appendix 2.

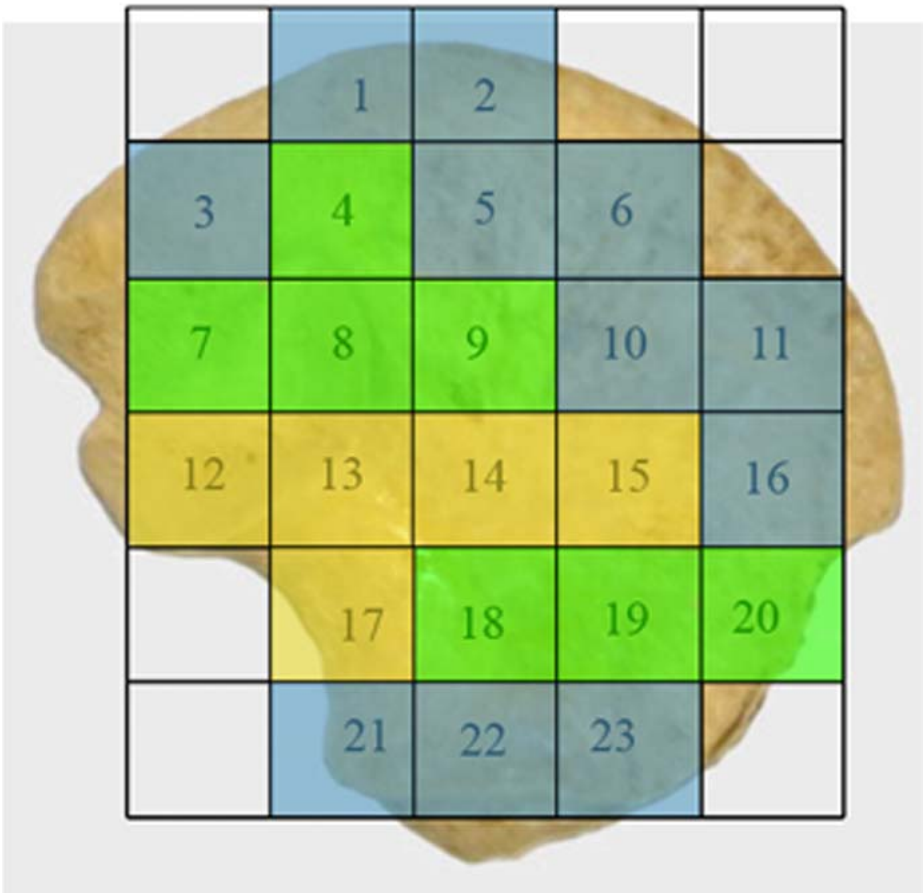

Figure 6.19. Coloured map representing regional groupings with statistically similar trabecular characteristics taken from Table 6.5. High (yellow), medium (green) and low (blue) trabecular separation (Tb.Sp).

Trabecular Number (Tb.N)

Table 6.6 displays the descriptive statistics for trabecular number (Tb.N) at each volume of interest (VOI). Tb.N within the neonatal ilium can be defined by three different groupings (Figures 6.20 - 6.22). Volumes of interest that contribute to a single group display no statistical difference between values, with one exception (VOI 9v10) (Figure 6.21). The highest values of Tb.N (2.818 – 2.335 mm^{-1}) are observed in the superior perimeter (VOIs 1,2&6), posterior auricular (VOI 3), superior body (VOI 5), anterior perimeter regions (VOIs 11&16), and in the acetabular component of the ilium (VOIs 21-23). Reduced values of Tb.N (2.087 – 1.405 mm^{-1}) are observed in regions

corresponding to the superior body volume (VOI 4), posterior auricular (VOI 7), cranial and caudal auricular volumes (VOIs 8, 12&13), the central body (VOI 9&10) and inferior body regions (VOIs 18-20). The final and lowest values of average Tb.N (1.277 - 0.907 mm^{-1}) are observed in the trabecular chiasma (VOIs 14&15), and greater sciatic notch region (VOI 17).

Coefficient of variation for trabecular number was again observed to be a low value within the majority of trabecular bone volumes. Regions which displayed higher values for coefficient of variation, reflective of increased inter-specimen variation, included volumes associated with the cranial auricular, central body, trabecular chiasma and inferior body.

	Tb.N (1/mm)				
	MEAN	RANGE		SD (±)	CV (%)
VOI		MIN	MAX		
1	2.533	1.958	2.963	0.197	7.777
2	2.723	2.452	3.215	0.201	7.382
3	2.335	1.807	2.848	0.283	12.120
4	1.995	1.247	2.657	0.374	18.747
5	2.338	1.825	3.094	0.302	12.917
6	2.46	1.618	2.905	0.242	9.837
7	2.011	1.564	2.589	0.221	10.990
8	1.538	1.065	2.040	0.208	13.524
9	1.405	1.033	2.339	0.292	20.783
10	2.087	1.329	2.751	0.325	15.573
11	2.514	1.760	3.055	0.3	11.933
12	1.492	1.195	1.859	0.188	12.601
13	1.457	0.969	1.865	0.205	14.070
14	0.907	0.580	1.200	0.138	15.215
15	1.046	0.660	1.795	0.283	27.055
16	2.63	2.010	3.053	0.269	10.228
17	1.277	0.872	1.625	0.169	13.234
18	1.763	1.337	2.468	0.285	16.166
19	1.816	1.448	2.329	0.327	18.007
20	1.546	0.794	1.988	0.321	20.763
21	2.818	1.784	3.821	0.392	13.911
22	2.583	1.744	3.290	0.302	11.692
23	2.77	1.803	3.229	0.273	9.856

Table 6.6. Descriptive statistics (mean, range, standard deviation and coefficient of variation) for neonatal trabecular number (Tb.N) at each volume of interest (VOI). Data for individual specimens can be found in Appendix 1.

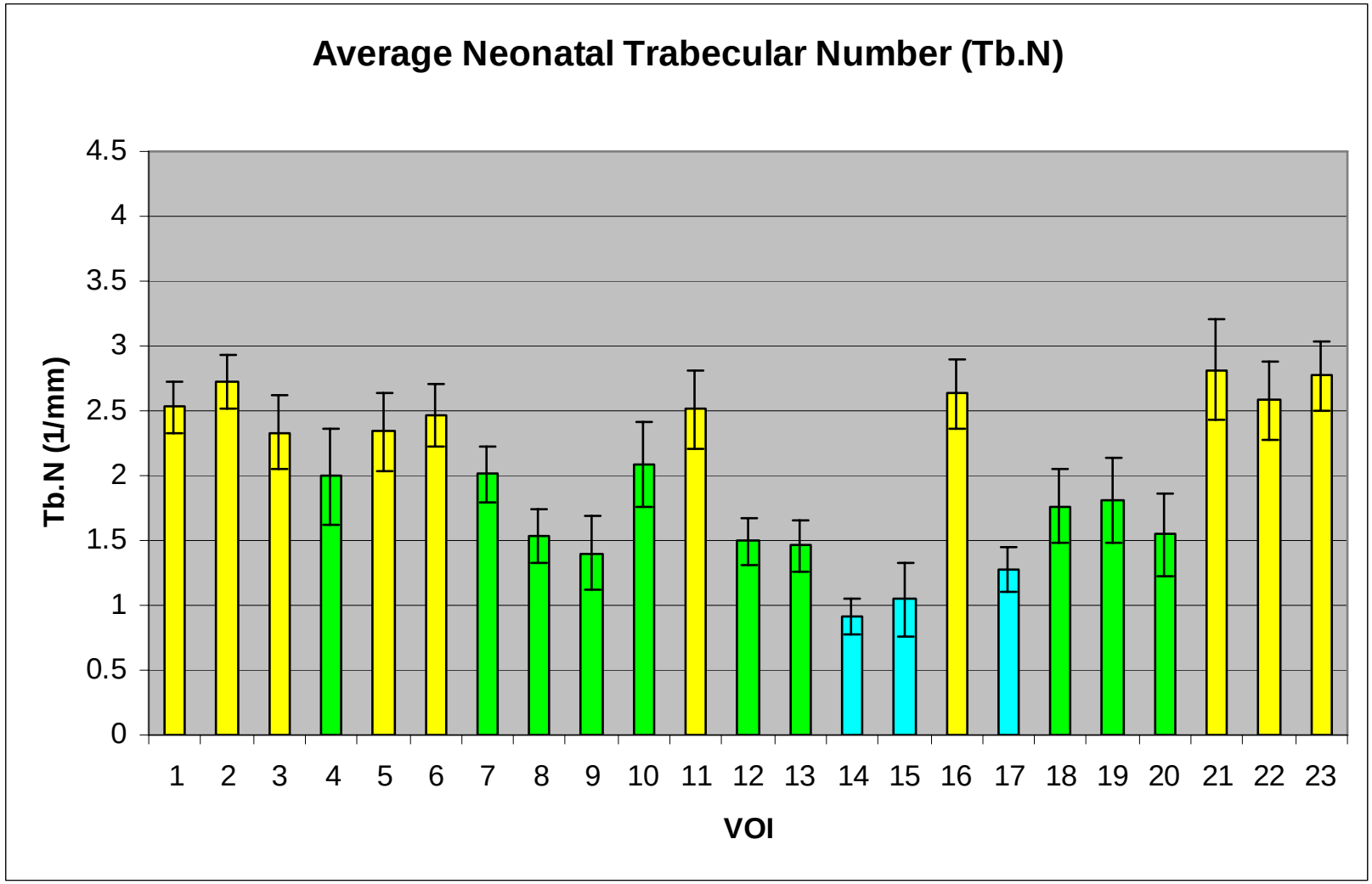

Figure 6.20. Graphic representation of mean (± SD) trabecular number at each volume of interest. High (yellow), medium (green) and low (blue) trabecular number.

Tb.N																						
2	N																					
3	N	N																				
4	N	Y	N																			
5	N	N	N	N																		
6	N	N	N	N	N																	
7	N	Y	N	N	N	N																
8	Y	Y	Y	N	Y	Y	N															
9	Y	Y	Y	N	Y	Y	N	N														
10	N	Y	N	N	N	N	N	N	Y													
11	N	N	N	N	N	N	N	Y	Y	N												
12	Y	Y	Y	N	Y	Y	N	N	N	N	Y											
13	Y	Y	Y	N	Y	Y	N	N	N	N	Y	N										
14	Y	Y	Y	Y	Y	Y	Y	N	N	Y	Y	N	N									
15	Y	Y	Y	Y	Y	Y	Y	N	N	Y	Y	N	N	N								
16	N	N	N	Y	N	N	Y	Y	Y	N	N	Y	Y	Y	Y							
17	Y	Y	Y	Y	Y	Y	Y	N	N	Y	Y	N	N	N	N	Y						
18	Y	Y	N	N	N	Y	N	N	N	N	Y	N	N	Y	N	Y	N					
19	Y	Y	N	N	N	Y	N	N	N	N	Y	N	N	Y	Y	Y	N	N				
20	Y	Y	Y	N	Y	Y	N	N	N	N	Y	N	N	N	N	Y	N	N	N			
21	N	N	N	Y	N	N	Y	Y	Y	Y	N	Y	Y	Y	Y	N	Y	Y	Y	Y		
22	N	N	N	N	N	N	N	Y	Y	N	N	Y	Y	Y	Y	N	Y	Y	Y	Y	N	
23	N	N	N	Y	N	N	Y	Y	Y	Y	N	Y	Y	Y	Y	N	Y	Y	Y	Y	N	N
VOI	1	2	3	4	5	6	7	8	9	10	11	12	13	14	15	16	17	18	19	20	21	22

Figure 6.21: Pairwise multiple comparison of parameters between individual volumes. Non-parametric data was produced using Dunn's test. Statistical output has been summarised to illustrate which volumes are statistically similar. Y=significant difference; N=no significant difference. VOI groupings have been coloured to aid interpretation. High (yellow), medium (green), low (blue) trabecular number (Tb.N). Full statistical data can be found in Appendix 2.

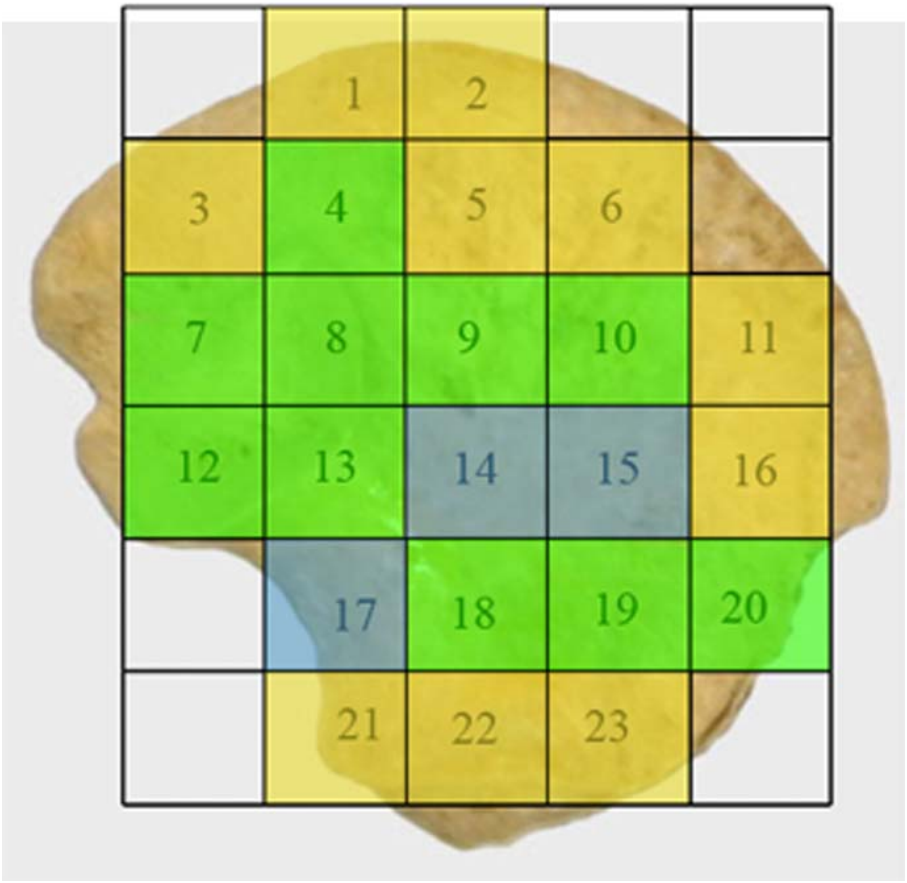

Figure 6.22. Coloured map representing regional groupings with statistically similar trabecular characteristics taken from Table 6.6. High (yellow), medium (green), low (blue) trabecular number (Tb.N).

Structural Model Index (SMI)

Table 6.7 displays the descriptive statistics for structural model index (SMI) at each volume of interest (VOI). SMI for the neonatal ilium is observed within a range of values indicative of a more plate-like model of trabecular organisation (an SMI of between 0-3) (Figure 6.23). Although significant differences for SMI are observed between certain volumes of interest all values lie within the more plate-like morphology category. Within the plate-like morphology, the values for the SMI within the neonatal ilium can be defined by three different groupings (Figures 6.23 - 6.25). Volumes of interest contributing to a single group display no statistical difference between values

(Figure 6.24). Highest values of SMI which tend more towards a rod-like morphology (2.011 – 1.977) are located in the trabecular chiasma region (VOIs 14&15). Intermediate values of plate-like morphology (1.678 – 1.418) are located at the greater sciatic notch (VOI 17), inferior body (VOIs 18-20), auricular surface (VOIs 8, 12&13) and superior and central body (VOIs 5, 9&10). Lowest values of SMI (1.352 – 1.155) are located in superior and anterior perimeter volumes (VOIs 1,2,4,6,11&16), posterior auricular (VOIs 3&7) and acetabular (VOIs 21-23) volumes of interest.

Coefficient of variation for structural model index presented with higher values than those observed for previous trabecular indices. This is due to the fact that when the mean value is near zero, the coefficient of variation is sensitive to small changes in the mean, thus limiting its usefulness.

	SMI				
	MEAN	RANGE		SD (±)	CV (%)
VOI		MIN	MAX		
1	1.27	0.769	1.749	0.241	18.976
2	1.155	0.814	1.600	0.25	21.645
3	1.224	0.387	1.860	0.311	25.408
4	1.249	0.716	1.929	0.29	23.219
5	1.418	1.028	1.975	0.288	20.310
6	1.351	0.841	1.978	0.279	20.651
7	1.352	0.435	1.883	0.352	26.036
8	1.632	0.948	2.105	0.287	17.586
9	1.547	1.001	1.993	0.281	18.164
10	1.532	1.023	1.977	0.273	17.820
11	1.26	0.748	1.662	0.223	17.698
12	1.498	1.046	1.897	0.23	15.354
13	1.424	0.943	1.867	0.243	17.065
14	2.011	1.285	2.488	0.313	15.564
15	1.977	1.545	2.621	0.337	17.046
16	1.254	0.223	1.832	0.329	26.236
17	1.505	0.573	2.089	0.441	29.302
18	1.432	0.908	2.037	0.298	20.810
19	1.469	1.044	1.889	0.272	18.516
20	1.678	1.191	2.423	0.367	21.871
21	1.328	1.016	1.193	0.223	16.792
22	1.206	0.131	1.794	0.358	29.685
23	1.325	0.813	1.818	0.311	23.472

Table 6.7. Descriptive statistics (mean, range, standard deviation and coefficient of variation) for neonatal structural model index (SMI) at each volume of interest (VOI). Data for individual specimens can be found in Appendix 1.

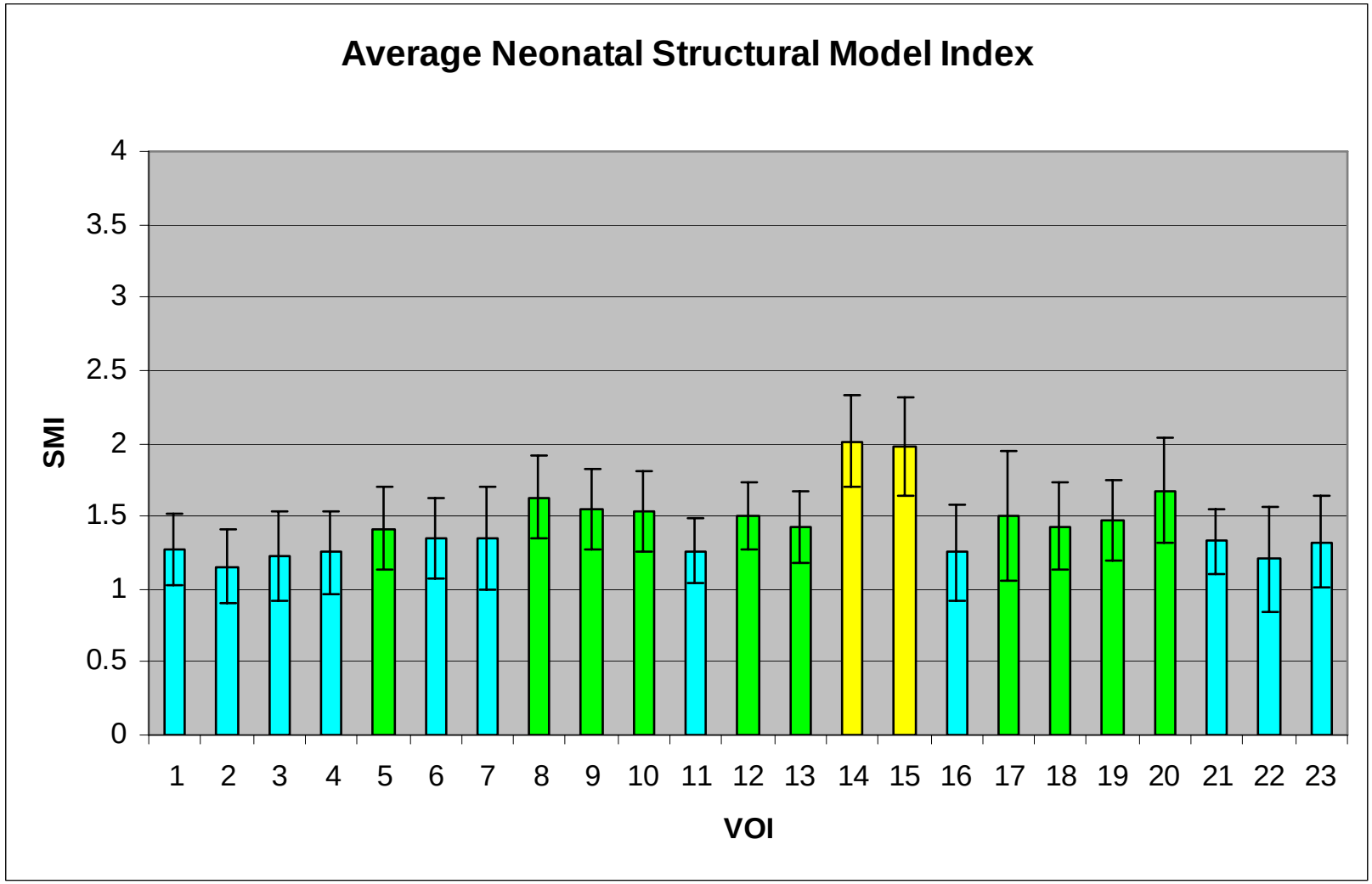

Figure 6.23. Graphic representation of mean (± SD) structural model index at each volume of interest. High (yellow), intermediate (green) and low (blue) values of structural model index.

SMI																						
2	N																					
3	N	N																				
4	N	N	N																			
5	N	N	N	N																		
6	N	N	N	N	N																	
7	N	N	N	N	N	N																
8	Y	Y	Y	Y	N	N	N															
9	N	Y	Y	Y	N	N	N	N														
10	N	Y	Y	N	N	N	N	N	N													
11	N	N	N	N	N	N	N	Y	N	N												
12	N	Y	N	N	N	N	N	N	N	N	N											
13	N	N	N	N	N	N	N	N	N	N	N	N										
14	Y	Y	Y	Y	Y	Y	Y	Y	Y	Y	Y	Y	Y									
15	Y	Y	Y	Y	Y	Y	Y	Y	Y	Y	Y	Y	Y	N								
16	N	N	N	N	N	N	N	Y	N	N	N	N	N	Y	Y							
17	N	Y	N	N	N	N	N	N	N	N	N	N	N	Y	Y	N						
18	N	N	N	N	N	N	N	N	N	N	N	N	N	Y	Y	N	N					
19	N	Y	N	N	N	N	N	N	N	N	N	N	N	Y	Y	N	N	N				
20	Y	Y	Y	Y	N	Y	Y	N	N	N	Y	N	N	Y	N	Y	N	N	N			
21	N	N	N	N	N	N	N	Y	N	N	N	N	N	Y	Y	N	N	N	N	Y		
22	N	N	N	N	N	N	N	Y	Y	Y	N	N	N	Y	Y	N	N	N	N	Y	N	
23	N	N	N	N	N	N	N	Y	N	N	N	N	N	Y	Y	N	N	N	N	Y	N	N
VOI	1	2	3	4	5	6	7	8	9	10	11	12	13	14	15	16	17	18	19	20	21	22

Figure 6.24: Pairwise multiple comparison of parameters between individual volumes. Non-parametric data was produced using the Holm-Sidak test. Statistical output has been summarised to illustrate which volumes are statistically similar. Y=significant difference; N=no significant difference for structural model index (SMI). Full statistical data can be found in Appendix 2. High (yellow), medium (green) and low (blue) values of structural model index.

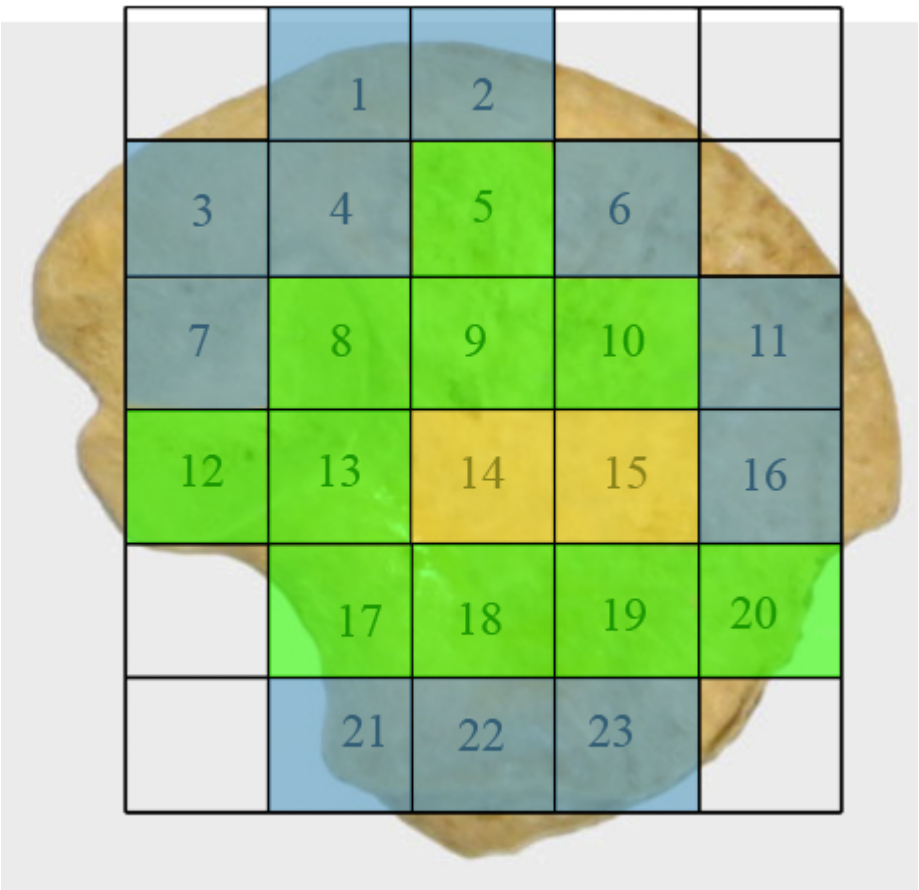

Figure 6.25. Coloured map representing regional groupings with statistically similar trabecular characteristics taken from Table 6.7. High (yellow), medium (green), low (blue) structural model index (SMI).

Degree of Anisotropy (DA)

Table 6.8 displays the descriptive statistics for DA at each volume of interest (VOI). Although the average DA for the neonatal ilium tends towards anisotropy there were three distinct regions of structural anisotropy observed (Figures 6.26 - 6.28). Volumes of interest contributing to a single group displayed no statistical difference between values (Figure 6.27). Highest values of DA which tend towards total anisotropy (0.886 – 0.794) are observed over the majority of the iliac blade, inclusive of superior and anterior superior perimeter volumes (VOIs 1,2,6,11&16), posterior auricular (VOI 3), superior and central iliac body (VOIs 4,5,9&10) cranial auricular volume (VOI 8) and

trabecular chiasma volumes (VOIs 14&15). Reduced values for degree of anisotropy (0.729 – 0.684) were observed in both caudal auricular and adjacent posterior auricular volumes (VOIs 7&12). Finally, lowest values of DA which tend towards a more organised structural conformation (0.647 – 0.487) are observed at the greater sciatic notch volumes (VOIs 13&17), inferior body (VOIs 18-20) and acetabular volumes of interest (VOIs 21-23). Although trabeculae in these volumes display lower values of DA representative of a more aligned morphology, they still remain distinctly anisotropic.

Coefficient of variation for degree of anisotropy again presents as a low value across all volumes of interest representing a low level of inter-specimen variation for this parameter.

	DA				
	MEAN	RANGE		SD (±)	CV (%)
VOI		MIN	MAX		
1	0.881	0.709	0.999	0.087	9.875
2	0.867	0.709	0.999	0.078	8.997
3	0.794	0.708	0.974	0.083	10.453
4	0.851	0.650	0.991	0.127	14.924
5	0.872	0.719	0.994	0.087	9.977
6	0.861	0.699	0.995	0.088	10.221
7	0.684	0.560	0.897	0.083	12.135
8	0.861	0.540	0.997	0.109	12.660
9	0.804	0.693	0.997	0.087	10.821
10	0.886	0.719	0.976	0.08	9.029
11	0.853	0.718	0.980	0.081	9.496
12	0.729	0.581	1.919	0.071	9.739
13	0.583	0.401	0.731	0.081	13.894
14	0.818	0.588	0.970	0.097	11.858
15	0.815	0.667	0.993	0.096	11.779
16	0.839	0.716	0.993	0.098	11.681
17	0.487	0.304	0.571	0.06	12.320
18	0.538	0.402	0.765	0.085	15.799
19	0.52	0.402	0.622	0.071	13.654
20	0.629	0.512	0.778	0.083	13.196
21	0.571	0.413	0.764	0.1	17.513
22	0.647	0.504	0.853	0.082	12.674
23	0.565	0.383	0.699	0.077	13.628

Table 6.8. Descriptive statistics (mean, range, standard deviation and coefficient of variation) for neonatal degree of anisotropy (DA) at each volume of interest (VOI). Data for individual specimens can be found in Appendix 1.

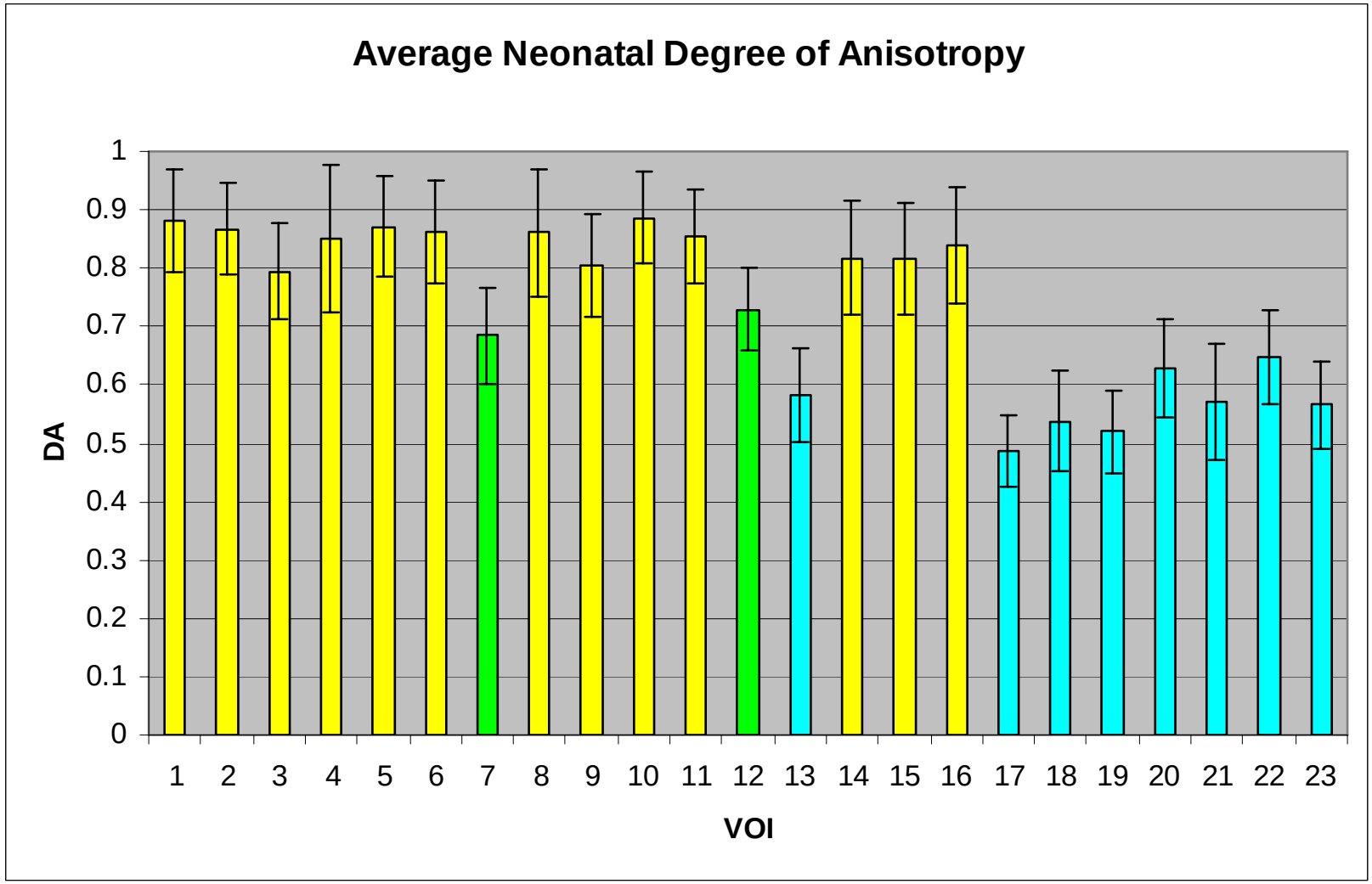

Figure 6.26. Graphic representation of mean (± SD) degree of anisotropy at each volume of interest. High (yellow), medium (green) and low (blue) values of DA.

DA																						
2	N																					
3	N	N																				
4	N	N	N																			
5	N	N	N	N																		
6	N	N	N	N	N																	
7	Y	Y	N	Y	Y	Y																
8	N	N	N	N	N	N	Y															
9	N	N	N	N	N	N	N	N														
10	N	N	N	N	N	N	Y	N	N													
11	N	N	N	N	N	N	Y	N	N	N												
12	Y	N	N	N	N	N	N	N	N	Y	N											
13	Y	Y	Y	Y	Y	Y	N	Y	Y	Y	Y	N										
14	N	N	N	N	N	N	N	N	N	N	N	N	Y									
15	N	N	N	N	N	N	N	N	N	N	N	N	Y	N								
16	N	N	N	N	N	N	Y	N	N	N	N	N	Y	N	N							
17	Y	Y	Y	Y	Y	Y	N	Y	Y	Y	Y	Y	N	Y	Y	Y						
18	Y	Y	Y	Y	Y	Y	N	Y	Y	Y	Y	Y	N	Y	Y	Y	N					
19	Y	Y	Y	Y	Y	Y	N	Y	Y	Y	Y	Y	N	Y	Y	Y	N	N				
20	Y	Y	Y	Y	Y	Y	N	Y	Y	Y	Y	N	N	Y	Y	Y	N	N	N			
21	Y	Y	Y	Y	Y	Y	N	Y	Y	Y	Y	N	N	Y	Y	Y	N	N	N	N		
22	Y	Y	N	Y	Y	Y	N	Y	Y	Y	Y	N	N	Y	Y	Y	N	N	N	N	N	
23	Y	Y	Y	Y	Y	Y	N	Y	Y	Y	Y	N	N	Y	Y	Y	N	N	N	N	N	N
VOI	1	2	3	4	5	6	7	8	9	10	11	12	13	14	15	16	17	18	19	20	21	22

Figure 6.27: Pairwise multiple comparison of parameters between individual volumes. Non-parametric data was produced using Dunn's test. Statistical output has been summarised to illustrate which volumes are statistically similar. Y=significant difference; N=no significant difference for degree of anisotropy (DA). Full statistical data can be found in Appendix 2. High (yellow), medium (green) and low (blue) values of DA.

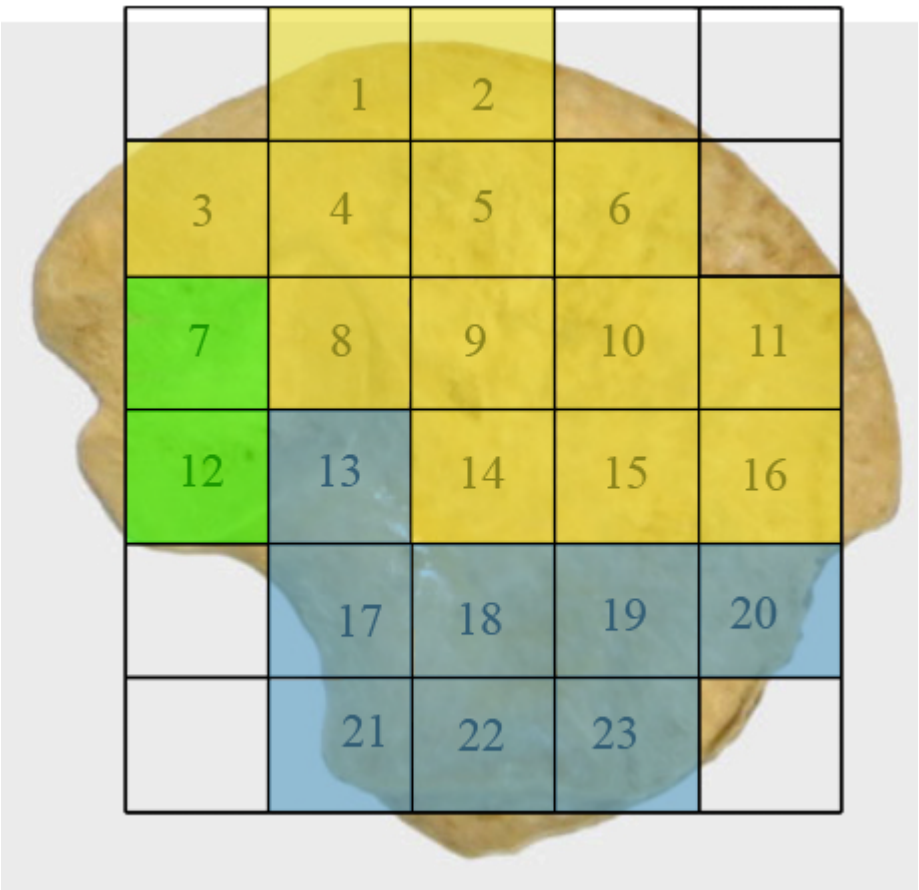

Figure 6.28. Coloured map representing regional groupings with statistically similar trabecular characteristics taken from Table 6.8. High (yellow), medium (green), low (blue) values for degree of anisotropy (DA).

6.9 Neonatal trabecular data discussion

The skeleton is a metabolically active structure which undergoes continuous change throughout life from early fetal developmental modeling to the constantly changing structural remodeling of the older skeleton (Hadjidakis and Androulakis, 2006; Robling *et al*, 2006). However, the rate of bone remodeling during the neonatal period and during the first two years of life is much higher than is exhibited in the adult, with neonatal remodeling estimated at 50% *per annum* compared to 5% *per annum* in the adult (Walker, 1991). With emphasis on this and with the knowledge that bone is highly responsive to stresses and strains in that it is laid down and remodelled at sites of

increased mechanical force or microdamage (Evans, 1957; Turner, 1998; Raisz, 1999; Huiskes *et al*, 2000), it has been proposed that trabecular characteristics in the ilium may be explained predominantly in terms of direct stance related bipedal weight transfer and associated ground reaction forces. However, it has become apparent that there is a significant degree of organisation of trabecular morphology in the neonatal ilium, prior to any possible direct locomotive forces. Trabeculae appear to be aligned in radiating trajectories that essentially mirror those observed in the adult. Therefore, this characteristically mature patterning must be explained by other factors. Discussion of regional trabecular characteristics will be made and paralleled with previous radiographic observations.

Consideration has been given to the influences of progressive ossification on the trabecular patterning observed in the neonatal ilium. The recognised point of primary ossification and the concomitant location of nutrient invasion in the ilium are observed anterio-superior to the greater sciatic notch (Laurenson, 1964). This landmark, demonstrated radiographically by increased bone density, equates to the position of the trabecular chiasma. This is, by necessity, the most mature region of the ilium. This region displays greater density than surrounding regions due to its advanced modeling and remodeling resulting in an increased mineral component characterised by increased radiopacity. The resultant progression of ossification from this centre can then be observed to radiate superiorly into the iliac blade and inferiorly into the acetabular component, illustrated by the distinctive density gradient produced radiographically (Figure 6.29). This is based on the assumption that remodelled bone has differentiating characteristics when compared to *de novo* bone formation (the initial laying down of bone from an osteoid template). It is suggested that *de novo* ossification is located furthest away from the centre of ossification and consequently the most remodelled

bone is located furthest away from the growth fronts in the neonatal ilium. Continuous growth of the ilium is known to proceed by modeling at the growth plates (Scheuer and Black, 2000). Therefore, to permit a full explanation of how growth and normal ossification may contribute to the trabecular characteristics observed in the growing ilium, it is necessary to consider the ilium as a diaphysis with active metaphyseal fronts at both the iliac crest and the acetabular component.

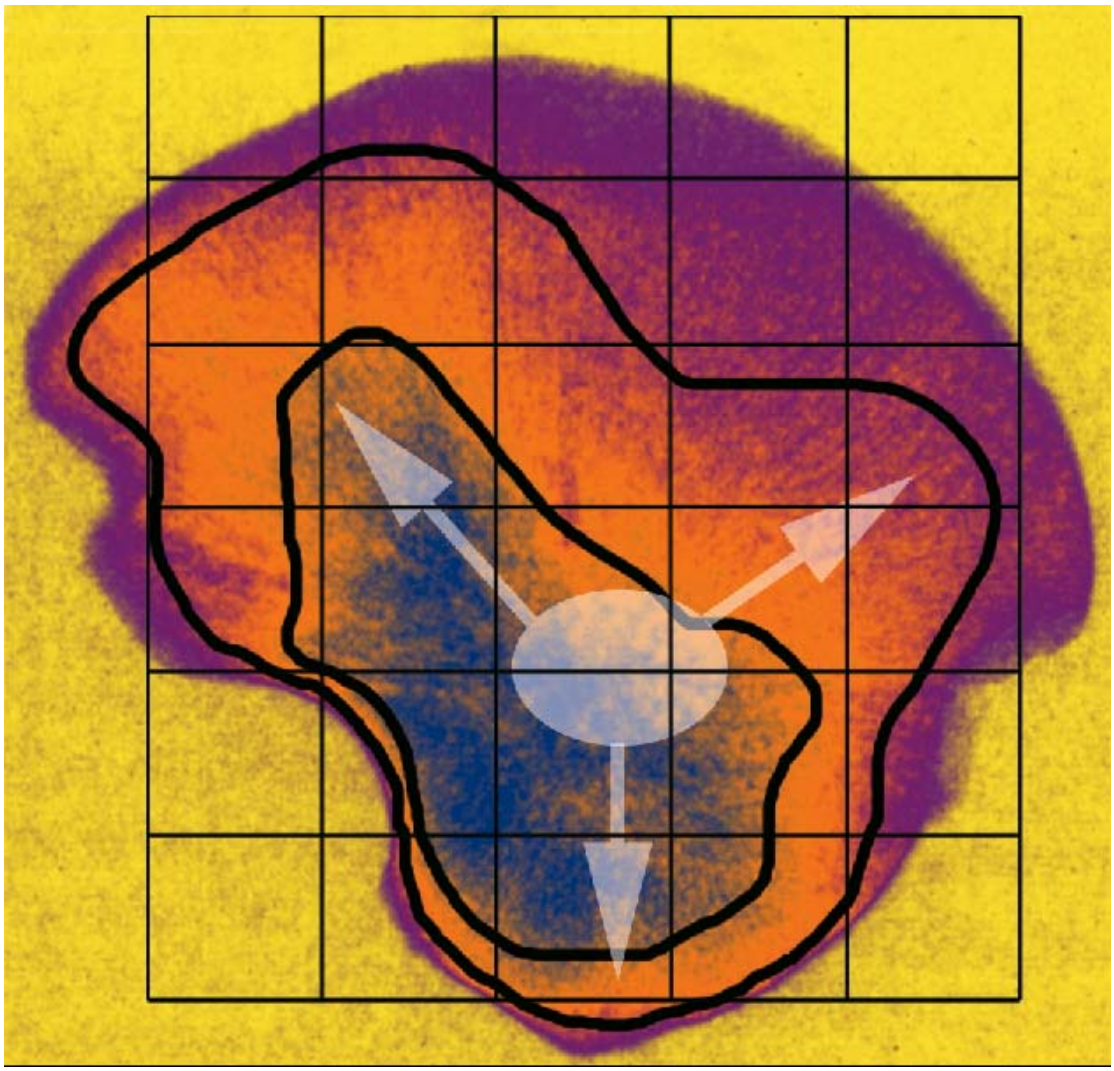

Figure 6.29. Gradient enhanced radiograph of a neonatal ilium with VOI grid overlay. Radiopacity is illustrated by high values (blue), intermediate values (orange), and low values (magenta). The position of the primary centre of ossification is located in the blue region (white oval) with proposed ossification fronts radiating cranially and caudally represented by colour gradient (white arrows).

Prior to discussion of the regional trabecular characteristics observed in the neonatal ilium, it should be noted that the structural model index was observed to be relatively uniform throughout the entire trabecular volume, being a combination of both rods and plates with a tendency towards plate-like structure. Although there were regions of statistically significant difference in values of SMI within the trabecular volume, these values were all within the range defined for a plate-like structural composition. A plate-like structural model index for the entire iliac trabecular morphology is most likely to be related to the pelvic and gluteal muscular interactions acting on the iliac cortices. These anatomical interactions are considered to encourage the formation of plate like trabeculae which tend to be aligned parallel with resultant tensile forces, resulting in a biomechanically optimised structural conformation (Turner, 1992). Additionally, plate-like trabeculae have also been documented as being optimal in shear-loading structures such as the ilium (Dalstra, 1993), where the two cortical shells are being held together by plate-like trabecular 'ties' preventing the complex from being pulled apart by the functional interactions of potentially opposing musculature.

Additionally, inter-specimen variation must be considered in the context of the results obtained. Although the majority of VOI's for each trabecular parameter displayed a low value for coefficient of variation, regions which displayed marginally higher values, for the trabecular parameters outlined previously, include volumes associated with the cranial auricular, central body, trabecular chiasma and inferior body regions. These regions may display a higher coefficient of variation due to their proximity to the ossification centre and thus reflect the variation in remodeling influences which may be encountered during the early weeks after birth. This can be contrasted with volumes which displayed lower inter-specimen variation which are

hypothesised to be in regions which undergo predominantly modeling rather than combined modelling and remodeling pressures. It must be borne in mind that although specimens have been grouped into a single 'neonatal' age cohort, there may be an inherent degree of variability in the age range contained within this cohort. This variability may be in the order of several weeks which may be reflected in the range of values and the coefficients of variation obtained for each structural parameter volume of interest. Larger coefficients of variation must also be considered to reflect inconsistencies in volume of interest positioning between specimens, which are unavoidable due to the absence of developmental homology. This may explain the higher apparent inter-specimen variation in the cranial auricular region, due to this regions anatomical variability between specimens and the potential inconsistencies involved in placement of a VOI at the cranial auricular trabecular volume.

6.9.1 Regional Trabecular patterning

Superior and anterior perimeter (VOI 1,2,6,11,16)

The superior and anterior perimeter region equates roughly to the location of the future anterior crest epiphysis. The trabecular morphology observed in the perimeter volumes of interest is characterised by a high BV/TV consisting of a high number of thin, tightly packed plate-like trabeculae. This structural conformation is considered to be representative of normal early trabecular modeling and related to ossification of the cartilage septae in the hypertrophic zone (Byers *et al*, 2000). During normal bone proliferation, growth plate cartilage transforms, via endochondral ossification, into new trabecular bone where there is a close relationship between the growth plate matrix structure and the newly forming trabecular structure (Rodriguez *et al*, 1992; Byers *et al*, 2000). This combined with the fact that the process of endochondral ossification sets

the basic trabecular bone scaffold upon which all subsequent modeling and remodeling occurs (Gosman and Ketcham, 2009) allows for an understanding of growth plate trabecular architecture. In the perimeter growth regions it is suggested that when the primary spongiosa is formed from the calcified cartilage matrix it is laid down in an initial pure form characterised by the structural parameters observed. It is proposed that at the growing fronts, the newly formed trabeculae have had limited exposure to intrinsic forces and therefore limited opportunity to remodel and resorb into a more functionally aligned mature arrangement. The degree of anisotropy observed in the anterior and superior perimeter volumes reinforces this theory as it is characterised by an anisotropic arrangement which reflects the newly formed bone structure in the absence of any significant remodeling stresses which might act to align and therefore remodel the structural arrangement.

Acetabulum (VOI 21-23)

In the acetabulum, the trabecular architecture is similar to that observed in the perimeter volumes, in that it is characterised by a high bone volume fraction consisting of a high number of thin, tightly packed plate-like trabeculae. As described for the superior perimeter regions, the acetabular component is also a growth front for newly formed trabeculae which are essentially a baseline template of endochondral ossification which have had limited time to respond to intrinsic forces. However, the degree of anisotropy observed in the acetabular component is different to that observed in the perimeter regions and deviates from the proposed theory of trabecular structure reflecting initial unaltered endochondral ossification. In these volumes of interest there appears to be a degree of alignment of the trabecular structure. This reinforces the possibility that there may be the presence of functional forces which are sufficient in magnitude to initiate

early alignment of the trabecular structure, but are not yet great enough to initiate quantifiable changes in other architectural parameters. One theory which may be applied to explaining this characteristic degree of anisotropy in the acetabular component can be related to the fact that the acetabulum is a synovial joint involving the complex association of the three innominate bones, through a cartilaginous continuity, this structural association may have a bearing on the trabecular architecture of the acetabular component. Early reflexive limb movements, as discussed previously for radiographic analysis, may have an increased impact on the acetabular component as retrograde forces may be transferred from the ischium and pubis to the ilium via the cartilaginous acetabulum. This additional force component associated with the acetabular component may explain the altered values of degree of anisotropy in the acetabular component as compared to the iliac blade component. As a more isotropic trabecular arrangement can be attributed to advanced organisation of the trabecular structure in response to functional forces, the fact that the superior perimeter region and the acetabular component only differ significantly in their values of DA lends weight to the proposal that retrograde limb movement forces may contribute to the acetabular trabecular form.

A further theory for the different trabecular characteristics observed between the growing front of the superior perimeter and that of the acetabular component can be related to the likening of the ilium to a growing long bone with a diaphysis and proximal and distal metaphyseal growth fronts. In a long bone the direction of the dominant nutrient artery generally determines the dominant growing end and the reduced growing end of the bone whereby the dominant artery is directed towards the reduced growing end. The direction of the dominant nutrient artery can be deduced from a dry bone by the obliquity of the dominant nutrient foramen. In the ilium, the

advanced degree of anisotropy suggests that the acetabular component may be the "growing" end of the bone and this is confirmed by inspection of the nutrient foramen which has an obliquity towards the iliac crest inferring that the iliac crest is the reduced growth front and that the acetabular component is indeed the advanced growing front.

Additionally, the acetabular region of the ilium is significantly thicker than that of the iliac blade which may have implications on the degree of anisotropy due to the increased volume of trabeculae present. The increased volume of trabeculae in the acetabular component, as compared to the superior perimeter volumes which have a comparatively low trabecular volume, may impose the requirements to strengthen the trabecular network to prevent potential failure of the structure. The superior perimeter may not require this same reinforcement due to the support of the closely approximated cortices. This proposed strengthening requirement in the acetabular component may be reflected in the more isotropic trabecular values observed as the trabeculae become more aligned in order to confer increased strength and support to the increased inter-cortical trabecular volume.

Superior and inferior body (VOI 4,5,18-20)

In the superior and inferior body of the ilium, marginal changes in trabecular characteristics from those observed in the perimeter and acetabular regions are observed. The superior body can be generalised as displaying moderately high trabecular BV/TV consisting of a high to medium number of thin, moderately packed, anisotropic, plate-like trabeculae. Further to this, the inferior body is characterised by a medium to low trabecular BV/TV consisting of a low number of moderately spaced thin plate-like trabeculae which are more organised i.e. less anisotropic than the superior body volumes of interest. These alterations from the pattern seen at the growth front

most likely represent the effects of remodeling which can only have occurred in response to *in utero* intrinsic influences, as these changes predate the more recent pattern seen in the perimeter regions of the neonate. Therefore, the superior and inferior body regions are likely to represent the most recently remodelled regions behind the growth fronts. This remodeling, in regions parallel to the growth fronts may be in response to a host of influences which may act in unison or in isolation. Direct muscle activity may transmit a force component into the underlying trabeculae causing a resultant remodeling. Muscular interactions have been shown to have an influence on the trabecular architecture from the early fetal period, with studies in the fetal ilium suggesting that intrauterine muscular-related biomechanical constraints may have a bearing on certain trabecular characteristics (McColl *et al*, 2006). Further to this, responses to transferred forces from early reflexive limb movement may account for the apparently advanced remodeling and more anisotropic characteristics observed in the inferior body of the ilium. Finally, maturation of internal anatomical tissues such as vascular channels and the formation of marrow spaces may have influenced the approximated trabecular characteristics (Crock, 1996). Specifically, within the inferior body the trabecular parameters reflect the proximity of this region to the centre of ossification and point dominant nutrient invasion more so than the superior body which is located further from these loci. This pattern of graded change in trabecular architecture can be paralleled with the radiographic representation where the superior and inferior body displays a changed morphology concomitant with the proposed localised influences. These areas of bone patterning can also be observed radiographically in the adult morphology suggesting that perhaps once this pattern is formed, it is retained.

Central body (VOI 9&10)

The central body of the ilium has a trabecular arrangement characterised by a low BV/TV consisting of a medium to low number of thin moderately spaced, anisotropic, plate-like trabeculae. The central body can be viewed as being the subsequent remodeled front behind the superior body, therefore reinforcing the theory of a remodeling gradient, radiating from the ossification centre, at the trabecular chiasma, towards the periphery. This architectural arrangement may be explained in terms of hypothetical directional force trajectories entering the ilium in a retrograde fashion, from early reflexive limb movement, converging upon the trabecular chiasma and continuing in antero-superior and postero-superior directions. In taking this course, these hypothesised forces essentially bypass the central body of the ilium resulting in a low BV/TV combined with weak trabecular characteristics. This can be paralleled with an area of structural redundancy highlighted in radiographic studies (Figure 6.29). This area of structural redundancy is also visible in the adult and represents an area of the iliac blade where the gluteal and pelvic shells of compact bone may fuse without any intervening cancellous bone.

Trabecular chiasma (VOI 13-15)

The trabecular chiasma represents volumes of significantly altered trabecular morphology (Figure 6.30). These volumes are characterised by low trabecular BV/TV consisting of a very low number of thickened, well spaced, anisotropic, plate-like trabeculae. Theoretically, the trabecular chiasma is the most mature region of the bone in terms of progressive ossification in relation to the original location of the primary centre of ossification (Laurenson, 1964; Scheuer and Black, 2000), and the location of the highest concentration of vascular channels (Brookes, 1971; Crock, 1996).

Therefore, this trabecular arrangement can most likely be attributed to an increase in the functional interactions acting at this region during the fetal and neonatal period from both anatomical (Brandi and Collin-Osdoby, 2006; Eriksen *et al*, 2007) and biomechanical sources (Walker, 1991, Thelen *et al*, 2002; Pitsillides, 2006; Nowlan *et al*, 2007), as well as reflecting the most mature location for remodeling. This is further reinforced by the higher values obtained for SMI within the trabecular chiasma region. Although these values are still representative of plate-like trabecular morphology, they are more intermediate in value between a plate-like and rod like morphology. This transition from one structural model towards another occurs through the process of bone remodeling in response to functional interactions (Lazenby *et al*, 2008) this extends evidence to the fact that the trabecular chiasma is a more mature region of trabecular bone.

Although a low value of trabecular bone volume is observed which may initially be considered as a feature of structural weakness, the trabecular indices which contribute to this BV/TV are characteristic of increased strength. This increased strength can be inferred as redundant thin trabeculae are considered to have been resorbed and remaining trabeculae to have thickened resulting in a more mature trabecular morphology which is better suited to accommodating inherent functional interactions. This architecturally distinct conformation can be paralleled with the defined trabecular chiasma observed by plane plate radiography. The trabecular chiasma has been partly attributed to the retrograde forces transferred into the ilium from early reflexive limb movement during the fetal and neonatal periods. The low BV/TV in this region combined with the dense radiographic representation reported previously, suggests that the cortical shell may have a significant contribution to the structural integrity of the trabecular chiasma as a region of increased neonatal force

transmittance. This theory is strengthened by the understanding of the ilium consisting of low density trabecular bone covered by layers of cortical bone forming a strong, low-weight structure that is well suited to accommodate high loads (Dalstra and Huiskes, 1995). This region of strengthened trabecular characteristics and overall increased bone density representation can again be paralleled with the adult representation (Macchiarelli *et al*, 1999; Rook *et al*, 1999).

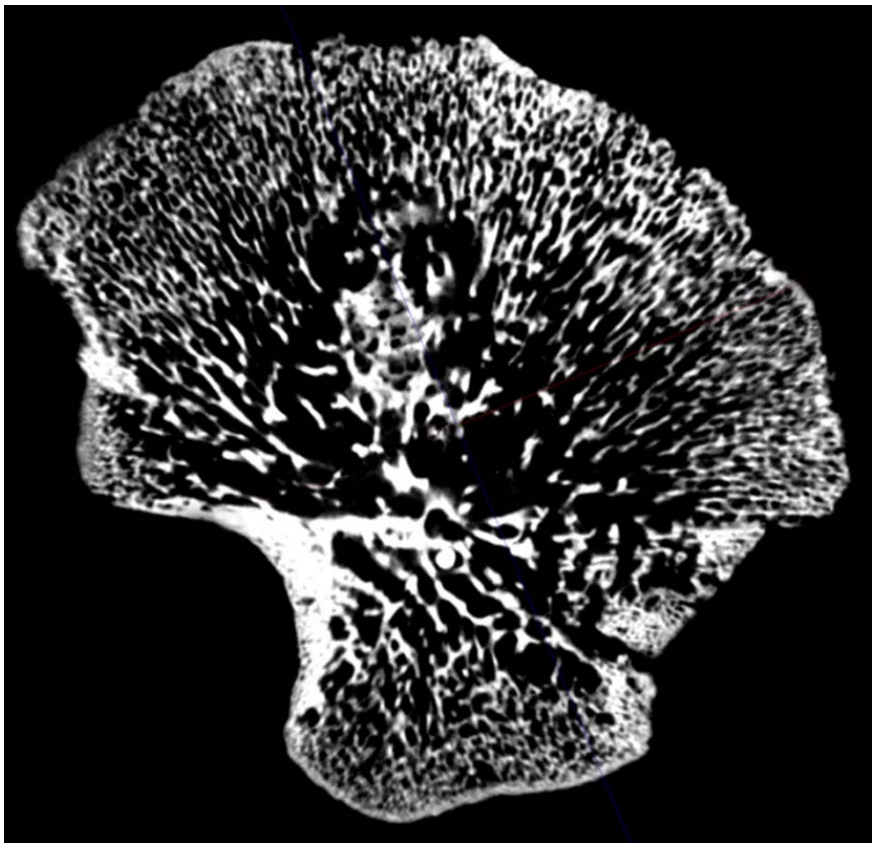

Figure 6.30. 2D μCT sagittal slice through a neonatal ilium illustrating trabecular characteristics across the trabecular volumes of interest in a single plane. Trabecular characteristics at the centre of ossification, the trabecular chiasma, reflect the site of nutrient invasion and subsequent radiation of vascular branches into the iliac blade and acetabular component.

Auricular surface (VOI 8, 12)

The cranial (VOI 8) and caudal (VOI 12) auricular regions differ in their trabecular characteristics. Volumes of interest relevant to the cranial auricular surface present with

a trabecular morphology characterised by a medium to low trabecular bone volume fraction consisting of a relatively low number of thin, moderately spaced trabeculae which are anisotropic and plate-like in their morphology. This is a similar morphology to the adjacent central body. Conversely, the trabecular morphology in the caudal auricular surface presents as a medium to high trabecular bone volume fraction consisting of a low number of thickened well spaced, plate-like trabeculae which are more organised in their arrangement. This is a similar morphology to the adjacent posterior region of the trabecular chiasma. In all trabecular parameters except Tb.N and SMI there appears to be a difference in trabecular morphology between these volumes, however, none of these differences reaches a statistically significant level. Therefore, although the cranial morphology is more similar to the appearance of the central body and the caudal limb to the chiasma trabecular morphology, they are essentially consistent within the morphology of their adjacent regions. As such, there is no evidence to suggest selective remodeling in the internal architecture specific to this joint. The overall architectural arrangement observed in these volumes may be attributed to functional influences on the joint during the neonatal period. Immediate focus in this case is directed towards the ligamentous associations which will already be well developed (Salsabili and Hogg, 1991). It is proposed that stresses and strains induced by the strong ligamentous interactions, which encapsulate the joint (Bowen and Cassidy, 1981; Vleeming *et al*, 1990), may cause a gradual remodeling process within the underlying trabecular bone perhaps influencing the changes in the auricular and surrounding volumes of interest. As discussed previously, in the adult, the sacro-iliac joint does not transmit weight *per se* from the upper body across the joint surfaces of the sacro-iliac joint (Last, 1973; Scheuer and Black, 2000). Instead, weight is known to be transferred through the strong ligamentous material which encapsulates the joint

(Bowen and Cassidy, 1981; Vleeming *et al*, 1990). As such, it is suggested that ligamentous interactions must be firmly established at the earliest of developmental stages in order to be strong enough to accommodate stance related forces at the adoption of a bipedal stance. Further to this, it must also be considered that the distribution of force transmittance generated during bipedal gait is not equally distributed through the two limbs of the sacro-iliac joint (Brooke, 1934). As such, it is possible that as a preparatory mechanism, the ligamentous material in the cranial part of the joint surface develops and attaches differently to that in the caudal auricular area, thus resulting in the more profound change in the trabecular morphology between the auricular volumes. The cranial limb of the SI joint articulates with S1 and the caudal limb of with S2 and sometimes S3 (Scheuer and Black, 2000). Any movement related forces transferred across the joint from torso-reflex movements are proposed to occur via S1 caudal limb interaction. Ultimately, when weight is transferred across this joint at the adoption of a bipedal stance, the wedging of the sacrum will ensure that S2 caudal limb interactions are initiated.

Greater sciatic notch (VOI 17)

Trabecular morphology in the greater sciatic notch volume of interest is characterised by a medium to low trabecular bone volume fraction consisting of a very low number of thickened well spaced plate-like trabeculae. The trabeculae in this volume of interest adopt a more aligned morphology similar to that described for the acetabular and inferior body volumes. Again consideration is given to immediate soft tissue structures and in particular to the large and closely approximated sciatic nerve. It is possible that neurogenic influences may alter the morphology of the underlying trabeculae. Indeed, proximity of nervous tissue has been considered to be responsible for thickening of the

cortical shell as a protective mechanism to the sciatic nerve and thought has also been placed on the potential for neurogenesis being an initiator of endochondral ossification in the ilium (Laurenson, 1964; Scheuer and Black, 2000). Neurogenic influences on the skeleton have also been demonstrated by the occurrence of anencephaly, in the absence of neurological tissue the vault bones do not ossify (Nakano, 1973). Also, ossification of the posterior vertebral column is observed to initiate in response to the peripheral nervous system (Kjaer *et al*, 1993; Scheuer and Black, 2000). As neurogenic influences can induce profound changes in bone it may be possible that the significantly altered trabecular characteristics within the sciatic notch volume, consisting of low trabecular bone volume fraction combined with a very low number of thickened well spaced trabeculae, may in part be attributable to this. Recent studies have also highlighted that the metabolic control of bone is influenced heavily by the nervous system (Jones *et al*, 2004). When paralleling the structural quantification in the sciatic notch region to the radiographic representation, further inferences can be made regarding the structural composition of this region and the potential contribution to this strength from the sciatic nerve. This region was represented as an area of increased structural density radiographically which parallels the trabecular phenotype of increased thickening of structurally significant trabeculae in order to confer strength and protection (Figures 6.29 & 6.30). This region is also reputedly an area of particular strength in the adult due to the passage of the sacro-ischial trabecular bundle (Aiello and Dean, 1990; Scheuer and Black, 2000). Further investigations in relation to cortical thickness and the inter-relationship with internal architecture will be presented later.

Finally, although it is likely that normal growth combined with local anatomical and biomechanical influences have a predominant and marked influence on cortical and

trabecular characteristics, consideration must also be given to the potential genetic influences which act upon the trabecular architecture and the skeleton as a whole. It is feasible that a predetermined genetic template of trabecular structure may be evident and thus a precocious development of progressive organised bone architecture may ensue. This genetic template may then be acted upon and altered by various mechanical, anatomical, angiogenic and neurogenic factors in order to shape the trabecular architecture into an optimal conformation for a particular temporal developmental window. Thus a potential genetic component of early cortical morphology and trabecular architectural organisation may act as a preparatory mechanism, in unison with proposed extragenetic influences, enabling the structural composition of the ilium to accommodate a life-time of functionally inherent ontogenetic stresses and strains.

In summary, this part of the study revealed that a recognisable and regional organisation of internal trabecular architecture is established at a very early maturational stage in the human ilium. Remarkably, the observed morphology can be paralleled with the generalised patterning observed in the adult which is more usually and specifically attributed to locomotive influences. Therefore, the early presence of this mature trabecular morphology suggests that previous attribution of iliac trabecular patterning primarily or solely to locomotor weight transfer may be too simplistic. Other factors including progressive remodeling in response to normal growth and ossification, inherent anatomical interactions and early reflex limb movement must be considered. It is therefore suggested that the neonatal trabecular pattern may yield an insight into the developmental origins of future load bearing structures. Further to this, it must also be postulated that the observed patterning may be indicative of a predetermined template upon which early non-weight bearing and later, stance-related, locomotive influences

may be superimposed and perhaps reinforced at a later age. This part of the study contributes to a greater understanding of early developmental trabecular organisation in the ilium and has core implications for understanding the origins of trabecular characteristics attributed to load bearing structures in the adult by providing a foundation for subsequent ontogenetic development.

6.10 Neonatal cortical results

In this part of the study average thicknesses of the pelvic and gluteal cortices were measured to investigate the cortical bone patterning of the ilium during the neonatal developmental period. Descriptive statistics for thickness measurements on both pelvic and gluteal surfaces are summarised in Table 6.9, full raw data are presented in Appendix 3. To establish the degree of statistical significance between corresponding regions of interest (ROI's) on pelvic and gluteal shells an ANOVA test was performed. All non-parametric data were subjected to a Kruskal-Wallis one way analysis of variance on ranks test. This test determined the overall significance between the pelvic and gluteal cortical thicknesses from a single ROI. Summarised statistical significance is also displayed in Table 6.9. The data showed that for all ROI's apart from 1,2,11,16,21,22, and 23 (where there was no statistical difference), the gluteal cortex was always significantly thicker than the pelvic cortex within any single ROI.

Analysis highlighted regions of differing cortical thickness on both the pelvic and gluteal shells of the neonatal ilium. The average thickness and standard deviation for each ROI is given in Table 6.9. The differences in cortical thickness over the iliac shells appear to occur in almost concentric waves emanating from a locus approximating to the position of the initial site of ossification and dominant nutrient invasion. To aid interpretation of this pattern, a colour map of cortical thickness

gradients is shown in (Figure 6.31). Patterning of cortical thickness will be examined for both pelvic and gluteal cortices in isolation in the first instance.

	Pelvic thickness					Gluteal thickness		
ROI	Mean (mm)	SD (±)	CV (%)	*H*	*P*	Mean (mm)	SD (±)	CV (%)
1	0.184	0.013	7.065	0.12	0.733	0.184	0.015	8.152
2	0.184	0.012	6.522	1.17	0.28	0.183	0.015	8.197
3	0.266	0.026	9.774	167.96	< 0.001*	0.388	0.034	8.763
4	0.29	0.013	4.483	172.06	< 0.001*	1.119	0.125	11.171
5	0.243	0.017	6.996	174.71	< 0.001*	0.757	0.113	14.927
6	0.206	0.01	4.854	179.47	< 0.001*	0.341	0.055	16.129
7	0.27	0.016	5.926	168.88	< 0.001*	0.842	0.069	8.195
8	0.288	0.032	11.111	179.75	< 0.001*	1.604	0.253	15.773
9	0.473	0.089	18.816	176.39	< 0.001*	1.292	0.124	9.598
10	0.285	0.013	4.561	179.08	< 0.001*	0.639	0.087	13.615
11	0.183	0.012	6.557	0.61	0.434	0.184	0.016	8.696
12	0.316	0.013	4.114	182.43	< 0.001*	0.726	0.043	5.923
13	0.415	0.101	24.337	179.45	< 0.001*	1.451	0.088	6.065
14	0.791	0.102	12.895	179.35	< 0.001*	1.521	0.17	11.177
15	0.524	0.068	12.977	179.55	< 0.001*	0.987	0.172	17.427
16	0.186	0.012	6.452	1.51	0.219	0.19	0.019	10.000
17	0.881	0.054	6.129	179.41	< 0.001*	1.889	0.184	9.741
18	0.793	0.062	7.818	173.39	< 0.001*	1.648	0.175	10.619
19	0.72	0.036	5.000	173.54	< 0.001*	1.437	0.18	12.526
20	0.353	0.016	4.533	171.62	< 0.001*	0.928	0 233	25.108
21	0.236	0.017	7.203	0.05	0.821	0.237	0.026	10.970
22	0.242	0.013	5.372	3.72	0.054	0.236	0.023	9.746
23	0.243	0.015	6.173	2.27	0.132	0.239	0.024	10.042

Table 6.9. Average pelvic and gluteal cortical thickness with standard deviations and coefficients of variation for each region of interest (ROI). ANOVA between pelvic and gluteal cortical thicknesses for each ROI produced the H statistic and p value. * denotes a statistically significant difference. Statistical significance from this table is summarised in Figure 6.34.

Pelvic cortex (Figure 6.31A and 6.32; Table 6.9)

The thickness of the neonatal pelvic cortex ranges between an average of 0.183mm (ROI 11) and 0.881mm (ROI 17). The peripheral regions of the iliac blade and the acetabular margin are composed of the thinnest cortical bone ranging between 0.183±0.012mm (ROI 11) and 0.353±0.016mm (ROI 20). On the blade, the regions of thinnest cortex were located around outer perimeter regions of the ilium, including posterior auricular (ROI 7), iliac crest (ROI's 1,2,3&6) and anterior superior and anterior inferior regions (ROI's 10,11,16&20). In addition to this, similarly low values of cortical thickness were observed in the superior body of the ilium (ROI's 4&5), the auricular surface (ROI's 8&12) and acetabular component (ROI's 21-23). Increased values of cortical thickness, ranging between 0.415±0.101mm and 0.524±0.068mm, were located in the central region of the ilium (ROI's 9,13&15). Finally, maximal values of cortical thickness, ranging between 0.720±0.036 and 0.881±0.054mm, were located in the region of the trabecular chiasma (ROI 14), greater sciatic notch (ROI 17) and inferior body of the ilium (ROI's 18&19).

The coefficient of variation for the pelvic cortex regions of interest presented as a low value across the majority of regions of interest, reflecting the low level of inter-specimen variation. Regions of interest where marginally increased values for coefficient of variation were observed include those associated with the central body and the trabecular chiasma.

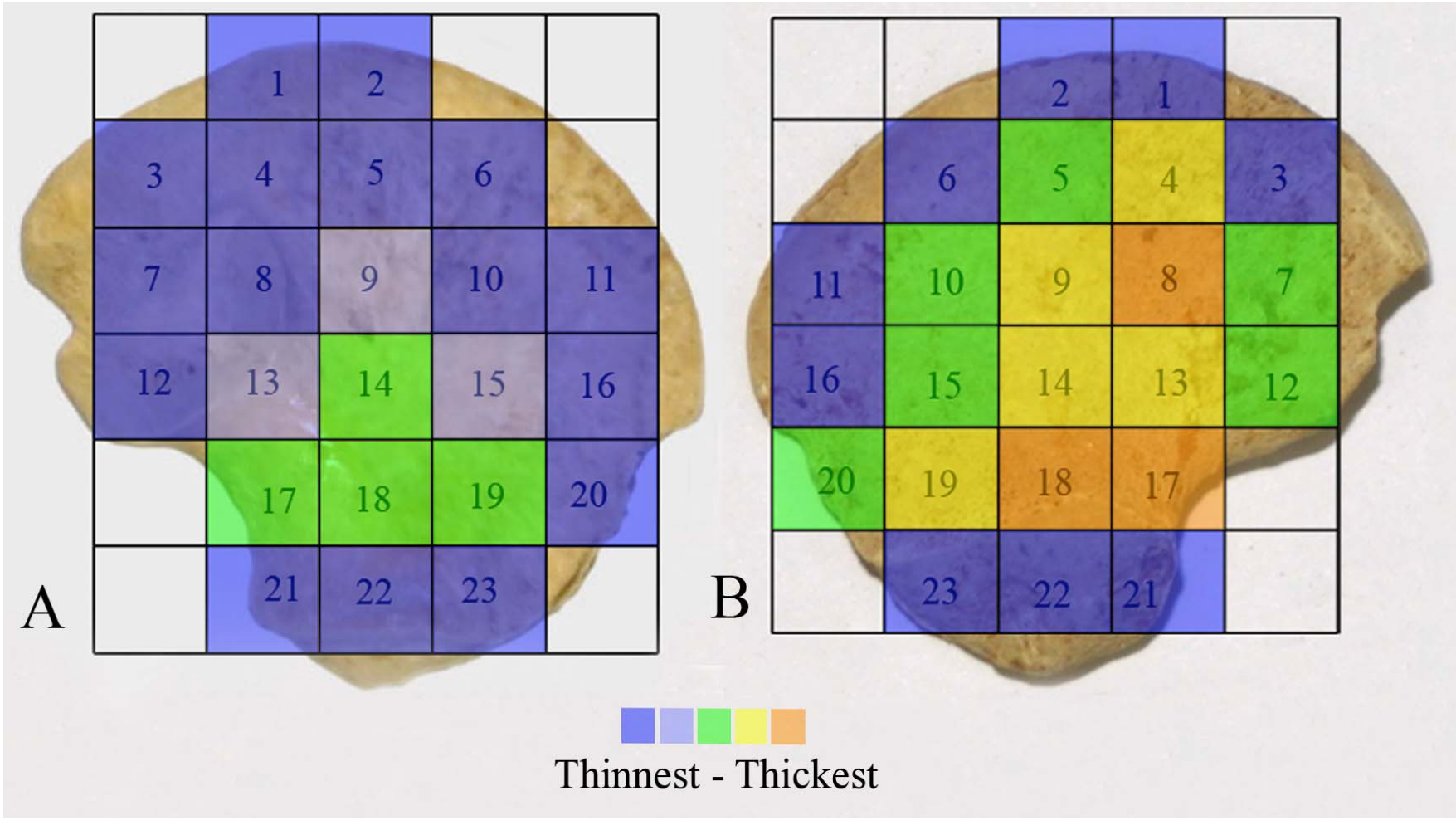

Figure 6.31. Colour map of cortical thickness on pelvic (A) and gluteal (B) surfaces of neonatal ilium.

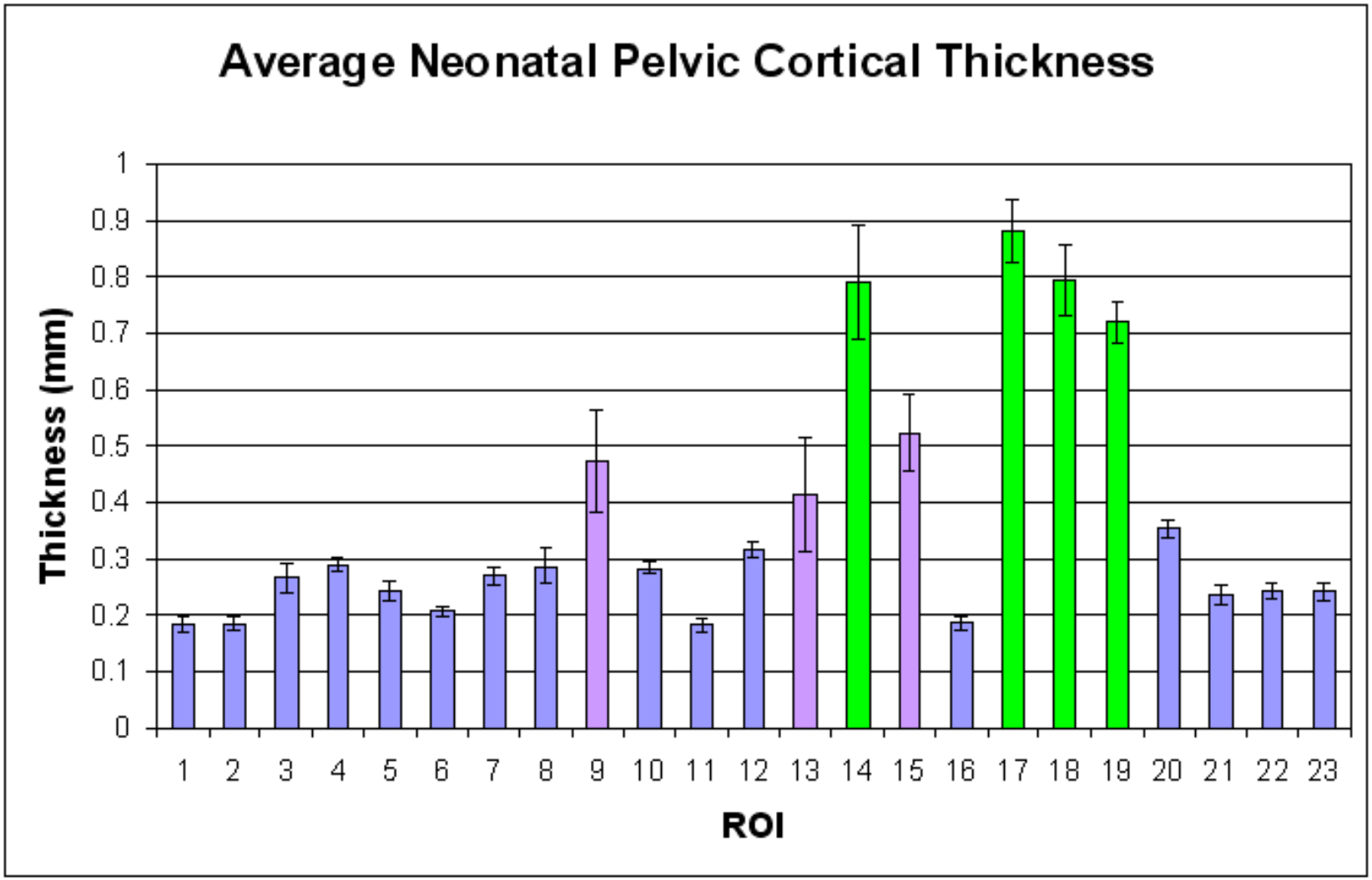

Figure 6.32. Average neonatal pelvic cortical thicknesses (±SD) for each region of interest (ROI).

Gluteal cortex (Figure 6.31B and 6.33; Table 6.9)

Thickness values for the neonatal gluteal cortex have a larger range than those of the pelvic cortex with values ranging between an average of 0.183mm (ROI 2) and 1.889mm (ROI 17). Lowest values of gluteal cortical thickness, ranging between 0.183±0.015mm and 0.388±0.034mm were again located peripherally across the iliac crest (ROI's 1,2, 3&6) extending into anterior superior (ROI 11&16) regions of interest as well as the acetabular component of the ilium (ROI 21-23). Increased cortical thickness values, ranging between 0.639±0.087mm and 0.987±0.170mm, were located in the superior body (ROI 5), anterior central body (ROI 10), caudal auricular region (ROI 12), posterior auricular region (ROI 7), anterior central body (ROI 15) and anterior inferior perimeter (ROI 20) regions of interest. An increase in gluteal cortical thickness, ranging between 1.119±0.125mm and 1.521±0.170mm, was observed in the posterior superior body (ROI 4), central body (ROI 9), chiasma (ROI 13&14) and anterior inferior body (ROI 19). Finally, maximal values of gluteal cortical thickness, ranging between 1.604±0.253mm and 1.889±0.184mm were located in the cranial auricular region (ROI 8), inferior body (ROI 18) and greater sciatic notch (ROI 17) regions of interest.

Coefficient of variation for gluteal cortex regions of interest again presented as low values over the majority of regions reflective of a low level of inter-specimen variation. Those regions which displayed increased values for coefficient of variation included anterior superior, central body, trabecular chiasma and anterior inferior regions.

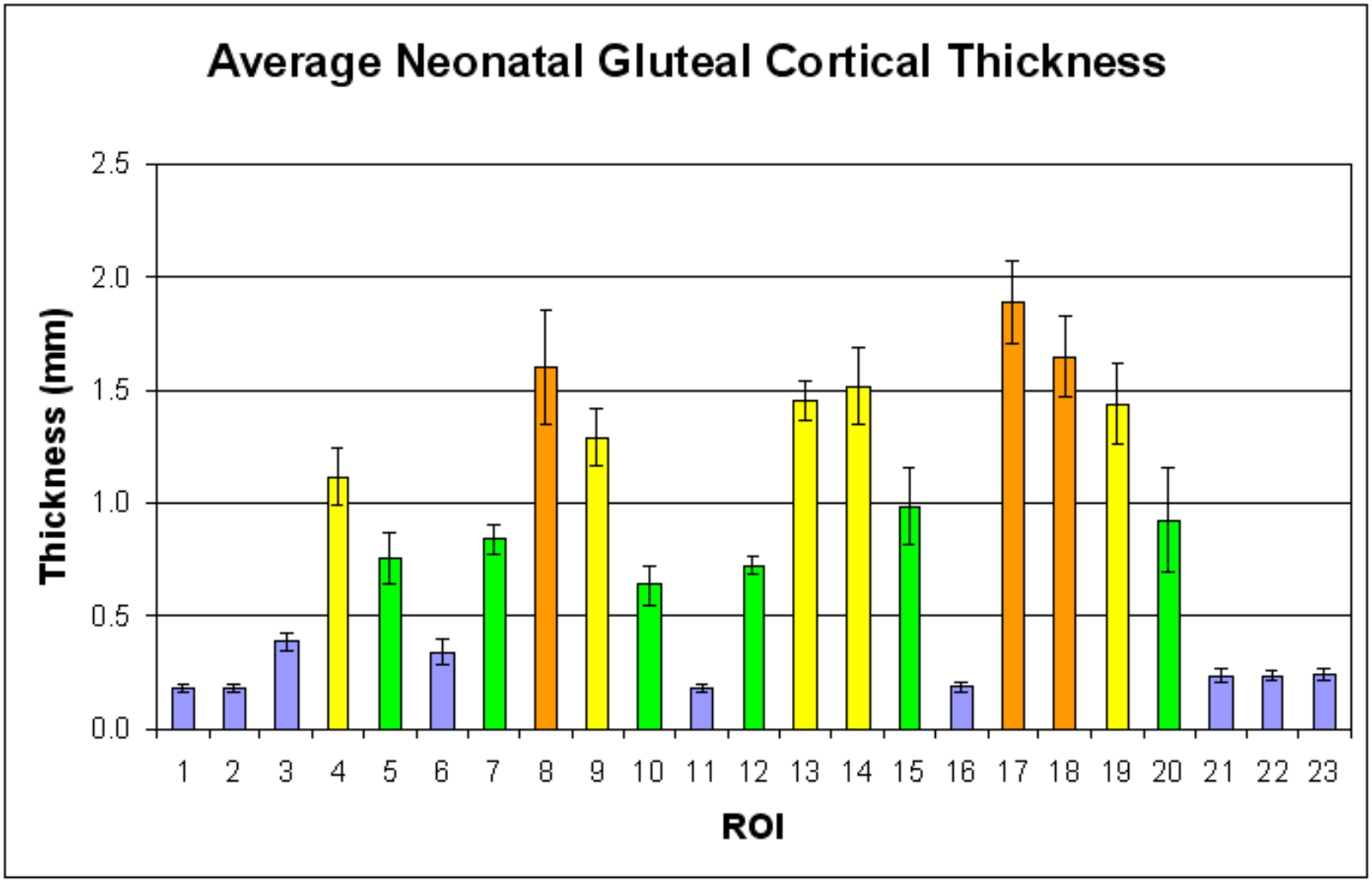

Figure 6.33. Average neonatal gluteal cortical thicknesses (±SD) for each region of interest (ROI).

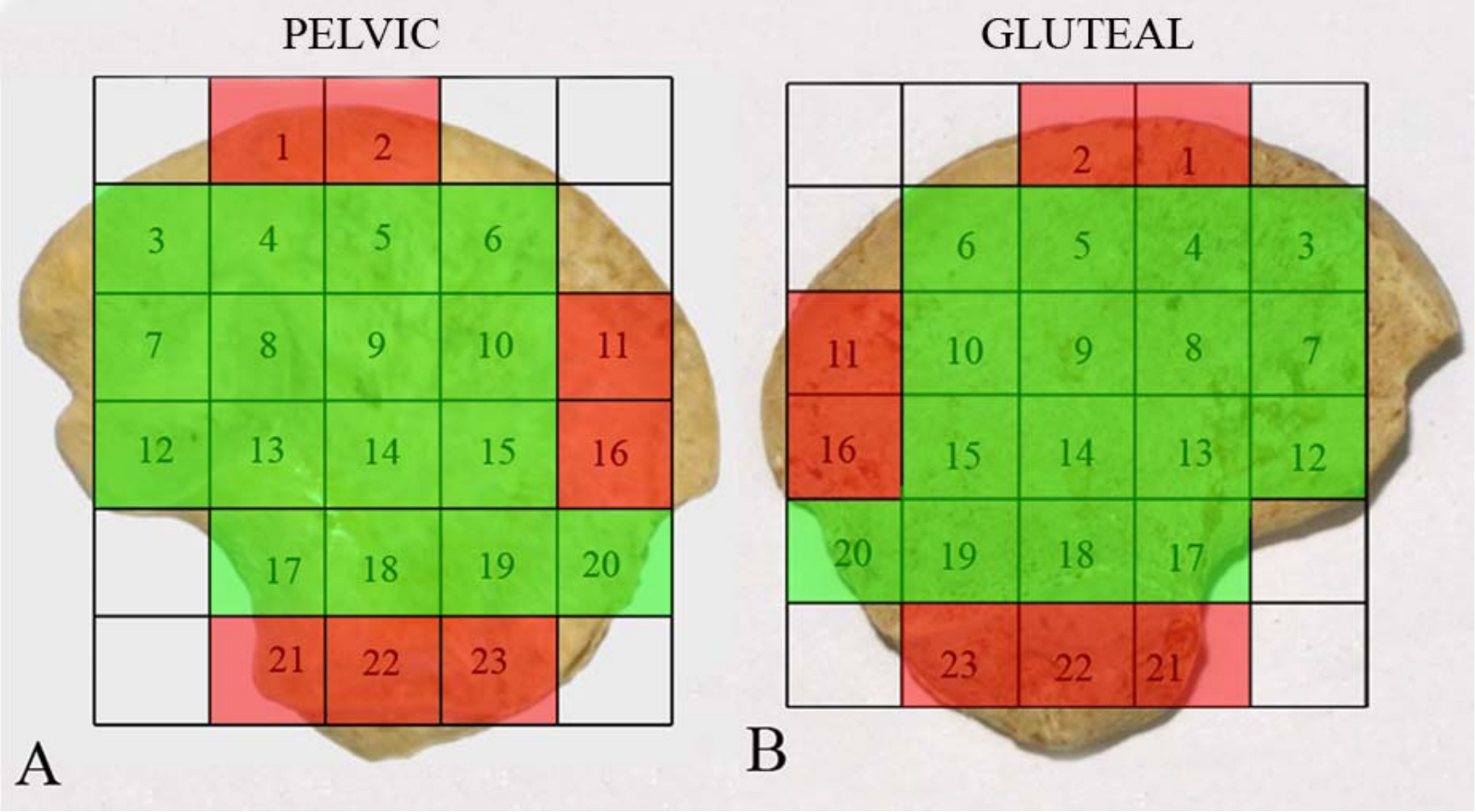

Figure 6.34. Colour map of ROI's showing regions of statistically significant difference between thickness values on pelvic (A) and gluteal (B) surfaces. Red = no statistical significance between thickness of cortex. Green = statistically significant difference between surfaces, with the gluteal thickness always greater than pelvic in all ROI's.

6.11 Neonatal cortical thickness discussion

Initial bone growth on the gluteal and pelvic shells of the ilium is reportedly achieved through the progressive process of periosteal apposition in response to localised stimuli (Raisz, 1999). Subsequent resorption and formation mechanisms remodel the bone in due course as it responds to changing requirements. During growth, formation tends to predominate and as such, bone modeling results in the apposition of bone tissue brought about by the disequilibrium of apposition and resorption processes. This apposition of bone tissue has been suggested to be most active in the early developmental years and tends to subside after skeletal maturity is achieved (Frost, 1990a). Collectively, modeling increases the outer cortex and inner marrow cavity diameters, as well as producing trabecular and cortical drift (Cowin, 2001). In the developing ilium, modeling is considered to be a well controlled process achieved through lateral modeling drift (Parfitt *et al*, 2000), which causes the cortical and trabecular compartments to enlarge only marginally (Schnitzler *et al*, 2009). A recent study by Schnitzler *et al* (2009), investigated cortical growth at the iliac crest via histomorphometric analysis. This study documented that lateral modeling drift ensues through the deposition of appositional bone onto the gluteal periosteal surface and resorption on the pelvic periosteal surface. As growth proceeds, and to prevent excessive thickening of the gluteal surface and excessive thinning of the pelvic surface, compensatory endosteal resorption and deposition occurs on respective gluteal and pelvic surfaces. Also during lateral modeling drift, trabeculation of the cortex, the process of trabecular production from unresorbed gluteal endosteal bone takes place as does compaction, the process of trabecular incorporation into the pelvic endosteal bone (Parfitt *et al*, 2000). In taking these aspects into account, the iliac cortex has been

shown to grow through a combination of gluteal periosteal and pelvic endosteal bone deposition.

In the current study, a range of gluteal and pelvic cortical thicknesses are evident across the neonatal ilium indicating that the cortex is not a uniform structure. Due to the early developmental stage of the ilia examined in this study, few biomechanical influences are proposed to have acted upon the bone. Therefore, the predominant functional interactions are hypothesised to be those associated with normal growth, progressive muscle activity and progressive ossification. As has been previously discussed, initial periosteal ossification, which is responsible for the formation of the cortex, is thought to commence in an area of the perichondrium superior to the region of the greater sciatic notch (Laurenson, 1964b), at the region of dominant nutrient artery invasion. This ossification is then considered to spread both cranially and caudally over the blade and acetabular component of the ilium (Scheuer and Black, 2000). In following this reasoning, when the ilium reaches the neonatal stage, the most "mature" bone will be present in the region of the trabecular chiasma as this is the area of primary bone formation and has had the greatest opportunity to remodel. From this locus, it would be expected that a thickness gradient might be evident radiating towards thinner peripheral active growth regions as these are the areas of newest bone formation and have had limited opportunity for remodeling.

This theory appears to support the results of this study as the pelvic cortex displays a well defined thickness gradient. This gradient begins with regions of thickest cortex located at the greater sciatic notch region (ROI 17), trabecular chiasma (ROI 14) and inferior body (ROI's 18 & 19), all regions which are adjacent to the site of primary ossification or the direct influence of a major nerve and as such would be expected to display most mature ossification. Reduced thickness is observed in regions superiorly

adjacent to thickest regions (ROI's 9, 13 & 15), and are likely to represent more recent areas of bone deposition and have thus had less time to remodel. Finally, lowest cortical thickness is observed over the majority of the peripheral iliac blade and acetabular components (all remaining ROI's). These regions are furthest from the primary centre of ossification and are therefore the "newest" areas of cortical bone formation that are still in the modeling phase due to their immediate proximity to the metaphyseal growth plate.

The pattern of cortical thickness for the gluteal surface also follows this general pattern, but is more complex than the pattern observed for the pelvic cortex. This may be attributed to the fact that during the growing years, the iliac bone cortices differ with regard to cellular activity on their surfaces, most likely reflecting a modeling drift (Rauch *et al*, 2006). On the gluteal cortex, a thickness gradient is observed extending from regions of thickest cortex at the greater sciatic notch gradually becoming thinner towards the periphery. However, the cortex is generally thicker on this surface and displays a greater staging of thickness than is observed on the pelvic surface. The variation in thickness of the gluteal cortex may also be partly explained by normal appositional growth. The thickest regions of cortex are observed at the greater sciatic notch and adjacent regions (ROI's 17&18) which dissipate into reduced cortical thickness regions radiating anteriorly, superiorly and postero-superioly (ROI's 4,9,13,14&19). Subsequently, a decreased thickness is observed in a circumferential pattern (ROI's 5,7,10,12,15&20), and finally, a similar low value of cortical thickness, to those observed on the pelvic surface, is located peripherally (ROI's 1,2,3,6,11,16,21-23). However, although a grading of thickness is observed, the majority of gluteal ROI's are significantly thicker than their pelvic counterpart. This differential patterning between surfaces is supported by the statistically significant difference between pelvic

and gluteal thicknesses in all regions except extreme peripheral areas (Table 6.9, Figure 6.34). If the pattern of cortical thickness seen on the pelvic surface was to be accepted as 'normal' growth then it would be reasonable to infer that the variation seen for the gluteal cortical thickness might represent a modified response which may require additional functional interactions to be considered.

It is possible that the gluteal thickness may be influenced by additional requirements and influences including muscular development and early reflex contraction of gluteal musculature. The gluteal cortex provides attachment for a large developing mass of musculature, which in itself is considered to be the initiator of periosteal ossification of the iliac blades (Laurenson, 1964b; Delaere *et al*, 1992; Scheuer and Black, 2000). This muscle mass, from its early development, may induce functional forces on the developing cortex through reflex contractions. In support of this theory, a previous study on the ossification of the fetal ilium noted a thickening of the gluteal cortex and attributed this to the presence of the gluteal musculature (Delaere *et al*, 1992). This is important, as strong evidence exists to suggest that bone mass and strength are related to muscle function (Schoenau and Fricke, 2008), with muscle contraction placing the largest physiological load on bone, creating an inherent need for bone stability to be adapted to muscle strength (Schoenau, 2006). Therefore, it is possible that the reflex contractions of gluteal musculature, which result in altered bone morphology in the adult, may cause the gluteal cortex to remodel during early development resulting in an increased cortical thickness in regions of direct muscular attachment. It is acknowledged that there is also a large muscle mass on the pelvic surface in the form of the iliacus muscle, which may also be considered to initiate a remodeling of the pelvic cortex. However, the advanced remodeling of the gluteal cortex is proposed to be caused by the much larger muscle volume and strength of the

gluteus minimus and medius, thus inferring that the differential thickening of the cortices may simply be attributed to differences in sheer muscle mass.

Finally, it is appropriate to consider the inherent limitations of this study and discuss these in the context of the results. As developmental homology cannot be assumed due to the cross-sectional nature of the study and the use of a uniform grid, some degree of variation may exist between the absolute positioning of each ROI. However, this variation is considered to be minimal due to the analysis of a single developmental cohort which contains specimens of a very similar shape and size. Therefore, ROIs are considered to be broadly representative of the same functional region in each specimen analysed. Further to this, the selection of an appropriate point within a ROI which is representative of average thickness may be ambiguous. To limit this error, four random points within each ROI were selected and averaged in order to give a thickness value which was more representative of the whole ROI. The raw data for this analysis is presented in Appendix 3. One final potential limitation which must be addressed is relevant to ROIs which are non-uniform in their cortical appearance. Such ROIs are those associated with the auricular surface and the greater sciatic notch regions. On the gluteal cortex the auricular surface occupies parts of ROI's 7, 8 & 13. In these ROIs care was taken to avoid the cortex of the joint surface and concentrate the sampling points to non-auricular regions of the cortex. Additionally, on both gluteal and pelvic cortices the greater sciatic notch region (ROI 17) contains a convex surface morphology. Placement of analysis points on this convex surface may lead to exaggerated thickness data. To limit this, placement of analysis points within ROI 17 was confined to regions which represented cortex in plane with the blade of the ilium.

6.12 Relationship of trabecular and cortical data to normal growth

The implied mode of growth and ossification in the ilium has been well documented in the literature, with initial periosteal ossification followed by endochondral bone production radiating progressively over the anlage in a relatively uniform pattern (see Chapter 2, section 2.3 for review). This implied mode of ossification in the ilium is summarised in Figure 6.35. However, advanced analysis of the trabecular and cortical data obtained for the neonatal ilium requires a somewhat modified view of progressive ossification to be considered.

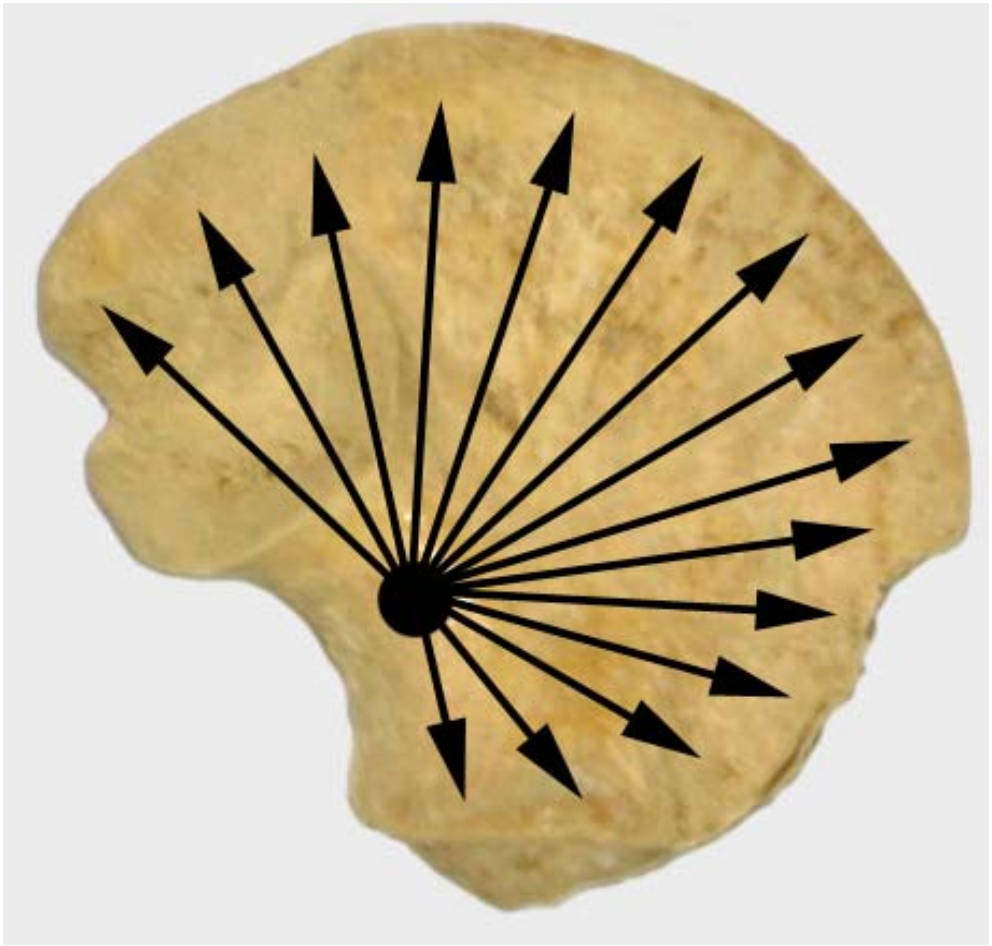

Figure 6.35. Simplified view of the current concept of ossification progression in the human ilium. Uniform radiating endochondral growth from the centre of ossification in the vicinity of the greater sciatic notch.

This part of the study builds upon previous quantitative structural data presented on the trabecular patterning within the neonatal ilium and proposes that growth is governed by multifunctional influences that do not support a uniform pattern of concentric progressive ossification. Alternatively, evidence of a distinctive pattern of regionalised growth, characterised by appositional cortical growth, compartmentalised endochondral ossification and vascularisation directed towards defined growth plates, is presented. This analysis is based upon statistical differences between trabecular parameters and cortical thicknesses from selected adjacent volumes and regions of interest.

Trabecular structural parameters obtained from histomorphometric analysis of three-dimensional slice data were further analysed to investigate specific regions of trabecular patterning. Overall statistical significance between all VOI's for each trabecular parameter is summarised in Figure 6.36 (full statistical data can be found in Appendix 2). To achieve specific regional statistical analysis, pairwise multiple comparisons were restricted to adjacent volumes of interest, where a VOI was compared with neighbouring VOI's in the superior, inferior, anterior or posterior positions based on Figure 6.2. For levels of statistical significance between each 'adjacent VOI' see Figure 6.37.

Statistically significant differences were analysed between adjacent volumes of interest for each of the measured trabecular indices. Adjacent volumes of interest which demonstrate a statistically significant difference between values are summarised in Figure 6.38. Overall statistical significance, where a significant difference is observed in one or more trabecular indices is summarised in Figure 6.39.

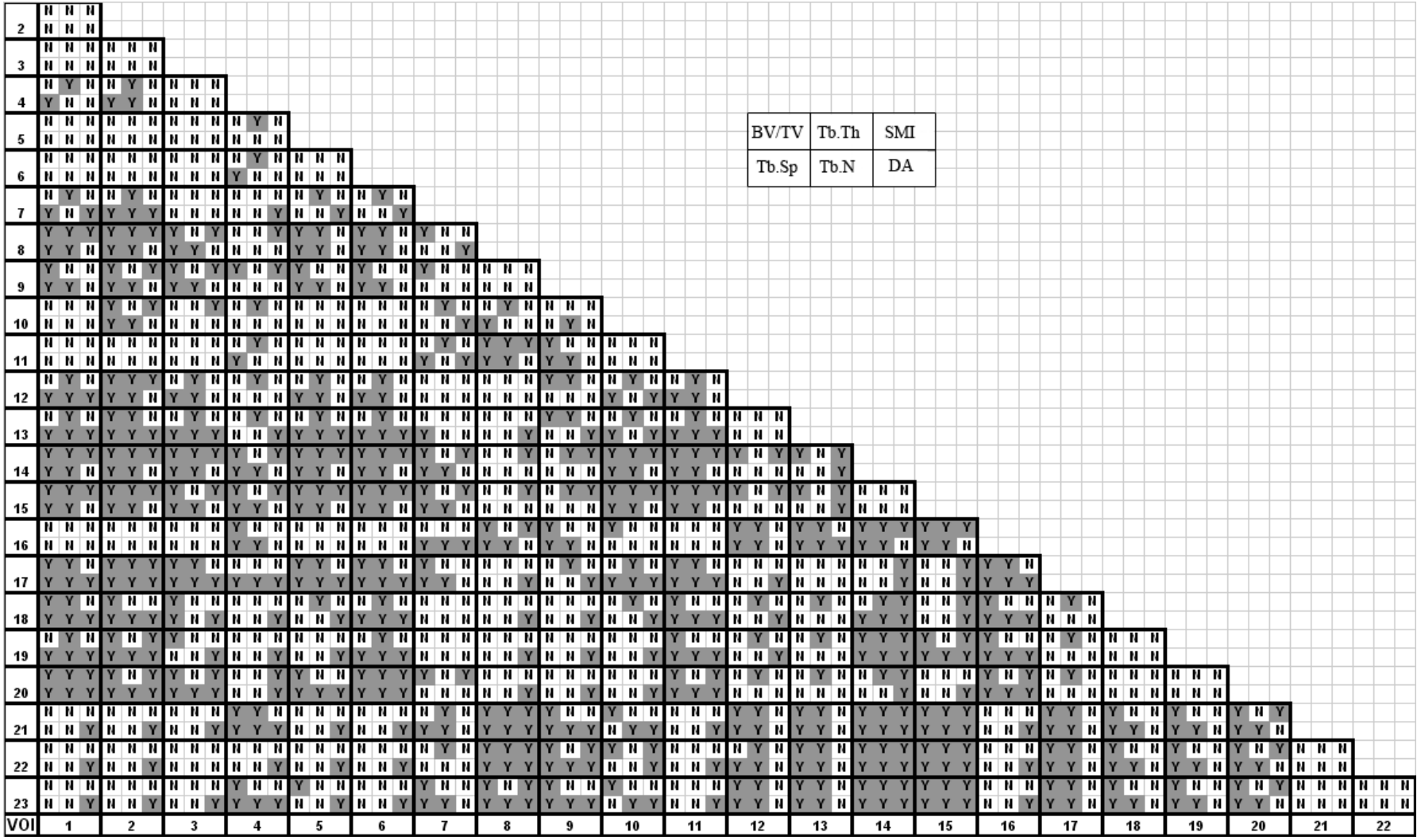

Figure 6.36. Summarised statistical significance between all volumes of interest from ANOVA pairwise multiple comparison procedure. Y=statistically significant difference (shaded); N=no statistically significant difference (not shaded).

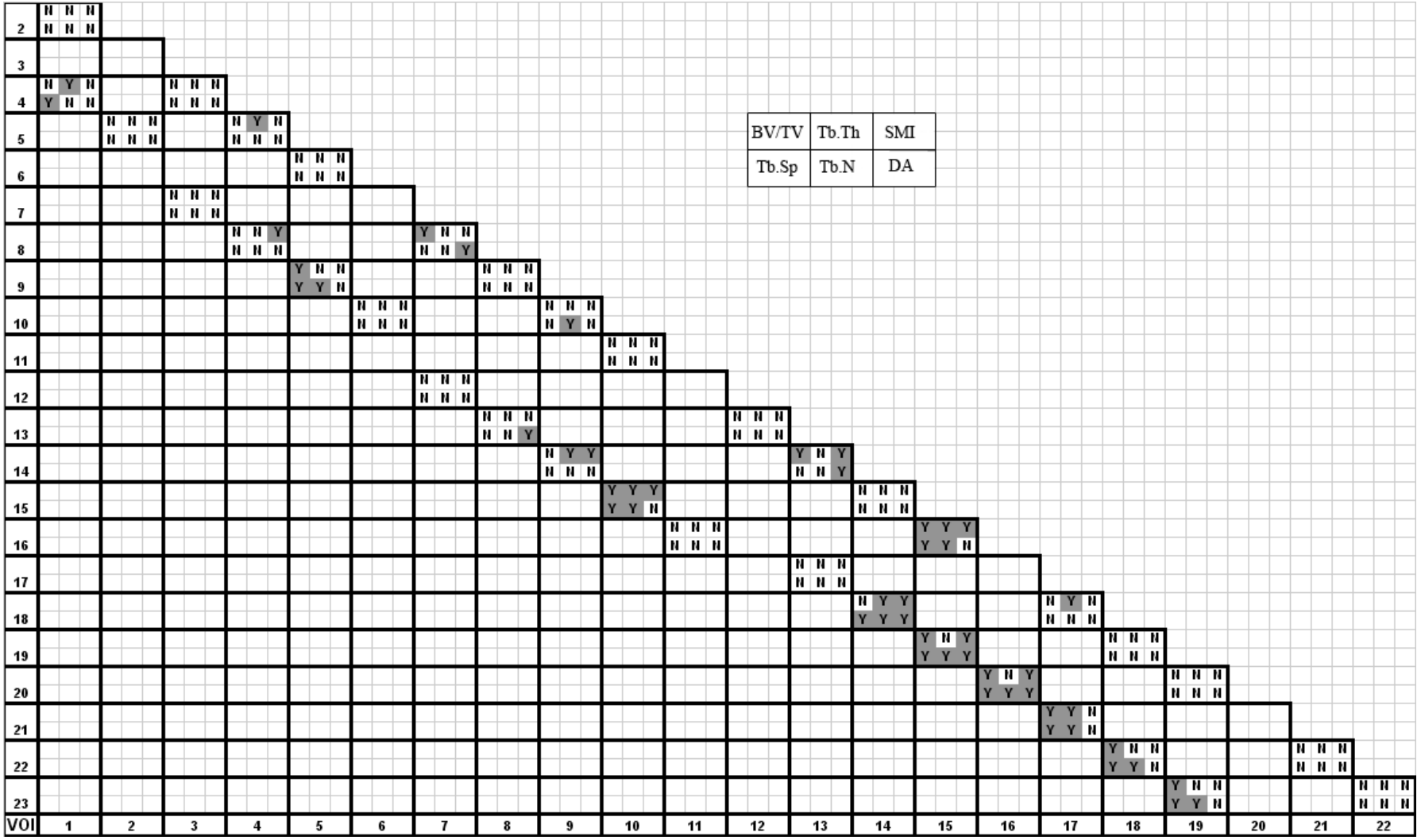

Figure 6.37. Summarised statistical significance between immediately adjacent volumes of interest from ANOVA pairwise multiple comparison procedure. Y=statistically significant difference (shaded); N=no statistically significant difference (not shaded).

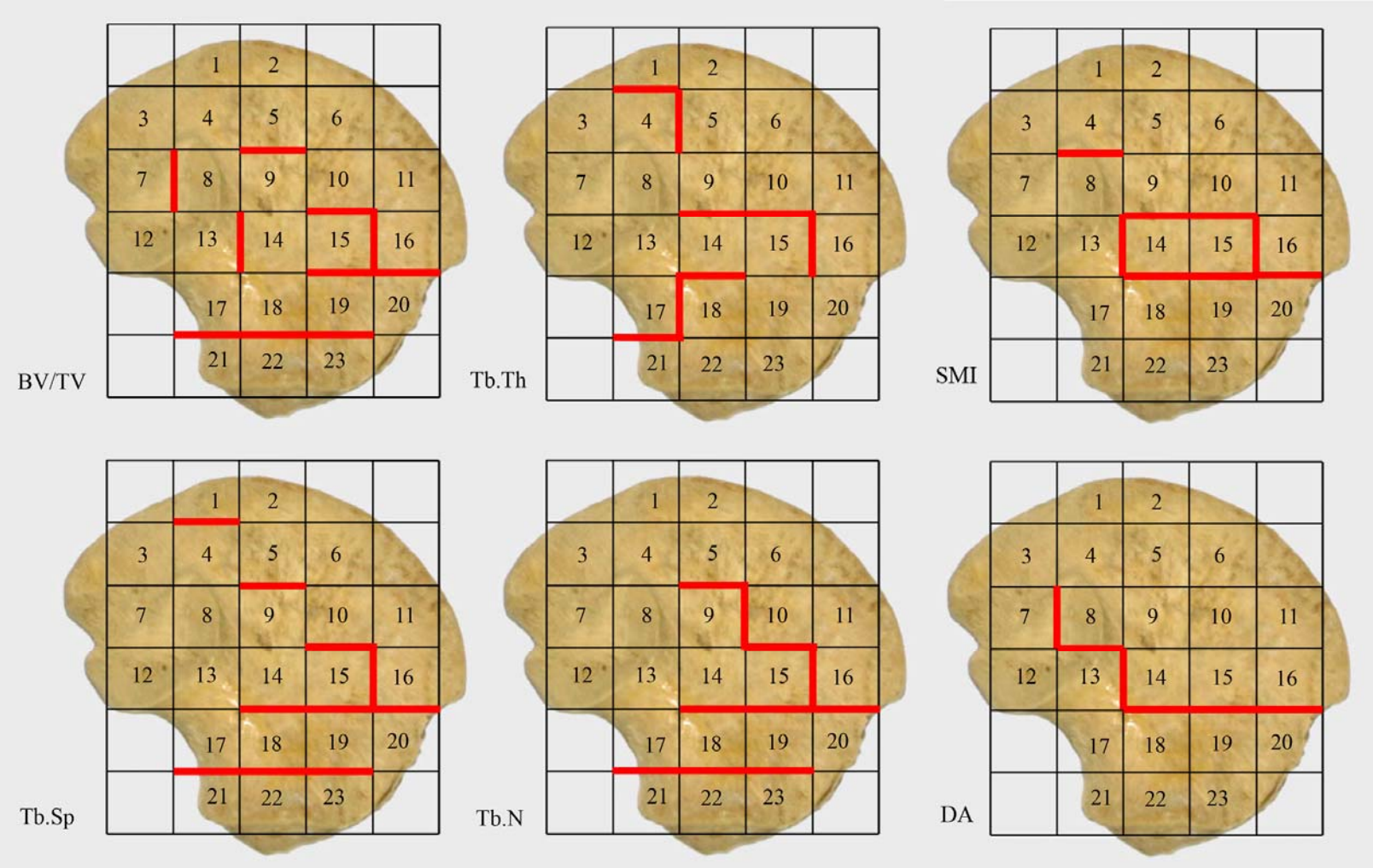

Figure 6.38. Statistically significant difference between individual trabecular parameters in immediately adjacent VOI's. A thickened red line represents that a statistically significant difference exists between VOI's that border the line.

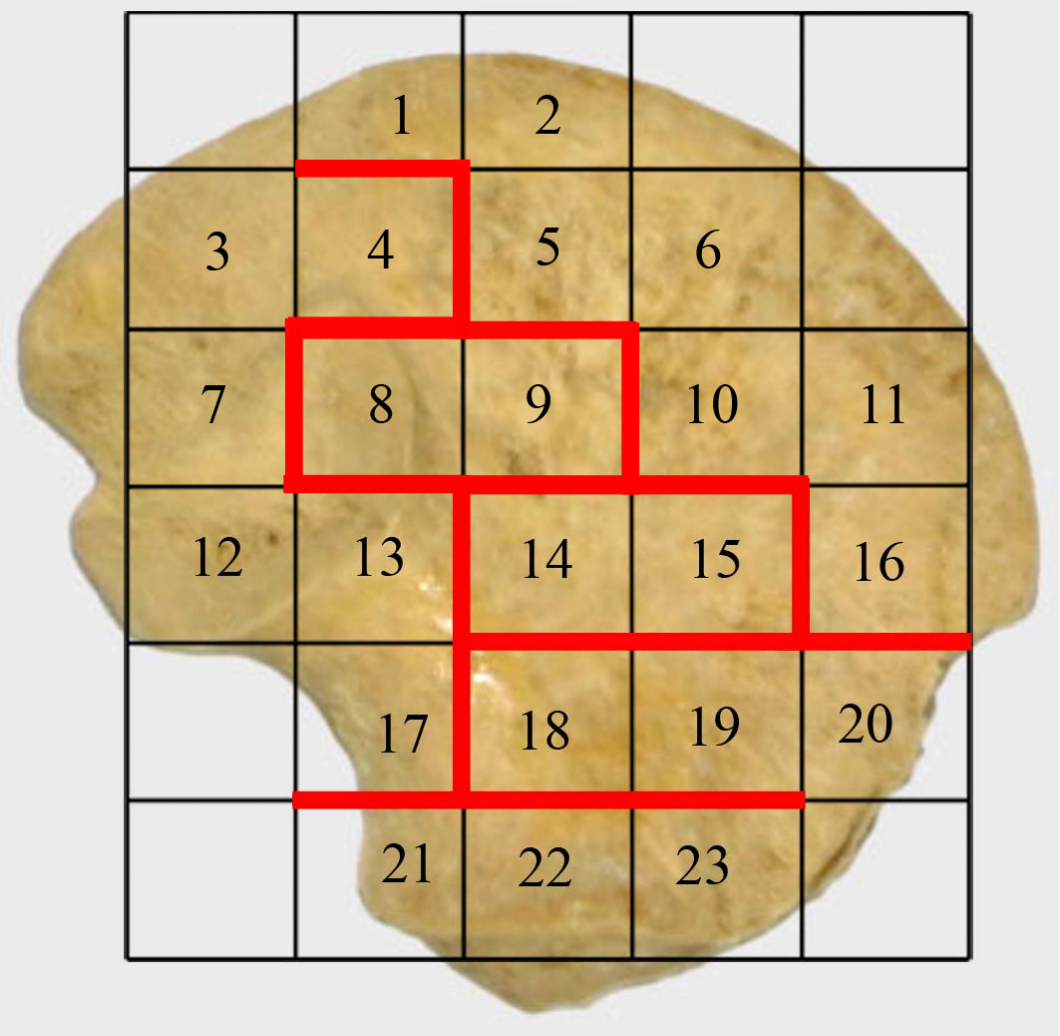

Figure 6.39. Illustration of statistically significant difference between one or more parameters in adjacent VOI's. A thickened red line represents that a statistically significant difference exists between VOI's that border the line.

Bone Volume Fraction (BV/TV)

Adjacent volumes of interest which displayed a statistically significant difference between values of bone volume fraction included: 5v9; 7v8; 10v15; 13v14; 15v16; 15v19; 16v20; 17v21; 18v22; and 19v23 (Figure 6.38). In the neonatal ilium statistically significant differences in BV/TV separated the trabecular volume into a distinct acetabular component (VOI's 21-23) which was characterised by high values of BV/TV (Table 6.3), an anterior inferior component (VOI's 19&20) which demonstrated reduced BV/TV and an iliac blade component which in itself contained a general

demarcation of anteriorly and posteriorly associated volumes. Each of these regions was distinct from the trabecular chiasma (VOI's 14&15) which demonstrated a low value of BV/TV (18.909% and 19.013% respectively). Within the iliac blade trabecular volume, statistically significant differences (Figure 6.37) were observed between the central ilium (VOI 9) (21.710%) and the superior body (VOI 5) (34.415%), the trabecular chiasma (VOI 15) (19.013%) and central body (VOI 10) (30.857%), the posterior auricular (VOI 7) (34.866%) and cranial auricular volumes (VOI 8) (26.734%), the caudal auricular (VOI 13) (31.953%) and trabecular chiasma volume (VOI 14) (18.909%), as well as the anterior superior perimeter (VOI 16) (41.044%) and trabecular chiasma volumes (VOI 15) (19.013%). This division of the iliac trabecular volume from early in the developmental period, evidenced via BV/TV, demonstrates not only a compartmentalisation of progressing ossification but also highlights a modeling gradient within particular compartments. All average values of BV/TV are taken from Table 6.3.

Trabecular Thickness (Tb.Th)

From the early developmental period distinguishable differences in Tb.Th are observed across the ilium. Adjacent volumes of interest which displayed a statistically significant difference between values of Tb.Th included: 1v4; 4v5; 9v14; 10v15; 14v18; 15v16; 17v18; and 17v21 (Figure 6.38). Statistically significant differences (Figure 6.37) are observed between regions associated with the greater sciatic notch (VOI 17) (0.204mm) and surrounding volumes (VOI's 18&21) (0.166mm and 0.151mm). Additionally the trabecular chiasma (VOI 14&15) (0.209mm and 0.186mm) is demarked by statistical differences between VOI's 9,10,16&18 (range of 0.148 – 0.166mm). Differences in Tb.Th were also observed between the superior perimeter of the iliac crest (VOI 1)

(0.146mm) and the superior body (VOI 4) (0.169mm). Finally, differences were observed between volumes constituting the superior body (VOI's 4&5) (0.169mm and 0.148mm respectively). All average values of trabecular thickness are taken from Table 6.4.

Trabecular Separation (Tb.Sp)

Adjacent volumes of interest which displayed a statistically significant difference between values of Tb.Sp included: 1v4; 5v9; 10v15; 14v18; 15v16; 15v19; 16v20; 17v21; 18v22; and 19v23 (Figure 6.38). Statistically significant differences in Tb.Sp between volumes (Figure 6.37), divide the ilium into an acetabular component (VOI's 21-23) (range of 0.218 - 0.239mm), an inferior body component (VOI's 18-20) (range of 0.317 – 0.341mm) and an iliac blade component. Within the iliac blade there are further statistical differences which are considered to separate the blade into anterior and posterior portions. These differences occur between the trabecular chiasma (VOI 15) (0.509mm) and the anterior superior perimeter (VOI 16) (0.225mm) , the trabecular chiasma (VOI 15) and the central body (VOI 10) (0.27mm), the central body (VOI 9) (0.359mm) and the superior body (VOI 5) (0.252mm) and finally between the superior body (VOI 4) (0.304mm) and the superior perimeter (VOI 1) (0.226mm). All average values of trabecular separation are taken from Table 6.5.

Trabecular Number (Tb.N)

Adjacent volumes of interest which displayed a statistically significant difference between values of Tb.N included: 5v9; 9v10; 10v15; 14v18; 15v16; 15v19; 16v20; 17v21; 18v22; and 19v23 (Figure 6.38). In the neonatal ilium statistically significant differences between values of Tb.N (Figure 6.37) follow a similar pattern to that for

Tb.Sp in that a defined acetabular component (VOI's 21-23) (range of 2.583 – 2.818mm^{-1}), an inferior body region (VOI's 18-20) (range of 1.546 – 1.816 mm^{-1}) and a blade component of the ilium are observed. Within the trabecular volume of the blade there are demarcations between the central body (VOI 9) (1.405mm^{-1}) and the superior body (VOI 5) (2.335mm^{-1}), the trabecular chiasma (VOI 15) (1.046mm^{-1}) and the central body (VOI 10) (2.087mm^{-1}) as well as between the trabecular chiasma (VOI 15) (1.046mm^{-1}) and the anterior superior perimeter (VOI 16) (2.63mm^{-1}). All average values of trabecular number are taken from Table 6.6.

Structural Model Index (SMI)

Adjacent volumes of interest which displayed a statistically significant difference between values of SMI, although still within the range of values for a plate-like model of bone architecture included: 4v8; 9v14; 10v15; 13v14; 14v18; 15v16; 15v19; and 16v20 (Figure 6.38). These statistical differences (Figure 6.37) illustrate that the SMI for the trabecular chiasma volumes (VOI's 14&15) (2.011 and 1.977 respectively) are significantly higher in value than all surrounding volumes. Additionally, differences are observed between the anterior superior perimeter (VOI 16) (1.254) and the anterior inferior body (VOI 20) (1.678), as well as the cranial auricular volume (VOI 8) (1.632) and the superior body (VOI 4) (1.249). All average values of structural model index are taken from Table 6.7.

Degree of Anisotropy (DA)

Adjacent volumes of interest which displayed a statistically significant difference between values for the degree of anisotropy included: 7v8; 8v13; 13v14; 14v18; 15v19; 16v20 (Figure 6.38). The statistical differences observed divide the ilium into a superior

blade component and an inferior body/acetabular component through differences observed between the trabecular chiasma volumes (VOI's 14&15) (0.818 and 0.815 respectively) and the inferior body (VOI's 18&19) (0.538 and 0.520 respectively), as well as the anterior superior perimeter (VOI 16) (0.839) and the anterior inferior body (VOI 20) (0.629). Additional areas of significant difference are located between the cranial auricular volume (VOI 8) (0.861) and the posterior auricular volume (VOI 7) (0.684), the cranial auricular volume (VOI 8) (0.861) and caudal auricular volume (VOI 13) (0.583), and finally between the caudal auricular/trabecular chiasma volume (VOI 13) (0.583) and the trabecular chiasma (VOI 14) (0.818). All average values of degree of anisotropy are taken from Table 6.8.

Collectively, statistical differences between adjacent VOI's appear to divide the trabecular volume into six regions which are relatively isolated on the basis of trabecular characteristics. This differentiation can be visualised using a 2D sagittal slice through the ilium (Figure 6.40). Each of these regions, identified through quantification and gross visualisation, focus from a central region, previously referred to as the trabecular chiasma (Macchiarelli *et al*, 1999; Rook *et al*, 1999). The positioning of this trabecular chiasma coincides approximately with the location of the primary centre of ossification and dominant nutrient artery invasion (Region 1 on Figure 6.40).

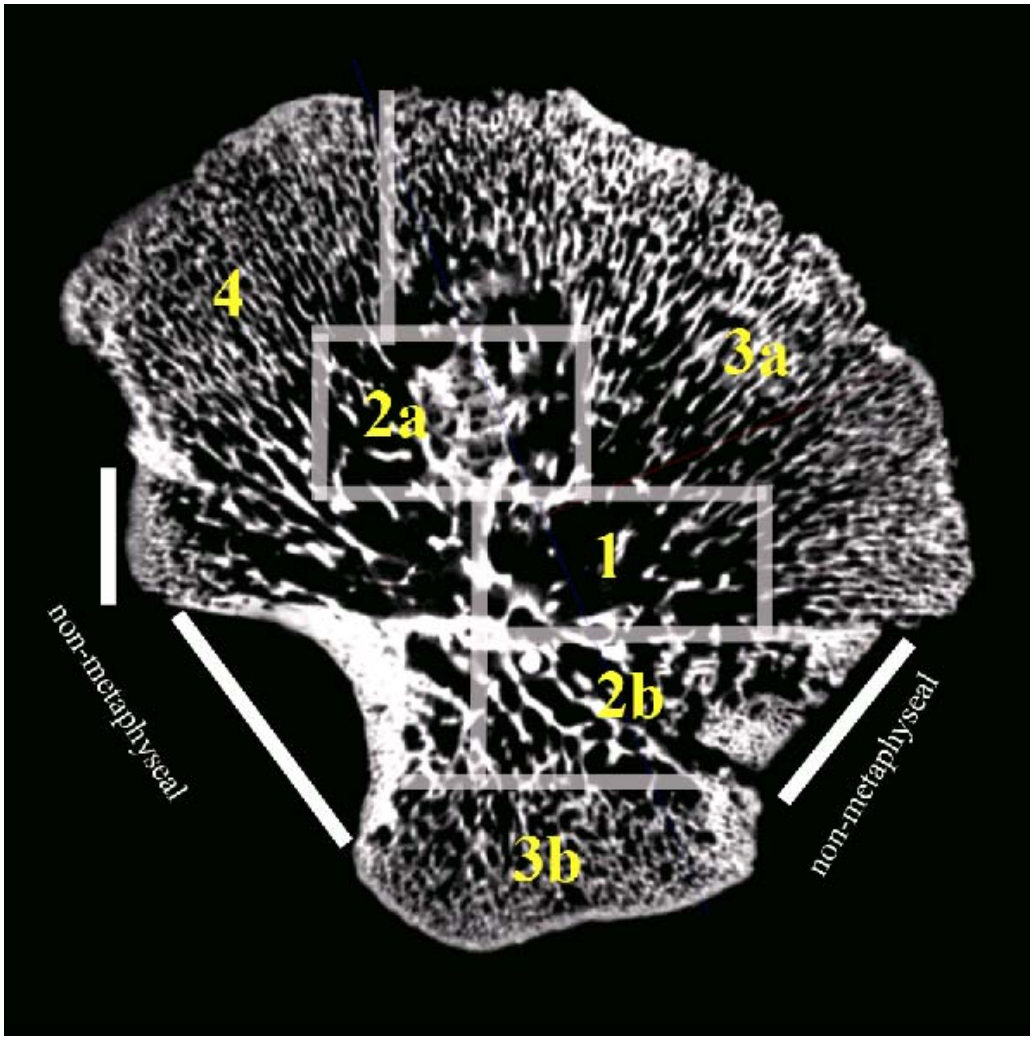

Figure 6.40. Two-dimensional sagittal microCT slice through a neonatal ilium. Gross visualisation of trabecular patterning demonstrates regions of differential 'growth'.
1 - most mature region of trabecular bone; 2a&b – regions of bone growth which are less mature; 3a&b – regions of most recent bone modeling; 4 – recently modelled region which is different from 3a&b possibly due to multifunctional influences.

The regions observed to radiate from this central locus are directed postero-superiorly, antero-superiorly and inferiorly. The postero-superior directed radiation first presents as a volume of trabecular bone which is less mature than that of the chiasma (Region 2a), and then as a terminal region of most recently modelled trabecular bone (Region 4). In addition to the recently modelled architecture in region 4, there appears to be a distinctive trabecular pattern associated with growth towards the greater sciatic notch. The antero-superior directed radiation is observed to extend towards the iliac crest as a volume of recently modelled trabecular bone (Region 3a). Finally, the inferiorly

directed radiation is observed to extend towards the acetabular metaphyseal region, first presenting as a volume of less mature trabecular bone than that of the chiasma (Region 2b), then as a volume of most recently modelled trabecular bone (Region 3b). Each of these trabecular growth trajectories are illustrated in Figure 6.41. It must be noted that there are no differences between regions 2a and 2b other than degree of anisotropy. This is also true between regions 3a and 3b where the only statistical differences observed are between degree of anisotropy. Each of the compartmentalised regions outlined will be fully discussed by relating bony morphology to specific functional influences.

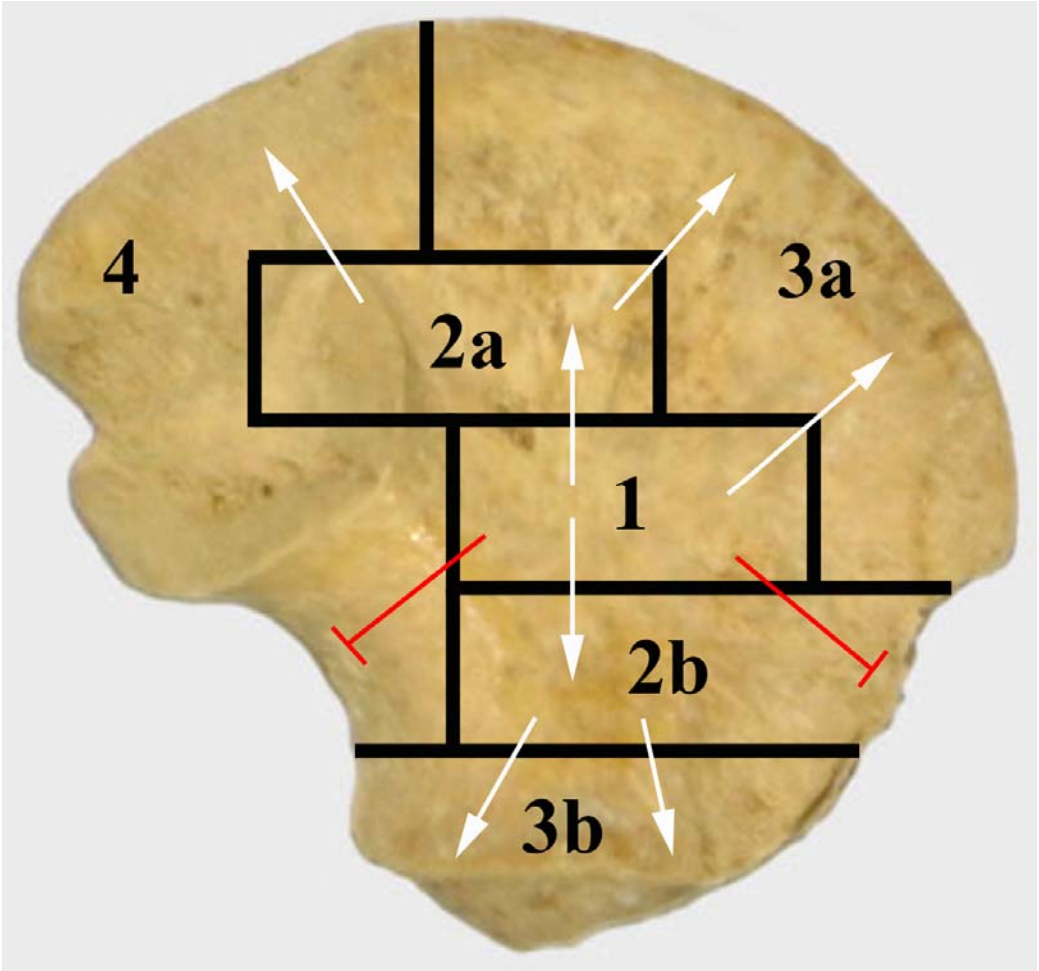

Figure 6.41. Revised view of ossification progression in the human ilium. The schematic demonstrates the position of six distinct trabecular regions within the neonatal ilium. White arrows are representative of growth towards a metaphyseal surface. Red lines are representative of restricted growth regions associated with non-metaphyseal surfaces.

The results for trabecular volume statistical analysis revealed a structural patterning which compartmentalises the trabecular volume into well defined regions. This structural patterning may be explained through a revised model of endochondral ossification which is partially driven by three active 'growth' regions relating to metaphyseal influences; two at the iliac crest and one at the acetabular component, as well as three 'restricted growth' regions relating to non-metaphyseal influences; one at the anterior inferior iliac spine, one at the greater sciatic notch and one at the caudal limb of the sacro-iliac joint. Analysis of regional cortical thicknesses has also reinforced this theory by demonstrating a statistically significant differential thickening between pelvic and gluteal cortices in 'restricted growth' perimeter regions and no statistical difference between cortices in 'growing' perimeter regions (Table 6.9; Figure 6.34).

6.13 Discussion of progressive trabecular and cortical growth and morphology

Initial bone modeling in the ilium occurs at specific metaphyseal growth fronts which are present at the iliac crest and acetabular component (Scheuer and Black, 2000). It is proposed that initial modeling in the ilium is partly responsible for the characteristic trabecular architecture and cortical morphology observed during the early developmental period. Furthermore, it is suggested that modeling is partially controlled by 'metaphyseal drivers' which cause a radiation of trabecular and cortical bone growth from specific metaphyseal growth fronts. The statistical analysis for this part of the study indicated the presence of three 'growth regions' directed by metaphyseal drivers at the iliac crest (anterior and posterior) and acetabular component, and three 'restricted growth regions' located at the anterior inferior iliac spine region, the greater sciatic

notch region and the caudal sacro-iliac joint where there are no metaphyseal growth fronts.

The pattern of bone architecture in the neonatal ilium is proposed to be a composite of regions of bone modeling and regions of bone remodeling. Firstly, during early bone development in the ilium, prior to the influences of remodeling, a baseline template is proposed to result from the initial modeling of the primary spongiosa which is intimately related to primary chondrocyte arrangement, initial mineralisation, vascular invasion of the tissue and subsequent calcification. Several studies have demonstrated that the structure of the cartilaginous growth plate matrix and the subsequent primary trabecular bone structure are closely associated (Byers *et al*, 2000; Olsen *et al*, 2000). Subsequently, after formation of the primary spongiosa, the structure undergoes initial remodeling in response to developing functional forces and associated anatomical interactions which occur concomitant with ongoing modeling at growth fronts.

It is therefore suggested, that initial and continued modeling is partially directed by metaphyseal drivers which cause the trabecular architecture to adopt a specific morphology which radiates from the centre of ossification towards growth fronts at the iliac crest and acetabular component. These metaphyseal drivers direct the formation of initial immature primary spongiosa and early thin cortical bone production. Further to this, subsequent remodeling is proposed to alter regions of more mature bone formation and have an influence on regions of the ilium which are not constantly being extended by modeling. Additionally, it is suggested that initial modeling and subsequent remodeling of the trabecular bone may be influenced by the presence of the dominant vascular arrangement within the ilium which is necessary to support active growth. As the ilium grows in size, its vascularity also increases proportionately, therefore, as

vascular elements are space occupying tissues, they will be a driver for remodeling causing Tb.N to decrease, Tb.Sp to increase, BV/TV to decrease and will result in a compensatory increase in Tb.Th. This vascular arrangement is proposed to cause primary bone formation and subsequent remodeling to proceed around its distribution, ultimately dictating where the trabeculae will be arranged in broad terms.

Vascular invasion is thought to have a definite and profound influence on the trabecular morphology of the iliac cancellous bone during the earliest stages of development. Initial consideration is given to the presence of the dominant osteogenetic nutrient artery of the ilium and its function as an organiser of bone formation (Trueta, 1963). It can be hypothesised that the close relationship between the positioning of the vascular network and timing of vascular invasion, which initiates endochondral ossification, may have an impact on the structural organisation of the proceeding ossifying architecture. Further to this, it is well documented that angiogenesis is closely associated with bone resorption and formation mechanisms (Brandi and Collin-Osdoby, 2006; Eriksen *et al*, 2007), resulting in a direct remodeling relationship. The dominant nutrient artery of the ilium is observed to enter the cortical bone at a location superior-medial to the greater sciatic notch in response to angiogenic signals from disintegrating cartilage cells (Alini *et al*, 1996; Carlevaro *et al*, 1997; Ortega *et al*, 2004). This artery proceeds by invading the underlying cartilaginous anlage, initiating the process of trabecular bone formation in a position corresponding to the future trabecular chiasma. Once inside the cartilaginous body of the ilium the vascular network is thought to radiate in a fan-like orientation superiorly into the iliac body towards the iliac crest and inferiorly into the acetabular component, indicative of the driving forces of the opposing metaphyseal growth plates. Arterial injection and Spalteholz clearing of this vascular network has intimated the positioning of the nutrient artery and its resultant bifid diffuse

fanning (Crock, 1996). The distribution of arterial invasion ranges from the most substantial dominant vessels which first enter the bone, to the fine arteriole network in the superior blade and acetabular regions (Figure 6.42). As the presence of nutrient vessels is observed prior to the formation of the first trabecular elements (Laurenson, 1964b; Scheuer and Black, 2000), growth and remodeling of trabeculae proceed around the invading, proliferating and growing vessels. Furthermore, with continued growth and angiogenesis of the nutrient vessels, trabeculae may become further remodelled (Trueta, 1963). As the trabeculae become separated by the vascular elements it is necessary for structural strength to be regained so as to prevent the trabecular structure from becoming weakened leading to functional failure. Functional failure in the neonate would most likely arise from muscle pull on weakened plates that could perhaps separate.

Figure 6.42. Arterial distribution of neonatal ilium. Modified from Crock (1996).

In order to describe the pattern in more detail and in relation to the positioning of nutrient invasion and subsequent endochondral ossification it is appropriate to first consider the most mature area of initial bone formation followed by the pattern of radiating endochondral growth. Initial consideration is therefore given to the trabecular chiasma (Region 1) where the observed trabecular morphology is considered to be heavily influenced by proximity to the primary centre of ossification and the concomitant point of dominant nutrient invasion. This is reflected in the fact that the trabecular chiasma is statistically different from surrounding VOI's in one or more trabecular characteristics. Within this region the largest nutrient vessels for the neonatal ilium will be present as they pierce the periosteum and diffusely radiate throughout the trabecular network (Brookes, 1971; Crock, 1996). The presence of this comparatively large vascular network is considered to have implications on the surrounding trabecular network resulting in a low BV/TV which consists of a low number of thickened, well spaced trabeculae. This region is likely to be most affected by the vascular demand of the rest of the bone. Combined with increasing vascular demands, the proximity of the ossification centre is also considered to further contribute to the observed morphology. As this is the site of initial bone formation, this region has had an extended time for advance modeling and potential remodeling of trabeculae associated with developing functional forces. This advanced development may serve to explain the more robust trabecular characteristics in this region. This region also displays significant cortical thickness on both pelvic and gluteal cortices, which is in line with this region being the locus of primary ossification and a site of significant muscle attachment (Rosse and Gaddum-Rosse, 1997).

Each subsequent compartment of trabecular architecture is observed to diverge from the trabecular chiasma in a pattern of radiating endochondral growth. This has

been confirmed by statistically significant differences in trabecular morphology between the trabecular chiasma and surrounding VOI's. The first of these to be considered are the regions which radiate superiorly and inferiorly from the trabecular chiasma region and are represented by a trabecular morphology which is considered to be less mature than that of the trabecular chiasma. Region 2a is observed to radiate postero-superiorly from the trabecular chiasma and region 2b is evident radiating antero-inferiorly from the trabecular chiasma (Figure 6.41). These areas encompass VOIs 8&9 and 18-20 respectively and are both quantifiable by an increased BV/TV, comprising increased Tb.N as well as decreased Tb.Th and Tb.Sp. The altered trabecular characteristics may be primarily attributed to the fact that this trabecular volume is less mature than the trabecular chiasma and as such has undergone reduced remodeling resulting in the observed trabecular characteristics. Additionally, the space occupying vascular supply within these regions has finer branches which have not forced full remodeling of the trabecular scaffold. The metaphyses are heavily influential over vascular morphology and probably dictate the directionality of the vascular network towards growth fronts. This is reflected in the fact that vascular presence is directed towards metaphyseal growth plates and to a lesser extent towards non-metaphyseal regions. In region 2b, the morphology of the anterior section may be attributable to the fact that this region is associated with a 'restricted growth' region where the endochondral ossification is not progressing towards a growth plate but is instead juxtaposed between the trabecular chiasma and a non-metaphyseal cortex at the anterior inferior iliac spine. As such, the trabecular morphology within this region is different to that observed in surrounding growth regions resulting in the statistically significant differences between volumes of interest; 14-18, 15-19, 16-20, 17-18, 18-22, and 19-23. When considering the vasculature of region 2b, it is somewhat different to

that observed in “growing” regions as there are no significant branches of arterial supply directed antero-inferiorly (Figure 6.42) (Crock, 1996). As the passage of the nutrient artery and its branches are proposed to supply areas of growth which are directed towards a growth plate it not surprising that the arterial supply does not extend fully into these VOI’s due to the absence of a growth plate. This is considered to contribute to the characteristic ‘restricted growth’ trabecular morphology observed towards the anterior inferior iliac spine. The altered morphology can be grossly visualised on a 2D sagittal microCT slice (Figure 6.40). The endochondral progression within this region of the ilium is considered to be different from “growing” regions as there is not a continuous modeling front and instead trabeculae which have been laid down are now beginning to be remodelled into a more mature form. The only difference between regions 2a and 2b are their respective values for degree of anisotropy, where region 2b tends towards a more organised morphology. The fact that all other parameters are not statistically different fits with the theory that these regions represent modeling fronts behind the most mature region at the ossification centre. However, the more isotropic trabecular conformation in region 2b may be explained by its potential to be influenced by hypothesised retrograde limb movement forces. Although these regions are similar in their trabecular characteristics they differ in their cortical thickness distributions. Region 2a and 2b have similarly thick gluteal cortices however region 2a displays thin to average thickness on the pelvic cortex with region 2b displaying average thickness on the pelvic shell. This results in region 2b possessing the most robust overall morphology when considered in terms of pelvic and gluteal cortical thickness and trabecular characteristics. It is suggested that this advanced thickening in region 2b may be associated with its closer proximity to the ossification centre, thus resulting in advanced cortical bone remodeling.

The subsequent regions of distinct trabecular morphology are observed to radiate antero-superiorly towards the iliac crest (Region 3a) from region 2a and the trabecular chiasma as well as inferiorly into the acetabular component (Region 3b) from the inferior body. Both of these regions have been termed peripheral 'growing regions' due to their trabecular morphology which is characterised by a high bone volume fraction consisting of a high number of thin, tightly packed trabeculae. This morphology is explainable as these volumes are directed towards the iliac crest and acetabular metaphyseal growth plates respectively, which are modeling fronts for advancing endochondral growth. Due to the continuous modeling towards growth regions during the neonatal developmental period these regions can be classified as 'growing'. The presence of antero-superiorly and inferiorly directed branches of the dominant nutrient vessels (Figure 6.42) (Crock, 1996), contributes to evidence that these regions of the ilium are actively growing through continuous modeling. These regions display very similar trabecular morphology reflected in all trabecular indices except degree of anisotropy. As discussed previously the more isotropic trabecular alignment in the acetabular component suggests that potential retrograde forces, proposed to be transmitted across the cartilaginous acetabulum from reflexive limb movement, may indeed induce a precocious alteration within the trabecular architecture making it distinct from other newly modelled peripheral trabecular volumes. The cortical bone thickness in regions 3a and 3b is of a maintained low value which is also considered to be reflective of newly modelled bone.

The final region of demarked trabecular morphology is observed postero-superiorly (Region 4). This is a large region which encompasses volumes of interest from the greater sciatic notch through to the posterior iliac crest. In this region, gross visualisation of trabecular distribution from 2D μCT slices (Figure 6.40), highlighted a

differentiation in trabecular characteristics within the trabecular volume which were not reflected in the statistical differences between quantitative values. This is surprising as it would be expected that this volume of trabeculae would reflect multiple influences including the position of the auricular surface, the proximity of the sciatic nerve, the modeling front associated with the postero-superior metaphyseal driver and any potential forces induced from reflexive limb movements. However, these individual influences are indistinguishable as reflected by statistical differences in the trabecular architecture. This may be due to the proposed multiple influences being superimposed and ultimately masking one another, leading to the composite trabecular pattern observed which cannot be defined by statistically significant differences. Specifically, within region 4, the trabecular architecture associated with the greater sciatic notch may be described as a further 'restricted growth' region of trabecular patterning. As described previously for the antero-inferior region, it is not expected that this trabecular volume should have a significant contribution from the trabecular arterial system due to its endochondral progression being directed towards a non-metaphyseal border and not an active growth plate. This is once again confirmed by analysis of the iliac vascular distribution, where a defined arterial void is situated in the trabecular volume associated with the greater sciatic notch (Figure 6.42) (Crock, 1996). Additionally, within the postero-superior perimeter of region 4 the trabecular architecture reflects a growing front where continued modeling results in a trabecular morphology characterised by a high bone volume fraction, again consisting of numerous, thin, tightly packed trabeculae. This is a similar morphology to that observed in the anterior superior and acetabular trabecular volumes.

As outlined, when considering the modeling progression superiorly within the iliac blade, respective anterior and posterior metaphyseal drivers can be hypothesised to

control the proceeding growth at the iliac crest. This dual focused modeling progression divides the superior peripheral iliac trabecular volume into a distinct anterior and posterior extension. Therefore, these two trabecular areas have been termed ‘growing regions’ and may explain the trabecular differences which divide the iliac blade into anterior and posterior extensions. It has previously been considered that the iliac crest epiphysis ossified from a midline point on the iliac crest and proceeded to extend anteriorly and posteriorly (Francis, 1940). However, this view has been expelled by the recognition that the iliac crest epiphysis instead ossifies from two individual ossification centres (Scheuer and Black, 2000). The anterior iliac crest epiphysis forms the anterior part of the crest and the posterior iliac crest epiphysis forms the posterior part of the crest (Stevenson, 1924). The positioning of the future anterior and posterior epiphysis corresponds to the two different regions of trabecular arrangement (regions 3a and 4). It is proposed that the formation of this bi-partite iliac crest epiphysis and the associated underlying trabecular rays may be partly directed by the attachment of musculature to the iliac crest. Muscle attachment sites along the iliac crest can be divided into defined muscle compartments and individual muscles which reflect the two parts of the iliac crest. Anteriorly, the internal and external oblique’s and transversus abdominus muscles take attachment, whereas posteriorly, gluteus maximus, latissimus dorsi, quadratus lumborum and erector spinae muscles take attachment (Rosse and Gaddum-Rosse, 1997). The differing forces induced by these distinct muscle groups may act to partly induce the trabecular differences observed between the two regions.

The presence of two iliac crest epiphyses suggests the presence of two separate, but synchronised, growth fronts for which there must be an associated growth trajectory of ensuing endochondral ossification and an associated nutrient supply. The presence of a bidirectional growth trajectory from the trabecular chiasma and the presence of an

vascular supply for each trajectory (Figure 6.42) (Crock, 1996), may explain the trabecular differences between these regions. Differences in vascular distribution between regions 3a and 4 can be visualised in Figure 6.42 where there is a defined increased vascular density associated with the posterior region. Although this illustration of differential vascular distribution lends further evidence for the different trabecular characteristics observed between the two regions, it must be treated with caution as it is the sole illustration available. Additionally, gross visualisation of this pattern can be observed on a sagittal microCT cross-section (Figure 6.40). Within each of the anterior and posterior growth trajectories there is a defined modeling gradient which although not reaching statistical significance between most VOI's, is evident from inspection of absolute values. This gradient is reflected in an increasing BV/TV and Tb.N towards the periphery combined with a gradual decrease in Tb.Th and Tb.Sp. This modeling gradient may be attributable to the pattern of trabecular formation mirroring the arrangement of mineralised cartilage columns at the metaphyseal growing front (Byers *et al*, 2000; Olsen *et al*, 2000). This results in peripheral regions maintaining a newly modelled trabecular appearance which gradually becomes influenced by functional remodeling and advanced modeling towards the trabecular chiasma.

Further adding to the theory of multiple regions of growing metaphyseal and restricted growing non-metaphyseal origin is the statistical significance observed between values of cortical thickness for pelvic and gluteal cortices. This analysis demonstrated that no statistical difference was observed for cortical values between pelvic and gluteal shells in growing perimeter regions (ROI's 1, 2, 11, 16, 21, 22, 23). This may suggest that there is a continuous modeling front laying down new bone which has yet to experience any significant remodeling influences. Conversely, a

statistically significant difference between pelvic and gluteal cortices in proposed ‘restricted growth’ peripheral regions was observed. It is suggested that this differential thickening is due to restricted growth regions being subjected to remodeling forces, opposed to renewed appositional modeling, due to their distance from an active growth zone.

This part of the study proposes a revised model for progressive endochondral ossification in the neonatal ilium. The presence of defined regions of distinguishable trabecular characteristics arising from a central trabecular chiasma suggests that there is a compartmentalised radial growth. This growth is observed to extend towards growth plates in ‘growing’ trabecular trajectories and towards non-metaphyseal peripheral regions in ‘non-growing’ trabecular rays. This pattern of growth has been related to the presence, positioning and expansion of the vascular supply to the ilium of which dominant invading branches and subsequent radial fanning correspond well with the trabecular compartmentalisation observed. Additionally, within ‘growing’ compartments a modeling gradient is observed which is indicative of primary trabecular ossification which mirrors the columnar alignment of the initial cartilaginous template in peripheral regions. This primary spongiosa is then gradually remodelled in response to temporal functional interactions ultimately converging towards the most advanced region of growth at the trabecular chiasma. Therefore, this part of the study contributes towards an advanced understanding of the trabecular patterning and progressing ossification within the ilium during the neonatal developmental period.

6.14 Summarised relationship between qualitative morphology and quantitative results.

When paralleling the quantified trabecular and cortical data with the radiographic gradient maps a full interpretation of neonatal iliac form can be achieved. Within the ilium, the trabecular chiasma region represents a common locus of unique form in both qualitative and quantitative studies from which all other regions can be described. Therefore, this is a natural starting point to begin to understand the relationship between the quantitative and qualitative results of this project. Radiographically, the trabecular chiasma and inferior body regions were represented by dominant density gradients, this was supported by the high values of pelvic and gluteal cortical thickness observed in these regions. Underlying the thickened cortices, the trabecular architecture was observed to have adopted a remodeled conformation which is characteristic of increased structural strength i.e. trabeculae of increased thickness and decreased number. In summary, the chiasma and inferior body region are suggested to be more mature remodeled regions of the ilium due to the positioning of dominant nutrient invasion and concomitant centre of ossification. In addition to this, it is suggested that retrograde limb forces passing both antero-superiorly and postero-superiorly from the acetabular component and movement of the axis of the body via the sacro-iliac joint may converge in the region of the chiasma and inferior body resulting in the requirement for increased buttressing of the cortices and a remodeling of the trabecular bone. Therefore it is suggested that the chiasma region displays an internal and external architecture that is perhaps modified through three distinct influences – mature ossification, arterial invasion and movement.

From the trabecular chiasma, the most dominantly represented radiographic region presented as a posteriorly directed trajectory which has, in the literature, been

associated with weight transfer from the sacro-iliac joint to the acetabulum in bipedal locomotion. It is suggested that its presence in the neonate may well indicate an area of remodelled bone that is designed to respond to the forces associated with movement at the neonatal sacro-iliac joint as it responds to reflexive movements of the trunk. Therefore this trajectory may well represent a conjoined area of alteration reflecting movement related stresses towards the chiasma from the sacro-iliac joint and the pubis in relation to lower limb movement. Inspection of the quantitative data illustrated that the posterior trajectory was represented by thickened pelvic and gluteal cortices in the inferior portion of the posterior trajectory which tapered to become thinner towards the superior most aspects of the trajectory. This is in keeping with the tapering of density displayed radiographically. The trabecular parameters in this region displayed a more complicated arrangement which has been attributed to the multifunctional influences acting in this region from the sacro-iliac joint, retrograde limb forces, as well as endochondral growth towards both metaphyseal and non-metaphyseal borders. The positioning of the VOI's and ROI's does not permit a direct comparison between the quantitative and qualitative data but this could not be avoided. However the nature of the bone in the region of the posterior trajectory is consistent with bone that is in the process of remodelling i.e. number is reduced, thickness is increasing and the BV/TV is decreasing.

Passing anteriorly, from the trabecular chiasma a less pronounced trabecular trajectory was observed and attributed to an anteriorly directed retrograde force component of primitive limb movement. Analysis of the quantified data again demonstrated a cortical thickness which was in keeping with this pattern whereby a thicker pelvic and gluteal cortex was observed at the inferior portion of the anterior trajectory which thinned as the trajectory extended antero-superiorly. Inspection of the

trabecular parameters in this trajectory again display a graded appearance from the chiasma region towards the periphery and are in keeping with the hypothesised influences of vascular presence and ossification progression in the growing ilium and the nature of remodelled bone. It is suggested that this trajectory may be less marked than the posterior trajectory as it only transfers forces of retrograde movement from the lower limb and is not reinforced by stresses passing in the opposite direction.

Between the anterior and posterior trajectories a reduced density region was observed radiographically. This was described as an apparently structurally redundant area interspersed between two functionally significant rays of structural density. Analysis of the cortical thicknesses in this region demonstrated that although values are reduced in comparison to the chiasma, values are similar to the terminal regions of the anterior and posterior trajectories. Trabecular values in this region are indicative of a less remodeled volume than that of the trabecular chiasma which is in line with hypothesised endochondral growth towards the iliac crest with a larger number of finer trabeculae. With remodelling occurring in the anterior and posterior trajectories in response to limb movement, there will be no corresponding forces placed on this supero-medial region and in due course it will remodel to meet the requirements placed on it i.e. sites of cortical bone for muscle attachment. There will be no need for intervening cancellous bone to retain the 'sandwich' effect as the function of the bone reverts solely to the requirement of the muscle attachment.

Perimeter regions of the ilium were represented by reduced density areas radiographically, attributed to the absence of any significant remodeling forces during the neonatal period and to the fact that the perimeter regions were most recently modeled and thus presented with the most immature density pattern. Inspection of the cortical and trabecular values for these regions confirmed this suggestion by

demonstrating that the cortices were characterised by reduced cortical thickness and internal architecture that was indicative of newly modeled bone i.e. thin densely packed trabeculae.

A significant density representation presented at the greater sciatic notch which was attributed to its proximity to the sciatic nerve and the potential neurogenic influences from this nerve to bone formation. The pelvic and gluteal cortical values are high in this region which lends support to the hypothesis of bone apposition in response to a neurogenic stimulus. This is the only area of the ilium to display this response and the only area to have immediate relations to a nerve of such significant size. Additionally, values of trabecular architecture are indicative of a remodeled trabecular architecture which is hypothesised to be partly attributable to the closely approximated sciatic nerve and partly to the proximity to the trabecular chiasma region and the factors influencing its morphology.

Finally the acetabular component of the neonatal ilium was represented by a significant density representation radiographically, primarily attributed to the three dimensional thickness in this region when compared to the rest of the blade-like expanse of the ilium. The thin cortices and the recently modeled trabecular characteristics suggest that this region should be represented by a less dense overall pattern. However, the significantly increased three-dimensional volume of trabecular bone in this region is indeed considered to contribute to the density representation observed radiographically. The change in degree of anisotropy does go some way towards describing the altered appearance in this region as the orientation of the bone plates are realigned to likely respond to the retrograde forces associated with limb movement that will pass across this joint. The periphery of the acetabular surface remains consistent with the metaphyseal growth regions seen throughout the remainder

of the bone but in the qualitative radiographic images it was clear that an area of increased density 'the acetabular roof' could be identified. This would be consistent with the development of more compacted subchondral bone which is characteristic of a joint surface.

There is no denying that the human ilium is governed by genetic control as the external morphology of the bone is characteristically identifiable from a very early age and therefore there is no reason to suggest that genetics will not play a large part in determining the baseplate for internal architectural characteristics. Being provided with a 'human' template may form the starting point for subsequent alterations (internal and external) but it will act as a constraint so that changes must be contained within the confines of the basic genetic anlage. There are several features that can affect both the internal and external architecture of the bone and these include:

- Significant space occupying requirements by the vascular system to supply an actively growing bone that has at least two (if not three) regions of metaphyseal activity.
- The growth of the bone around a large and significant peripheral nerve that will not appreciably increase in size from the neonatal stage.
- Reflex movements of the fetus both in utero and as a neonate which must be transmitted to the bone through the joint connections. These movements will occur both from the axis of the body via the sacroiliac joint and from the acetabulum from the pubis, the ischium and the femur as muscles contract and limbs move.
- Muscle mass will increase as the child grows requiring an altered surface for attachment.

Both qualitative and quantitative analysis has demonstrated that defined regions of cortical and trabecular morphology in the neonatal ilium can be paralleled with proposed gait-related features in the adult. However, alternative explanations regarding the observed form are suggested. These explanations involve normal anatomical interactions and progressive ossification in the growing ilium and appear to be unrelated to any direct load bearing mechanisms although they may reflect the effects of force transfer across joints which require accommodation of the internal architecture. For the effectively adult pattern of internal structure to be present in the neonate, suggests that either:

1. This genetic pattern is inherent in the human and is laid down in advance of any bipedal requirements that the child may subsequently require, or more likely
2. It is an indication that the basic template is laid down at an early stage through influences that are not directly related to bipedality but that when bipedality occurs it must utilise the existing scaffold for this new function and make such alterations as are required. However, given that the space occupying vascular tissue is mature in its form by this stage, it may well take precedence. This leads to an interesting theory that perhaps the ilium is not after all a weight bearing structure but is efficient in load transfer. Previous work (Ali and MacLaughlin, 1990) has shown that the sacroiliac joint is not sexually dimorphic in the adult and such dimorphism is generally interpreted as a clear indication of a joint that is weight bearing. It has been suggested that the sacro-iliac joint does not weight bear and therefore that the forces associated with an upright stance may therefore be transferred across the joint region but not directly transmitted by it. Therefore, if the forces associated with bipedalism are largely transferred via soft tissue then the adaptations required by the bone to bipedality may not be as

significant as first predicted and therefore the architectural pattern that has previously been associated with bipedality may have been incorrectly attributed. It may simply be that a standardised pattern of cortical and trabecular bone form is developed in the ilium which may be maintained into the mature form.

CHAPTER 7 – Wider Context Discussion

7.1 Introduction

The original aim of this thesis was to document the changing cortical and trabecular architecture of the developing ilium. However, this aim required modification to focus on the earliest developmental periods, specifically the fetus and the neonate. In concentrating on this developmental cohort, extended analysis enabled the detailed investigation of an unexpected early structural patterning of internal trabecular architecture and cortical dimensions. This chapter discusses the bone patterning found in the neonatal ilium and discusses these in light of trabecular and cortical bone organisation reported in previous human and animal postcranial developmental studies. This comparison will provide a basis upon which to explore the theories proposed for patterns of bone structure observed in the human neonatal ilium.

This chapter also outlines how the data obtained may be applied in extended areas of research and proposes instances where the raw data and theories postulated may be used in professional disciplines for predictive and practical applications. In addition to the applicability of the study data, a discussion of the study strengths and limitations will be presented, which will provide recommendations as to how future and extended studies may be improved to provide a more reliable and detailed perspective of trabecular and cortical morphology. This will be followed by an outline of suggestions for future research which may be conducted to answer outstanding questions or may be designed to investigate new theories which were posed throughout the duration of the current investigation. Finally, this chapter will document the conclusions of this research.

7.2 Relevance of study results to existing literature

The results of this study can be compared and contrasted with a comprehensive literature which has aimed to investigate the trabecular architecture and cortical dimensions of the mammalian skeletal system from a variety of perspectives. This large literature base has been derived through the application of an ever increasing suite of analytical techniques which have produced data sets that can be directly and indirectly compared with the data obtained in the current study. These analyses have attempted to document skeletal form throughout development, in the adult skeleton and subsequently in the aging skeleton when degenerative conditions become prevalent. It is predominantly studies of the human fetal and neonatal skeletal form which are of most interest but few have yielded data which are numerically comparable to the results of the current study. However, analysis of adult bone patterning and the results obtained from animal developmental studies are also useful for paralleling theories of gross bone patterning to the trabecular and cortical appearance observed during early development.

This section attempts to present a cross-section of the most relevant developmental trabecular and cortical bone analyses conducted in the human and animal skeleton. These studies will be paralleled with the results of the current study to interrogate the theories generated regarding the patterns of bone formation observed during the earliest stages of development in the human neonatal ilium.

7.2.1 Studies of early structural development in the ilium

Several recent studies, many of which were published after the commencement of the current study, have attempted to address aspects of structural form in the human ilium during early development, from the fetal period through to the early years of life (Glorieux *et al*, 2000; Parfitt *et al*, 2000; Abel, 2006; McColl *et al*, 2006; Rauch *et al*,

2006; Volpato, 2008). Although similar in their aims, these investigations have analysed a limited number of trabecular parameters and a significantly reduced number of analytical fields when compared to the current study. However, regardless of their reduced investigative scope, their results are still extremely important for substantiating the structural patterning of the trabecular architecture and cortical morphology observed in this study. One of the most relevant of these recent studies, which was conducted as part of a larger investigation, set out to test the hypothesis that the fetal iliac trabecular tissue of modern humans displayed an ordered structure throughout fetal ontogeny (Abel, 2006). This investigation was carried out on 137 fetal specimens using two measures of macroscopic and microscopic quantification, trabecular bone density and trabecular anisotropy respectively. Similar to the current investigation, this study applied microCT to analyse these trabecular parameters within three different areas of interest across the iliac blade. These areas of interest were situated anteriorly in line with the anterior superior iliac spine, posteriorly in line with the posterior superior iliac spine and superiorly at the midpoint of the iliac crest.

The results of Abel's study showed that at 16 intra uterine weeks, the fetal ilium demonstrated a higher bone density in the anterior and posterior trabecular volumes compared to the superiorly oriented trabecular volume. Subsequently, at 36 intrauterine weeks the fetal ilia demonstrated comparable bone density across all examined areas of interest. At term, this uniformity was maintained, as bone density was not shown to vary significantly across the iliac blade. This study concluded that modern humans have an ordered trabecular tissue arrangement from the earliest stages of fetal development (16 intrauterine weeks) reflected in the fact that bone is not evenly distributed across the iliac blade. Following on from this, later in the fetal period and into the neonatal period,

it was suggested that trabecular bone becomes more evenly distributed so that trabecular characteristics cannot be differentiated between trabecular volumes.

The primary observation that bone density differed between the anterior, posterior and superior trabecular volumes during the earliest of fetal periods correlates well with the qualitative observations made in the initial part of the current study. As discussed in Chapter 5, qualitative radiographic observations of early fetal specimens demonstrated distinct differences in apparent bone density, as defined by radiopacity, between anterior, posterior and superior regions. However, it must be borne in mind that a radiographic representation is a composite of trabecular and cortical bone distribution, therefore, conclusions pertaining solely to trabecular structure must be treated with caution. Advanced analysis of the trabecular pattern in the neonate using μCT, which isolated the trabecular structure from the involvement of cortical bone, again confirmed the observations of Abel, (2006), for the more advanced developmental cohorts, by demonstrating that no statistically significant differences exist between the trabecular parameters in the anterior, posterior and superior trabecular volumes. However, although apparently arriving at similar results, the current study also challenges the ultimate conclusions made by Abel, (2006). It was suggested that the absence of differences between trabecular parameters in the anterior, posterior and superior trabecular volumes was indicative of a structural uniformity across the entire iliac trabecular volume in the neonate. This appears to be somewhat over-simplified as only very isolated trabecular regions located on the periphery of the ilium were investigated in Abel's study. In restricting the analysis to these regions Abel, (2006) did not investigate, in any detail, the trabecular volumes associated with the main body and acetabular component of the ilium. It is within these volumes, in the current study, where statistically significant differences in trabecular parameters are observed. This

leads to an alternative conclusion which proposes that there is indeed a structural organisation within the trabecular volume during the neonatal developmental period.

Abel, (2006), suggested the finding that fetal iliac trabecular tissue becomes more evenly distributed across the iliac blade throughout early ontogeny was not consistent with the notion that fetal bone density adapts to meet the applied loads associated with early muscle contraction. This resulted in a conclusion that the data were not consistent with the hypothesis of fetal and neonatal iliac trabecular bone re-orientating to meet alterations in the direction of applied loads. This conclusion is not in line with the results obtained in the current study which suggests that a defined trabecular organisation is developed throughout early iliac trabecular development as a function of the temporal stresses and strains encountered by the bone. The different conclusions between the two studies may be attributed to the limited trabecular parameters and volumes of interest analysed by Abel (2006).

A final observation by Abel (2006), although not investigated quantitatively, was that there appeared to be a bone density gradient extending from the centre of ossification towards the periphery in all directions. It was suggested that this trabecular bone distribution may be a product of the ossification process. This theory of progressive endochondral ossification supports one of the theories outlined in the current study which suggests that initial endochondral ossification is responsible, as part of a multifunctional set of influences, for early developmental trabecular patterning.

In addition to the investigations of Abel (2006), a further related study by McColl *et al* (2006), proposed an automated method for measuring trabecular thickness from micro-CT scans and applied this to the calculation of trabecular thickness in the fetal ilium. Measurements of average trabecular thickness were taken from 38 specimens using transects positioned at two specific regions of interest, at the posterior

iliac crest and inferior acetabular component. The results of this study demonstrated that there was no statistically significant difference in values of trabecular thickness between these two regions which is in line with the findings of the current study. McColl *et al* reported that there was evidence of increasing trabecular thickness throughout fetal development from values of 99μm at 16 intra uterine weeks up to an average trabecular thickness of 240μm at term. They reported that this trend of increasing trabecular thickness during the fetal developmental period was similar to that observed in the femur (Salle *et al*, 2002). The values of average trabecular thickness reported for the most mature neonatal specimens are higher than the values reported in the current study for comparative trabecular volumes which range between 0.145 and 0.162μm in posterior superior perimeter volumes and between 0.151 and 0.157 in acetabular component trabecular volumes. McColl *et al*, (2006) in their discussion made reference to the fact that the values of trabecular thickness reported were higher than would be expected when comparisons were made to other studies investigating trabecular architecture in human fetal and neonatal bone. It was initially proposed that the increased values of trabecular thickness in the ilium at term, as compared to other postcranial bones, may be attributable simply to the fact that different bones possess different trabecular characteristics (Macho *et al*, 2005) due to functionally related differences. However, comparison with results of the current study suggests that the trabecular thickness values reported by McColl *et al*, (2006) for the neonatal ilium may have been overestimated. This overestimation may be attributed to the analysis techniques used, which employed parallel plate model assumptions to the calculation of trabecular thickness. These techniques have been well reported in the literature to overestimate trabecular measures (Ding and Hvid, 2000). This may aid in explaining the discrepancies observed between these high values of trabecular thickness and the

significantly lower values demonstrated in the current study, which applies model independent measures of trabecular parameter calculation for a more reliable assessment of structural form. A final consideration for the larger trabecular thickness values reported by McColl *et al* (2006), when compared to existing literature values for other postcranial bones, may be attributed to the analysis methods applied. As previous studies which provide comparative data on human trabecular thickness have applied histological sectioning to the assessment of trabecular thickness, its inherent tissue shrinkage limitation (Uchiyama *et al*, 1997) may have exacerbated the absolute difference in average trabecular thickness values between the studies.

A further recent study by Volpato, (2008), aimed to address the structural changes to the trabecular and cortical bone of the ilium from the neonatal developmental period through to the adult representation, in response to the progressive acquisition of bipedal locomotive abilities. This investigation again applied microCT as the primary analysis technique. The results of this study demonstrated that between the ages of 1 and 2 the trabecular architecture displayed the main topographic features observed in the adult from a qualitative perspective. Volpato, (2008) suggested that prior to this developmental period, during the neoperinatal period (0-3months) the density representation was homogenous and radial, of the type commonly observed in immature animals. This is contradictory to the results obtained for qualitative and quantitative analysis of the neonatal developmental cohort in the current study, which defined a distinctive patterning of bone density, which possessed the characteristic features described for the adult density representation. Indeed further examination of the radiographic images of the neoperinatal age cohort presented by Volpato (2008), calls into question the accuracy of the study's structural interpretation, as it seems apparent that there is indeed a defined structural arrangement during this period and not a

uniform homogenous density distribution as suggested. The veracity of the early developmental sample in the Volpato study is also questionable due to the very small sample size which consisted of only two specimens. Also the sampling volumes applied were poorly defined and appeared to be sporadically arranged with little emphasis on repeatability between specimens. Additionally, the study provided very limited quantitative data regarding specific trabecular characteristics and cortical thicknesses. Of the data presented, from the seven different regions of interest analysed, it can be deduced that the trabecular thickness across the neoperinatal ilium ranges from approximately 130μm to 150 μm. Additionally bone volume fraction was observed to range in value from approximately 25% to 40%. In the current study, values of trabecular thickness range in value from 0.145 μm to 0.223 μm, and values of bone volume fraction range from 18.9% to 43.5%. This difference in the range of values between the two studies may be attributable to the different volumes of interest analysed. In the current study, an increased number of trabecular volumes were sampled taking into account large trabecular volumes which were neglected by the Volpato study. However, although the range of values does differ, there is a general agreement regarding the magnitude of these two trabecular indices within synonymous volumes of the neonatal ilium.

Furthermore, in addition to trabecular bone analysis, Volpato (2008) reported that the major cortical thickness in the neoperinatal ilium was found on the lateral (gluteal) side of the bone located between the trabecular chiasma (1.75mm lateral (gluteal); 1.08mm medial (pelvic)) and the central part of the iliac wing (1.23mm lateral (gluteal); 1.00mm medial (pelvic)). This observation of differential iliac cortical thickness reiterates the observations of a previous investigation which documented the transiliac bone histomorphometry in juvenile individuals and concluded that the gluteal

and pelvic surfaces of the ilium differed with regard to bone cell activity on their surfaces (Rauch *et al*, 2006). These observations are in agreement with the current study where a differential thickness pattern is observed between the two cortices. The thickest cortex was located on the lateral (gluteal) surface extending between the inferior body and central body of the ilium encompassing the trabecular chiasma. The highest mean cortical thickness for this region in the current study was 1.89mm lateral (gluteal); 0.881mm medial (pelvic).

Additional studies have considered the developing trabecular architecture and cortical thickness of the ilium at defined isolated landmarks using traditional histomorphometric techniques (Glorieux *et al*, 2000; Parfitt *et al*, 2000). These studies, although not providing an interpretation of overall structural composition, produce trabecular and cortical values generally representative of an isolated region within a developmental cohort which can be compared to the results of the current study. The first relevant such study was conducted by Glorieux *et al* (2000), to investigate the trabecular parameters and cortical widths at the iliac crest in five age groups. They concluded that there were significant age-dependant increases in both cortical width and trabecular bone volume fraction, the latter being due to an increase in trabecular thickness. This study examined individuals between the ages of 1.5 and 22.9 years to provide an account of normative data for iliac bone histomorphometry in growing children. Unfortunately, the results are presented in wide age ranges (1.5-6.9 yr; 7.0-10.9 yr; 11.0-13.9 yr; 14.0-16.9 yr; and 17.0-22.9 yr), and therefore provide limited information regarding the very early developmental sample. Comparison of the results presented in their study for the early developmental age cohort (1.5-6.9 yrs) with data from the current study investigating the trabecular architecture of the fetal and neonatal ilium cannot be conducted as averaging across age ranges has resulted in a masking of

true early developmental trabecular and cortical bone characteristics. The trabecular values reported are in line with those expected with more mature development and are certainly not representative of trabecular and cortical values expected for the early developmental period at the iliac crest. The more mature values reported by Glorieux *et al*, (2000) may be explained by the proposal that bone begins to adopt a more adult morphology from between the ages of 1-2 (Ryan and Krovitz, 2006; Gosman and Ketcham, 2009), which is the earliest age cohort examined in their study. It is therefore suggested that this study provides limited information regarding the early developmental periods. This further reinforces the requirement for the current study to provide the literature with a more extensive representation of the trabecular and cortical bone characteristics for this developmental period which may be used to supplement existing histomorphometric data (Glorieux *et al*, 2000). It must be acknowledged that Glorieux *et al,* (2000) noted that the results of their study should only be used for comparisons if the same analytical methods are employed. Therefore, comparisons of their results with the results of the current study should not be over analysed.

A further histomorphometric study analysed bone parameters from the anterior superior iliac spine in subjects aged 1.5-23 years (Parfitt *et al*, 2000). This study demonstrated that there were significant increases in core width of the iliac blade with increasing age which corresponded to increased cortical width and trabecular bone volume. Specifically, the trabecular bone was shown to increase in bone volume fraction and trabecular thickness however, trabecular number remained relatively constant. In the earliest age cohort bone volume fraction was observed to be a low value at ~20%, trabecular thickness was presented with values of ~0.090mm and trabecular number presented with values of ~2.1mm^{-1}. The values reported in this study for individuals at 1.5 years of age are significantly lower than the values obtained for the

anterior superior iliac spine trabecular volume in the current study due to the advanced age cohort analysed.

7.2.2 Studies of early structural development in other postcranial bones

An increasing number of studies investigating the trabecular architecture of the human skeleton during the early developmental period have been conducted in postcranial bones other than the ilium. Although these studies cannot be directly compared to the results of the current study, analysis of their results is useful for identifying common patterns of trabecular bone formation and remodeling during the neonatal developmental period.

An initial study of this kind by Ryan and Krovitz, (2006), attempted to quantify the trabecular changes in the human proximal femur which are associated with the acquisition of bipedal locomotion. This study applied microCT and associated trabecular analysis software. In the fetal specimens analysed in this study, a dense, relatively undifferentiated trabecular structure was observed. This structural arrangement was reported to present as interconnected parallel columns of bone matrix which did not resemble mature trabecular bone and was not differentiated into recognisable structural zones. This early structural template was then observed to differentiate into a more mature architectural pattern after around one year of age. In the youngest individuals analysed, which were of a similar developmental stage to the iliac specimens in this study, bone volume fraction presented as a high value, ranging between 45% and 59%. Trabecular number presented as a high value ranging between 3-4.5 mm^{-1}. Trabecular thickness was reported to be variable during the fetal period, however, the mean trabecular thickness presented as a low value ranging between

0.093-0.134 mm. Finally, bone structure was shown to be highly anisotropic in the youngest specimens.

A further similar study attempting to document the ontogenetic alterations of the trabecular architecture in response to the acquisition of normal functional activities and changing body mass was undertaken in the subadult proximal tibia (Gosman and Ketcham, 2009). In the proximal tibia, trabecular bone at birth was again characterised by a dense, undifferentiated structure which possessed a large number of small trabeculae organised in interconnected parallel columns, similar to those described for the proximal femur (Ryan and Krovitz, 2006). Gosman and Ketcham, (2009), suggested that the initial high trabecular number observed appeared to be determined early in development under strict constraints. Specifically, it is considered that the trabecular number is related to the numerical density of the cartilage septae which become ossified (Byers *et al*, 2000). At birth the bone volume fraction in the proximal tibia was shown to be high (range 40.41%-46.06%), trabecular thickness was demonstrated as being very low (range 0.078-0.096 mm), trabecular number was observed to be very high (range 4.504-5.118 mm^{-1}), and the overall trabecular structure was again shown to be highly anisotropic.

The volumes of interest selected for the proximal femur and tibia were located at the ossification front just below the growth plate. Therefore, these results may generally parallel with those obtained from the perimeter growth regions of the neonatal ilium which are considered to be synonymous trabecular volumes in terms of progressive endochondral growth. Values of trabecular architecture in perimeter growth regions of the neonatal ilium were represented by a high bone volume fraction (maximal = 43.5%), a low trabecular thickness (minimal = 0.146mm), a high trabecular number (maximal = 2.8 mm^{-1}), and a highly anisotropic trabecular architecture. Comparisons between this

study and those of the long bones highlight that certain individual trabecular parameters presented for the proximal femur and tibia, during the fetal period, are similar in value to those obtained for the neonatal ilium. This suggests that there is some degree of standardisation in the way in which the trabecular architecture is laid down at growth plate regions during early development. However, although absolute values of trabecular architecture are similar between the growth fronts in each of these bones, the conclusions presented for the overall femoral and tibial trabecular characteristics contrast with those proposed for the trabecular architecture of the neonatal ilium. In the fetal and neonatal proximal femur and tibia it has been concluded that the trabecular patterning is uniformly distributed and does not begin to organise until at least one year of age (Ryan and Krovitz, 2006; Gosman and Ketcham, 2009). This is very different from the rather precocious structural organisation observed in the neonatal ilium. This difference is surprising as all lower limb bones are non-load bearing during the early developmental periods. This discrepancy may be attributed to the fact that the sampling volumes applied to the analysis of the proximal femur and tibia are too large and do not provide enough detailed information regarding the variation in trabecular parameters across the full trabecular volume. This may lead to an apparent over-simplification of the trabecular structure during the fetal period in these bones. Ryan and Krovitz, (2006), attempted to address this by applying heterogeneity analysis to determine the variation within the trabecular structure using multiple non-overlapping volumes of interest. Their results demonstrated that there was indeed heterogeneity within the trabecular structure during the early developmental sample, however, they did not comment upon this and instead concentrated on the advanced level of heterogeneity in more mature specimens. This level of variation within the trabecular architecture during the fetal period, prior to any weight bearing influences, reinforces the results of the current study

by demonstrating the potential of the trabecular volume to have a high degree of structural organisation prior to the influences of direct stance weight transfer. Finally, although inferences regarding the trabecular volume can be made between bones, it must be acknowledged that direct comparisons between the femoral and tibial trabecular results and the results of this thesis should be made with caution due to the different bones under investigation.

In addition to studies applying microCT to the analysis of trabecular architecture in postcranial bones, other studies have applied more traditional histomorphometric techniques (Byers *et al*, 2000; Salle *et al*, 2002; Nuzzo *et al*, 2003). One such histomorphometric analysis conducted on the fetal and newborn proximal femoral metaphysis suggested that modeling rather than remodeling was principally responsible for the development of metaphyseal trabecular bone production during *in utero* development (Salle *et al*, 2002). It was demonstrated that from the second to the third trimester, bone volume fraction increased steadily due to an increase in trabecular thickness and maintenance of trabecular number. Salle *et al,* (2002) demonstrated that several trabecular parameters varied depending on their distance from the growth plate. Bone volume fraction was shown to increase with increasing distance from the growth plate. Surprisingly, this is the opposite of what is observed in the current study, where BV/TV decreases with increasing distance from the growth plate. This may be explained by a number of reasons including the variations in bone patterning dependant on the different bones examined to the differences in associated anatomical interactions. An initial consideration is given to the positioning of the nutrient artery for the ilium which is proposed to have a greater influence on the trabecular BV/TV of the ilium than the dominant femoral nutrient artery has on the femur. The location of the dominant nutrient artery invasion in the ilium is located centrally within the trabecular bone

architecture, whereas in the femur, the invading nutrient artery enters the bone at a region corresponding to the medullary cavity, within which there is no significant trabecular architecture. Therefore, in the ilium, arterial presence, in the form of the large dominant nutrient artery, may have a direct influence on surrounding trabecular bone, whereas, in the femur it is terminal arterial branches which may influence the trabecular form, as the large dominant branches are confined to the diaphysis. Additionally, differences in BV/TV patterning between the ilium and the femur may be due to the fact that the femoral data is from the fetal period compared to the neonatal period for the iliac trabecular data. It is suggested that with increased developmental status and the proposed rapid modeling during the perinatal period, the pattern of fetal BV/TV may alter to conform to the pattern observed in the current study for the neonatal ilium.

Furthermore, during the neonatal period, increased osteoid volume i.e. increased apposition of bone, will influence a relative increase in BV/TV at peripheral growth plate regions which are experiencing continued modeling. However, the degree of bone apposition or osteoid deposition at more mature regions of bone formation, i.e. those furthest from the growth plate, will not be so substantial. This differential rate of bone apposition is proposed to cause increased values of BV/TV in peripheral growth plate regions and decreased BV/TV values in more distant regions as the bone matures. This theory is supported by Salle *et al*, (2002) who demonstrated that osteoid volume is highest at growth plate regions and decreases with distance from the growth plate, which with increased development will result in a net increase in BV/TV, as is evidenced in this study during the neonatal period. Further to BV/TV, values reported by Salle *et al,* (2002) for trabecular thickness and trabecular number were in keeping with the results of the current study where trabecular thickness increased with

increasing distance from the growth plate and trabecular number decreased with increasing distance from the growth plate.

A further quantitative histomorphometric study investigating the trabecular bone development from the growth palate was carried out in the costochondral junction of children between the ages of 11 days and 13.5 years (Byers *et al*, 2000). The primary spongiosa was quantified in terms of bone volume fraction, trabecular thickness, trabecular separation and trabecular number. In the neonatal period, BV/TV was observed to be 29%, Tb.Th presented as a low value of 0.081 mm, Tb.Sp also presented with a low value of 0.200 mm, and finally Tb.N presented with a high value of 3.75 mm^{-1}. These trabecular characteristics were considered to reflect the active growth unit which contributed to longitudinal growth and accumulation of bone mass. This generalised trabecular pattern reflects that of modeling peripheral volumes in the ilium. This also reinforces the suggestion that certain trabecular parameters are determined early in development, and are therefore under more strict constraints.

Finally, a study by Nuzzo *et al*, (2003) studied the ossification process in human vertebrae during the early developmental period using micro-computed tomography. This study demonstrated that a more dense trabecular network was present in fetal bone compared with the trabecular network of adult bone. The early developmental representation demonstrated a defined central core of trabecular bone surrounded peripherally by what was described as more immature bone. The trabecular arrangement observed in the fetus when compared to the more mature representation, was explained by the absence of biomechanical constraints during the early developmental period. This study suggested that the differential patterning of trabecular structure between the central core and the peripheral region corresponded to the pattern of early deposited mineral. This suggests that the ossification process in the fetal vertebrae may be an

expansion from a central region. This observation can be paralleled with the results of neonatal trabecular patterning in the ilium where a radiating trabecular pattern is observed to emanate from a central region and is thought to be partly directed by early ossification.

7.2.3 Studies of trabecular and cortical development in animal models

As outlined, recent studies in human bone have begun to investigate isolated regional trabecular and cortical characteristics from single developmental cohorts. However, few of these studies have documented the trabecular architecture from a full ontogenetic perspective. This has resulted in a restricted quantitative perspective of the developmental progression of trabecular architecture and cortical morphology. In response to this neglected area of investigation, animal models have been employed to study these adaptations with increasing developmental status (Tanck *et al*, 2001; Mulder *et al*, 2006; Mulder *et al*, 2007).

An initial such study by Tanck *et al*, (2001) investigated the trabecular bone volume fraction and morphological anisotropy at various stages of development (6, 23, 56, 104, and 203 weeks) using pig vertebrae and proximal tibiae. Bone volume fraction was shown to increase rapidly during the initial stages of development whereas morphological anisotropy lagged behind, increasing at a later stage of development. The rapid increase in bone volume fraction, explained by the weight gain of the pigs, was proposed to induce loading onto the skeletal system. It was concluded that bone density, reflected in the bone volume fraction, was adapted to external load from the early phases of growth, whereas the trabecular architecture, reflected in the morphological anisotropy, was adapted later in development. The results and conclusions of this study can be related to the results of the trabecular data obtained in the current study where a

high bone volume fraction combined with a high degree of anisotropy is reported at peripheral growth regions in the neonatal human ilia which has been related in part to early biomechanical influences.

A further such study by Mulder *et al* (2005), which forms part of a series, investigated the architecture and mineralisation of the developing trabecular bone in the pig mandibular condyle. This was considered by the authors to be the first study to present substantial quantitative data regarding the trabecular bone changes which may occur throughout development. The relevance of this study to the current investigation was the observation that there were regional differences within the trabecular architecture observed during the early developmental period. This trabecular compartmentalisation was considered to be a combined reflection of the pattern of progressive growth and mechanical loading on bone during development. This theory can be related to the compartmentalised trabecular growth observed in the neonatal ilium which has also been related to multifunctional influences.

A further study in this series by Mulder *et al*, (2006), again analysed the trabecular architecture of the mandibular condyle of the pig during the fetal and neonatal period of development. The mandible was consistently chosen as it is one of the first bones in the body to ossify during fetal development, therefore providing the opportunity to study the changing trabecular architecture from the earliest stages of development. This study demonstrated that trabecular architectural parameters reflect the developmental growth direction of the bone. Specifically, a defined orientation of the trabecular architecture in the fetal period was observed which was maintained into the neonatal developmental period. This orientation of the trabecular elements was considered to be a reflection of the growth course of the mandibular condyle. This is an interesting theory which may be applied to the more isotropic morphology observed in

the acetabular and inferior body regions of the neonatal ilium in the current study. It may be possible that this degree of orientation of the trabeculae, as reflected by a reduced value of anisotropy, may be in response to the growth of the ilium inferiorly into the wide acetabular expanse.

The most recent addition to this series by Mulder *et al*, (2007) investigated the contribution of altered trabecular architecture to the mechanical properties of the trabecular structure throughout development in the pig mandibular condyle. This study was based on the premise that bone develops into a load bearing structure during early development. This is proposed to be in response to incremental increases in loading from involuntary contraction of developing muscles which initiate movement during the early fetal period. The results of this investigation demonstrated that during early development, the trabecular framework does develop into a load bearing structure reflected by an increasing degree of mineralisation combined with distinct alterations in trabecular architectural form, including increased values of trabecular thickness and separation along with combined decreases in trabecular number. These results support the hypothesis that the trabecular architecture in the neonatal ilium may be partially influenced by reflexive muscle contraction and resultant limb movements imposing forces on the trabecular structure.

It is predicted that further such studies conducted on animal models will continue to dominate the literature on the developmental changes associated with trabecular architecture and cortical morphology. This trend will predominate due to the potential to conduct longitudinal studies of bone structural modification and the ability to obtain multiple specimens, enabling reliable structural testing. The ability to conduct longitudinal studies in animals has been made possible by the introduction of *in vivo*

micro-CT where a sedated animal can be monitored under controlled conditions during scanning (Holdsworth and Thornton, 2002).

7.2.4 Studies of trabecular and cortical structure in the adult

Several studies investigating the trabecular architecture and cortical morphology of the human adult ilium have been conducted (Dalstra and Huiskes, 1995; Macchiarelli *et al*, 1999; Martinon-Torres, 2003). However, most quantitative studies have been confined to isolated volumes of interest generally located around the periphery of the bone at the iliac crest and spines (Uchiyama *et al*, 1997; Hildebrand *et al*, 1999). This trend of investigation has continued due to the main focus of these studies being towards understanding bone competency in degenerative conditions rather than to understanding the overall structural composition of the bones internal and external form (Chappard *et al*, 1988). Absolute values of trabecular architecture will not be presented here due to the inability to compare these values with younger developmental cohorts. Additionally, as the regions of trabecular architecture and cortical morphology analysed are restricted to specific regions, namely the iliac crest, little information can be deduced regarding comparative adult form.

7.3 Application of study results

The results of this study have the potential to be applied directly to current disciplines and speciality areas for both theoretical and diagnostic purposes. In addition, the data produced in this study has laid a foundation which may be expanded upon for future investigation in these areas. This extended interpretation is likely to stem from advanced analysis of the neonatal sample and extension of this analysis to the full ontogenetic sample. It is considered that the current study results may be applied in a

variety of manners, from increasing current anthropological and anatomical knowledge to speciality areas associated with medicine and forensics.

7.3.1 Anthropological theory

Anthropology, literally meaning ‘human discourse’ is the branch of science concerned with the origin and development of humans in all their physical, social, and cultural relationships (Stedman, 2005). This study adds to the physical anthropological literature by presenting previously undocumented aspects of skeletal form. This is considered to be particularly important as the ilium is a key skeletal structure associated with the attainment of future bipedal capabilities. The fundamental basis of this research was an innovative developmental study, which aimed to document the way in which internal trabecular architecture was arranged throughout early development. Its primary contribution to the literature is one of elementary understanding of early biological skeletal development in the human ilium. The pelvic complex is a fundamental structure within the appendicular skeleton for many requirements including load transfer and muscular attachment. However, despite the structural organisation of the pelvis being extremely important, there is still little known about its development. As such, the primary contribution of this research was to produce a record of its initial developmental form during early ontogeny.

As this is a field of skeletal biology and skeletal dynamics which has been relatively neglected, the results of this study have provided advanced data and theories to a previously undocumented and poorly understood ontogenetic representation of early trabecular and cortical bone form in the ilium.

7.3.2 Evolutionary theory

It is proposed that the findings of this study may have significant implications on current evolutionary theory. As has been discussed for modern adult *Homo sapien* iliac specimens, previous studies have also demonstrated well defined trabecular bundles throughout the Hominin lineage, from the genus *Homo* and *Australopithecus* to the youngest of the Miocene hominoids *Oreopithecus bambolii* (7 – 9 million years old). Each of these trabecular bundles have been discussed in relation to gait related forces (Aiello and Dean, 1990; Macchiarelli *et al*, 1999; Rook, 1999; Martinon-Torres, 2003). The presence of these proposed gait related trabecular features lends support to the claim that apes early in the Hominin lineage were in part bipedal (Latimer and Ward, 1998; Saunders, 1998), combining arboreal climbing with a bipedal gait (Macchiarelli *et al*, 1999). However, the presence of well defined internal and external bone structure during the early developmental period as evidenced in this study for modern *Homo* leads to a re-evaluation of mature trabecular arrangement being used as an indicator of bipedal capabilities. This may lead to a reconsideration of the trabecular evidence in the early Hominin lineage as being indicative of a proposed bipedal posture and may ultimately result in a re-evaluation of the evolutionary origin of bipedalism.

7.3.3 Force function relationships

The results of this study contribute to an increased knowledge of force:function relationships in the ilium during the early developmental period. Primary attention in this regard was directed towards the relationship between the early reflexive lower limb movements and the proposed structural response of the trabecular architecture to the forces generated by this action. Characteristic alterations to the internal trabecular architecture which were restricted to the inferior portion of the ilium suggested that a

retrograde force component was a predominant remodeling factor. It is well documented that trabecular bone is influenced by force:function relationships, however, with regards to the pelvis these have predominantly concerned the adult form and have been attributed to mature anatomical influences and load transfer associated with bipedal capabilities (Dalstra and Huiskes, 1995; Macchiarelli *et al*, 1999; Martinon-Torres, 2003). The suggested presence of a force:function relationship associated with the trabecular architecture in a neonatal individual is a new finding which adds significantly to knowledge of the relationship between inherent forces and bone alterations during the early developmental period.

As well as the proposed retrograde force:function relationship between reflexive muscular contractions initiating primitive limb movement and the trabecular structure, further information has been deduced regarding the relationship between the anatomical structures which are directly associated with the ilium. These anatomical interactions are proposed to induce functional forces upon the cortex and underlying trabecular architecture. This is a further area which has been given relatively little attention in the literature other than a brief mention as parts of larger communications (Delaere et al, 1992). The specific anatomical interactions which have been further elucidated by this research include both muscular and ligamentous attachments and their resultant influences. Muscular interactions associated with the gluteal shell are considered to be significant determinants of early form. Like-wise ligamentous tissue attachment associated with the sacro-iliac joints is considered to influence both external and internal morphology as evidenced by the qualitative data.

Further structure:function relationships have been proposed relating to the positioning and approximation of anatomical structures and the trabecular and cortical bone arrangement. Firstly, the relationship between the trabecular architectural form and

the internal vascular network is one which has been given little consideration in the literature other than illustrative documentation (Crock, 1996). The results and hypotheses of this study suggest that there may indeed be a defining intimate relationship between the vascular arrangement and the associated trabecular structure in the neonatal ilium. It is proposed that this relationship maybe maintained throughout development and into the adult form where a change in vascular arrangement will be reflected in the trabecular arrangement. A further structure:function relationship proposed by this study has extended further evidence to the previously suggested interaction between neurological tissue and bone formation. It is suggested that the proximity of neurological tissue may induce an increased level of bone production as evidenced at the greater sciatic notch in response to the sciatic nerve. Previous literature has eluded to this (Laurenson, 1964a), and the results of this study appear to support these previous observations and suggestions by demonstrating a characteristic trabecular and cortical morphology at the greater sciatic notch.

This study has proposed that force:function and structure:function relationships are likely major determinants, alongside progressing ossification, of the trabecular architecture and cortical structure during the neonatal developmental period.

7.3.4 Clinical interpretation

Trabecular bone architecture is often assessed from a clinical perspective in order to establish the competency of a specific skeletal element (Cummings *et al*, 2002). This form of assessment is often conducted when there is a suspected degenerative skeletal disorder and is generally confined to adults with advancing age (Scottish Intercollegiate Guidelines Network, 2003). The assessment of the trabecular architecture and cortical morphology from a developmental perspective is an area which

lacks any substantial research and to which there appears to have been limited emphasis. This lack of previous research can most likely be attributed to the enormous task involved in analysing the developing form of individual skeletal elements across an ontogenetic range. In modern medicine, with an ever increasing range of corrective devices and surgical procedures, an interpretation of the structural composition in the ilium, as well as the other bones of the skeleton, is required for advanced understanding of normal form and for planning the correction of potential pathologies and traumas which may be encountered by the skeleton.

The potential is now also available for this kind of research due to the availability of suitable imaging media which provide sufficient imaging resolution for visualisation of trabecular parameters from the youngest human fetal specimens through to the most mature adult individuals. The results of the current study have initiated this type of research and have formed a foundation template of bone structural arrangement in the ilium upon which future ontogenetic studies of trabecular architectural and external cortical morphology can be based and may begin to reach clinical potential. Currently, the neonatal trabecular and cortical data may have limited clinical implications, however, knowledge that the structural composition of the ilium during early development is not of uniform distribution and is instead precociously organised may provoke a re-evaluation of the way in which the correction of pelvic anomalies may be managed during early development.

Although certain pathologies of the pelvis, such as congenital hip dysplasia, are present at birth, most anomalies of the pelvis which require correction are normally dealt with during the period of attainment of an obligate bipedal stance. Therefore, an interpretation of the structural composition throughout an ontogenetic range of specimens will allow for a documentation of the normal pattern of specific temporal

structural organisation. This pattern of normal cortical thickness and internal trabecular architectural form may be utilised by a clinician to plan a corrective procedure in order to reposition skeletal elements resulting in a realignment of the forces influencing the pelvis, ultimately achieving a remodeling towards the normal pattern.

Most bone loss pathologies in relation to major issues of healthcare e.g osteoporosis are viewed from the perspective of what goes wrong at the advanced age range of the spectrum. It is proposed that further focus and investigation on how the adult pattern develops may aid in understanding what happens when the pattern degenerates later in life. It is therefore suggested that investigators studying medical healthcare issues may be well advised to start by looking at the earlier template.

7.3.5 Forensic potential

It is proposed that the results of this study have the potential to be utilised as an accessory technique for aging individuals and for identifying fragmentary remains as being of iliac origin. It is possible that fragmentary sections of bone may be primarily identified as iliac upon examination of the cortical and trabecular structural arrangement. Further examination of this structural patterning, via micro-CT, may allow for the assessment of developmental status based upon the signature values for individual trabecular indices as documented for the neonatal age cohort investigated in this study. Although these types of potential analyses would be currently restricted to the neonatal age cohort it is possible that further examination of the entire ontogenetic spectrum would allow for the development of a more comprehensive analysis tool for the identification and aging of fragmentary skeletal remains of iliac origin. This may then be used in conjunction with other techniques to allow for a more reliable investigative interpretation.

Previous studies have considered changes in the trabecular architecture associated with age (Lips *et al*, 1978; Macho *et al*, 2005; Cui et al, 2008), however, no studies have been conducted to determine age from the trabecular architecture. Despite this, trabecular bone architecture in the distal femur and proximal tibia has been applied to establish positive identity (Mann, 1998). It is suggested that this area of investigation and analysis could be further expanded for the ilium.

7.4 Study limitations

The primary limitations of this study are related to the juvenile skeletal sample and are issues which have been repeatedly highlighted as limiting factors when conducting developmental studies using small sample sizes of undocumented provenance (Ryan and Krovitz, 2006; Gosman and Ketcham, 2009). The principal limitation is considered to be the relatively small sample size used. However, as the Scheuer collection is one of the largest juvenile skeletal collections of its kind available for this type of research, this is offered simply as an explanation. As reduced sample sizes are common in studies considering human bone development, particularly during the early stages of development, consideration of this fact must always be addressed when discussing results. A further limiting factor of this study is associated with sample mortality which is an additional important issue which must be considered in the context of the results obtained. As most specimens used in this study are undocumented in terms of cause of death it cannot be completely ascertained whether the child died from a condition which was likely to have affected the ilium. However, gross assessment of the bones and careful inspection of their internal representation strongly suggests that there was no obvious pathology associated with the skeleton at death. As such, the skeletal sample used is considered to be free from any associated skeletal

pathology which will likely influence the qualitative and quantitative results obtained. Furthermore, the majority of specimens had limited associated documentation regarding age or sex. Therefore, aging of the specimens was undertaken using standard metric evaluations of the ilium (Fazekas and Kosa, 1978), as outlined previously (Chapter 5). Although the measurements taken, placed each specimen analysed within the neonatal developmental period, it must be acknowledged that there may be a lack of precision in age estimation, this limitation however, is considered to be minimal and should not impact on the fact that these individuals are highly unlikely to have achieved unassisted bipedal stance. Additionally, all specimens were pooled into a single cohort regardless of sex due to the inability to establish sex with any certainty during early development. It is unlikely that significant sexual differences in skeletal form will be present during the neonatal period, therefore this was not considered to introduce a significant degree of error to the results (Cox and Mays, 2000).

Further limitations associated with the imaging equipment used were deemed to be a significant limiting factor in the collection of reliable trabecular and cortical bone data. A full documentation of these limitations, as associated with each of the imaging modalities trialled, was made in Chapter 4. However, the final imaging modality and analysis protocol applied to the data are considered to be the best available and provide the most reliable interpretation of iliac structural composition.

7.5 Study strengths

Although several limitations have been associated with this study it must also be acknowledged that there are several strengths which add to the innovative nature of the investigations and to the veracity of the data obtained. The primary strengths of this study can be attributed to the recent developments in three-dimensional imaging

techniques which have made non destructive, 3D quantification of trabecular bone micro-structure possible. Non-invasive structural analysis has enabled the detailed internal investigation of skeletal elements from the Scheuer collection. This type of investigation was previously unjustifiable due to the requirement for destructive assessment techniques. High-resolution micro-CT scanning of whole bone elements is a very recent advancement in the imaging field and the availability of such a scanner for the assessment of the neonatal developmental cohort is considered to be a significant strength of this research.

Additionally, the availability of model-independent analysis software allowed for a more accurate assessment of trabecular and cortical structure than has been obtained in previous studies. Structural parameters such as architectural anisotropy, bone volume fraction, structural model index and trabecular thickness, number and separation can be calculated directly from micro-CT scan images. As with micro-CT imaging modalities model-independent analysis software is a recent development in the field of bone structural analysis which has allowed the current gold standard in structural calculation to be applied in this investigation.

Furthermore, although many issues relating to the skeletal sample were discussed as potential limiting factors, the availability of the Scheuer collection of juvenile skeletal remains is also regarded as a great strength of this research. As juvenile material in any quantity is difficult to obtain, it is a significant attribute of this research that a resource such as the Scheuer collection was made available. Additionally, the preservation quality of the material contained within this collection is extremely good, allowing for a detailed structural analysis of the entire ilium.

7.6 Future applications and recommendations for improvement

Throughout the duration of this project several limitations were identified which have been predominantly associated with the level of imaging and analytical technology currently available. This provided several problems during the data collection and analysis phases of the project which required various interim solutions to be applied in order to provide a reliable data set using the materials and methods available. Although these solutions were considered appropriate for this research and enabled a thorough insight into early bone patterning in the ilium, it is appropriate to suggest aspects where the research methodology may have been improved or could be enhanced in the future. This is likely to occur with the advent of more advanced imaging systems and analytical software, however, certain alternative analysis methods are currently available and warrant discussion.

7.6.1 Alternative methods of quantification

In addition to the methods of quantification outlined in this thesis there are alternative means available for cortical and trabecular bone parameter calculation. These methods involve quantification of bone structure in cases where resolution or image quality insufficiencies make direct interpretation of bone parameters difficult. Such methods range in application from trabecular quantification of greyscale radiographic images to the interpretation of clinical CT scans using micro-CT as a standard comparison. These additional techniques may have specific applications in the clinical context for predicting bone competency, where it may not be possible to obtain high resolution micro-CT images of whole bones. Instead a plain plate radiograph or clinical CT may be available and could be analysed in terms of bone structural composition.

7.6.1.1 Texture analysis

Texture analysis as applied to trabecular bone images offers the potential to obtain information from low resolution plain plate radiographs (Geraets *et al*, 1990; Pothuaud *et al*, 1998; Benhamou *et al*, 2001) and clinical CT images (Ito *et al*, 1995; Showalter *et al*, 2006). This eliminates the limitations associated with application of complex, costly and inaccessible imaging devices by providing an alternative method of structural assessment (Genant *et al*, 1999). Texture analysis involves extracting parameters characterising the arrangement of the regular patterns which constitute the image (Apostol *et al*, 2006). Several methods of texture analysis have been employed in an attempt to define the optimal technique for characterisation of trabecular architecture. These methods include both structural and statistical applications such as skeletonisation, run-length distribution, spectrum and fractal analysis techniques (Apostol *et al*, 2006; Guggenbuhl *et al*, 2006). Skeletonisation is a classic structural method achieved by reducing all trabecular structures down to a single pixel thickness which runs in the median line of each traebcula. This is used for calculation of simple indices such as length, number of nodes and end points, however, this method requires thresholding which can introduce limitations due to the inherent poor quality of radiographic and clinical CT images. Fractal models of trabecular bone in low resolution greyscale images are examples of statistical texture analysis techniques and are commonly used to provide a single numeric evaluation (the fractal dimension) representative of bone structure (Pothuaud *et al*, 1998; Benhamou *et al*, 2001).

Texture analysis of plain plate radiographs has been shown to be well correlated with trabecular bone histomorphometry and provides a suitable means for investigating structural organisation in degenerative bone diseases such as osteoporosis (Chappard *et al*, 2005). Studies investigating the relationship between texture analysis of radiographic

images and three-dimensional histomorphometric parameters assessed by micro-CT have demonstrated that when multiple correlations are used, radiographic texture analysis proves to be a suitable approach for bone microarchitecture assessment (Guggenbuhl *et al*, 2006).

Early studies applying texture analysis to CT images for the determination of fracture risk in conditions such as osteoporosis have suggested that this technique may be useful in characterising bone structure, specifically in relation to spinal fractures (Ito *et al*, 1995). A more recent study by Showalter *et al*, (2006) determined whether three-dimensional texture measures calculated from low resolution CT images of trabecular bone correlated with three dimensional structural indices measured using high-resolution micro-CT images. It was concluded that texture features were highly correlated with structural indices and that this technique may be utilised to obtain structural information regarding the trabecular environment when high resolution imaging is unavailable. However, further development and refinement of this technique is recommended prior to any clinical application.

The application of texture analysis to lowered resolution images for the calculation of trabecular characteristics is a field which is currently under development and requires further research in order to firmly establish best practice procedures and applicability to routine structural assessment. Therefore, although initial studies have indicated its usefulness in assessing certain trabecular indices its full potential may not yet be realised.

7.6.2 New generation imaging equipment

The primary limitation in advancing knowledge in the field of bone architecture, from a developmental, clinical and anthropological perspective, is the inability to image

whole human bones at sufficient resolution for reliable structural quantification. This limitation is a function of the imaging equipment which is currently available for routine clinical examination or whole bone structural research. Fortunately new micro-CT equipment is continually being developed and being made available to enable more advanced analysis of bone structure in areas of the skeleton which were previously inaccessible by detailed imaging studies.

New generation micro-CT scanners are now capable of resolving much larger structures at greatly increased spatial resolutions allowing the potential for future detailed structural information to be gained in large bones and in full ontogenetic studies. It is anticipated that scanner specifications will continue to improve so that even larger fields of view with a maintained high spatial resolution will be achieved. The advent of such imaging equipment may prompt a re-evaluation of past studies which have applied reduced resolution images to structural quantification of bone. Currently, high-resolution assessment of bone is being conducted in studies applying synchrotron radiation tomography (SRμCT) as a more powerful alternative to micro-CT. However, this modality remains relatively inaccessible for most research projects due to the scarcity of SR facilities (Kazakia *et al*, 2008).

7.6.3 Automation of VOI/ROI placement

In this study the manual definition and placement of volumes and regions of interest was an extremely laborious and time consuming process. Therefore, the implementation of an automated method of analysis field generation would significantly reduce the labour intensive nature of such a study. Furthermore automation of this procedure as defined by recognisable anatomical landmarks would contribute to significantly improving the accuracy of analysis field placement within and between

specimens, as well as enhancing the reliability of resulting quantification. Additionally, the development of an automated analysis field generator and placement algorithm may allow the analysis of a substantial increase in the number of analysis fields used. For example instead of the twenty three volumes and regions of interest as employed in this study, several hundred analysis fields could potentially be generated and analysed. This would contribute to a greatly increased amount of detail regarding the overall structural patterning of the ilium. In order to achieve this, a computer code is required for the automated identification of 3D objects based on landmark data which could be used in conjunction with current model-independent analysis software. At present, there is no available commercial software specifically for this type of image processing. Development of software for this type of analysis field automation should be seriously considered when designing future studies on the assessment of whole bone trabecular architecture.

7.6.4 Selection of a threshold algorithm

A wide range of previous studies have attempted to establish a thresholding protocol for application to images of trabecular bone structure. However, no completely reliable thresholding technique has been established. Identification of such a technique would greatly improve trabecular bone investigations as accurate pre-processing of digital data is essential for accurate quantification (Scherf and Tilgner, 2009).

Previous studies applying calculated thresholding methods to CT data have applied the half-maximum height (HMH) thresholding protocol (Spoor *et al*, 1993; Fajardo *et al*, 2002; Coleman and Colbert, 2007) or the adaptive iterative thresholding method (Ryan and Ketcham 2002a; 2002b; Fajardo *et al*, 2007). Both of these thresholding methods refer to calculated single grey value thresholds between the

trabecular bone and the background but differ in their method of calculation. Manual segmentation, as applied in this study, is an additional and widely used alternative to these computational methods. However, each of these calculated and manual thresholding techniques have inherent limitations which must be factored into the results obtained from a quantitative study and discussed in terms of their impact on any conclusions drawn. As a result of these limitations there is a constant drive to develop a thresholding algorithm which can reduce inaccuracies and provide a more reliable means of structural quantification from digital images.

A recently published study by Scherf and Tilgner, (2009), proposed a new method for image thresholding in relation to complex objects such as trabecular bone. They presented the ray casting algorithm which is constructed upon the three-dimensional grey value gradient within the image rather than defined greyscale values. This is significant as the grey value gradient is not affected by gray value variations with low frequencies and can be applied to images produced with degenerated signals. This technique uses the maxima of the 3D gray value gradients in an image to define the boundaries of a structure. The main advantage of this algorithm is that it is unaffected by slight variations in brightness caused by variations in material density or beam hardening, which are often the primary source of error in other thresholding procedures.

7.6.5 Radiographic quantification

The initial part of this study analysed radiographic images of the ilium from a qualitative point of view which allowed for a gross structural interpretation for subsequent three-dimensional quantification. However, the preliminary analysis of radiographic images may be improved by the application of quantitative procedures. It is possible that greyscale values from isolated regions of interest within the raw

radiographic images may be assigned an arbitrary value which can then be compared with other regions across the ilium. This would then allow for a more thorough interpretation of the radiographic images to be used in association with the qualitative representation. The quantification of the greyscale patterning may be achieved by applying a software package such as ImageJ, which would provide values such as min/max, mean and standard deviation of the grey values. As the radiographs were collected using the same settings and exposure times and were scanned in the same manner, the actual grey values obtained when applying such a method should be comparable across specimens and should indicate a relative density of bone. In order to obtain calibrated true bone densities, a bone phantom would be required.

7.7 Future research

The current study, although providing a detailed insight into the early developmental structure of the human ilium, has presented many additional questions and lines of research which have yet to be investigated and which extend beyond the scope of the current project. These research questions are diverse and some can be regarded as natural extensions of the current study where others are related research branches which although stemming from the principles of this research, aim to address wider issues of anthropological theory.

It is appropriate to first consider future work that may be conducted which forms a direct extension from the current work. In the first instance this is aimed at documentation of the complete innominate so that a perspective of early developmental structural composition can be gained for the ischium and pubis in addition to the ilium. Following on from documentation of the early developmental pattern it would be appropriate to produce a complete ontogenetic documentation of changing cortical and

trabecular structure for the entire innominate. This would aid the evaluation of changes that occur to the primitive pattern as more mature influences of locomotion manifest in older juveniles as the child moves from sitting, to crawling and finally to a mature bipedal gait. However, this requires that imaging technology continues to develop to the point where large specimens of adult size can be imaged in three dimensions with a maintained high degree of spatial resolution to allow for the accurate quantification of bone parameters. Production of an ontogenetic record of structural modification could then be related to specific developmental milestones. This could be utilised in many different ways for the purposes of clinical diagnosis and therapeutic intervention to the forensic examination of age of an individual when presented with fragmentary skeletal remains. From the fundamental documentation of changing internal pelvic architecture there is the potential for application to several other anthropological concepts. Construction of the modern human template of biomechanical alteration will allow for deductive extrapolation to issues of human evolution and adaptation, as well as application to fragmentary remains having the potential to be a maturity indicator. The contribution to the current literature may take the form of evolutionary and adaptive theory, and research could also be formulated from an archaeological perspective. There is also potential for further comparative osteological analysis between species based on the normal template produced in this research.

Further research may consider the bone architecture of the sacrum and how this relates to the trabecular and cortical bone patterning in the pelvis. To date several studies have analysed the trabecular architecture and cortical thickness of the vertebral column for assessment of degenerative conditions such as osteoporosis (Ritzel *et al*, 1997; Chen *et al*, 2008). However, no study has considered the vertebral column and specifically the sacrum from an ontogenetic perspective and in relation to the loads

which are being transferred through the vertebral bodies towards the sacro-iliac joint. The need for additional research into the microstructure of vertebral bodies is reinforced by previous researchers calling for better characterisation of the microstructure within the vertebral column (Sun *et al*, 2004). Following analysis of the skeletal components which contribute to the lower limb it would be appropriate to analyse the remainder of the postcranial skeleton in terms of developing trabecular architecture and cortical thickness. This information could then be related to temporal functional interactions and applied in a variety of disciplines.

Another aspect of trabecular and cortical bone quantification, which was highlighted as a significant methodological factor which had potential implications on reliability and accuracy of results, was the quantification software applied. The potential inherent limitations when using bone structural quantification software highlights the requirement for comparative studies to be conducted looking at the compatibility of software for calculating various indices of bone structure. Due to the significant number of software packages available for analysis of trabecular and cortical bone parameters, it is suggested that all available model-dependant and model-independent software packages should be applied in a comparative study to assess the trabecular and cortical bone parameters within an individual bone.

Imaging resolution was an important aspect of this study which had significant implications on the accuracy of the results obtained. As such, further investigations may be conducted to establish trabecular bone accuracy at differing resolutions. Several studies have investigated the effects of resolution on structural quantification by artificially degrading high resolution images and quantifying before and after degradation. However, to provide a true assessment of how imaging resolution influences trabecular and cortical bone quantification in the ilium a study employing

various high and low scanning resolutions could be applied. This would allow an insight into the optimal imaging parameters which could be used during studies which aim to quantify the trabecular structure. A study of this nature would again require the potential for imaging systems to resolve the smallest of trabeculae in larger specimens.

Vascular distribution within the ilium was a significant structural interaction proposed to influence the trabecular form. As little work has concentrated on the vascular network of the internal ilium, a study investigating the true arterial distribution may be conducted to reinforce the results and discussions regarding the trabecular architecture and its relationship to arterial presence. This could be conducted using modern infiltration techniques whereby the dominant nutrient artery for the ilium is identified, washed with saline solution and injected with non-viscous latex solution under pressure. Once the latex solution has been allowed to harden the surrounding soft and hard tissues are chemically dissolved in a solution of sodium hydroxide. This type of arterial casting has been conducted previously (Crock, 1996), however, the only documented evidence is presented in photographic form which provides limited information regarding the extent of the arterial network in three dimensions. Arterial casting of the entire ontogenetic series of human ilia may provide a valuable insight into the associated trabecular patterning. However, the availability of fleshed specimens is very limited, therefore, as the investigation proposed would be destructive in nature a thorough investigation in the human may be restricted.

An additional area for future study which was identified throughout the duration of the current study involved documenting the dimensions of the greater sciatic notch in relation to the developing sciatic nerve. It is proposed that the size and positioning of the sciatic nerve may have a significant influence of the morphology of this landmark at different stages throughout development. A future project may investigate the

morphology of this notch and the size of the associated nerve through analysis and measurement from imaging studies of specimens with both soft and hard tissues present. The effects of nerve proximity may also be examined in other areas of the skeleton, such as the lesser sciatic notch morphology in relation to the internal pudendal nerve.

A further study may consider the effects of movement and muscle attachment on the cortical morphology and trabecular architecture in more detail. The effects of movement and muscle action on the ilium may be investigated through the application of finite element analysis, where the material properties of the neonatal ilium can be simulated by a computer reconstruction of the bone from micro-CT scans. This model can then be stressed in a manner which mirrors the physiological stresses induced by muscles and movements on the actual bone during the neonatal period. This model then predicts how the cortical and trabecular morphology would respond to these stresses thereby providing evidence for the bone changes associated with muscle attachment and limb movement. Finally, a further study which would advance the knowledge of the iliac trabecular architecture involves an investigation solely directed towards understanding the architecture and morphology of the auricular region of the ilium. The unique structure of the sacro-iliac joint and the peculiar way in which forces are transmitted through the joint complex make this a particularly significant locus for extended study.

A final area of research which has been identified throughout the duration of the current investigation involves the assessment of iliac structural morphology between species. Through the investigation of animal models, patterns of cortical and trabecular development and alteration in response to different functional forces and requirements may be assessed and compared to the human form. This type of analysis may allow for

a greater insight into the potential gene-environment influences on bone form and may provide evidence of common evolutionary patterns of bone formation.

7.8 Conclusion

This study presented data on iliac trabecular bone architecture and cortical bone dimensions from the early human developmental period. Through a systematic analysis protocol, the mechanically optimised lightweight structure of the neonatal ilium (Dalstra and Huiskes, 1995), which consists of two cortical shells and an internal cancellous bone core, was documented. The initial findings of this study pertain to recommendations for best practice analysis protocols for the imaging and analysis of trabecular and cortical bone structure in protected skeletal collections. The investigation and application of multiple imaging modalities highlighted that micro-computed tomography imaging was the optimal non-destructive modality for the assessment of skeletal microstructure. This investigation also highlighted that other imaging modalities (clinical computed tomography and magnetic resonance imaging) can be applied to gain a gross perspective of bone form, however, cannot be applied for the direct quantitative assessment of trabecular architecture. Additionally, this study also highlighted that model-independent assessment of trabecular bone indices should be employed as a gold standard when analysing bone structure from computer generated images.

With specific reference to the ilium, the main results of this study have revealed, through both qualitative and quantitative analysis, that a recognisable and regional organisation of internal trabecular architecture and external cortical morphology is established at a very early age in the human ilium. This is evidenced by a characteristic radiographic density representation which is composed of a defined

compartmentalisation of the trabecular structure combined with a distinctive patterning of cortical thickness across both pelvic and gluteal surfaces of the ilium. This early developmental pattern has distinctive traits which can be paralleled with the gross density template seen in the adult which has been attributed in the past to a biomechanical response to weight bearing bipedal locomotive influences. However, as the fetal and neonatal representation is free from direct stance related load transfer, a full discussion of potential influencing factors were considered to elucidate the origins and progression of structured bone patterning in the ilium. Interestingly, the early presence of this precociously mature trabecular and cortical morphology suggests that previous attribution of iliac trabecular patterning to locomotor load transfer may be too simplistic. It is therefore suggested that the neonatal trabecular and cortical patterning may yield an insight into the developmental origins of future load bearing structures.

It is proposed that the trabecular structural observations made in this study in non-load bearing fetal and neonatal pelves may be a preliminary response to multifunctional influences acting during this developmental period. These include progressive modeling and remodeling in response to normal progressive growth and ossification; inherent external and internal anatomical interactions from soft tissues; early reflex limb movements which have the potential to transmit retrograde remodeling forces into the ilium; and finally the potential for the presence of a pre-determined genetic template of skeletal form which may prove to be a ‘human’ scaffold or indeed perhaps even a ‘primate’ genetic blueprint..

Additionally, the cortical patterning observed on both pelvic and gluteal surfaces are consistent with expected gradients of bone thickness driven by progressive ossification radiating from the central ossification centre for the ilium. Further to this, increased gluteal cortical thickening has been attributed, with caution, to the presence of

the large gluteal muscle mass which may induce accelerated remodeling forces within the cortex through reflex muscle contraction resulting in a thickening response in areas of direct muscle attachment, reinforcing previous similar observations (Delaere *et al*, 1992).

The results of this study have also proposed a revised model for proceeding endochondral ossification during early development in the ilium. The presence of defined regions of distinguishable trabecular characteristics arising from a central trabecular chiasma suggests that the compartmentalised growth is radial and directed by metaphyseal growth drivers. This growth is observed to extend towards growth plates in 'growing' trabecular trajectories and towards non-metaphyseal peripheral regions in 'non-growing' trabecular rays. This pattern of growth has been related to the presence and positioning of the vascular supply of the ilium of which dominant invading branches and subsequent radial fanning corresponds well with the trabecular compartmentalisation observed. Additionally, within 'growing' compartments a modeling gradient is observed which is indicative of primary trabecular ossification which mirrors the columnar alignment of the initial cartilaginous template in peripheral regions. This primary spongiosa is then gradually remodelled in response to temporal functional interactions, ultimately converging towards the most advanced region of growth at the trabecular chiasma.

Through an examination of the relationship between cortical and trabecular structure in relation to the functional demands placed upon the pelvic complex during its early growth phase, this study contributes to a greater understanding of early developmental trabecular organisation and cortical bone structure in the ilium. This analysis has core implications for understanding the origins of trabecular and cortical bone characteristics attributed to load bearing structures in the adult by providing a

foundation for subsequent ontogenetic development. Additionally, this study contributes to an advanced understanding of the progressive ossification within the ilium during the earliest developmental stages.

References

Abel, R.L. (2006). Ontogenetic Change in Primate Pelvic Morphology: The Hominoid Ilium. Liverpool University: Unpublished PhD Thesis.

Adair, F.L. (1918). The ossification centres of the fetal pelvis. *American Journal of Obstetrics and Diseases of Women and Children*. **78**: 175-199.

Adolph, K.E. (1997). Learning in the Development of Infant Locomotion. *Monographs of the Society for Research in Child Development.* **62(3)**:1-15.

Adolph, K.E. (2002). Babies' steps make giant strides towards a science of development. *Infant Behaviour and Development*. **25**:86-90.

Advani, S., LaFrancis, D., Bogdanovic, E., Taxel, P., Raisz, L.G. and Kream, B.E. (1997). Dexamethasone suppresses in vivo levels of bone collagen synthesis in neonatal mice. *Bone*. **20**:41-46.

Aiello, L. and Dean, C. (1990). *An Introduction to Human Evolutionary Anatomy*. London: Academic Press.

Ali, R.S. and MacLaughlin, S.M. (1990). The relationship between sex, body size and the auricular surface of the ilium. *Journal of Anatomy* **170**: 237-238.

Alini, M., Marriott, A., Chen, T., Abe, S. and Poole, R. (1996). A novel angiogenic molecule produced at the time of chondrocyte hypertrophy during endochondral bone formation. *Developmental Biology.* **176**: 124-132.

Amling, M., Takeda, S. and Karsenty, G. (2000). A neuro(endo)crine regulation of bone remodelling. *BioEssays*. **22**:970-975.

Anderson, H.C. (1995). Molecular biology of matrix vesicles. *Clinical Orthopaedics and Related Research*. **314**:266-280.

Anderson, F.C. and Pandy, M.G. (2003). Individual muscle contributions to support in normal walking. *Gait and Posture*. **17**:159-169.

Apostol, L., Boudousq, V., Basset, O., Odet, C., Yot, S., Tabary, J., Dinten, J-M., Boller, E., Kotzki, P-O. and Peyrin, F. (2006). Relevance of 2D radiographic texture analysis for the assessment of 3D bone microarchitecture. *Medical Physics*. **33(9)**:3546-3556.

Aspden, R.M., Rudman, K.E. and Meakin, J.R. (2006). A mechanism for balancing the human body on the hips. *Journal of Biomechanics*. **39**:1757-1759.

Augat, P., Margevicius, K., Simon, J., Wolf, S., Suger, G. and Claes, L. (1998). Local tissue properties in bone healing: influence of size and stability of the osteotomy gap. *Journal of Orthopaedic Research*. **16**:475-481.

Bagi, C.M., Hanson, N., Andresen, C., Pero, R., Lariviere, R., Turner, C.H. and Laib, A. (2006). The use of micro-CT to evaluate cortical bone geometry and strength in nude rats: correlation with mechanical testing, pQCT and DXA. *Bone*. **38(1)**:136-144.

Bagnal, K.M., Harris, P.F. and Jones, P.R.M. (1977). A radiographic study of the human fetal spine. 2. The sequence of development of ossification centres in the vertebral column. *Journal of Anatomy*. **124**:791-802.

Bardeen, C.R. (1905). Studies of the development of the human skeleton. *American Journal of Anatomy.* **4**:265-302.

Barker, S.L. and Scheuer, J.L. (1998). Predictive value of human footprints in a forensic context. *Medicine Science and the Law*. **38(4)**: 341-346.

Baron, R. (1999). Anatomy and ultrastucture of bone. In: *Primer on the Metabolic Bone Disease and Disorder of Mineral Metabolism*, 4th ed., Favus, M.J., Lippincott/Williams and Wilkins, Chapter 1.

Beaupied, H., Chappard, C., Basillais, A., Lespessailles, E. and Benhamou, C.L. (2006). Effect of specimen conditioning on the microarchitectural parameters of trabecular bone assessed by micro-computed tomography. *Physics in Medicine and Biology*. **51**:4621-4634.

Benhamou, C.L., Poupon, S., Lespessailles, E., Loiseau, S., Jennane, R., Siroux, V., Ohley, W. and Pothuaud, L. (2001). Fractal analysis of radiographic trabecular bone texture and bone mineral density: two complementary parameters related to osteoporotic fracture. *Journal of Bone and Mineral Research*. **16(4)**:697-704.

Bernard, T.N. and Cassidy, J.D. (1991). The sacroiliac syndrome. Pathophysiology, diagnosis and management. In: Frymoyer JW, ed. *The Adult Spine: Principles and Practice*. New York: Raven. pp2107–2130.

Bertram, J.E. and Swartz, S.M. (1991). The "law of bone transformation": a case of crying Wolff? *Biological Reviews of the Cambridge Philosophical Society*. **66**:245-273.

Bevill, G., Eswaran, S.K., Gupta, A., Papadopoulos, P. and Keaveny, T.M. (2006). Influence of bone volume fraction and architecture on computed large-deformation failure mechanisms in human trabecular bone. *Bone*. **39(6)**:1218-1225.

Biewener, A.A., Fazzalari, N.L., Konieczynski, D.D. and Baudinette, R.V. (1996). Adaptive changes in trabecular architecture in relation to functional strain patterns and disuse. *Bone*. **19**:1-8.

Bilezikian, J.P., Morishima, A., Bell, J. and Grumbach, M.M. (1998). Increased bone mass as a result of estrogen therapy in a man with aromatase deficiency. *New England Journal of Medicine*. **339**:559-603.

Birkner, R. (1978). *Normal Radiographic Patterns and Variances of the Human Skeleton – An X-ray Atlas of Adults and Children*. Baltimore (Munich): Urban and Schwarzenberg.

Bobroff, E.D., Chambers, H.G., Sartoris, D.J., Wyatt, M.P. and Sutherland, D.H. (1999). Femoral anteversion and neck-shaft angle in children with cerebral palsy. *Clinical Orthopedics and Related Research*. **364**:194-204.

Bonucci, E. (1967). Fine structure of early cartilage calcification. *Journal of Ultrastructural Research.* **20**:33-50.

Boucher, B.J. (1957). Sex difference in the foetal pelvis. *American Journal of Physical Anthropology*. **15**:581-600.

Bourgery, J.M. (1832). *Traitè Complet de l'Anatomie de l'Homme. I. Osteologie*. Paris.

Bowen, V. and Cassidy, J.D. (1981). Macroscopic and microscopic anatomy of the sacroiliac joint from embryonic life until the eighth decade. *Spine.* **6(6)**: 620-628.

Boyd, S.K., Davison, P., Muller, R. and Gasser, J.A. (2006). Monitoring individual morphological changes over time in ovariectomized rats by *in vivo* micro-computed tomography. *Bone*. **39**:854-862.

Brandi, M.L. and Collin-Osdoby, P. (2006) Vascular biology and the skeleton. *Journal of Bone and Mineral Research*. **21**:183-192.

Bril, B and Brenière, Y. (1992). Postural requirements and progression velocity in young walkers. *Journal of Motor Behaviour*. **24**:105-116.

Bronner, F. and Worrell, R.V. (1999). *Orthopaedics, Principles of Basic and Clinical Science*. Florida: CRC Press.

Brooke, R. (1934). The sacro-iliac joint. PhD Thesis. University of London.

Brookes, M. (1971). *The Blood Supply of Bone*. London: Butterworths.

Brunner, C., Kissling, R. and Jacob, H.A. (1991). The effects of morphology and histopathologic findings on the mobility of the sacroiliac joint. *Spine*. **16**:1111–1117.

Bruzek, J. and Soustal, K. (1981). Contribution to ontogenesis of human bony pelvis. *Acta Universitatis Carolinae-Biologica*. **12**:37-45.

Burnside, L.H. (1927). Coordination in the locomotion of infants. *Genetic Psychology Monographs*. **2**:279-372.

Burr, D.B., Robling, A.G. and Turner, C.H. (2002). Effects of biomechanical stress on bones in animals. *Bone*. **30**:781-786.

Byers, S., Moore, A.J., Byard, R.W. and Fazzalari, N.L. (2000). Quantitative histomorphometric analysis of the human growth plate from birth to adolescence. *Bone*. **27(4)**:495-501.

Canalis, E. (1996). Mechanisms of glucocorticoid action in bone: implications to glucocorticoid-induced osteoporosis. *Journal of Clinical Endocrinology and Metabolism*. **81**:3441-3447.

Canalis, E. and Delany, A.M. (2002). Mechanisms of glucocorticoid action in bone. *Annals of the New York Academy of Sciences*. **966**:73-81.

Canalis, E., McCarthy, T. and Centrella, M. (1988). Growth factors and the regulation of bone remodelling. *Journal of Clinical Investigation*. **81**:277-281.

Carey, E.J. (1929). Studies in the dynamics of histogenesis. Experimental, surgical, and roentgenographic studies in the architecture of human cancellous bone, the resultant of back pressure vectors of muscle action. *Radiology*. **13**:127-168.

Carlevaro, M.F., Albini, A., Ribatti, D., Gentili, C., Benelli, R., Cermelli, S., Cancedda, R. and Descalzi Cancedda, F. (1997). Transferrin promotes endothelial cell migration and invasion: implication in cartilage neovascularization. *Journal of Cell Biology*. **136**:1375–1384.

Carruth, B.R. and Skinner, J.D. (2002). Feeding behaviours and other motor development in healthy children (2-24 months). *Journal of the American College of Nutrition*. **21(2)**: 88-96.

Carter, D.R. and Beaupre, G.S. (2001). *Skeletal Form and Function. Mechanobiology of Skeletal Development, Aging and Regeneration*. Cambridge: Cambridge University Press.

Carter, D.R. and Hayes, W.C. (1977). The compressive behaviour of bone as a two phase porous structure. *American Journal of Bone and Joint Surgery*. **59**:954-962.

Carter, D.R., Orr, T.E. and Fyrhie, D.P. (1989). Relationships between loading history and femoral cancellous bone architecture. *Journal of Biomechanics.* **22**: 231-244.

Cendre, E., Mitton, D., Roux, J-P., Arlot, M.E., Duboeuf, F., Burt-Pichat, B., Rumelhart, C., Peix, G. and Meunier, P.J. (1999). High-resolution computed tomography for architectural characterization of human lumbar cancellous bone. Relationships with histomorphometry and biomechanics. *Osteoporosis International*. **10**:353-360.

Chappard, D., Guggenbuhl, P., Legrand, E., Basle, M.F. and Audran, M. (2005). Texture analysis of X-ray radiographs is correlated with bone histomorphometry. *Journal of Bone and Mineral Metabolism*. **23**:24-29.

Chappard, D., Retailleau-Gaborit, N., Legrand, E., Basle, M, F. and Audran, M. (2005). Comparison insight bone measurements by histomorphometry and μCT. *Journal of Bone and Mineral Research*. **20(7)**:1177-1184.

Chappard, D., Legrand, E., Pascaretti, C., Basle, M.F. and Audran, M. (1999). Comparison of eight histomorphometric methods for measuring trabecular bone

architecture by image analysis on histological sections. *Microscopy Research and Technique*. **45**:303-312.

Chappard, D., Alexandre, C. and Riffat, G. (1988). Spatial distribution of trabeculae in iliac bone from 145 osteoporotic females. *Acta Anatomica*. **132**:137-142.

Chen, H., Shoumura, S., Emura, S. and Bunai, Y. (2008). Regional variations of vertebral trabecular bone microstructure with age and gender. *Osteoporosis International*. **19**:1473-1483.

Cho, P.S., Rudd, A.D. and Johnson, R.H. (1996). Cone-beam CT from width-truncated projections. *Computerized Medical Imaging and Graphics*. **20(1)**:49-57.

Ciarelli, M.J., Goldstein, S.A., Kuhn, J.L., Cody, D.D. and Brown, M.B. (1991). Evaluation of orthogonal mechanical properties and density of human trabecular bone from the major metaphyseal regions with materials testing and computed tomography. *Journal of Orthopaedic Research*. **9**:674-682.

Ciarelli, T.E., Fyhrie, D.P., Schaffler, M.B. and Goldstein, S.A. (2000). Variations in three-dimensional cancellous bone architecture of the proximal femur in female hip fractures and in controls. *Journal of Bone and Mineral Research*. **15:**32-40.

Clark, K.C., Swallow, R.A., Naylor, E., Roebuck, E.J. and Whitley, A.S. (1984). *Positioning in Radiography. Clark's Positioning in Radiography*. Oxford, UK: Heinemann, p405-411.

Cody, D.D., Flynn, M.J. and Vickers, D.S. (1989). A technique for measuring regional bone mineral density in human vertebral bodies. *Physics in Medicine and Biology*. **16**:766-772.

Cohen, S.P. (2005). Sacroiliac Joint Pain: A Comprehensive review of anatomy, diagnosis, and treatment. *Anaesthesia and Analgesia*. **101**:1440 –1453.

Coleman, M.N. and Colbert, M.W. (2007). Technical note: CT thresholding protocols for taking measurements on three-dimensional models. *American Journal of Physical Anthropology*. **133**:723-725.

Collet, P.H., Uelbelhart, D., Vico, L., Moro, L., Hatmann, D., Roth, M. and Alexandre, C. (1997). Effects of 1- and 6-month spaceflight on bone mass and biochemistry in two humans. *Bone*. **20**:547-551.

Cooper, D.M.L., Turinsky, A.L., Sensen, C.W. and Hallgrimsson, B. (2003). Quantitative 3D analysis of the canal network in cortical bone by micro-computed tomography. *The Anatomical Record (Part B: The New Anatomist)*. **274(B)**:169-179.

Correia, H., Balseiro, S. and De Areia, M. (2005). Sexual dimorphism in the human pelvis: testing a new hypothesis. *Homo*. **56(2)**:153-160.

Correnti, V. (1955). Le basi morfomeccamiche della struttura dell'osso iliaco. *Rivista di Antropologia*. **42**:289-336.

Correnti, V. (1957). L'architettura del bacino umano ed il suo piano di orientamento fisiologico. *Rivista di Antropologia*. **44**:3-68.

Courteix, D., Lespessailles, E., Peres, S.L., Obert, P., Germain, P. and Benhamou, C.L. (1998). Effect of physical training on bone mineral density in prepubertal girls: A comparative study between impact-loading and non-impact-loading sports. *Osteoporosis International*. **8**:152-158.

Cowin, S.C., Moss-Salentijn, L. and Moss, M.L. (1991). Candidates for the mechanosensory system in bone. *Journal of Biomechanical Engineering*. **113(2)**:191-197.

Cowin, S. (2001). *Bone Mechanics Handbook*, 2nd Edition. Florida: CRC Press.

Cox, M. and Mays, S. (2000). Human Osteology In Archaeology and Forensic Science. Greenwich Medical Media: London. pp 117-127.

Crock, H.V. (1996). *An Atlas of Vascular Anatomy of the Skeleton & Spinal Cord*. London: Martin Dunitz.

Cui, W.Q., Won, Y.Y., Baek, M.H., Lee, D.H., Chung, Y.S., Hur, J.H. and Ma, Y.Z. (2008). Age and region dependant changes in three-dimensional microstructural properties of proximal femoral trabeculae. *Osteoporosis International*. **19**:1579-1587.

Cummings, S.R., Bates, D. and Black, D.M. (2002). Clinical use of bone densitometry: Scientific review. *Journal of the American Medical Association*. **288(15)**:1889-1897.

Currey, J. (1986). Power law models for the mechanical properties of cancellous bone. *Engineering in Medicine*. **15:**53-54.

Dalle Carbonare, L., Valenti, M.T., Bertoldo, F., Zanatta, M., Zenari, S., Realdi, G., Lo Cascio, V. and Giannini, S. (2005). Bone microarchitecture evaluated by histomorphometry. *Micron*. **36**:609-616.

Dalstra, M., Huiskes, R., Odgaard, A. and Van Erning, L. (1993). Mechanical and textural properties of pelvic trabecular bone. *Journal of Biomechanics*. **26**:523-535.

Dalstra, M. and Huiskes, R. (1995). Load transfer across the pelvic bone. *Journal of Biomechanics*. **28(6)**:715-724.

Davidson, R.A. and Bowman, S. (2002). Macroradiography using conventional X-ray equipment. *The British Journal of Radiology*. **75**:831-836.

Davidson, R.M., Lingenbrink, P.A. and Norton, L.A. (1996). Continuous mechanical loading alters properties of mechanosensitive channels in G292 osteoblastic cells. *Calcified Tissue International*. **59**:500-504.

Davis, G.R. and Elliott, J.C. (2006). Artefacts in x-ray microtomography of materials. *Materials Science and Technology*. **22(9)**:1011-1018.

Day, J.S., Ding, M., Odgaard, A., Sumner, D.R., Hvid, I. and Weinans, H. (2000). Parallel plate model for trabecular bone exhibits volume fraction-dependant bias. *Bone*. **27(5)**:715-720.

Delaere, O., Kok, V., Nyssen-Behets, C. and Dhem, A. (1992). Ossification of the human fetal ilium. *Acta Anatomica*. **143**: 330-334.

Delaere, O. and Dhem, A. (1999). Prenatal development of the human pelvis and acetabulum. *Acta Orthopaedica Belgica*. **65(3)**:225-260.

Dempster, D.W., Cosman, F., Kurland, E.S., Zhou, H., Nieves, J., Woelfert, L., Shane, E., Plavetic, K., Muller, R., Bilezikian, J. and Lindsay, R. (2001). Effects of daily treatment with parathyroid hormone on bone architecture and turnover in patients with osteoporosis: a paired biopsy study. *Journal of Bone and Mineral Research*. **16**:1846-1853.

Diederichs, G., Link, T.M., Kentenich, M., Schwieger, K., Huber, M.B., Burghardt, A.J., Majumdar, S., Rogalla, P. and Issever, A.S. (2009). Assessment of trabecular bone structure of the calcaneus using multi-detector CT: correlation with microCT and biomechanical testing. *Bone*. doi:10.1016/j.bone.2009.01.372.

Ding, M. and Hvid, I. (2000). Quantification of age-related changes in the structure model type and trabecular thickness of human tibial trabecular bone. *Bone*. **26**:291-295.

Ding, M., Odgaard, A. and Hvid, I. (1999). Accuracy of cancellous bone volume fraction measured by micro-CT scanning. *Journal of Biomechanics*. **32**:323-326.

Ding, M., Day, J.S., Burr, D., Mashiba, T., Hirano, T., Weinans, H., Sumner, D.R. and Hvid, I. (2003). Canine cancellous bone microarchitecture after one year of high dose bisphosphonates. *Calcified Tissue International.* **72**:737-744.

Drake, R.L., Vogl, W. and Mitchell, A.W.M. (2005). *Gray's Anatomy for Students*. Churchill Livingstone: Philadelphia.

Drapeau, M.S.M. and Streeter, M.A. (2006). Modelling and remodelling responses to normal loading in the human lower limb. *American Journal of Physical Anthropology*. **129(3)**:403-409.

Ducy, P., Schinke, T. and Karsenty, G. (2000). The osteoblasts: A sophisticated fibroblast under central survalence. *Science*. **289**:1501-1504

Ehrlich, P.J. and Lanyon, L.E. (2002). Mechanical strain and bone cell function: a review. *Osteoporosis International*. **13**:688-700.

Engel, J. (1851). *Über die Gesetze der Knochenentwicklung*. Sitzungsberichte der Wiener Academie der Wissenschaften 1851, VII, p591, Tables 25-28.

Engelke, K., Graeff, W., Meiss, L., Hahn, M. and Delling,G. (1993). High spatial resolution imaging of bone mineral using computed tomography. Comparison with

microradiography and undecalcified histologic sections. *Investigative Radiology*. **28**:341-349.

Eriksen, E.F. (1986). Normal and pathological remodelling of human trabecular bone: three dimensional reconstruction of the remodelling sequence in normals and in metabolic bone disease. *Endocrinology Reviews*. **7**:379-406.

Eriksen, E. F., Eghbali-Fatourechi, G.Z. and Khosla, S. (2007). Remodeling and vascular spaces in bone. *Journal of Bone and Mineral Research*. **22(1)**:1-6.

Erlebacher, A., Filvaroff, E.H., Gitelman, S.E. and Derynck, R. (1995). Toward a molecular understanding of skeletal development. *Cell*. **80**:371-378.

Evans, F.G. (1957). *Stress and Strain in Bones.* Charles C. Thomas, Springfield, Illinois.

Evans, F.G. (1973). *Mechanical Properties of Bone*. Charles C. Thomas. Springfield: Illinois.

Fajardo, R.J. and Müller, R. (2001). Three-dimensional analysis of nonhuman primate trabecular architecture using micro-computed tomography. *American Journal of Physical Anthropology*. **115**:327-336.

Fajardo, R.J., Ryan, T.M. and Kappelman, J. (2002). Assessing the accuracy of high-resolution X-ray computed tomography of primate trabecular bone by comparisons with histological sections. *American Journal of Physical Anthropology.* **118**:1-10.

Fajardo, R.J., Müller, R., Ketcham, R.A. and Colbert, M. (2007). Nonhuman anthropoid primate femoral neck trabecular architecture and its relationship to locomotor mode. *Anatomical Record: Advances in Integrative Anatomy and Evolutionary Biology*. **290**:422-436.

Fazekas, I.Gy. and Kosa, F. (1978). *Forensic Fetal Osteology*. Budapest: Akademiai Kiado.

Feldkamp, L.A., Goldstein, S.A., Parfitt, A.M., Jesioil, G. and Kleerekoper, M. (1989). The direct examinantion of three-dimensional bone architecture in vitro by computed tomography. *Journal of Bone and Mineral Research*. **4**:3-11.

Fernández-Seara, M.A., Song, H.K. and Wehrli, F.W. (2001).Trabecular bone volume fraction mapping by low-resolution MRI. *Magnetic Resonance in Medicine* **46**:103-113.

Forssberg, H. (1985). Ontogeny of human locomotor control I. Infant stepping, supported locomotion and transition to independent locomotion. *Experimental Brain Research*. **57**:480-493.

Francis, C.C. (1940). The appearance of centres of ossification from 6-15 years. *American Journal of Physical Anthropology*. **27**:127-138.

Frazer, J.E. (1948). *The Anatomy of the Human Skeleton*, 4th edition. London: Churchill.

Freund, W.A. (1868). *Tageblatt der Dresdner Versammlung Deutscher Naturforscher und Arzte*, p73

Freund, W.A. (1878). *Gynacologische Klinik*. Strasburg, p.14

Frost, H.M. (1964). *The Laws of Bone Structure*, CC Thomas: Springfield, Illinois.

Frost, H.M. (1987). Bone 'mass' and the 'mechanostat'. *Anatomical Record*. **219**:1-9.

Frost, H.M. (1990a). Skeletal structural adaptations to mechanical usage (SATMU): 1. Redefining Wolff's Law: the bone modelling problem. *Anatomical. Record*. **226**:403-413.

Frost, H.M. (1990b). Skeletal structural adaptations to mechanical usage (SATMU): 2. Redefining Wolff's Law: the remodeling problem. *Anatomical Record*. **226**:414-422.

Frost, H.M. (2003). Bone's mechanostat: A 2003 update. *Anatomical Record*. **275A**:1081-1101.

Fung, F.C. (1981). *Biomechanics. Mechanical Properties of Living Tissues*. Springer, Berlin.

Galichon, V. and Thackeray, J.F. (1997). CT scans of trabecular bone. structure in the ilia of Sts 14 *(Australopithecus africanus), Homo sapiens and Pan paniscus. South African Journal of Science.* **93**:179–180.

Gardner, E. and Gray, D.J. (1950). Prenatal development of the human hip joint. *American Journal of Anatomy*. **87**: 163-211.

Gardner, E. and O'Rahilly, R. (1972). The early development of the hip joint in staged human embryos. *Anatomical Record*. **172**: 451-452.

Garvey, C.J. and Hanlon, R. (2002). Computed tomography in clinical practice. *British Medical Journal*. **324**:1077-1080.

Gefen, A. and Seliktar, R. (2004). Comparison of the trabecular architecture and the isostatic stress flow in the human calcaneus. *Medical Engineering and Physics*. **26**:119-129.

Genant, H.K., Gordon, C., Jiang, Y., Lang, T.F., Link, T.M. and Majumdar, S. (1999). Advanced imaging of bone macro and micro structure. *Bone*. **25(1)**:149-152.

Genant, H.K., Gordon, C., Jiang, Y., Link, T.M., Hans, D., Majumdar, S. and Lang, T.F. (2000). Advanced imaging of macrostructure and microstructure of bone. *Hormone Research*. **54**:24-30.

Genant, H.K. and Jiang, Y. (2006). Advanced imaging assessment of bone quality. *Annals of the New York Academy of Sciences*. **1069(1)**:410-428.

Geraets, W.G.M., Van Der Stelt, P.F., Netelenbos, C.J. and Elders, P.J.M. (1990). A new method for automatic recognition of the radiographic trabecular number. *Journal of Bone and Mineral Research*. **5**:227-233.

Germiller, J.A. and Goldstein, S.A. (1997). Structure and function of embryonic growth plate in the absence of functioning skeletal muscle. *Journal of Orthopaedic Research*. **15**:362-370.

Gesell, A. and Thompson, H. (1938). *The Psychology of Early Growth including Norms of Infant Behaviour and a Method of Genetic Analysis*. New York: Macmillan.

Gibson, L.J. (1985). The mechanical behaviour of cancellous bone. *Journal of Biomechanics*. **18**:317-328.

Gilbert, S.R., Gilbert, A.C. and Henderson, R.C. (2004). Skeletal maturation in children with quadriplegic cerebral palsy. *Journal of Pediatric Orthopedics*. **24**:292-297.

Glorieux, F.H., Travers, R., Taylor, A., Bowen, J.R., Rauch, F., Norman, M. and Parfitt, A.M. (2000). Normative data for iliac bone histomorphometry in growing children. *Bone*. **26(2)**:103-109.

Goel, V.K., Valliappan, S. and Svensson, N.L. (1978). Stresses in the normal pelvis. *Computers in Biology and Medicine*. **8**:91-104.

Goldstein, S.A. (1987). The mechanical properties of trabecular bone: dependence on anatomic location and function. *Journal of Biomechanics*. **20**:1055-1061.

Gosman, J.H. and Ketcham, R.A. (2009). Patterns in Ontogeny of Human Trabecular Bone from SunWatch Village in the Prehistoric Ohio Valley: General Features of Microarchitectural Change. *American Journal of Physical Anthropology*. **138(3)**:318-332.

Goulet, R.W., Goldstein, S.A., Ciarelli, M.J., Kuhn, J.L., Brown, M.B. and Feldkamp, L.A. (1994). The relationship between the structural and orthogonal compressive properties of trabecular bone. *Journal of Biomechanics*. **27**:375-389.

Greenspan, S.L. and Greenspan, F.S. (1999).The effect of thyroid hormone on skeletal integrity. *Annals of Internal Medicine*. **130**:750-758.

Guggenbuhl, P., Bodic, F., Hamel, L., Basle, M.F. and Chappard, D. (2006). Texture analysis of X-ray radiographs of iliac bone is correlated with bone micro-CT. *Osteoporosis International*. **17(3)**:447-454.

Guggino, S.E., Lajeunesse, D., Wagner, J.A. and Snyder, S.H. (1989). Bone remodeling signalled by a dihydropyridine- and phenylalkylamine-sensitive calcium channel. *Proceedings of the National Academy of Science USA*. **86**:2957-2960.

Guldberg, R.E., Lin, A.S.P., Coleman, R., Robertson, G. and Duvall, C. (2004). Microcomputed tomography imaging of skeletal development and growth. **72(3)**: 250-259.

Hadjidakis, D.J. and Androulakis, I.I. (2006). Bone Remodelling. *Annals of the New York Academy of Sciences*. **1092**:385-396.

Haidekker, M.A., Andresen, R. and Werner, H.J. (1999). Relationship between structural parameters, bone mineral density and fracture load in lumbar vertebrae, based on high-resolution computed tomography, quantitative computed tomography and compression tests. *Osteoporosis International*. **9**:433-440.

Hall, B.K. and Herring, S.W. (1990). Paralysis and growth of the musculoskeletal system in the embryonic chick. *Journal of Morphology*. **206**:45-56.

Hangartner, T.N. and Gilsanz, V. (1996). Evaluation of cortical bone by computed tomography. *Journal of Bone and Mineral Research*. **11**:1518-1525.

Hara, T., Tanck, E., Homminga. J. and Huiskes, R. (2002). The influence of microcomputed tomography threshold variations on the assessment of structural and mechanical trabecular bone properties. *Bone*. **31(1)**:107-109.

Harcourt-Smith, W.E.H. and Aiello, L.C. (2004). Fossils, feet and the evolution of human bipedal locomotion. *Journal of Anatomy*. **204**:403-416.

Henderson, R.C., Gilbert, S.R., Clement, M.E., Abbas, A., Worley, G. and Stevenson, R.D. (2005). Altered skeletal maturation in moderate to severe cerebral palsy. *Developmental Medicine and Child Neurology*. **47**:229-236.

Hercz, G. (2001). Regulation of Bone Remodeling: Impact of Novel Therapies. *Seminars in Dialysis*. **14(1)**:55-60.

Hert, J., Liskova, M. and Landrgot, B. (1969). Influence of the long term, continuous bending on bone. *Folia Primatologica*. **17**:389-399.

Hildebrand, T. and Ruegsegger, P. (1997a). A new method for the model independent assessment of thickness in three dimensional images. *Journal of Microscopy.* **185**: 67-75.

Hildebrand, T. and Ruegsegger, P. (1997b). Quantification of bone microarchitecture with the structural model index. *Computer Methods in Biomechanical and Biomedical Engineering*. **1(1)**:15-23.

Hildebrand, T., Laib, A., Müller, R., Dequeker, J. and Ruegsegger, P. (1999). Direct three-dimensional morphometric analysis of human cancellous bone: Microstructural data from spine, femur, iliac crest, and calcaneus. *Journal of Bone and Mineral Research*. **14(7)**:1167-1174.

Hoa, S. T. and Hutmacher, D.W. (2006). A comparison of micro CT with other techniques used in the characterisation of scaffolds. *Biomaterials.* **27**:1362–1376.

Hodges, P.W., Gurfinkel, V.S., Brumagne, S., Smith, T.C. and Cordo, P.C. (2002). Coexistence of stability and mobility in postural control: evidence from postural compensation for respiration. *Experimental Brain Research*. **144**:293-302.

Holdsworth, D.W. and Thornton, M.M. (2002). Micro-CT in small animal and specimen imaging. *Trends in Biotechnology*. **20(8)**: S34-S39.

Holm, N.J. (1980). The internal stress pattern of the os coxae. *Acta Orthopedica Scandinavica*. **51**:421-428.

Hosseini, A. and Hogg, D.A. (1991). The effects of paralysis on skeletal development in the chick embryo. I. General effects. *Journal of Anatomy*. **177**:159-168.

Hounsfield, G.N. (1973). Computerized transverse axial scanning (tomography). 1. Description of system. *British Journal of Radiology*. **46**:1016-1022.

Hsieh, Y.F., Robling, A.G., Ambrosius, W.T., Burr, D.B. and Turner, C.H. (2001). Mechanical loading of diaphyseal bone in vivo: the strain threshold for an osteogenic response varies with location. *Journal of Bone and Mineral Research*. **16**:2291-2297.

Huiskes, R. and Chao, E.Y.S. (1983). A survey of finite element analysis in orthopaedic biomechanics: the first decade. *Journal of Biomechanics*. **16(6)**:385-409.

Huiskes, R. (2000). If bone is the answer, what is the question? *Journal of Anatomy*. **197**:145-156.

Huiskes, R., Ruimerman, R., van Lenthe, G. and Janssen, J.D. (2000). Effects of mechanical forces on maintenance and adaptation of form in trabecular bone. *Nature*. **405**:704-706.

Humphry, G.M. (1858). *A Treatise of the Human Skeleton*. Cambridge: MacMillan and Co.

Inman, V.T., Ralston, H.J. and Todd, F. (1981). *Human Walking*. London: Williams and Wilkins.

Ippolito, E., Tovaglia, V. and Caterini, R. (1984). Mechanisms of acetabular growth in the foetus in relation to pathogenesis and treatment of congenital dislocation of the hip. *Italian Journal of Orthopaedics and Traumatology*. **10(4)**:501-510.

Ito, M., Ikeda, K., Nishiguchi, M., Shindo, H., Uetani, M., Hosoi, T. and Orimo, H. (2005). Multi-detector row CT imaging of vertebral microstructure for evaluation of fracture risk. *Journal of Bone and Mineral Research*. **20(10)**:1828-1836.

Ito, M., Nakamura, T., Matsumoto, T., Tsurusaki, K. and Hayashi, K. (1998). Analysis of trabecular microarchitecture of human iliac bone using microcomputed tomography in patients with hip arthrosis with or without vertebral fracture. *Bone*. **23(2)**:163-169.

Ito, M., Ohki, M., Hayashi, K., Yamada, M., Uetani, M. and Nakamura, T. (1995). Trabecular texture analysis of CT images in the relationship with spinal fracture. *Radiology*. **194**:55-59.

Jackson, S. and Thomas, R. (2004). *Cross-sectional Imaging Made Easy*. Edinburgh: Churchill-Livingstone.

Jacob, H.A.C., Huggler, A.H., Dietschi, C. and Schreiber, A. (1976). Mechanical function of subchondral bone as experimentally determined on the acetabulum of the human pelvis. *Journal of Biomechanics*. **9**:625-627.

Janssen, M. (1920). On *Bone Formation: Its Relation to Tension and Pressure*. London, Longmans.

Jarvinen, L.N., Sievanen, H., Jokihaara, J. and Einhorn, T.A. (2005). Revival of bone strength: the bottom line. *Journal of Bone and Mineral Research*. **20**:717-720.

Jee, W.S.S. (2001) Integrated bone tissue physiology: Anatomy and Physisology. In: Cowin, S. *Bone Mechanics Handbook*, 2nd Edition. Florida: CRC Press.

Jee, W.S.S. (2005). The past, present, and future of bone morphometry: its contribution to an improved understanding of bone biology. *Journal of Bone and Mineral Metabolism*. **23(S)**:1-10.

Jensen, K.S., Mosekilde, L. and Mosekilde, L. (1990). A model of vertebral bone architecture and its mechanical properties. *Bone*. **11(6)**:417-423.

Jiang, Y., Zhao, J., White, D.L. and Genant, H.K. (2000). Micro CT and Micro MR imaging of 3D architecture of animal skeleton. *Journal of Musculoskeletal and Neuronal Interactions*. **1**:45-51.

Johnstone, W.H., Keats, T.E. and Lee, M.E. (1982). The anatomic basis for the superior acetabular roof notch "Superior acetabular notch". *Skeletal Radiology*. **8**:25-27.

Jones, K.B., Mollano, A.V., Morcuende, J.A., Cooper, R.R. and Saltzman, C.L. (2004). Bone and brain: A review of neural, hormonal, and musculoskeletal connections. *The Iowa Orthopaedic Journal*. **24**:123-132.

Jones, J.R., Poologasundarampillai, G., Atwood, R.C., Bernard, D. and Lee, P.D. (2007). Non-destructive quantitative 3D analysis for the optimisation of tissue scaffolds. *Biomaterials*. **28**:1404-1413.

Jovanovic, S. and Zivanovic, S. (1965). The establishment of the sex by the great schiatic notch. *Acta Anatomica*. **61**:101-107.

Kang, C., Paley, M., Ordidge, R. and Speller, R. (1999). R'_2 measured in trabecular bone in vitro : Relationship to trabecular separation. *Magnetic Resonance Imaging*. **17(7)**:989-995.

Kapandji, I.A. (1987). *The Physiology of the Joints. Volume Two: Lower Limb*. 5th Edition. Edinburgh: Churchill Livingstone.

Kawaguchi, H., Pilbeam, C.C. and Raisz, L.G. (1994). Anabolic effects of 3,3',5-triiodothyronine and triiodothyroacetic acid in cultured neonatal mouse parietal bones. *Endocrinology*. **135**: 971-976.

Kazakia, G.J., Burghardt, A.J., Cheung, S. and Majumdar, S. (2008). Assessment of bone tissue mineralisation by conventional x-ray microcomputed tomography: Comparison with synchrotron radiation microcomputed tomography and ash measurement. *Medical Physics*. **35(7)**:3170-3179.

Keaveny, T.M., Morgan, E.F., Niebur, G.L. and Yeh, O.C. (2001). Biomechanics of trabecular bone. *Annual Review of Biomedical Engineering*. **3**:307-333.

Keen, M. (1993). Early development and attainment of normal mature gait. *Journal of Prosthetics Orthotics*. **5**:35-38.

Khosla, S. (2008). Estrogen and bone: Insights from estrogen-resistant aromatase-deficient, and normal men. *Bone*. **43**:414-417.

Kim, D.G., Christopherson, G.T., Dong, X.N., Fyhrie, D.P. and Yeni, Y.N. (2004). The effect of microcomputed tomography scanning and reconstruction voxel size on the accuracy of stereological measurements in human cancellous bone. *Bone*. **35**:1375-1382.

Kissling, R.O. and Jacob, H.A. (1996). The mobility of the sacroiliac joint in healthy subjects. *Bulletin (Hospital for Joint Diseases)*. **54(3)**:158-164.

Kjaer, I., Kjaer, T.W. and Gream, N. (1993). Ossification sequence of occipital bone and vertebrae in human fetuses. *Journal of Craniofacial Genetics and Developmental Biology*. **13**:83-88.

Klein-Nulend, J., Van der Plas, A., Semeins, C.M., Ajubi, N.E., Frangos, J.A., Nijweide, P.J. and Burger, E.H. (1995). Sensitivity of osteocytes to biomechanical stress in vitro. *The Federation of American Studies for Experimental Biology*. **9**:441-445.

Klein-Nulend, J., Nijweide, P.J. and Burger, E.H. (2003). Osteocyte and bone structure. *Current Osteoporosis Reports*. **1(1)**:5-10.

Knothe Tate, M.L., Adamson, J.R., Tami, A.E. and Bauer, T.W. (2004). The osteocyte. *International Journal of Biochemistry and Cell Biology*. **36**:1-8.

Kobayashi, S., Takahashi, H.E., Ito, A., Saito, N., Nawata, M., Horiuchi, H., Ohta, H., Ito, A., Iorio, R., Yamamoto, N. and Takaoka, K. (2003). Trabecular minimodeling in human iliac bone. *Bone*. **32**:163-169.

Koch, J.C. (1917). The laws of bone architecture. *American Journal of Anatomy*. **21**:177-298.

Kothari, M., Keaveny, T.M., Lin, J.C., Newitt, D.C., Genant, H.K. and Majumdar, S. (1998). Impact of spatial resolution on the prediction of trabecular architecture parameters. *Bone*. **22**:437-443.

Krogman, W.M and Íşçan, M.Y. (1986). *The Human Skeleton in Forensic Medicine*. Springfield, Illinois: Charles C. Thomas.

Kubo, M. and Ulrich, B.D. (2006). Early stage of walking: Development of control in mediolateral and anteropoterior directions. Journal of Motor Behaviour. **38(3)**:229-237.

Kuhn, J.L., Goldstein, S.A., Feldkamp, L.A., Goulet, R.W. and Jesion, G. (1990). Evaluation of a microcomputed tomography system to study trabecular bone structure. *Journal of Orthopaedic Research*. **8**:833-842.

Lacey, D.L., Timms, E., Tan, H.L., Kelley, M.J., Dunstan, C.R., Burgess, T., Elliott, R., Colombero, A., Elliott, G., Scully, S., Hsu, H., Sullivan, J., Hawkins, N., Davy, E., Capparelli, C., Ali, E., Qian, Y.X., Kaufman, S., Sarosi, I., Shalhoub, V., Senaldi, G., Gou, J., Delaney, J. and Boyle, W.J. (1998). Osteoprotegrin ligand is a cytokine that regulates osteoclasts differentiation and activation. *Cell*. **93**:165-176.

Lai, Y.M., Quin, L., Yeung, H.Y., Lee, K.K.H. and Chan, K.M. (2005). Regional differences in trabecular BMD and micro-architecture of weight-bearing bone under habitual gait loading: a pQCT and microCT study in human cadavers. *Bone*. **37**:274-282.

Laib, A., Kumer, J.L., Majumdar, S. and Lane, N.E. (2001). The temporal changes of trabecular architecture in ovariectomized rats assessed by microCT. *Osteoporosis International*. **12**:936-941.

Lanyon, L.E. (1974). Experimental support for the trajectorial theory of bone structure. *Journal of Bone and Joint Surgery*. **56B(1)**:160-166.

Lanyon, L.E. (1982). *Mechanical function and bone remodelling.* In:Sumner-Smith, G, editor. *Bone in Clinical Orthopaedics*. Philidelphia: Saunders. pp273-304.

Lanyon, L.E. (1993). Osteocytes, strain detection, bone modelling and remodeling. *Calcified Tissue International*. **53**:S102-S107.

Lanyon, L.E., Goodship, A.E., Pye, C.J. and Macfie, J.H. (1982). Mechanically adaptive bone remodelling. *Journal of Biomechanics*. **15**:141-154.

Lanyon, L.E. (1984). Functional strain as a determinant for bone remodelling. *Calcified Tissue International*. **36(1)**:S56-S61.

Lanyon, L.E. and Rubin, C.T. (1984). Static vs dynamic loads as an influence on bone remodelling. *Journal of Biomechanics*. **17(12)**:897-905.

Lanyon, L.E. and Skerry, T. (2001). Postmenopausal osteoporosis as a failure of bone's adaptation to functional loading: a hypothesis. *Journal of Bone and Mineral Research*. **16**:1937-1947.

Lanyon, L.E. (1996). Using functional loading to influence bone mass and architecture: objectives, mechanisms and relationship with estrogen of the mechanically adaptive process in bone. *Bone*. **18**:S37-S43.

Last, R.J. (1973). *Anatomy, Regional and Applied*, 5th Edition. Edinburgh: Churchill Livingstone.

Latarjet, A. and Gallois, A. (1910). L'architecture interiere de l'os iliaque et de la ceinture pelvienne. *Bibliography Anatomy*. **20**:55-69.

Latimer, B.M. and Ward, C.V. (1998). Locomotion in Australopithecus: evidence from the leg and foot. *Dual Congress*. Sun City (abstract).

Laurenson, R.D. (1963). *The Chondrification and Primary Ossification of the Human Ilium*. MD Thesis. University of Aberdeen.

Laurenson, R.D. (1964a). The primary ossification of the human ilium. *Anatomical Record.* **148**:209-217.

Laurenson, R.D. (1964b). The chondrification of the human ilium*. Anatomical Record*. **148**:197-202.

Lazenby, R.A., Angus, S., Cooper, D.M.L. and Hallgrimsson, B. (2008). A three-dimensional microcomputed tomographic study of site-specific variation in trabecular microarchitecture in the human second metacarpal. *Journal of Anatomy*. **213(6)**:698-705.

Lee, T.C. and Taylor, D. (1999). Bone remodelling: Should we cry Wolff? *Irish Journal of Medical Science*. **168(2)**:102-105.

Lee, C.A. and Einhorn, T.A. (2001). *Osteoporosis*. Chapter 1:The bone organ system: form and function. Second edition. Academic, San Diego.

Lee, M.C. and Eberson, C.P. (2006). Growth and development of the child's hip. *Orthopedic Clinics of North America.* **37**:119-132.

Leong, A. (2006). Sexual dimorphism of the pelvic architecture: A struggling response to destructive and parsimonious forces by natural and mate selection. *McGill Journal of Medicine*. **9**:61-66.

Li, X., Liu, J., Davey, M., Duce, S., Jaberi, N., Liu, G., Davidson, G., Tenent, S., Mahood, R., Brown, P., Cunningham, C., Bain, A., Beattie, K., McDonald, L., Schmidt, K., Towers, M., Tickle, C. and Chudek, S. (2007). Micro-magnetic resonance imaging of avian embryos. *Journal of Anatomy*. **211(6)**:798-809.

Li, Y., Crompton, R.H., Alexander, R.McN., Gunther, M.M. and Wang, W.T. (1996). Characteristics of ground reaction forces in normal and chimpanzee-like bipedal walking by humans. *Folia Primatologica*. **66**:137-159.

Li, Y.C., Amling, M., Pirro, A.E., Priemel, M., Meuse, J. and Baron, R. (1998). Normalisation of mineral ion homeostasis by dietary means prevents hyperparathyroidism, rickets, and osteomalacia, but not alopecia in vitamin D receptor-ablated mice. *Endocrinology*. **139**:4391-4396.

Lieberman, D.E. and Pearson, O.M. (2001). Trade-off between modelling and remodeling responses to loading in the mammalian limb. *Bulletin of the Museum of Comparative Zoology*. **156**:269-282.

Lieberman, D.E., Pearson, O.M., Polk, J.D., Demes, B. and Crompton, A.W. (2003). Optimization of bone growth and remodeling in response to loading in tapered mammalian limbs. *Journal of Experimental Biology*. **206**: 3125-3138.

Linde, F., Norgaard, P., Hvid, I., Odgaard, A. and Soballe, K. (1991). Mechanical properties of trabecular bone. Dependancy on strain rate. *Journal of Biomechanics*. **24**:803-809.

Link, T.M., Majumdar, S., Lin, J.C., Augat, P., Gould, G., Newitt, D., Ouvang, X., Lang, T.F., Mathur, A. and Genant, H.K. (1998). Assessment of trabecular structure using high resolution CT images and texture analysis. *Journal of Computer Assisted Tomography*. **22**:15-24.

Link, T.M., Vieth, V., Stehling, C., Lotter, A., Beer, A., Newitt, D. and Majumdar, S. (2003). High-resolution MRI vs multislice spiral CT: which technique depicts the trabecular bone structure best? *European Journal of Radiology*. **13**:663-671.

Lips, P., Courpron, P. and Meunier, P.J. (1978). Mean wall thickness of trabecular bone packets in the human iliac crest: changes with age. *Calcified Tissue Research*. **26**:13-17.

Liskova, M. and Hert, J. (1971). Reaction of bone to mechanical stimuli. *Folia Primatologica*. **19**:301-317.

Liu, X.S., Sajda, P., Saha, P.K., Wehrli, F.W. and Guo, X. E. (2006). Quantification of the roles of trabecular architecture and trabecular type in determining the elastic modulus of human trabecular bone. *Journal of Bone and Mineral Research.* **21(10)**:1608-1617.

Louis, O., Van den Winkel, P., Covens, P., Schoutens, A. and Osteaux, M. (1993). Size of cortical bone and relationship to bone mineral density assessed by quantitative computed tomography image segmentation. *Investigative Radiology*. **28**:802-805.

Lovejoy, C.O., Meindl, R.S., Ohman, J.C., Heiple, K.G. and White, T.D. (2002). The *Maka* femur and its bearing on the antiquity of human walking: applying contemporary concepts of morphogenesis to the human fossil record. *American Journal of Physical Anthropology*. **119**:97-133.

Luthje, P., Nurmi, I., Kataja, M., Heliovaara, M. and Santavirta, S. (1995). Incidence of pelvic fractures in Finland in 1988. *Acta Orthopaedica Scandinavica*. **66(3)**:245-248.

Macchiarelli, R., Bondioli, L., Galichon, V. and Tobias, P.V. (1999). Hip bone trabecular architecture shows uniquely distinctive locomotor behaviour in South African australopithecines. *Journal of Human Evolution*. **36**:211-232.

Macho, G.A., Abel, R.L. and Schutkowski, H. (2005). Age changes in bone microstructure: do they occur uniformly? *International Journal of Osteoarcheology.* **15**:421-430.

MacLatchy, L. and Müller, R. (2002). A comparison of the femoral head and neck trabecular architecture of Galago and Perodicticus using micro-computed tomography (μCT). *Journal of Human Evolution*. **43**:89-105.

MacLaughlin, S.M. and Bruce, M.F. (1986). The sciatic notch/acetabular index as a discriminator of sex in European skeletal remains. *Journal of Forensic Sciences.* **31(4)**:1380-1390.

MacRae, V.E., Harvat, S., Pells, S.C., Dale, H., Collinson, R.S., Pitsillides, A.A., Ahmed, S.F. and Farquharson, C. (2008). Increased bone mass, altered traebcular architecture and modified growth plate organisation in the growing skeleton of SOCS2 deficient mice. *Journal of Cellular Physiology*. **218(2)**:276-284.

MacWilliams, B.A., Cowley, M. and Nicholson, D.E. (2003). Foot kinematics and kinetics during adolescent gait. *Gait and Posture*. **17(3)**:214-224.

Maga, M., Kappelman, J., Ryan, T.M. and Ketcham, R.A. (2006). Preliminary observations on the calcaneal trabecular microarchitecture of extant large-bodied hominids. *American Journal of Physical Anthropology*. **129**:410-417.

Majumdar, S., Kothari, M., Augat, P., Newitt, D.C., Link, T.M., Lin, J.C., Lang, T., Lu, Y. and Genant, H.K. (1998). High-resolution magnetic resonance imaging: three-dimensional trabecular bone architecture and biomechanical properties. *Bone*. **22(5)**:445-454.

Majumdar, S., Newitt, D.C., Mathure, A., Osman, D., Gies, A., Chiu, E., Lotz, J., Kinney, J. and Genant, H.K. (1996). Magnetic resonance imaging of trabecular bone structure in the distal radius: Relationship with x-ray tomographic microscopy and biomechanics. *Osteoporosis International*. **6**:376-385.

Majumder, S., Roychowdhury, A. and Pal, S. (2004). Variations of stress in pelvic bone during normal walking, considering all active muscles. *Trends in Biomaterials and Artificial Organs*. **17(2)**:48-53.

Mann, R.W (1998). Use of bone trabeculae to establish positive identification. *Forensic Science International*. **98(1-2)**:91-99.

Manolagas, S.C. and Olefsky, J.M. (1988). *Contemporary Issues in Endocrinology and Metabolism.. Metabolic Bone and Mineral Disorders*. Vol 5. New York: Churchill Livingstone.

Manolagas, S.C. and Jilka, R.L. (1995). Bone marrow, cytokines, and bone remodelling. *New England Journal of Medicine*. **332**:305-311.

Marchal, F. (2000). A new morphometric analysis of the hominid pelvic bone. *Journal of Human Evolution*. **38**:347-365.

Martin, R.B., Burr, D.B. and Sharkey, N.A. (1998). *Skeletal Tissue Mechanics*. Springer: New York.

Martin-Badosa, E., Elmoutaouakkil, A., Nuzzo, S., Amblard, D., Vico, L. and Peyrin, F. (2003). A method for the automatic characterization of bone architecture in 3D mice tomographic images. *Computerized Medical Imaging and Graphics*. **27**:447-458.

Martinon-Torres, M. (2003). Quantifying trabecular orientation in the pelvic cancellous bone of modern Humans, Chimpanzees, and the Kebara 2 Neanderthal. *American Journal of Human Biology*. **15**:647-661.

Mays, S., Lees, B. and Stevenson, J.C. (1998). Age dependant bone loss in the femur in a medieval population. *International Journal of Osteoarchaeology*. **8**:97-106.

McColl, D.J., Abel, R., Spears, I.R. and Macho, G.A. (2006). Automated method to measure trabecular thickness from microcomputed tomographic scans and its application. *The Anatomical Record Part A*. **288A**:982-988.

McGraw, M.B. (1945). *The Neuromuscular Maturation of the Human Infant*. New York: Columbia University Press.

Miller, J.A., Schultz, A.B. and Andersson, G.B. (1987). Load-displacement behavior of the sacroiliac joints. *Journal of Orthopaedic Research*. **5**:92–101.

Miller, F., Moseley, C. and Koreska, J. (1990). Pelvic anatomy relative to lumbosacral instrumentation. *Journal of Spinal Disorders*. **3(2)**:169-173.

Molina, P.E. (2006). *Endocrine Physiology*. Second Edition. New York: McGraw-Hill.

Moore, K.L. and Dalley, A.F. (1999). *Clinically Oriented Anatomy*. Fourth Edition. Philidelphia: Lippincott Williams and Wilkins.

Moore, R.J., Durbridge, T.C., Woods, A.E. and Vernon-Roberts, B. (1989). Variation in histomorphometric estimates across different sites of the iliac crest. *Journal of Clinical Pathology*. **42**:814-816.

Mosekilde, L., Eriksen, E.F. and Charles, P. (1990). Effects of thyroid hormone on bone and mineral metabolism. *Endocrinology Metabolism Clinics of North America*. **19**:35-63.

Mosekilde, L. and Mosekilde, L. (1989). Normal vertebral body size and compressive strength: relation to age and to vertebral and iliac trabecular bone compressive strength. *Bone*. **6**:291-295.

Mulder, L., Koolstra, J.H., Weijs, W.A. and van Eijden, T.M.G.J. (2005). Architecture and mineralisation of developing trabecular bone in the pig mandibular condyle. *The Anatomical Record*. **285A**:659-667.

Mulder, L., Van Groningen, L.B., Potgieser, Y. A., Koolstra, J. H. and Van Eijden, M.G.J. (2006). Regional differences in architecture and mineralisation of developing mandibular bone. *The Anatomical Record*. **288A**:954-961.

Mulder, L., van Ruijven, L.J., Koolstra, J.H. and van Eijden, T.M.G.J. (2007). Biomechanical consequences of developmental changes in trabecular architecture and mineralization of the pig mandibular condyle. *Journal of Biomechanics*. **40**:1575-1582.

Mullender, M.G. and Huiskes, R. (1995). Proposal for the regulatory mechanism of Wolff's law. *Journal of Orthopaedic Research*. **13**: 503-512.

Müller, R., Koller, B., Hildebrand, T., Laib, A., Gianolini, S. and Ruegsegger, P. (1996). Resolution dependency of microstructural properties of cancellous bone based on three-dimensional m-tomography. *Technology and Health Care*. **4**:113-119.

Müller, R. and Ruegsegger, P. (1997). Micro-tomographic imaging for the non-destructive evaluation of trabecular bone architecture. *Bone Research in Biomechanics.* **40**:61-79.

Müller, R., Van Campenhout, H., Van Damme, B., Van der Perre, G., Dequeker, J., Hildebrand, T. and Rüegsegger, P. (1998). Morphometric Analysis of Human Bone Biopsies: A Quantitative Structural Comparison of Histological Sections and Micro-Computed Tomography. *Bone*. **23(1)**:59-66.

Müller, R. (2003). Bone microarchitecture assessment: current and future trends. *Osteoporosis International*. **14(5)**:S89-S99.

Müller, R. (2005). Long-term prediction of three-dimensional bone architecture in simulations of pre-, peri- and post-menopausal microstructural bone remodelling. *Osteoporosis International*. **16**:S25-S35.

Murray, P.D.F. (1936). *Bones. A Study in the Development and Structure of the Vertebrate Skeleton*. i-x, Cambridge University Press, 1-203.

Musemeche, C.A., Fisher, R.P., Cotler, H.B. and Andrassy, R.J. (1987). Selective management of paediatric pelvic fractures: a conservative approach. *Journal of Pediatric Surgery*. **22(6)**:538-540.

Nagaraja, S., Lin, A.S.P. and Guldberg, R.E. (2007). Age-related changes in trabecular bone microdamage initiation. *Bone*. **40**:973-980.

Nakano, K.K. (1973). Anencephaly: A review. *Developmental Medicine and Child Neurology*. **15**:383-400.

Nakano, H., Watahiki, J., Kubota, M., Maki, K., Shibasaki, Y., Hatcher, D. and Miller, A.J. (2003). Micro X-ray computed tomography analysis for the evaluation of asymmetrical condylar growth in the rat. *Orthodontic Craniofacial Research*. **6**(Suppl. 1):168-172.

Newman, D.L., Dougherty, G., al Obaid, A. and Hajrasy, H. (1998). Limitations of clinical CT in assessing cortical thickness and density. *Physics in Medicine and Biology*. **43**:619-626.

Nilsson, B.E. and Westlin, N.E. (1971). Bone density in athletes. *Clinical Orthopaedics*. **77**:179-182.

Noback, C.R. (1944). The developmental anatomy of the human osseous skeleton during the embryonic, fetal and circumnatal periods. *Anatomical Record.* **88**: 91-125.

Noback, C.R. and Robertson, G.G. (1951). Sequences of appearance of ossification centres in the human skeleton during the first five prenatal months. *American Journal of Anatomy.* **89**:1-28.

Nowlan, N.C., Murphy, P. and Prendergast, P.J. (2007). Mechanobiology of embryonic limb development. *Annals of the New York Academy of Science*. **1101**:389-411.

Nuzzo, S., Meneghini, C., Braillon, P., Bouvier, R., Mobilio, S. and Peyrin, F. (2003). Microarchitectural and physical changes during fetal growth in human vertebral bone. *Journal of Bone and Mineral Research*. **18(4)**:760-768.

Odgaard, A., Jensen, E.B. and Gundersen, H.J.G. (1990). Estimation of structural anisotropy based on volume orientation. A new concept. *Journal of Microscopy*. **157**:149-162.

Odgaard, A. (1997). Three-dimensional methods for quantification of cancellous bone architecture. *Bone*. **20**:315-328.

Ogden, J.A., Conlogue, G.J., Bronson, M.L. and Jensen, P.S. (1979). Radiology of postnatal skeletal development. II. The manubrium and sternum. *Skeletal Radiology*. **4**:189-195.

Ogden, J.A. and Phillips, S.B. (1983). Radiology of Postnatal Skeletal Development. VII. The scapula. *Skeletal Radiology*. **9**:157-169.

Ohlsson, C., Bengtsson, B., Isaksson, G.P., Andreassen, T.T. and Stootweg, M.C. (1998). Growth hormone and bone. *Endocrine Reviews*. **19(1)**:55-79.

Olsen, B.R., Reginato, A.M. and Wang, W. (2000). Bone development. *Annual Review of Cell and Developmental Biology*. **16**:191-220.

O'Rahilly, R. and Gardner, E. (1975). The timing and sequence of events in the development of the limbs in the human embryo. *Anatomy and Embryology*. **148**: 1-23.

Ortega, N., Behonick, D.J. and Werb, Z. (2004). Matrix remodeling during endochondral ossification. *Trends in Cell Biology*. **14(2)**:86-93.

Osborne, D., Effmann, E., Broda, K. and Harrelson, J. (1980). The development of the upper end of the femur with special reference to its internal architecture. *Radiology.* **137**:71-76.

Oxnard, C.E. and Yang, H.C.L. (1981). Beyond biometrics: Studies of complex biological patterns. *Symposia of the Zoological Society London.* **46**: 127-167.

Pacifici, R. (1996). Estrogen, cytokines and pathogenesis of postmenopausal osteoporosis. *Journal of Bone and Mineral Research*. **11**:1043-1051.

Pacifici, R. (1998). Cytokines, estrogen and postmenopausal osteoporosis-the second decade. *Endocrinology*. **139**:2659-2661.

Pal, G.P. and Routal, R.V. (1998). Architecture of the cancellous bone of the human talus. *The Anatomical Record.* **252**:185-193.

Papadimitriou, A. and Chrousos, G.P. (2005). Recognising the sex differences in the incidence of pubertal disorders. *Hormone and Metabolic Research*. **37(11)**:708-710.

Parfitt, A.M., Drezner, M.K., Glorieux, F.H., Kanis, J.A., Malluche, H. and Meunier, P.J. (1987). Bone histomorphometery: standardization of nomenclature, symbols, and units. *Journal of Bone and Mineral Research*. **2**:595-610.

Parfitt, A.M., Travers, R., Rauch, F. and Glorieux, F.H. (2000). Structural and cellular changes during bone growth in healthy children. *Bone*. **27**:487-494.

Patel, P.V., Prevrhal, S., Bauer, J.S., Phan, C., Eckstein, F., Lochmuller, E-M., Majumdar, S. and Link, T.M. (2005) Trabecular bone structure obtained from multislice spiral computed tomography of the calcaneus predicts osteoporotic vertebral deformities. *Journal of Computer Assisted Tomography*. **29(2)**:246-253.

Pearson, O.M. and Lieberman, D.E. (2004). The aging of Wolff's "law": Ontogeny and responses to mechanical loading in cortical bone. *Yearbook of Physical Anthropology*. **47**:63-99.

Pel, J.J.M., Spoor, C.W., Pool-Goudzwaard, A.L., Hoek Van Duke, G.A. and Snijders, C.J. (2008). Biomechanical analysis of reducing sacroiliac joint shear load by optimization of pelvic muscle and ligament forces. *Annals of Biomedical Engineering*. **36(3)**:415-424.

Perry, J. (1992). *Gait Analysis: Normal and Pathological Function*. New Jersey: SLACK Incorporated.

Petersson, J., Brismar, T. and Smedby, O. (2006). Analysis of skeletal microstructure with clinical multislice CT. *Medical Image Computing and Computer Assisted Intervention: MICCAI*. **9(2)**:880-887.

Pierroz, D.D., Bouxsein, M.L., Rizzoli, R. and Ferrari, S.L. (2006). Combined treatment with a B-blocker and intermittent PTH improves bone mass and microarchitecture in ovariectomized mice. *Bone*. **39**:260-267.

Pitsillides, A.A. (2006). Early effects of embryonic movement: 'a shot out of the dark'. *Journal of Anatomy*. **208**:417-431.

Ponseti, I.V. (1978). Growth and development of the acetabulum in the normal child. *The Journal of Bone and Joint Surgery.* **60(A)**:575-585.

Popova, T. (1935). *Issledovaniia po biodinamike lococotsii*. Chapter 3, vol 1: Biodinamika khod'by normal'nogo vzroslogo muzhchiny. Idat Vsesoiuz. Insit. Eksper. Med. Moscow.

Pothuaud, L., Lespessailles, E., Harba, R., Jennane, R., Royant, V., Eynard, E. and Benhamou, C.L. (1998). Fractal analysis of trabecular bone texture on radiographs: discriminant value in postmenopausal osteoporosis. *Osteoporosis International*. **8**:618-625.

Pothuaud, L., van Rietbergen, B., Mosekilde, L., Beuf, O. and Levitz, P. (2002). Combination of topological parameters and bone volume fraction better predicts the mechanical properties of trabecular bone. *Journal of Biomechanics*. **35**:1091-1099.

Prendergast, P.J. and Huiskes, R. (1995). The biomechanics of Wolff's law: recent advances. *Irish Journal of Medical Sciences*. **164(2)**:152-154.

Preuschoft, H. (2004). Mechanisms for the acquisition of habitual bipedality: are there biomechanical reasons for the acquisition of upright bipedal posture? *Journal of Anatomy*. **204(5)**:363-384.

Qin, L., Genant, H.K., Griffith, J. and Leung, K.S. (2007). *Advanced Bioimaging Techniques in Assessment of the Quality of Bone and Scaffold Materials, Techniques and Application*. Springer Berling Heidelberg, pp 79-84.

Raisz, L.G. (1999). Physiology and pathophysiology of bone remodelling. *Clinical Chemistry*. **45(8B)**:1353-1358.

Rajput, B., Arnold, G., Gibbs, S., Wang, W., Cochrane, L., Leese, G. and Abboud, R.J. (2008). Integrating pressure distribution measurement and gait analysis: A contribution to the diabetic foot. *Clinical Biomechanics*. **23**:715-716.

Rapillard, L., Charlebois, M. and Zysset, P.K. (2006). Compressive fatigue behaviour of human vertebral trabecular bone. *Journal of Biomechanics*. **39(11)**:2133-2199.

Rauch, F., Travers, R. and Glorieux, F.H. (2006). Cellular activity on the seven surfaces of iliac bone: A histomorphometric study in children and adolescents. *Journal of Bone and Mineral Research*. **21(4)**:513-519.

Ripamonti, U. (2006). Soluble osteogenic molecular signals and the induction of bone formation. *Biomaterials*. **27**:807-822.

Rissech, C., Sanudo, J.R. and Malgosa, A. (2001). The acetabular point: a morphological and ontogenetic study. *Journal of Anatomy*. **198(6)**:743-748.

Ritman, E.L. (2004). Micro-computed tomography-current status and developments. *Annual Review of Biomedical Engineering*. **6**:185-208.

Ritzel, H., Amling, M., Posl, M., Hahn, M. and Delling, G. (1997). The thickness of human vertebral bone and its changes in aging and osteoporosis: A histomorphometric analysis of the complete spinal column from thirty-seven autopsy specimens. *Journal of Bone and Mineral Research*. **12:**89-95.

Robling, A.G., Hinant, F.M., Burr, D.B. and Turner, C.H. (2002). Improved bone structure and strength after long term mechanical loading is greatest if loading is separated into short bouts. *Journal of Bone and Mineral Research*. **17**:1545-1554.

Robling, A.G., Castillo, A.B. and Turner, C.H. (2006). Biomechanical and molecular regulation of bone remodelling. *Annual Review of Biomedical Engineering*. **8**:455-498.

Robson, P. (1984). Prewalking locomotor movements and their use in predicting standing and walking. *Child: Care, Health and Development*. **10**:317- 330.

Rodriguez, J.I., Razquin, S., Palacios, J. and Rubio, V. (1992). Human growth plate development in the fetal and neonatal period. *Journal of Orthopaedic Research*. **10**:62-71.

Roesler, H. (1987). The history of some fundamental concepts in bone biomechanics. *Journal of Biomechanics*. **20(11/12)**:1025-1034

Roodman, G.D. (1992). Role of cytokines in the regulation of bone resorption. *Calcified Tissue International*. **53(1)**: S94-S98.

Roodman, G.D. (1996). Advances in bone biology: the osteoclast. *Endocrine Reviews*. **17**:308-332.

Rook, L., Bondioli, L., Kohler, M., Moya-Sola, S. and Macchiarelli, R. (1999). *Oreopithecus* was a bipedal ape after all: Evidence from the iliac cancellous architecture. *Proceedings of the National Academy of Sciences of the United States of America.* **96(15)**:8795-8799.

Rose, J. and Gamble, J.G. (1994). *Human Walking.* Second Edition. Baltimore: Williams and Wilkins.

Rosen, C.J. and Donahue, L.R. (1998). Insulin-like growth factors and bone-the osteoporosis connection revisited. *Proceeding of the Society for Experimental Biology and Medicine*. **219**:1-7.

Ross, D.S. (1994). Hyperthyroidism, thyroid hormone therapy, and bone. *Thyroid*. **4**:319-326.

Rosse, C. and Gaddum-Rosse, P. (1997). *Hollinshead's Textbook of Anatomy*. 5th Edition. Lippincott-Raven: Philadelphia.

Roux, W. (1881). *Der Kampf der Teile im Organismus*. Leipzig: Engelmann.

Rubin, C.T. and Lanyon, L.E. (1984). Regulation of bone formation by applied dynamic loads. *Journal of Bone and Joint Surgery*. **66A**:397-402.

Rubin, C., Turner, A.S., Mallinckrodt, C., Jerome, C., McLeod, K. and Bain, S. (2002). Mechanical strain, induced noninvasively in the high frequency domain, is anabolic to cancellous bone, but not cortical bone. *Bone*. **30(3)**:445-452.

Rudman, K.E., Aspden, R.M. and Meakin, J.R. (2006). Compression or tension? The stress distribution in the proximal femur. *Biomedical Engineering Online.* **5**:12-18.

Ruegsegger, P., Koller, B. and Muller, R. (1996). A microtomographic system for the non-destructive evaluation of bone microarchitecture. *Calcified Tissue International*. **58**:24-29.

Ruff, C.B., Walker, A. and Trinkaus, E. (1994). Postcranial robusticity in *Homo*. III: ontogeny. *American Journal of Physical Anthropology*. **93**:35-54.

Ruff, C., Holt, B. and Trinkaus, E. (2006). Who's afraid of the big bad Wolff?: "Wolff's law" and bone functional adaptation. *American Journal of Physical Anthropology*. **129**:484-498.

Ruimerman, R. (2005). *Modeling and Remodeling in Bone Tissue*. Dissertation, University Press Facilities: Eindhoven.

Rupprecht, M., Pogoda, P., Mumme, M., Rueger, J.M., Puschel, K. and Amling, M. (2006). Bone microarchitecture of the calcaneus and its changes in ageing: a histomorphometric analysis of 60 human specimens. *Journal of Orthopaedic Research*. **24(4)**: 664-674.

Ryan, T.M. and Ketcham, R.A. (2002). Femoral head trabecular bone structure in two omomyid primates. *Journal of Human Evolution.* **43**:241-263.

Ryan, T.M. and van Rietbergen, B. (2005). Mechanical significance of femoral head trabecular bone structure in Loris and Galagos evaluated using micromechanical finite element analysis. *American Journal of Human Evolution.* **126**:82-96.

Ryan, T.M. and Krovitz, G.E. (2005). Ontogeny of three-dimensional trabecular bone architecture in the human proximal femur. *American Journal of Physical Anthropology*. Supplement. **40**:180-181.

Ryan, T.M. and Krovitz, G.E. (2006). Trabecular bone ontogeny in the human proximal femur. *The Journal of Human Evolution*. **51(6)**:591-602.

Ryan, T.M, van Rietbergen, B., and Krovitz, G.E. (2007). Mechanical adaptation of the trabecular bone in the growing human femur and humerus. *American Journal of Physical Anthropology.* Supplement. **44**:p203.

Salle, B.L., Rauch, F., Travers, R., Bouvier, R. and Glorieux, F.H. (2002). Human fetal bone development: Histomorphometric evaluation of the proximal femoral metaphysis. *Bone*. **30(6)**:823-828.

Salsabili, N., and Hogg, D.A. (1991). Development of the human sacroiliac joint. *Clinical Anatomy*. **4**:99-108

Samei, E., Seibert, J.A., Willis, C.E., Flynn, M.J., Mah, E. and Junck, K.L. (2001). Performance evaluation of computed radiography systems. *Medical Physics*. **28(3)**:361-371.

Sandor, T., Felsenberg, D., Kalendar, W.A., Clain, A. and Brown, E. (1992). Compact and trabecular components of the spine using quantitative computed tomography. *Calcified Tissue International*. **50**:502-506.

Saparin, P., Thomsen, J.S., Kurths, J., Beller, G. and Gowin, W. (2006). Segmentation of bone CT images and assessment of bone structure using measures of complexity. *Medical Physics*. **33(10)**:3857-3873.

Saunders, J.B., Inman, V.T. and Eberhart, H.D. (1953). The major determinants in normal and pathological gait. *Journal of Bone and Joint Surgery*.**35(3A)**:543-558.

Saunders, W.J. (1998). Comparative morphometric study of the australopithecine vertebral series Stw-H8/841. *Journal of Human Evolution*. **34**:249-302.

Sawamura, C., Takahashi, M., McCarthy, K.J., Shen, Z., Fukai, N., Rodriguez, E.K. and Snyder, B.D. (2006). Effect of in ovo immobilization of development of chick hind-limb articular cartilage: an evaluation using micro-MRI measurement of delayed gadolinium uptake. *Magenetic Resonace in Medicine*. **56**:1235-1241.

Schaetzing, R. (2003). Computed Radiography. Advances in Digital Radiography: RSNA Categorical Course in Diagnostic Radiology Physics. pp7-22.

Scherf, H. and Tilgner, R. (2009). A new high-resolution computed tomography (CT) segmentation method for trabecular bone architectural analysis. *American Journal of Physical Anthropology*. DOI: 10.1002/ajpa.21033.

Scheuer, L. and Black, S. (2000). *Developmental Juvenile Osteology*. London: Academic Press.

Scheuer, L. and Black, S. (2004). *The Juvenile Skeleton*. London: Academic Press.

Schnitzler, C.M., Mesquita, J.M. and Pettifor, J.M. (2009). Cortical bone development in black and white South African children: Iliac crest histomorphometry. *Bone*. **44(4)**:603-611.

Schoenau, E. (2006). Muscular system is the driver of skeletal development. *Annales Nestlé*. **64**:55-61.

Schoenau, E. and Fricke, O. (2008). Mechanical influences on bone development in children. *European Journal of Endocrinology*. **159(1)**:S27-S31.

Schutkowski, H. (1993). Sex determination of infant and juvenile skeletons: 1. Morphognostic features. *American Journal of Physical Anthropology*. **90**:199-205.

Scottish Intercollegiate Guidelines Network (SIGN). (2003). *Management of Osteoporosis*. Guideline No. 71, Edinburgh.

Shapiro, L.G. and Stockman, G.C. (2002). *Computer Vision*. Prentice Hall. New Jersey.

Shen, H., Nutt, S. and Hull, D. (2004). Direct observation and measurement of fiber architecture in short fiber-polymer composite foam through micro-CT imaging. *Composites Science and Technology*. **64(13-14)**:2113-2120.

Shirley, M.M. (1931). *The first two years: A study of 25 babies. Vol. 1. Postural and locomotor development*. Minneapolis: University of Minnesota Press.

Showalter, C., Clymer, B.D., Richmond, B. and Powell, K. (2006). Three-dimensional texture analysis of cancellous bone cores evaluated at clinical CT resolutions. *Osteoporosis International*. **17**:259-266.

Siffert, R.S. and Levy, R.N. (1981). Trabecular patterns and the internal architecture of bone. *The Mount Sinai Journal of Medicine*. **48(3)**:221-229.

Silva, M.J., Wang, C., Keaveny, T.M. and Hayes, W.C. (1994). Direct and computed tomography thickness measurements of the human lumbar vertebral shell and endplate. *Bone*. **15**:409-414.

Simmons, C.A. and Hipp, J.A. (1997). Method-based differences in the automated analysis of the three-dimensional morphology of trabecular bone. *Journal of Bone and Mineral Research*. **12(6)**:942-947.

Simon, S.R. (1994). *Orthopaedic Basic Science, American Academy of Orthopaedic Surgeons*. Ohio.

Skedros, J.G. and Baucom, S.L. (2007). Mathematical analysis of trabecular 'trajectories' in apparent trajectorial structures: The unfortunate historical emphasis on the human proximal femur. *Journal of Theoretical Biology*. **244**:15-45.

Skedros, J.G., Sorenson, S.M., Hunt, K.J. and Holyoak, J.D. (2007). Ontogenetic structural and material variations in ovine calcanei: a model for interpreting bone adaptation. *Anatomical Record (Hoboken)*. **290(3)**:284-300.

Slyper, A.H. (2006). The pubertal timing controversy in the USA, and a review of possible causative factors for the advance in timing of onset of puberty. *Clinical Endocrinology.* **65**:1-8.

Sommerfeldt, D.W. and Rubin, C.T. (2001). Biology of bone and how it orchestrates the form and function of the skeleton. *European Spine Journal*. **10**:86-95.

Sonoda, M., Takano, M., Miyahara, J. and Kato, H. (1983). Computed radiography utilizing scanning laser stimulated luminescence. Radiology. **148**:833-838.

Soutis, M. (2006). Ancient Greek terminology in pediatric surgery: about the word meaning. *Journal of Pediatric Surgery*. **41**:1302-1308.

Spadaro, J.A., Werner, F.W., Brenner, R.A., Fortino, M.D., Fay, L.A. and Edwards, W.T. (1994). Cortical and trabecular bone contribute strength to the osteopenic distal radius. *Journal of Orthopaedic Research*. **12**:211-218.

Spoor, C.F., Zonneveld, F.W. and Macho, G.A. (1993). Linear measurements of cortical bone and dental enamel by computed tomography: Applications and problems. *American Journal of Physical Anthropology*. **91**:469-484.

Stanitski, C.L. (2005). Subsequent orthotic management of developmental dysplasia of the hip. *Journal of Pediatric Orthopedics*. **25(6)**:815-816.

Stauber, M. and Müller, R. (2006). Age-related changes in trabecular bone microstructures: global and local morphometry. *Osteoporosis International*. **17**:616-626.

Stauber, M. and Müller, R. (2008). Microcomputed tomography: a method for the non-destructive evaluation of the three dimensional structure of biological specimens. *Methods in Molecular Biology*. **455**:273-292.

Stedman (2005). *Stedman's Medical Dictionary*. 28th Edition. Lippincott Williams and Wilkins: Baltimore.

Stevenson, P.H. (1924). Age order of epiphyseal union in man. *American Journal of Physical Anthropology*. **7**:53-93.

Straus, W.L. (1929). Studies on primate ilia. *American Journal of Anatomy*. **43**:403-460.

Sturesson, B., Selvik, G. and Uden, A. (1989). Movements of the sacroiliac joints – A roentgen stereophotogrammetric analysis. *Spine* **14**:162-165.

Streeter, G.L. (1949). A review of the histogenesis of cartilage and bone. *Contributions to Embryology*. **33**:211-245.

Sudarsky, L. (1990). Geriatrics: Gait disorders in the elderly. *The New England Journal of Medicine.* **322**(20):1441-1446.

Sun, K. and Liebschner, M.A. (2004). Biomechanics of prophylactic vertebral reinforcement. *Spine*. **29**:1428-1435.

Sundaram, M., Brodeur, A.E., Burdge, R.E., Joyce, P.F., Riaz, M.A. and Poling, E.R. (1978). The clinical value of direct magnification radiography in orthopedics. **3(2)**:85-90.

Sutherland, D.H., Olshen, R., Cooper, L. and Woo, S.L.Y. (1980). The development of mature gait. *The Journal of Bone and Joint Surgery.* **62**:336-353.

Sutherland, D.H. (1997). The development of mature gait. *Gait and Posture*. **6(2)**:163-170.

Swartz, S.M., Parker, A. and Huo, C. (1998). Theoretical and empirical scaling patterns and theoretical homology in bone trabeculae. *Journal of Experimental Biology*. **201**:573-590.

Tanck, E., Homminga, J., van Lenthe, G.H. and Huiskes, R. (2001). Increase in bone volume fraction preceeds architectural adaptation in growing bones. *Bone*. **28**:650-654.

Tanck, E., Hannink, G., Ruimerman, R., Buma, P., Burger, E.H. and Huiskes, R. (2006). Cortical bone development under the growth plate is regulated by mechanical load transfer. *Journal of Anatomy*. **208**:73-79.

Teitelbaum, S. (2000). Bone Resorption by Osteoclasts. *Science.* **289**:1504-1508.

Thelen, E. (1981). Rhythmical behaviour in infancy: An ethological perspective. *Developmental Psychology.* **17**:237-257.

Thelen, E., Fisher, D.M. and Ridley-Johnson, R. (1984). The relationship between physical growth and a newborn reflex. *Infant Behaviour and Development*. **7**:479-493.

Thelen, E., Fisher, D.M. and Ridley-Johnson, R. (2002). The relationship between physical growth and a newborn reflex. *Infant Behaviour and Development*. **25**:72-85.

Thomason, J.J. (1985). The relationship of trabecular architecture to inferred loading patterns in the third metacarpal of the extinct equids *Merychippus* and *Mesohippus*. *Paleobiology*. **11**:323-335.

Thomsen, J.S., Ebbesen, E.N. and Mosekilde, L.I. (2002). Static histomorphometry of human iliac crest and vertebral trabecular bone: a comparative study. *Bone*. **30(1)**:267-274.

Thomsen, J.S., Laib, A., Koller, B., Prohaska, S., Mosekilde, L. and Gowin, W. (2005). Stereological measures of trabecular bone structure: comparison of 3D micro computed

tomography with 2D histological sections in human proximal tibial bone biopsies. *Journal of Microscopy*. **218(2)**:171-179.

Thomson, A. (1899). The sexual differences of the foetal pelvis. *Journal of Anatomy and Physiology*. **33**:359-380.

Tile, M. and Pennal, G.F. (1980). Pelvic disruption: principles of management. *Clinical Orthopaedics and Related Research*. **151**:56-64.

Torrance, A.G., Mosley, J.R., Suswillo, R.F. and Lanyon, L.E. (1994). Noninvasive loading of the rat ulna in vivo induces a strain-related modelling response uncomplicated by trauma or periosteal pressure. *Calcified Tissue International*. **54**:241-247.

Torry, M.R., Schenker, M.L., Martin, H.D., Hogoboom, D. and Philippon, M.J. (2006). Neuromuscular hip biomechanics and pathology in the athlete. *Clinics in Sports Medicine*. **25**:179-197.

Tronzo, R.G. and Okin, E.M. (1975). Anatomic restoration of congenital hip dysplasia in adulthood by total hip displacement. *Clinical Orthopaedics and Related Research*. **106**:94-98.

Trueta, J. (1963). The role of the vessels in osteogenesis. *The Journal of Bone and Joint Surgery*. **45B(2)**:402-418.

Turner, C.H., Akhtar, M.P., Raab, D.M., Kimmel, D.B. and Recker, R.R. (1991). A noninvasive, in vivo model for studying strain adaptive bone remodelling. *Bone*. **12**:73-79.

Turner, C.H. (1992). On Wolff's law of trabecular architecture. *Journal of Biomechanics*. **25**:1-9.

Turner, C.H. (1998). Three rules for bone adaptation to mechanical stimuli. *Bone*. **23(5)**:399-407.

Uchiyama, T., Tanizawa, T., Muramatsu, H., Endo, N., Takahashi, H.E. and Hara, T. (1997). A morphometric comparison of trabecular structure of human ilium between microcomputed tomography and conventional histomorphometry. *Calcified Tissue International*. **61**:493-498.

Ulrich, D., Van Rietbergen, B., Laib, A. and Ruegsegger, P. (1999a). Load transfer analysis of the distal radius from in-vivo high resolution CT-imaging. *Journal of Biomechanics*. **32**:821-828.

Ulrich, D., Van Rietbergen, B., Laib, A. and Ruegsegger, P. (1999b). The ability of three-dimensional structural indices to reflect mechanical aspects of trabecular bone. *Bone*. **25(1)**:55-60.

Väänanen, H.K. and Horton, M. (1995). The osteoclast clear zone is a specialised cell-extracellular matrix adhesion structure. *Journal of Cell Science*. **108(8)**:2729-2732.

Väänanen, H.K., Zhao, H., Mulari, M. and Halleen, J.M. (2000). The cell biology of osteoclast function. *Journal of Cell Science*. **113**:377-381.

Van der Eerden, B.C.J., Karperien, M. and Wit, J.M. (2003). Systemic and local regulation of the growth plate. *Endocrine Reviews*. **24(6)**:782-801.

Van Rietbergen, B., Weinans, H., Huiskes, R. and Odgaard, A. (1995). A new method to determine trabecular bone elastic properties and loading using micromechanical finite-element models. *Journal of Biomechanics*. **28**: p69.

Van Rietbergen, B., Odgaard, A., Kabel, J. and Huiskes, R. (1996). Direct mechanics assessment of mechanical symmetries and properties of trabecular bone architecture. *Journal of Biomechanics*. **29**:1653-1657.

Van Rietbergen, B. (2001). Micro-FE analyses of bone: state of the art. In: Majumdar, S. and Bay, B.K. *Noninvasive Assessment of Trabecular Bone Architecture and the Competence of Bone*. Kluwer Academic/Plenum Publishers: New York.

Verhulst, J. (2003). *Developmental Dynamics in Humans and Other Primates*. New York: Adonis Press.

Vleeming, A., Stoeckart, R. and Volkers, A.C.W. (1990). Relation between form and function in the sacroiliac joint (I): The clinical anatomical aspects. (II): The biomechanical aspects. *Spine*. **15**: 130-132.

Vleeming, A., van Wingerden, J.P., Dijkstra, P.F., Stoeckart, R., Snijders, C. J. and Stijnen, T. (1992). Mobility in the sacroiliac joints in the elderly: a kinematic and radiological study. *Clinical Biomechanics*. **7**:170–176.

Volpato, V. (2008). Morphogenèse de l'endostructure osseuse de l'ilion humain. *Computes Rendus Palevol*. **7**:463-471.

Von Mayer, H.V. (1867). *Die Architectur der Spongiosa*. Reickert und du Bois-Reymond's Archiv: 627.

Wachter, N.J., Augat, P., Krischak, G.D., Sarkar, M.R., Mentzel, M,. Kinzl, L. and Claes, L. (2001). Prediction of strength of cortical bone in vitro by microcomputed tomography. *Clinical Biomechanics*. **16**:252-256.

Walker, J.M. (1991). Musculoskeletal development: a review. *Physical Therapy*. **71(12)**:878-889.

Walker, J.M. (1992). The sacroiliac joint: a critical review. *Physical Therapy*. **72(12)**:903–916.

Wallach, S., Rousseau, G., Martin, l. and Azria, M. (1999). Effects of calcitonin on animal and in vitro models of skeletal metabolism. *Bone*. **25(5)**:509-516.

Ward, F.O. (1838). *Outlines of Human Osteology*. London: Renshaw.

Weaver, D.S. (1980). Sex differences in the ilia of a known sex and age sample of fetal and infant skeletons. *American Journal of Physical Anthropology*. **52**:191-195.

Webb, P.A.O. and Suchey, J.M. (1985). Epiphyseal union of the anterior iliac crest and medial clavicle in a modern sample of American males and females. *American Journal of Physical Anthropology.* **68**:457-466.

Wehrli, F.W., Hwang, S.N. and Song, H.K. (1998). New architectural parameters derived from micro-MRI for the prediction of trabecular bone strength. *Technology and Health Care*. **6**:307-320.

Wehrli, F.W. (2007). Structural and functional assessment of trabecular and cortical bone by micro magnetic resonance imaging. *Journal of Magnetic Resonance Imaging*. **25**:390–409.

Weinbaum, S., Cowin, S.C. and Zeng, Y. (1994). A model for the excitation of osteocytes by mechanical loading-induced bone fluid shear stresses. *Journal of Biomechanics*. **27(3)**:339-360.

Whitehouse, W.J. (1974). The quantitative morphology of anisotropic trabecular bone. *Journal of Microscopy*. **101**:153-168.

Whittle, M.W. (1991). *Gait Analysis: an Introduction*. Oxford: Butterworth-Heinemann.

Whittle, W. (2002). *Gait Analysis an Introduction*. Third Edition. Oxford: Butterworth-Heinemann.

Williams, P.L., Warwick, R., Dyson, M. and Bannister, L.H. (1989). *Gray's Anatomy*. Thirty-seventh edition. Churchill Livingstone: New York.

Wolff, J. (1892). *Das Gesetz der Transformation der Knochen*. Verlag von August Hirschwald, Berlin.

Wolff, J. (1986). *The Law of Bone Remodelling*. Springer-Verlag, Berlin Heidelberg. [Translated by P. Maquet and R. Furlong from the original (1892)].

Wyman, J. (1857). On the cancellated structure of the bones of the human body. *Boston Journal of Natural History*. **6**:125-140.

Zaidi, M., Moonga, B.S. and Abe, E. (2002). Calcitonin and bone formation: a knockout full of surprises. *Journal of Clinical Investigation*. **110(12)**:1769-1771.

Zerwekh, J.E., Ruml, L.A., Gottschalk, F. and Pak, C.Y.C. (1998). The effects of twelve weeks of bed rest on bone histology, biochemical markers of bone turnover, and calcium homeostasis in eleven normal subjects. *Journal of Bone and Mineral Research*. **13**:1594-1601.

APPENDIX 1: Raw specimen data for neonatal trabecular parameters

	BV/TV																						
VOI	1	2	3	4	5	6	7	8	9	10	11	12	13	14	15	16	17	18	19	20	21	22	23
Specimen																							
IP L	39.02957	38.96004	35.29915	34.37944	34.56763	34.29723	37.65927	24.92107	19.93751	28.88197	32.66479	31.30233	23.30635	18.21044	18.46525	39.8473	24.8587	22.97767	29.9359	29.27469	49.36186	43.10384	47.77359
LTH/E R	39.23439	42.12471	35.53971	41.94378	43.88335	39.15941	34.34597	31.22715	26.92258	37.92239	40.05447	36.67574	33.49586	D	21.78403	41.47883	30.65479	33.59988	34.76428	28.99794	51.20395	43.27396	48.75036
LTH/E L	34.02733	41.433	32.72303	35.32771	31.44749	39.32331	35.66323	30.89461	23.49767	34.03259	37.82775	35.1355	31.96698	14.42217	22.45189	38.59864	25.52715	28.8323	31.02883	25.07757	46.32672	40.66707	44.18311
LTH/G R	41.78184	42.28848	44.61557	41.60293	40.92973	32.30802	36.04222	25.79339	16.41432	36.57154	46.10094	35.98877	27.57296	12.83636	14.03946	45.99272	24.53406	27.67932	40.39863	22.37732	39.8185	35.18605	41.73655
LTH/F R	41.7968	48.74873	42.70313	40.50888	39.39992	39.16807	31.16997	33.81773	16.42506	34.93406	45.45575	36.27725	39.86477	16.3935	13.53839	39.3057	25.86932	30.27966	39.53415	27.62462	40.24685	43.21654	51.12673
LTH/F L	40.95919	48.77146	36.88064	40.49211	40.18961	41.80242	33.4548	26.5682	17.90202	37.05558	42.77858	27.46283	34.87087	20.66683	22.01115	40.66806	28.46132	30.79849	25.52446	28.6624	39.87407	44.57267	43.50611
NP1 R	31.59015	38.65927	35.98077	24.0887	26.68645	35.88814	27.77874	25.8038	22.86977	24.38699	39.37657	26.69971	21.34748	18.07185	19.8593	42.30046	18.02243	21.62102	21.62058	25.42098	38.76627	29.09437	42.79871
NP1 L	41.38394	41.39866	32.80949	31.10909	35.87671	34.81567	34.35443	25.69125	17.83278	24.82636	33.97143	32.61808	29.63859	17.5701	18.43594	37.76434	24.34964	28.3718	33.01909	20.77779	47.7916	41.27683	47.13404
NP2 R	30.31126	41.42071	32.13845	28.6603	28.36287	38.92695	39.22676	24.56714	20.0375	31.06961	28.29951	32.89695	D	26.18627	14.90511	44.49809	24.64852	25.21263	29.18384	32.71312	41.88046	46.94057	41.355
NP2 L	36.24032	43.3695	30.86431	31.41274	33.32562	39.80654	32.60312	21.95069	19.8024	28.98173	34.80605	32.78516	28.78367	21.45209	19.97104	32.67074	23.82985	25.61766	30.54879	26.32568	46.59405	42.62449	50.94044
P1 R	36.57835	40.53479	37.90292	33.24444	32.18503	37.92214	36.57835	24.86648	19.86692	34.34551	35.74836	32.1742	32.29591	23.32755	17.3687	44.06284	35.06804	30.83189	23.99566	28.96889	51.15815	44.9976	45.40135
P1 L	41.74926	48.19961	37.26686	29.66393	31.22144	35.85979	36.21753	27.62093	22.19674	38.0363	39.94446	33.75321	32.11372	18.36435	18.74317	40.29715	25.73729	34.78542	26.06466	31.17753	47.44949	38.94604	43.20967
SA/A R	35.14248	37.14385	D	31.01562	34.38685	37.85365	D	25.18644	24.4799	32.0181	34.29149	D	31.9316	18.51353	17.19861	36.81868	24.06679	26.4021	27.80865	26.84258	39.69012	40.37458	40.27409
SA/B R	40.98843	39.10808	47.26269	35.2011	36.42056	40.30021	29.73463	25.54405	15.62246	27.52136	44.65958	29.96516	28.37545	17.96577	13.50637	40.71817	D	D	D	D	D	D	D
SA/B L	35.09606	37.39625	44.21016	30.46422	35.86685	37.96554	38.59605	28.35242	17.14837	25.52244	41.89414	30.49699	27.39696	16.03902	16.86817	41.64983	22.18135	41.16494	36.61909	24.966	46.65688	46.90133	49.1216
SA/D R	35.7063	39.09439	36.10133	24.38763	26.88615	22.03382	31.37773	21.26517	24.43706	18.00693	27.86809	30.79637	33.98411	22.86753	20.73091	47.39683	21.19679	22.97187	28.23934	18.4422	40.58626	28.83544	33.24827
SA/E R	32.89744	39.24952	46.75291	31.90083	37.96709	42.43398	39.26095	26.84004	27.36516	40.11419	46.78091	35.76588	33.01711	20.59312	17.26813	47.80961	24.8933	27.87282	21.92065	32.11803	46.69447	40.56406	37.99133
SA/E L	33.09895	38.44745	39.28476	35.34759	38.06147	31.55183	43.94106	33.05702	32.25397	33.71879	39.24264	32.33416	39.21084	17.4134	23.94633	47.73926	31.38533	33.88644	40.05429	26.88968	48.28005	40.84514	42.99708
SA/F R	35.45133	38.72081	42.39965	32.66386	29.39335	28.94945	29.62052	24.50144	25.02203	20.694	40.93599	38.58349	32.36423	18.50741	13.20886	43.56407	27.46727	24.35314	29.97142	21.45618	24.72748	46.71653	38.26636
SA/F L	32.24183	41.7995	33.8845	35.40301	36.46156	32.40391	32.4431	29.94958	19.76558	31.1449	38.33378	37.52063	37.58501	19.11492	16.63301	40.32404	25.34851	37.81926	35.99432	24.80483	56.27165	36.06213	48.31491
SA/J R	34.87805	35.70908	36.79583	40.47644	34.69267	33.46885	38.02216	26.01881	D	D	39.50183	35.23415	31.4431	D	D	D	D	34.89172	34.89172	D	34.39012	37.60307	41.96571
SA/J L	38.15863	37.60167	33.49845	41.96864	38.29294	35.69461	38.95851	23.58798	23.29344	30.91077	32.36088	34.29712	35.55545	20.24031	17.56202	35.16258	29.04432	28.94309	24.42541	30.10767	40.51619	33.57567	40.81444
SS3 R	44.02801	37.23199	29.54704	27.31981	33.42118	33.66412	27.82938	28.30298	24.03179	29.60667	36.70797	28.4406	30.41752	20.95676	20.46892	42.24121	19.74838	30.17396	31.20458	15.87884	39.03887	42.54629	46.16275
SS3 L	39.25618	45.30954	38.13778	26.39118	30.63235	36.60818	36.98489	25.83755	25.05981	32.70511	34.1626	34.97541	35.20711	21.71227	25.92497	43.32009	29.4333	23.03826	20.83133	16.4	40.21506	33.18552	43.35911
STHB1 R	36.93051	38.50353	35.90468	32.30148	32.88387	34.09555	34.54772	24.79894	21.34917	29.82961	36.76018	34.50798	30.15238	17.3892	21.20807	38.7251	26.53039	28.72834	29.90159	24.81939	40.59896	38.51299	39.95049
STHB1 L	36.41255	36.13736	39.67637	35.00339	33.14637	36.31658	34.44604	24.24717	20.25797	30.85821	35.76546	33.12627	32.08947	17.9276	19.14828	41.59942	27.22648	29.5917	29.53213	28.21697	39.91295	37.10817	41.82247
STHB2 R	34.83759	40.55352	40.63204	31.85297	32.21308	32.89826	32.022	28.38427	18.75152	29.15942	35.58339	29.51749	34.41743	14.80445	21.19899	36.93559	26.39771	29.01347	24.97266	23.42691	39.84252	33.97772	38.17595
STHB2 L	33.15446	32.62745	42.34053	32.74726	34.81784	32.81747	38.48962	28.9564	23.62693	30.27878	32.46617	32.25215	34.31861	20.07865	26.90877	36.69869	29.4635	26.93619	28.56825	25.37219	36.37934	32.38686	43.44582

Full raw data set for each volume of interest within each individual specimen. Bone volume fraction (BV/TV).

	Tb.Th																						
VOI	**1**	**2**	**3**	**4**	**5**	**6**	**7**	**8**	**9**	**10**	**11**	**12**	**13**	**14**	**15**	**16**	**17**	**18**	**19**	**20**	**21**	**22**	**23**
Specimen																							
IP L	0.15976	0.15889	0.17406	0.1819	0.16569	0.14275	0.17765	0.17982	0.168	0.15195	0.14862	0.23939	0.24059	0.23178	0.20212	0.16886	0.18967	0.17137	0.17559	0.16134	0.17674	0.16863	0.17919
LTH/E R	0.14997	0.14238	0.14709	0.15786	0.14185	0.15088	0.15666	0.16769	0.17331	0.13972	0.14387	0.1973	0.23757	D	0.18612	0.15894	0.22844	0.17144	0.16229	0.15207	0.15066	0.14363	0.15834
LTH/E L	0.13839	0.14837	0.14487	0.16353	0.14105	0.14962	0.16605	0.18166	0.16655	0.14406	0.14436	0.2092	0.21167	0.21074	0.18714	0.14069	0.20466	0.16827	0.16222	0.15036	0.1521	0.15293	0.1585
LTH/G R	0.15539	0.16605	0.17714	0.17227	0.15707	0.1431	0.17203	0.16615	0.15307	0.17136	0.16261	0.25149	0.2288	0.2214	0.21047	0.17047	0.16842	0.16562	0.17344	0.16952	0.15833	0.1523	0.15631
LTH/F R	0.15331	0.15163	0.17014	0.16011	0.14587	0.14784	0.16177	0.17341	0.1585	0.14261	0.15977	0.24442	0.24998	0.21021	0.19077	0.17546	0.18161	0.16442	0.18236	0.18484	0.14488	0.15441	0.15858
LTH/F L	0.16712	0.16694	0.17274	0.17169	0.15903	0.15923	0.16045	0.17538	0.16656	0.14815	0.16313	0.22973	0.2132	0.20967	0.17757	0.15651	0.23637	0.16575	0.17144	0.17697	0.14039	0.16955	0.15047
NP1 R	0.14021	0.14526	0.16754	0.19311	0.13219	0.13607	0.14946	0.18773	0.16243	0.12111	0.13998	0.19487	0.19562	0.18913	0.16415	0.14136	0.18603	0.16169	0.16034	0.23326	0.13866	0.13051	0.15098
NP1 L	0.15597	0.1563	0.1523	0.17009	0.15757	0.14008	0.17559	0.18027	0.17266	0.13871	0.15101	0.26194	0.2255	0.21287	0.19235	0.17034	0.18775	0.17985	0.1714	0.15298	0.16814	0.1583	0.17251
NP2 R	0.12984	0.16231	0.16237	0.17573	0.14675	0.17998	0.1966	0.16777	0.16986	0.1843	0.1608	0.2624	D	0.24012	0.1966	0.17829	0.2108	0.16382	0.18971	0.16459	0.16005	0.17767	0.16895
NP2 L	0.15258	0.16025	0.17081	0.17062	0.15945	0.15736	0.18103	0.17757	0.17626	0.14987	0.15357	0.26045	0.2114	0.21342	0.19395	0.16251	0.18481	0.17654	0.1706	0.15976	0.16665	0.15882	0.17683
P1 R	0.18679	0.16404	0.16506	0.16796	0.16131	0.1704	0.18679	0.18575	0.15749	0.16618	0.16218	0.25257	0.22886	0.22565	0.2005	0.16746	0.21581	0.16994	0.16913	0.16476	0.17423	0.1611	0.15061
P1 L	0.1669	0.16986	0.16009	0.16631	0.17099	0.15715	0.17111	0.17418	0.16929	0.15994	0.15408	0.22979	0.19969	0.21584	0.21821	0.15784	0.22155	0.16677	0.17389	0.15924	0.16735	0.15981	0.15974
SA/A R	0.14491	0.14765	D	0.1642	0.14822	0.13405	D	0.15809	0.1565	0.14568	0.14757	D	0.1941	0.17815	0.17049	0.15012	0.21264	0.14475	0.16013	0.17445	0.13345	0.1576	0.14908
SA/B R	0.13832	0.12973	0.17777	0.15252	0.15025	0.15588	0.16408	0.17054	0.1229	0.14159	0.15119	0.20574	0.23348	0.20275	0.20455	0.16051	D	D	D	D	D	D	D
SA/B L	0.1367	0.13892	0.15523	0.18685	0.13903	0.14441	0.18727	0.17258	0.13809	0.13648	0.15759	0.21424	0.23838	0.21895	0.20499	0.15773	0.19697	0.16681	0.16351	0.1622	0.13367	0.15591	0.15214
SA/D R	0.14542	0.14335	0.16021	0.19313	0.14736	0.13621	0.19209	0.19977	0.18597	0.13549	0.13345	0.19059	0.23747	0.26609	0.1424	0.1661	0.24313	0.16537	0.17407	0.23232	0.14625	0.16534	0.18436
SA/E R	0.1219	0.15071	0.16436	0.15074	0.14634	0.14606	0.17235	0.15571	0.17543	0.14579	0.15311	0.20201	0.22357	0.20556	0.18414	0.15564	0.19963	0.15791	0.15778	0.16297	0.16401	0.15055	0.14721
SA/E L	0.13078	0.13993	0.15941	0.16278	0.13658	0.12104	0.16971	0.16204	0.13787	0.14899	0.1374	0.21604	0.21024	0.18342	0.15639	0.15459	0.21437	0.15854	0.14871	0.16463	0.15077	0.14285	0.15218
SA/F R	0.12585	0.12553	0.17473	0.17267	0.12338	0.12023	0.18939	0.18436	0.14907	0.13993	0.14453	0.21985	0.20876	0.22366	0.16742	0.1427	0.21745	0.13371	0.1567	0.16845	0.1386	0.14201	0.13597
SA/F L	0.13859	0.13924	0.15953	0.16833	0.14682	0.13161	0.17352	0.17802	0.13363	0.15336	0.1528	0.2146	0.23781	0.19568	0.18827	0.15982	0.19813	0.17169	0.16218	0.14739	0.14727	0.14657	0.16048
SA/J R	0.14401	0.13904	0.1658	0.16051	0.1454	0.14031	0.17673	0.1714	D	D	0.16123	0.22457	0.21995	D	D	D	D	0.18119	0.18119	D	0.1311	0.1323	0.15578
SA/J L	0.14562	0.13996	0.15446	0.17572	0.14597	0.13717	0.19103	0.17532	0.14018	0.14145	0.13535	0.21089	0.22905	0.16866	0.21409	0.1458	0.22211	0.14765	0.15141	0.1653	0.14241	0.13598	0.149
SS3 R	0.15598	0.14566	0.16336	0.18707	0.13989	0.15102	0.1714	0.1762	0.14082	0.1507	0.1542	0.22369	0.23292	0.20817	0.14606	0.15112	0.19263	0.17218	0.16784	0.151	0.16221	0.16924	0.15133
SS3 L	0.15442	0.15769	0.16611	0.17339	0.157785	0.15815	0.16487	0.1787	0.13064	0.15038	0.15122	0.22865	0.2087	0.21986	0.14441	0.1479	0.20434	0.17204	0.14214	0.17055	0.15468	0.14507	0.16924
STHB1 R	0.1417	0.1439	0.15389	0.16701	0.14056	0.13773	0.16565	0.16498	0.14539	0.14577	0.13621	0.20303	0.19226	0.1934	0.16296	0.14835	0.18478	0.16848	0.16582	0.15721	0.14329	0.14697	0.14885
STHB1 L	0.13838	0.14552	0.14493	0.15615	0.14	0.14584	0.16315	0.16802	0.1531	0.14009	0.15068	0.20112	0.2075	0.18306	0.16788	0.14716	0.18427	0.1532	0.15063	0.15344	0.13992	0.15445	0.15069
STHB2 R	0.13837	0.14962	0.16047	0.16967	0.14844	0.13735	0.17537	0.17712	0.14325	0.14896	0.15103	0.21229	0.20203	0.20156	0.22311	0.15188	0.19197	0.1621	0.15598	0.17157	0.15087	0.15076	0.14752
STHB2 L	0.1313	0.12888	0.15432	0.14782	0.14441	0.13287	0.17798	0.17828	0.16339	0.14995	0.13412	0.22288	0.2252	0.21459	0.2322	0.13855	0.2344	0.19337	0.16462	0.16685	0.13646	0.13675	0.15582

Full raw data set for each volume of interest within each individual specimen. Trabecular thickness (Tb.Th).

	Tb.Sp																						
VOI	1	2	3	4	5	6	7	8	9	10	11	12	13	14	15	16	17	18	19	20	21	22	23
Specimen																							
IP L	0.24326	0.23546	0.28096	0.32051	0.29391	0.2372	0.27718	0.43643	0.42062	0.29139	0.2652	0.47339	0.63533	0.68535	0.62656	0.27949	0.47502	0.4042	0.37087	0.32497	0.21613	0.24013	0.23521
LTH/E R	0.23291	0.20263	0.26517	0.2341	0.19565	0.22989	0.26511	0.29281	0.28551	0.22456	0.21706	0.33744	0.47627	D	0.49389	0.22358	0.49594	0.38197	0.30676	0.3313	0.18879	0.20574	0.21353
LTH/E L	0.24179	0.22092	0.25602	0.26614	0.25499	0.22474	0.26891	0.30872	0.31014	0.24123	0.22745	0.33442	0.3715	0.59584	0.59979	0.21573	0.50322	0.33589	0.29935	0.28479	0.21023	0.24676	0.23213
LTH/G R	0.20669	0.23253	0.23873	0.26835	0.23734	0.24465	0.28006	0.36027	0.39674	0.27112	0.21508	0.47394	0.53008	0.79956	0.69924	0.21815	0.35905	0.34305	0.27322	0.36722	0.23673	0.25615	0.2174
LTH/F R	0.22701	0.18315	0.24394	0.25531	0.23204	0.22397	0.35223	0.33779	0.4259	0.2349	0.21681	0.43462	0.44943	0.71293	0.45835	0.29473	0.38196	0.3763	0.3145	0.37308	0.22486	0.21805	0.19095
LTH/F L	0.23371	0.20882	0.2679	0.26568	0.24318	0.24231	0.31342	0.43223	0.4142	0.26519	0.23172	0.49309	0.39676	0.42095	0.46287	0.25182	0.47334	0.30698	0.34822	0.31967	0.21532	0.23048	0.21644
NP1 R	0.28554	0.24605	0.26436	0.44724	0.32486	0.2346	0.32534	0.52681	0.44267	0.29139	0.19619	0.41968	0.47317	0.68196	0.53131	0.20576	0.54125	0.30209	0.36111	0.42594	0.22211	0.25952	0.22955
NP1 L	0.21476	0.21613	0.26464	0.32666	0.26664	0.23048	0.32278	0.47217	0.48157	0.30759	0.23496	0.49797	0.45078	0.65743	0.60603	0.2713	0.50816	0.37412	0.31991	0.37282	0.19861	0.2302	0.22488
NP2 R	0.25222	0.23445	0.28285	0.33489	0.2983	0.25574	0.31439	0.4271	0.46591	0.32444	0.2933	0.47174	D	0.58524	0.68978	0.23067	0.54887	0.39656	0.38208	0.29445	0.22569	0.2449	0.25647
NP2 L	0.24826	0.20974	0.29796	0.32707	0.28087	0.22139	0.32823	0.48009	0.44284	0.28669	0.23204	0.51271	0.50326	0.59335	0.58103	0.26414	0.50554	0.38007	0.34525	0.31668	0.20071	0.22296	0.21346
P1 R	0.30473	0.22574	0.25849	0.32557	0.29584	0.25662	0.30473	0.39931	0.44739	0.27326	0.25127	0.53679	0.51473	0.43285	0.56158	0.23773	0.466	0.37121	0.39945	0.31621	0.21512	0.2342	0.20063
P1 L	0.2457	0.21414	0.24147	0.32451	0.3184	0.2443	0.28388	0.40049	0.3626	0.26267	0.24506	0.46828	0.45595	0.56052	0.55286	0.23969	0.53015	0.30998	0.41984	0.3187	0.21966	0.24921	0.22491
SA/A R	0.23306	0.21425	D	0.31344	0.25438	0.19856	D	0.35432	0.31786	0.22286	0.2259	D	0.3307	0.41703	0.47661	0.2072	0.49076	0.28693	0.26013	0.31798	0.24596	0.22629	0.23182
SA/B R	0.22177	0.20692	0.21185	0.29629	0.26989	0.21868	0.29115	0.39263	0.41741	0.25536	0.19907	0.4322	0.46843	0.57449	0.46968	0.25456	D	D	D	D	D	D	D
SA/B L	0.2229	0.20307	0.20859	0.30549	0.22167	0.223	0.2624	0.37045	0.32993	0.32154	0.21342	0.42153	0.50241	0.7441	0.60605	0.20954	0.4495	0.2338	0.24933	0.30801	0.16745	0.20284	0.18014
SA/D R	0.22276	0.18972	0.25925	0.43246	0.27989	0.26484	0.33663	0.42913	0.38501	0.353	0.23688	0.37419	0.37464	0.50048	0.36464	0.18118	0.58221	0.38678	0.33	0.5466	0.21864	0.30481	0.30579
SA/E R	0.22011	0.22411	0.21462	0.29789	0.23044	0.20174	0.27843	0.36934	0.31868	0.22142	0.20012	0.3968	0.4267	0.48416	0.4798	0.20179	0.35019	0.33761	0.33768	0.26953	0.22647	0.23849	0.23282
SA/E L	0.20178	0.1919	0.20706	0.2315	0.20092	0.20433	0.21033	0.2646	0.25064	0.25042	0.19344	0.31977	0.30286	0.54789	0.33167	0.19147	0.39938	0.2562	0.21461	0.29497	0.17852	0.21931	0.19937
SA/F R	0.18028	0.18402	0.2194	0.33766	0.24967	0.26062	0.33674	0.38011	0.29816	0.33147	0.19742	0.34808	0.38042	0.48423	0.49741	0.19673	0.43433	0.29153	0.29039	0.35635	0.2533	0.19518	0.19015
SA/F L	0.20991	0.17158	0.22466	0.25751	0.2126	0.21909	0.26297	0.31038	0.31229	0.25884	0.20339	0.3336	0.4197	0.39144	0.50076	0.22475	0.39374	0.25061	0.25137	0.34696	0.16658	0.23255	0.1935
SA/J R	0.20491	0.20037	0.23218	0.23872	0.22885	0.21308	0.25452	0.32972	D	D	0.20534	0.3728	0.36869	D	D	D	D	0.27578	0.27578	D	0.22057	0.2161	0.20071
SA/J L	0.20469	0.19699	0.23262	0.23378	0.20036	0.205	0.28282	0.35364	0.27923	0.23132	0.20995	0.3326	0.41181	0.43571	0.4168	0.20578	0.48167	0.24521	0.29869	0.33723	0.2029	0.23364	0.18903
SS3 R	0.19601	0.20692	0.23579	0.34377	0.22831	0.22953	0.3247	0.36994	0.2864	0.24991	0.22185	0.42372	0.47465	0.52356	0.36386	0.19612	0.53858	0.30116	0.29038	0.37533	0.24624	0.23144	0.21148
SS3 L	0.22457	0.19467	0.25795	0.33019	0.2488	0.21329	0.27104	0.39574	0.27308	0.23313	0.23037	0.43033	0.33664	0.49216	0.45009	0.18766	0.37417	0.39235	0.3265	0.33597	0.2715	0.27666	0.21524
STHB1 R	0.19928	0.20398	0.24	0.3379	0.23179	0.23402	0.26781	0.36683	0.30896	0.24751	0.21599	0.34496	0.39946	0.52372	0.40863	0.195	0.33719	0.30048	0.31007	0.32121	0.2167	0.26192	0.23802
STHB1 L	0.20248	0.20909	0.20119	0.27188	0.23041	0.22887	0.26992	0.38066	0.32033	0.24215	0.21417	0.34576	0.34583	0.41551	0.43248	0.19008	0.42439	0.29452	0.29121	0.26777	0.19877	0.23348	0.21384
STHB2 R	0.23595	0.22135	0.22457	0.3003	0.27571	0.23331	0.30894	0.34269	0.35712	0.30432	0.23305	0.42923	0.45197	0.55553	0.62565	0.24679	0.35211	0.35387	0.36415	0.41455	0.23434	0.27389	0.24919
STHB2 L	0.21777	0.23058	0.24586	0.28023	0.24693	0.2578	0.27485	0.35186	0.35491	0.28666	0.26496	0.415	0.43184	0.49088	0.45226	0.25509	0.42856	0.35367	0.33457	0.32288	0.25377	0.27704	0.22615

Full raw data set for each volume of interest within each individual specimen. Trabecular separation (Tb.Sp).

	Tb.N																						
VOI	1	2	3	4	5	6	7	8	9	10	11	12	13	14	15	16	17	18	19	20	21	22	23
Specimen																							
IP L	2.44294	2.45202	2.02793	1.89001	2.08633	2.40269	2.11991	1.3859	1.18676	1.9008	2.19785	1.30758	0.96872	0.78567	0.9136	2.35977	1.3106	1.34086	1.70487	1.81452	2.7929	2.55608	2.66605
LTH/E R	2.61616	2.95857	2.41621	2.65703	3.0937	2.59547	2.19237	1.86219	1.55342	2.71412	2.78413	1.85885	1.40996	D	1.17041	2.60967	1.34193	1.95988	2.14211	1.90687	3.39865	3.01296	3.07882
LTH/E L	2.45887	2.79249	2.25884	2.16029	2.22955	2.62825	2.14778	1.70072	1.41081	2.36235	2.62029	1.67948	1.51026	0.68435	1.19973	2.74356	1.24728	1.71346	1.91271	1.66784	3.04577	2.65914	2.7876
LTH/G R	2.68886	2.54681	2.51864	2.41498	2.60581	2.25768	2.09517	1.55241	1.07231	2.13425	2.83511	1.43105	1.2051	0.57979	0.66704	2.69795	1.45672	1.67125	2.32926	1.32006	2.51492	2.31029	2.67015
LTH/F R	2.72628	3.21492	2.50987	2.53009	2.70108	2.64932	1.92685	1.95018	1.03631	2.44956	2.84508	1.48423	1.59474	0.77987	0.70969	2.24021	1.42441	1.84163	2.16794	1.49453	2.77802	2.79884	3.22412
LTH/F L	2.4509	2.92152	2.13505	2.35841	2.52713	2.62526	2.085	1.51493	1.07479	2.50114	2.62241	1.19543	1.63556	0.98567	1.23956	2.59849	1.20412	1.8581	1.48883	1.61962	2.84033	2.62887	2.89135
NP1 R	2.25304	2.66138	2.14754	1.24739	2.01883	2.63754	1.85861	1.37448	1.40801	2.01355	2.81307	1.3701	1.09125	0.95555	1.20983	2.99245	0.96881	1.33721	1.34842	1.08982	2.79583	2.2293	2.83468
NP1 L	2.65331	2.64862	2.15423	1.82902	2.27691	2.48535	1.9565	1.42514	1.03283	1.78985	2.24959	1.24525	1.31433	0.8254	0.95848	2.21704	1.29691	1.57756	1.92644	1.35818	2.84239	2.60748	2.73217
NP2 R	2.33449	2.55191	1.97928	1.63097	1.9327	2.16291	1.9953	1.46435	1.17964	1.68582	1.75993	1.25369	D	1.09056	0.75814	2.49586	1.16927	1.53901	1.53837	1.98753	2.61676	2.64208	2.44781
NP2 L	2.37514	2.70639	1.8069	1.84114	2.09003	2.52969	1.80096	1.23615	1.12347	1.93373	2.26643	1.25879	1.36158	1.00516	1.02971	2.01037	1.28944	1.45107	1.79069	1.6478	2.79588	2.68379	2.88082
P1 R	1.9583	2.47105	2.29636	1.97931	1.99523	2.22551	1.9583	1.33869	1.26144	2.0668	2.20422	1.27388	1.41116	1.03381	0.86629	2.63121	1.62491	1.81427	1.4188	1.75828	2.93619	2.79318	3.0144
P1 L	2.5015	2.83761	2.3279	1.78364	1.82592	2.2819	2.11661	1.58574	1.31113	2.3781	2.59251	1.46886	1.60819	0.85083	0.85894	2.55306	1.1617	2.08583	1.49895	1.95789	2.83533	2.43707	2.70507
SA/A R	2.42511	2.51571	D	1.88894	2.31998	2.82377	D	1.59319	1.56423	2.1978	2.32376	D	1.64509	1.0392	1.00879	2.45254	1.13182	1.824	1.73664	1.53869	2.97416	2.56177	2.70144
SA/B R	2.96332	3.0145	2.65861	2.3079	2.42398	2.58537	1.81222	1.49785	1.27115	1.94379	2.95388	1.45646	1.21532	0.8861	0.6603	2.53672	D	D	D	D	D	D	D
SA/B L	2.56739	2.69188	2.84803	1.63043	2.57975	2.629	2.061	1.64282	1.24183	1.87001	2.65846	1.42347	1.14928	0.73256	0.82287	2.64056	1.12613	2.46779	2.2396	1.53922	3.4905	3.0082	3.22877
SA/D R	2.45535	2.72725	2.25342	1.26277	1.82458	1.61767	1.63352	1.0645	1.31402	1.32899	2.08823	1.61582	1.43106	0.85939	1.45582	2.85353	0.87182	1.38916	1.62226	0.79384	2.77505	1.74405	1.80341
SA/E R	2.69877	2.60433	2.84456	2.11629	2.59451	2.90523	2.27796	1.72373	1.55989	2.75146	3.05536	1.77054	1.47679	1.00183	0.93779	3.07181	1.24695	1.76513	1.38934	1.97075	2.84704	2.69431	2.58084
SA/E L	2.53092	2.74771	2.46435	2.17143	2.78678	2.60681	2.58917	2.04011	2.33942	2.26309	2.85605	1.49665	1.86507	0.94939	1.53123	3.08816	1.46406	2.13744	2.6935	1.63336	3.20228	2.85932	2.82536
SA/F R	2.8169	3.08457	2.42659	1.8917	2.3823	2.40784	1.56401	1.32898	1.67852	1.47892	2.83236	1.75503	1.55031	0.82748	0.78897	3.05275	1.26317	1.82128	1.91263	1.27376	1.78403	3.28962	2.81439
SA/F L	2.32647	3.00194	2.12403	2.10318	2.48339	2.46205	1.86975	1.68237	1.47917	2.03078	2.50877	1.74841	1.5805	0.97683	0.88347	2.52309	1.27937	2.20271	2.21943	1.68297	3.82102	2.46046	3.0106
SA/J R	2.42195	2.56834	2.21923	2.52177	2.38608	2.38529	2.15147	1.51802	D	D	2.45009	1.56894	1.42955	D	D	D	D	1.92575	1.92575	D	2.62316	2.84227	2.69386
SA/J L	2.62047	2.68657	2.16876	2.38842	2.62328	2.60224	2.03935	1.34541	1.66164	2.18521	2.39084	1.62629	1.55229	1.20003	0.8203	2.41168	1.30767	1.9602	1.61321	1.82136	2.84503	2.46911	2.73926
SS3 R	2.82263	2.55601	1.8087	1.46044	2.38913	2.22909	1.62366	1.60634	1.70652	1.96461	2.38055	1.27143	1.3059	1.00673	1.40137	2.79521	1.0252	1.75247	1.85913	1.05157	2.09847	2.51397	3.05049
SS3 L	2.5422	2.87339	2.29598	1.52206	1.98766	2.31478	2.24323	1.44588	1.91823	2.17488	2.2591	1.52966	1.687	0.98753	1.79526	2.92896	1.44044	1.33911	1.46553	0.96161	2.44205	2.28753	2.56193
STHB1 R	2.60632	2.67566	2.33312	1.9341	2.3395	2.47546	2.08563	1.50318	1.4684	2.04638	2.69879	1.69965	1.56831	0.89915	1.30142	2.61036	1.43576	1.70514	1.80322	1.57878	2.83329	2.62046	2.68393
STHB1 L	2.63131	2.48337	2.73754	2.24169	2.36754	2.4901	2.11126	1.44309	1.32317	2.20277	2.37362	1.64705	1.54645	0.97933	1.14061	2.82689	1.47756	1.93162	1.96061	1.83892	2.85261	2.40266	2.77537
STHB2 R	2.51765	2.71048	2.53214	1.87736	2.17015	2.39518	1.82593	1.60253	1.30903	1.95756	2.35602	1.39041	1.70355	0.73451	0.95015	2.43183	1.3751	1.78981	1.60104	1.36545	2.64085	2.25372	2.58786
STHB2 L	2.52506	2.53154	2.74368	2.2154	2.41099	2.46986	2.16257	1.62421	1.44605	2.01928	2.42062	1.44705	1.52393	0.93567	1.15886	2.6487	1.25697	1.39296	1.73539	1.52066	2.66596	2.36826	2.78825

Full raw data set for each volume of interest within each individual specimen. Trabecular number (Tb.N)

	SMI																						
VOI	**1**	**2**	**3**	**4**	**5**	**6**	**7**	**8**	**9**	**10**	**11**	**12**	**13**	**14**	**15**	**16**	**17**	**18**	**19**	**20**	**21**	**22**	**23**
Specimen																							
IP L	1.03333	1.16766	1.23857	1.34607	1.30591	1.3359	1.36962	1.89998	1.16581	1.42381	1.28527	1.52258	1.30875	2.04731	1.88245	1.0267	1.20005	1.15944	1.42908	1.81404	1.41781	1.19146	1.4605
LTH/E R	1.00195	1.13828	1.13626	1.06023	1.05109	1.1632	1.87719	1.45934	1.96799	1.58111	1.12824	1.84192	1.42822	D	1.79371	1.53039	1.45752	1.69166	1.55785	1.5421	1.67388	1.16949	1.72813
LTH/E L	1.33425	1.31747	1.6529	1.01583	1.97483	1.44685	1.86703	1.66167	1.98068	1.90842	1.28738	1.08986	1.76822	2.0005	1.71955	0.94676	1.75733	1.51107	1.31692	1.91667	1.14887	1.11525	1.20342
LTH/G R	1.06841	1.18689	1.23936	1.28421	1.30396	1.267	1.13978	1.61486	1.17974	1.30111	1.26594	1.89678	1.17616	2.13218	2.01997	1.20163	1.16866	1.55851	1.04975	1.4529	1.0777	1.14592	1.03466
LTH/F R	1.07661	1.38931	1.21705	1.14643	1.02813	1.12094	1.00803	1.40583	1.63054	1.56852	1.483	1.08691	1.08715	1.83375	2.55134	1.11835	1.50693	1.17352	1.04935	1.46284	1.17118	1.23514	1.7208
LTH/F L	1.18327	1.59143	1.52747	0.7934	1.17732	1.29278	1.02596	1.68631	1.55598	1.10108	1.06902	1.67612	1.53702	2.29859	1.89076	1.20061	1.5427	1.59206	1.77037	1.93542	1.27188	1.04448	1.14149
NP1 R	1.08989	1.01866	0.75011	1.4261	1.55012	1.28996	1.52186	1.98563	1.32669	1.97736	1.66217	1.42549	1.56648	1.28507	1.82596	1.14051	1.39192	1.9788	1.58109	1.71748	1.10452	1.17247	1.14039
NP1 L	1.07425	1.00889	1.25009	1.4514	1.18212	1.28767	1.0729	1.35569	1.43464	1.62962	1.31026	1.60814	0.94288	1.68675	1.88203	1.00671	0.70112	1.74992	1.10283	1.12099	1.28626	1.04028	1.5828
NP2 R	1.46336	1.02618	1.65265	0.75509	1.55747	1.26821	1.21119	1.52686	1.0013	1.91823	1.55523	1.5923	D	1.33591	1.69896	1.16815	0.98728	1.3386	1.79223	1.71448	1.30727	1.55725	1.01055
NP2 L	1.17141	1.0298	1.47935	1.36348	1.42925	1.06174	1.38016	1.77638	1.33486	1.41712	1.30467	1.60365	1.44885	1.52311	1.54526	1.34606	0.6469	1.00096	1.21023	1.52444	1.14394	1.13466	1.81825
P1 R	1.67362	1.4627	1.02346	1.29448	1.74283	1.84865	1.67362	1.31914	1.11554	1.84379	0.9052	1.36269	1.00663	2.08686	2.08573	1.49948	0.5731	1.23077	1.04379	1.1914	1.06523	1.70983	1.40237
P1 L	1.27868	1.59973	1.10487	0.75358	1.50165	1.49448	1.42321	1.92177	1.27892	1.08301	1.14248	1.04604	1.53957	2.10848	2.10813	1.15426	1.11909	1.00781	1.58706	1.35104	1.6968	1.01142	1.39987
SA/A R	1.74863	1.09121	D	1.30271	1.85512	1.84731	D	1.68781	1.59564	1.52658	1.21728	D	1.34193	2.12703	2.10979	1.0887	1.65894	1.67524	1.86562	2.05615	1.14551	1.76593	1.50348
SA/B R	1.04121	1.07905	1.1063	1.4915	1.56629	1.697	1.28671	1.59194	1.57603	1.59556	1.04405	1.22055	1.75814	2.22427	2.52524	1.0336	D	D	D	D	D	D	D
SA/B L	1.55526	1.42943	1.30952	1.64333	1.6279	1.54978	1.09352	1.85045	1.85546	1.02278	1.45051	1.49993	1.86745	2.09986	2.1959	1.5837	1.90966	0.90759	1.88936	1.64213	1.01565	1.11084	1.05251
SA/D R	0.97177	0.95236	0.72881	1.62934	1.6501	1.86423	1.39639	2.10545	1.451	1.87658	1.22274	1.48794	1.59512	2.12865	1.75944	1.69991	1.98736	1.19701	1.62945	2.28163	1.45612	1.72097	1.45328
SA/E R	1.25924	1.07077	1.51209	1.40996	1.08239	1.21278	1.26802	1.52774	1.73179	1.22971	1.47353	1.58261	1.57575	1.66987	2.13195	1.679	1.99654	1.65962	1.72073	1.29287	1.37007	1.22357	1.09041
SA/E L	1.20412	0.9441	1.144	1.32055	1.8668	1.01888	1.88279	1.32238	1.8197	1.94069	1.57348	1.75173	1.16005	2.10687	1.9123	1.01617	1.67093	1.15432	1.56386	1.93489	1.57601	1.25307	1.70672
SA/F R	1.2356	0.6323	0.97391	1.01976	1.09905	0.84094	1.85743	2.01404	1.59255	1.78413	0.74809	1.19862	1.4286	2.48754	2.37428	0.22031	1.8661	1.37526	1.12115	2.0425	1.89726	0.1311	0.81633
SA/F L	1.36196	0.81427	1.37601	1.13107	1.06174	1.07051	1.861	1.68094	1.99295	1.25458	0.95192	1.3086	1.69692	2.36517	2.22699	1.62871	1.89948	1.02937	1.07464	1.40549	1.19273	1.0822	1.1833
SA/J R	1.25824	0.94987	1.11338	1.61701	1.10558	1.20904	1.12814	1.68022	D	D	1.2002	1.45381	1.37976	D	D	D	D	1.43402	1.43402	D	1.25892	1.4365	0.93242
SA/J L	1.62872	0.80379	1.20938	0.71559	1.91188	1.97778	1.15061	2.10427	1.54466	1.35454	1.39929	1.46355	1.32297	1.86819	2.62126	1.23506	1.28655	1.56052	1.64458	1.25514	1.65722	1.79395	1.08411
SS3 R	1.66159	1.04132	1.8601	1.92894	1.12895	1.32589	1.41104	1.29685	1.83254	1.53243	1.07791	1.78943	1.4929	1.98152	1.65729	1.83207	1.90973	1.54087	1.29544	2.2717	1.37456	0.70219	1.51493
SS3 L	0.76868	1.57423	0.38722	1.28892	1.57785	1.32059	0.43537	0.94773	1.38726	1.33258	1.29463	1.5169	1.11001	2.16804	1.01867	1.63433	1.51868	1.54367	1.64248	2.42336	1.20161	0.65876	0.81268
STHB1 R	1.36094	1.16164	1.21221	1.23107	1.41391	1.08614	1.07276	1.79695	1.944	1.55383	1.067	1.6201	1.34751	2.39306	2.18051	1.42321	2.08857	2.03728	1.58718	1.89373	1.55462	1.42409	1.8767
STHB1 L	1.36309	1.34135	1.02032	1.07475	1.21157	1.2691	1.08046	1.86858	1.66406	1.47334	1.54767	1.62978	1.72192	2.37764	2.01031	1.09194	1.41443	1.51848	1.32931	1.84494	1.18953	1.40553	1.7041
STHB2 R	1.19307	1.06458	1.28884	1.24024	1.32373	1.30697	1.22138	1.24633	1.3685	1.50845	1.49594	1.42628	1.24902	2.19557	1.8099	1.05081	1.86927	1.76865	1.6456	1.27142	1.28372	1.29579	1.16823
STHB2 L	1.49037	1.44228	1.53288	1.24904	1.40355	1.33975	1.78354	1.34899	1.44397	1.62788	1.1092	1.75381	1.5969	1.76383	1.8344	1.29591	1.9901	1.27702	1.73024	1.27111	1.32839	1.01695	1.2386

Full raw data set for each volume of interest within each individual specimen. Structural model index (SMI).

	DA																						
VOI	1	2	3	4	5	6	7	8	9	10	11	12	13	14	15	16	17	18	19	20	21	22	23
Specimen																							
IP L	0.99885	0.81969	0.86629	0.76837	0.77202	0.9301	0.66208	0.91875	0.70962	0.92611	0.84853	0.63315	0.60318	0.73119	0.76207	0.71619	0.52676	0.44981	0.4016	0.76254	0.48296	0.76926	0.65726
LTH/E R	0.87135	0.998866	0.74909	0.9741	0.85246	0.86628	0.65407	0.82754	0.70478	0.83377	0.84373	0.71228	0.47473	D	0.75616	0.95458	0.5032	0.49411	0.49642	0.60053	0.5227	0.56925	0.6986
LTH/E L	0.96542	0.93893	0.80293	0.98685	0.91629	0.69948	0.70419	0.89247	0.71827	0.7194	0.96639	0.71578	0.40066	0.7004	0.69285	0.76898	0.3035	0.46697	0.60919	0.59839	0.63963	0.58965	0.6884
LTH/G R	0.97582	0.96571	0.88435	0.94292	0.98084	0.97665	0.75001	0.95455	0.87967	0.94662	0.82545	0.66719	0.54575	0.72398	0.73488	0.77539	0.47126	0.51288	0.53615	0.68453	0.56259	0.62288	0.60565
LTH/F R	0.70851	0.83241	0.71495	0.96188	0.72061	0.88662	0.55959	0.90297	0.85808	0.73961	0.89789	0.69422	0.62401	0.89124	0.81008	0.841	0.52872	0.48366	0.44577	0.77347	0.44106	0.50437	0.56285
LTH/F L	0.79127	0.85882	0.83974	0.99098	0.72815	0.7605	0.63334	0.90496	0.87095	0.84847	0.91388	0.76195	0.56098	0.80845	0.93918	0.7922	0.4812	0.47475	0.40411	0.77825	0.46338	0.56901	0.6081
NP1 R	0.95652	0.8026	0.97383	0.98394	0.71926	0.73385	0.71168	0.71699	0.79239	0.96946	0.85147	0.91891	0.6424	0.58779	0.74936	0.91502	0.54914	0.55844	0.45898	0.59279	0.5425	0.64549	0.62756
NP1 L	0.98812	0.82432	0.93617	0.92538	0.87918	0.86524	0.60505	0.77217	0.69034	0.92162	0.91743	0.7348	0.62456	0.65172	0.7169	0.73085	0.47577	0.47486	0.45777	0.56593	0.59883	0.71828	0.63797
NP2 R	0.92251	0.85311	0.85875	0.87929	0.77569	0.93754	0.60855	0.91401	0.74118	0.81689	0.84516	0.7082	D	0.93302	0.92587	0.97999	0.47323	0.40211	0.60847	0.76156	0.41333	0.85274	0.55688
NP2 L	0.96871	0.70938	0.80999	0.9864	0.78937	0.95993	0.6196	0.99384	0.7194	0.95829	0.80234	0.72327	0.56755	0.88488	0.73519	0.76684	0.41576	0.48802	0.51324	0.58257	0.52901	0.56213	0.537858
P1 R	0.92897	0.86777	0.78115	0.67321	0.83235	0.79064	0.64674	0.95713	0.77532	0.95186	0.91387	0.72604	0.60261	0.83998	0.66734	0.99282	0.47309	0.45292	0.5107	0.55659	0.41343	0.51532	0.38307
P1 L	0.97334	0.98073	0.80484	0.65006	0.94762	0.83323	0.66979	0.89601	0.77441	0.79752	0.76832	0.69581	0.55266	0.83514	0.70661	0.94005	0.44939	0.56356	0.50186	0.61483	0.50618	0.55456	0.53006
SA/A R	0.81771	0.76093	D	0.8569	0.89415	0.77477	D	0.91066	0.81	0.74259	0.85058	D	0.65403	0.78313	0.80992	0.73247	0.56535	0.62898	0.53745	0.69245	0.5483	0.6373	0.57469
SA/B R	0.76713	0.92559	0.70816	0.97347	0.94989	0.95638	0.74093	0.92984	0.70977	0.96538	0.8693	0.75586	0.62179	0.81275	0.83043	0.74781	D	D	D	D	D	D	D
SA/B L	0.77545	0.83353	0.65426	0.8072	0.91924	0.78322	0.70667	0.99736	0.83864	0.94953	0.7376	0.78702	0.67025	0.92974	0.86397	0.91524	0.50667	0.76521	0.51578	0.59307	0.70454	0.75078	0.55417
SA/D R	0.79491	0.80583	0.79775	0.70461	0.99447	0.78389	0.58545	0.7526	0.99666	0.97606	0.77312	0.82875	0.67309	0.95257	0.8216	0.79902	0.51762	0.57902	0.62204	0.68889	0.57722	0.66854	0.6095
SA/E R	0.83799	0.82712	0.79336	0.96977	0.81056	0.95234	0.65006	0.9426	0.92501	0.92481	0.76542	0.69765	0.58136	0.89455	0.92374	0.75501	0.42397	0.54147	0.46898	0.51207	0.47819	0.69148	0.58077
SA/E L	0.87867	0.9364	0.60911	0.93851	0.93106	0.93207	0.68361	0.75452	0.81824	0.84301	0.81827	0.72666	0.53069	0.69123	0.99289	0.77316	0.54627	0.51801	0.57597	0.54621	0.59904	0.6745	0.52916
SA/F R	0.81823	0.84694	0.71543	0.71088	0.86754	0.99488	0.58549	0.54002	0.93327	0.96147	0.94018	0.68293	0.48804	0.74398	0.86576	0.95176	0.51228	0.55959	0.65784	0.70909	0.76395	0.7466	0.51251
SA/F L	0.97793	0.81654	0.76361	0.72994	0.92263	0.86839	0.79535	0.94729	0.73843	0.9708	0.85823	0.69783	0.44076	0.91338	0.74389	0.84562	0.51139	0.67154	0.55687	0.71486	0.74807	0.67395	0.48685
SA/J R	0.89553	0.72902	0.7352	0.79966	0.90363	0.79885	0.82328	0.98255	D	D	0.72612	0.71834	0.52772	D	D	D	D	0.67151	0.55023	D	0.73763	0.70467	0.66617
SA/J L	0.97716	0.93536	0.74223	0.99141	0.98431	0.924	0.8509	0.7122	0.71227	0.86457	0.97129	0.74865	0.73067	0.81295	0.74479	0.97411	0.55457	0.56381	0.59188	0.59038	0.7296	0.69497	0.50482
SS3 R	0.84485	0.88171	0.82569	0.75899	0.96054	0.74963	0.63367	0.83103	0.70182	0.84091	0.96902	0.58062	0.66923	0.77767	0.89005	0.98454	0.54557	0.68623	0.55297	0.65533	0.54054	0.66758	0.5623
SS3 L	0.83393	0.92015	0.87187	0.68787	0.92055	0.9137	0.63644	0.72744	0.78153	0.9362	0.85409	0.68382	0.67819	0.82788	0.88499	0.72389	0.57091	0.56177	0.61979	0.51223	0.64392	0.66852	0.6485
STHB1 R	0.76129	0.97701	0.80812	0.61605	0.96809	0.95156	0.70739	0.88375	0.91809	0.79244	0.71781	0.71968	0.54626	0.81766	0.72349	0.95281	0.47168	0.50208	0.40635	0.58883	0.59685	0.57933	0.47876
STHB1 L	0.75959	0.98503	0.69884	0.70486	0.72415	0.95021	0.66763	0.79772	0.84881	0.90225	0.7244	0.69802	0.46802	0.86847	0.77234	0.72937	0.39652	0.4985	0.4995	0.54574	0.57402	0.66245	0.44338
STHB2 R	0.93309	0.81756	0.81769	0.93285	0.85203	0.75477	0.89716	0.95945	0.82677	0.86481	0.97952	0.76336	0.63479	0.97049	0.98028	0.82168	0.44764	0.46824	0.50462	0.53235	0.50607	0.62281	0.4932
STHB2 L	0.95162	0.82471	0.87484	0.91976	0.8864	0.77421	0.68255	0.78657	0.9174	0.96118	0.94776	0.9135	0.63757	0.87414	0.96701	0.76241	0.44844	0.48027	0.43362	0.599	0.56277	0.56565	0.52003

Full raw data set for each volume of interest within each individual specimen. Degree of anisotropy (DA).

APPENDIX 2: Raw statistical data for neonatal trabecular parameters

	BV/TV																						
	Q statistic	1.67																					
2	Significance	N																					
	Q statistic	0.35	1.31																				
3	Significance	N	N																				
	Q statistic	1.90	3.57	2.23																			
4	Significance	N	N	N																			
	Q statistic	1.40	3.07	1.74	0.50																		
5	Significance	N	N	N	N																		
	Q statistic	0.65	2.32	1.00	1.25	0.75																	
6	Significance	N	N	N	N	N																	
	Q statistic	1.15	2.81	1.49	0.73	0.24	0.50																
7	Significance	N	N	N	N	N	N																
	Q statistic	5.29	6.96	5.59	3.39	3.89	4.64	4.09															
8	Significance	Y	Y	Y	N	Y	Y	Y															
	Q statistic	6.90	8.56	7.19	5.02	5.52	6.26	5.70	1.66														
9	Significance	Y	Y	Y	Y	Y	Y	Y	N														
	Q statistic	3.17	4.83	3.49	1.29	1.78	2.52	2.00	2.08	3.70													
10	Significance	N	Y	N	N	N	N	N	N	N													
	Q statistic	0.26	1.41	0.09	2.16	1.66	0.91	1.41	5.55	7.16	3.43												
11	Significance	N	N	N	N	N	N	N	Y	Y	N												
	Q statistic	2.17	3.83	2.50	0.29	0.78	1.52	1.01	3.07	4.69	0.99	2.43											
12	Significance	N	Y	N	N	N	N	N	N	Y	N	N											
	Q statistic	2.72	4.38	3.04	0.84	1.33	2.07	1.55	2.53	4.15	0.45	2.98	0.54										
13	Significance	N	Y	N	N	N	N	N	N	Y	N	N	N										
	Q statistic	7.55	9.19	7.83	5.69	6.18	6.91	6.36	2.36	0.71	4.38	7.81	5.36	4.82									
14	Significance	Y	Y	Y	Y	Y	Y	Y	N	N	Y	Y	Y	Y									
	Q statistic	7.55	9.21	7.83	5.67	6.16	6.90	6.34	2.31	0.64	4.34	7.81	5.33	4.79	0.07								
15	Significance	Y	Y	Y	Y	Y	Y	Y	N	N	Y	Y	Y	Y	N								
	Q statistic	2.00	0.34	1.64	3.88	3.39	2.65	3.12	7.24	8.82	5.12	1.74	4.13	4.68	9.45	9.46							
16	Significance	N	N	N	Y	N	N	N	Y	Y	Y	N	Y	Y	Y	Y							
	Q statistic	5.44	7.08	5.74	3.58	4.07	4.80	4.26	0.25	1.38	2.28	5.70	3.26	2.73	2.07	2.02	7.36						
17	Significance	Y	Y	Y	N	Y	Y	Y	N	N	N	Y	N	N	N	N	Y						
	Q statistic	4.08	5.74	4.39	2.20	2.70	3.44	2.91	1.16	2.80	0.91	4.34	1.90	1.35	3.48	3.44	6.03	1.39					
18	Significance	Y	Y	Y	N	N	N	N	N	N	N	Y	N	N	N	N	Y	N					
	Q statistic	3.55	5.21	3.87	1.67	2.17	2.91	2.38	1.69	3.32	0.38	3.81	1.37	0.83	4.00	3.96	5.50	1.91	0.53				
19	Significance	N	Y	Y	N	N	N	N	N	N	N	Y	N	N	Y	Y	Y	N	N				
	Q statistic	5.49	7.13	5.79	3.63	4.12	4.85	4.31	0.30	1.34	2.33	5.74	3.31	2.77	2.03	1.97	7.40	0.05	1.43	1.95			
20	Significance	Y	Y	Y	N	Y	Y	Y	N	N	N	Y	N	N	N	N	Y	N	N	N			
	Q statistic	2.23	0.57	1.86	4.11	3.61	2.87	3.35	7.47	9.05	5.35	1.97	4.36	4.90	9.67	9.69	0.23	7.58	6.25	5.73	7.63		
21	Significance	N	N	N	Y	N	N	N	Y	Y	Y	N	Y	Y	Y	Y	N	Y	Y	Y	Y		
	Q statistic	1.11	0.55	0.75	2.99	2.50	1.76	2.24	6.36	7.94	4.24	0.85	3.25	3.80	8.58	8.58	0.09	6.49	5.15	4.62	6.53	1.11	
22	Significance	N	N	N	N	N	N	N	Y	Y	Y	N	N	Y	Y	Y	N	Y	Y	Y	Y	N	
	Q statistic	2.82	1.16	2.44	4.70	4.20	3.46	3.93	8.06	9.63	5.93	2.56	4.94	5.48	10.25	10.27	0.81	8.16	6.84	6.31	8.21	0.58	1.69
23	Significance	N	N	N	Y	Y	N	Y	Y	Y	Y	N	Y	Y	Y	Y	N	Y	Y	Y	Y	N	N
VOI		1	2	3	4	5	6	7	8	9	10	11	12	13	14	15	16	17	18	19	20	21	22

Full statistical data from one way analysis of variance with pairwise multiple comparison procedures for bone volume fraction (BV/TV). Q statistic is representative of the non-parametric distribution of data.

	Tb.Th																						
	Q statistic	0.47																					
2	Significance	N																					
	Q statistic	3.41	2.94																				
3	Significance	N	N																				
	Q statistic	4.77	4.30	1.32																			
4	Significance	Y	Y	N																			
	Q statistic	0.27	0.21	3.15	4.51																		
5	Significance	N	N	N	Y																		
	Q statistic	0.14	0.61	3.55	4.91	0.40																	
6	Significance	N	N	N	Y	N																	
	Q statistic	5.49	5.02	2.06	0.76	5.23	5.63																
7	Significance	Y	Y	N	N	Y	Y																
	Q statistic	5.86	5.39	2.40	1.09	5.60	6.00	0.32															
8	Significance	Y	Y	N	N	Y	Y	N															
	Q statistic	2.12	1.65	1.28	2.61	1.86	2.26	3.34	3.69														
9	Significance	N	N	N	N	N	N	N	N														
	Q statistic	0.23	0.24	3.15	4.50	0.03	0.37	5.21	5.58	1.87													
10	Significance	N	N	N	Y	N	N	Y	Y	N													
	Q statistic	0.70	0.22	2.72	4.08	0.43	0.84	4.80	5.17	1.43	0.46												
11	Significance	N	N	N	Y	N	N	Y	Y	N	N												
	Q statistic	9.01	8.54	5.55	4.28	8.75	9.15	3.49	3.20	6.82	8.70	8.32											
12	Significance	Y	Y	Y	Y	Y	Y	N	N	Y	Y	Y											
	Q statistic	8.98	8.51	5.53	4.25	8.72	9.12	3.46	3.17	6.80	8.67	8.29	0.02										
13	Significance	Y	Y	Y	Y	Y	Y	N	N	Y	Y	Y	N										
	Q statistic	8.32	7.86	4.90	3.64	8.06	8.46	2.86	2.57	6.17	8.02	7.64	0.59	0.57									
14	Significance	Y	Y	Y	N	Y	Y	N	N	Y	Y	Y	N	N									
	Q statistic	6.21	5.74	2.78	1.48	5.95	6.35	0.71	0.40	4.05	5.92	5.52	2.78	2.75	2.16								
15	Significance	Y	Y	N	N	Y	Y	N	N	Y	Y	Y	N	N	N								
	Q statistic	2.13	1.66	1.27	2.61	1.86	2.26	3.33	3.68	0.00	1.88	1.43	6.82	6.80	6.16	4.05							
16	Significance	N	N	N	N	N	N	N	N	N	N	N	Y	Y	Y	Y							
	Q statistic	8.11	7.64	4.69	3.42	7.85	8.25	2.65	2.36	5.95	7.81	7.42	0.81	0.78	0.21	1.94	5.95						
17	Significance	Y	Y	Y	N	Y	Y	N	N	Y	Y	Y	N	N	N	N	Y						
	Q statistic	4.12	3.65	0.71	0.61	3.86	4.26	1.35	1.69	1.98	3.86	3.43	4.84	4.82	4.20	2.07	1.98	3.99					
18	Significance	Y	N	N	N	Y	Y	N	N	N	Y	N	Y	Y	Y	N	N	Y					
	Q statistic	4.02	3.55	0.61	0.71	3.76	4.16	1.46	1.79	1.88	3.76	3.33	4.94	4.92	4.30	2.17	1.88	4.09	0.10				
19	Significance	Y	N	N	N	N	Y	N	N	N	N	N	Y	Y	Y	N	N	Y	N				
	Q statistic	3.98	3.52	0.60	0.70	3.73	4.12	1.44	1.77	1.87	3.72	3.30	4.89	4.87	4.26	2.15	1.86	4.05	0.10	0.00			
20	Significance	Y	N	N	N	N	Y	N	N	N	N	N	Y	Y	Y	N	N	Y	N	N			
	Q statistic	0.94	0.47	2.44	3.79	0.68	1.08	4.50	4.87	1.17	0.71	0.25	7.99	7.97	7.32	5.22	1.17	7.11	3.15	3.05	3.02		
21	Significance	N	N	N	Y	N	N	Y	Y	N	N	N	Y	Y	Y	Y	N	Y	N	N	N		
	Q statistic	1.31	0.84	2.08	3.42	1.05	1.44	4.14	4.50	0.81	1.07	0.62	7.63	7.61	6.97	4.86	0.81	6.76	2.79	2.69	2.67	0.36	
22	Significance	N	N	N	N	N	N	Y	Y	N	N	N	Y	Y	Y	Y	N	Y	N	N	N	N	
	Q statistic	2.25	1.78	1.14	2.48	1.99	2.39	3.21	3.56	0.13	2.00	1.56	6.69	6.67	6.04	3.92	0.13	5.83	1.85	1.75	1.74	1.30	0.94
23	Significance	N	N	N	N	N	N	N	N	N	N	N	Y	Y	Y	Y	N	Y	N	N	N	N	N
VOI		1	2	3	4	5	6	7	8	9	10	11	12	13	14	15	16	17	18	19	20	21	22

Full statistical data from one way analysis of variance with pairwise multiple comparison procedures for trabecular thickness (Tb.Th). Q statistic is representative of the non-parametric distribution of data.

	Tb.Sp																						
	Q statistic	1.17																					
2	Significance	N																					
	Q statistic	1.32	2.47																				
3	Significance	N	N																				
	Q statistic	4.29	5.46	2.94																			
4	Significance	Y	Y	N																			
	Q statistic	1.70	2.86	0.37	2.59																		
5	Significance	N	N	N	N																		
	Q statistic	0.39	1.55	0.93	3.91	1.31																	
6	Significance	N	N	N	Y	N																	
	Q statistic	3.91	5.06	2.57	0.35	2.23	3.53																
7	Significance	Y	Y	N	N	N	N																
	Q statistic	6.77	7.93	5.39	2.48	5.07	6.38	2.80															
8	Significance	Y	Y	Y	N	Y	Y	N															
	Q statistic	6.01	7.16	4.65	1.75	4.32	5.62	2.08	0.70														
9	Significance	Y	Y	Y	N	Y	Y	N	N														
	Q statistic	2.77	3.93	1.44	1.48	1.09	2.39	1.12	3.93	3.20													
10	Significance	N	Y	N	N	N	N	N	Y	N													
	Q statistic	0.14	1.03	1.45	4.43	1.84	0.53	4.05	6.91	6.14	2.91												
11	Significance	N	N	N	Y	N	N	Y	Y	Y	N												
	Q statistic	7.44	8.60	6.07	3.19	5.76	7.06	3.51	0.74	1.43	4.63	7.58											
12	Significance	Y	Y	Y	N	Y	Y	N	N	N	Y	Y											
	Q statistic	7.76	8.91	6.38	3.50	6.07	7.37	3.81	1.05	1.74	4.94	7.89	0.31										
13	Significance	Y	Y	Y	N	Y	Y	Y	N	N	Y	Y	N										
	Q statistic	8.86	9.99	7.50	4.69	7.21	8.48	4.99	2.29	2.95	6.09	8.99	1.55	1.25									
14	Significance	Y	Y	Y	Y	Y	Y	Y	N	N	Y	Y	N	N									
	Q statistic	8.69	9.85	7.31	4.44	7.01	8.31	4..745	1.99	2.67	5.87	8.83	1.24	0.93	0.33								
15	Significance	Y	Y	Y	Y	Y	Y	Y	N	N	Y	Y	N	N	N								
	Q statistic	0.08	1.07	1.38	4.33	1.76	0.46	3.95	6.79	6.03	2.83	0.06	7.46	7.77	8.86	8.70							
16	Significance	N	N	N	Y	N	N	Y	Y	Y	N	N	Y	Y	Y	Y							
	Q statistic	8.10	9.24	6.73	3.88	6.43	7.72	4.19	1.45	2.13	5.30	8.23	0.72	0.41	0.83	0.51	8.10						
17	Significance	Y	Y	Y	Y	Y	Y	Y	N	N	Y	Y	N	N	N	N	Y						
	Q statistic	5.16	6.31	3.81	0.91	3.48	4.78	1.24	1.55	0.84	2.36	5.30	2.27	2.57	3.77	3.50	5.19	2.96					
18	Significance	Y	Y	Y	N	N	Y	N	N	N	N	Y	N	N	Y	N	Y	N					
	Q statistic	4.78	5.94	3.44	0.53	3.10	4.40	0.87	1.92	1.21	1.99	4.92	2.64	2.95	4.41	3.88	4.82	3.33	0.39				
19	Significance	Y	Y	N	N	N	Y	N	N	N	N	Y	N	N	Y	Y	Y	N	N				
	Q statistic	5.54	6.68	4.20	1.33	3.87	5.16	1.65	1.11	0.41	2.77	5.67	1.82	2.13	3.32	3.05	5.57	2.51	0.42	0.79			
20	Significance	Y	Y	Y	N	Y	Y	N	N	N	N	Y	N	N	N	N	Y	N	N	N			
	Q statistic	0.48	0.68	1.78	4.73	2.16	0.86	4.35	7.19	6.43	3.22	0.34	7.85	8.16	9.25	9.09	0.39	8.49	5.59	5.21	5.96		
21	Significance	N	N	N	Y	N	N	Y	Y	Y	N	N	Y	Y	Y	Y	N	Y	Y	Y	Y		
	Q statistic	1.01	2.17	0.30	3.24	0.67	1.08	2.87	5.69	4.95	1.75	1.15	6.37	6.68	7.80	7.61	1.08	7.03	4.11	3.74	4.50	1.48	
22	Significance	N	N	N	N	N	N	N	Y	Y	N	N	Y	Y	Y	Y	N	Y	Y	Y	Y	N	
	Q statistic	0.48	0.68	1.78	4.73	2.16	0.86	4.35	7.19	6.43	3.22	0.34	7.85	8.16	9.25	9.09	0.39	8.49	5.59	5.21	5.96	0.00	1.48
23	Significance	N	N	N	Y	n	N	Y	Y	Y	N	N	Y	Y	Y	Y	N	Y	Y	Y	Y	N	N
VOI		1	2	3	4	5	6	7	8	9	10	11	12	13	14	15	16	17	18	19	20	21	22

Full statistical data from one way analysis of variance with pairwise multiple comparison procedures for trabecular separation (Tb.Sp). Q statistic is representative of the non-parametric distribution of data.

	Tb.N																						
	Q statistic	1.28																					
2	Significance	N																					
	Q statistic	1.29	2.56																				
3	Significance	N	N																				
	Q statistic	3.40	4.68	2.08																			
4	Significance	N	Y	N																			
	Q statistic	1.32	2.60	0.02	2.08																		
5	Significance	N	N	N	N																		
	Q statistic	0.50	1.78	0.79	2.89	0.81																	
6	Significance	N	N	N	N	N																	
	Q statistic	3.29	4.56	1.99	0.07	1.99	2.79																
7	Significance	N	Y	N	N	N	N																
	Q statistic	6.09	7.38	4.75	2.70	4.78	5.59	2.75															
8	Significance	Y	Y	Y	N	Y	Y	N															
	Q statistic	6.82	8.09	5.48	3.45	5.51	6.32	3.49	0.78														
9	Significance	Y	Y	Y	N	Y	Y	N	N														
	Q statistic	2.80	4.07	1.50	0.57	1.49	2.30	0.49	3.24	3.98													
10	Significance	N	Y	N	N	N	N	N	N	Y													
	Q statistic	0.13	1.41	1.16	3.27	1.19	0.38	3.17	5.97	6.69	2.67												
11	Significance	N	N	N	N	N	N	N	Y	Y	N												
	Q statistic	6.35	7.62	5.01	2.98	5.04	5.85	3.03	0.31	0.47	3.52	6.22											
12	Significance	Y	Y	Y	N	Y	Y	N	N	N	N	Y											
	Q statistic	6.49	7.76	5.16	3.13	5.19	5.99	3.17	0.45	0.33	3.66	6.36	0.14										
13	Significance	Y	Y	Y	N	Y	Y	N	N	N	N	Y	N										
	Q statistic	8.91	10.17	7.57	5.58	7.62	8.42	5.60	2.93	2.14	6.08	8.79	2.60	2.46									
14	Significance	Y	Y	Y	Y	Y	Y	Y	N	N	Y	Y	N	N									
	Q statistic	8.43	9.70	7.08	5.06	7.12	7.93	5.09	2.39	1.60	5.58	8.30	2.06	1.92	0.56								
15	Significance	Y	Y	Y	Y	Y	Y	Y	N	N	Y	Y	N	N	N								
	Q statistic	0.62	0.65	1.89	3.98	1.93	1.12	3.88	6.66	7.37	3.39	0.75	6.90	7.05	9.44	8.97							
16	Significance	N	N	N	Y	N	N	Y	Y	Y	N	N	Y	Y	Y	Y							
	Q statistic	7.52	8.78	6.19	4.19	6.23	7.03	4.22	1.54	0.76	4.71	7.40	1.23	1.09	1.36	0.82	8.06						
17	Significance	Y	Y	Y	Y	Y	Y	Y	N	N	Y	Y	N	N	N	N	Y						
	Q statistic	4.72	5.99	3.40	1.36	3.42	4.22	1.42	1.32	2.08	1.90	4.60	1.61	1.75	4.20	3.67	5.29	2.82					
18	Significance	Y	Y	N	N	N	Y	N	N	N	N	Y	N	N	Y	N	Y	N					
	Q statistic	4.40	5.67	3.08	1.03	3.09	3.90	1.10	1.64	2.40	1.58	4.27	1.93	2.07	4.52	4.00	4.97	3.14	0.32				
19	Significance	Y	Y	N	N	N	Y	N	N	N	N	Y	N	N	Y	Y	Y	N	N				
	Q statistic	5.82	7.08	4.51	2.49	4.53	5.33	2.54	0.16	0.92	3.02	5.70	0.46	0.60	3.03	2.51	6.38	1.67	1.14	1.45			
20	Significance	Y	Y	Y	N	Y	Y	N	N	N	N	Y	N	N	N	N	Y	N	N	N			
	Q statistic	1.57	0.30	2.83	4.93	2.87	2.06	4.81	7.60	8.31	4.33	1.69	7.84	7.98	10.37	9.90	0.94	8.99	6.23	5.91	7.31		
21	Significance	N	N	N	Y	N	N	Y	Y	Y	Y	N	Y	Y	Y	Y	N	Y	Y	Y	Y		
	Q statistic	0.29	0.98	1.56	3.65	1.60	0.79	3.55	6.33	7.04	3.06	0.42	6.58	6.72	9.12	8.64	0.33	7.74	4.97	4.65	6.05	1.26	
22	Significance	N	N	N	N	N	N	N	Y	Y	N	N	Y	Y	Y	Y	N	Y	Y	Y	Y	N	
	Q statistic	1.56	0.29	2.82	4.93	2.87	2.06	4.81	7.60	8.30	4.32	1.69	7.84	7.98	10.37	9.90	0.93	8.99	6.23	5.91	7.30	0.00	1.26
23	Significance	N	N	N	Y	N	N	Y	Y	Y	Y	N	Y	Y	Y	Y	N	Y	Y	Y	Y	N	N
VOI		1	2	3	4	5	6	7	8	9	10	11	12	13	14	15	16	17	18	19	20	21	22

Full statistical data from one way analysis of variance with pairwise multiple comparison procedures for trabecular number (Tb.N). Q statistic is representative of the non-parametric distribution of data.

	SMI																						
	t statistic	1.44																					
2	Significance	N																					
	t statistic	0.57	0.86																				
3	Significance	N	N																				
	t statistic	0.25	1.19	0.32																			
4	Significance	N	N	N																			
	t statistic	1.85	3.29	2.40	2.10																		
5	Significance	N	N	N	N																		
	t statistic	1.01	2.45	1.57	1.26	0.84																	
6	Significance	N	N	N	N	N																	
	t statistic	1.02	2.44	13571.00	1.27	0.81	0.02																
7	Significance	N	N	N	N	N	N																
	t statistic	4.53	5.97	5.05	4.78	2.68	3.52	3.47															
8	Significance	Y	Y	Y	Y	N	N	N															
	t statistic	3.44	4.87	3.97	3.69	1.61	2.44	2.40	1.05														
9	Significance	N	Y	Y	Y	N	N	N	N														
	t statistic	3.25	4.68	3.79	3.50	1.42	2.25	2.21	1.23	0.19													
10	Significance	N	Y	Y	N	N	N	N	N	N													
	t statistic	0.13	1.32	0.44	0.13	1.97	1.14	1.14	4.65	3.56	3.38												
11	Significance	N	N	N	N	N	N	N	Y	N	N												
	t statistic	2.83	4.26	3.37	3.09	1.00	1.83	1.80	1.65	0.60	0.41	2.96											
12	Significance	N	Y	N	N	N	N	N	N	N	N	N											
	t statistic	1.92	3.34	2.46	2.17	0.08	0.91	0.89	2.57	1.51	1.33	2.04	0.91										
13	Significance	N	N	N	N	N	N	N	N	N	N	N	N										
	t statistic	9.10	10.52	9.58	9.35	7.29	8.11	8.02	4.66	5.65	5.83	9.23	6.24	7.15									
14	Significance	Y	Y	Y	Y	Y	Y	Y	Y	Y	Y	Y	Y	Y									
	t statistic	8.76	10.19	9.25	9.01	6.93	7.76	7.68	4.28	5.28	5.46	8.89	5.88	6.79	0.42								
15	Significance	Y	Y	Y	Y	Y	Y	Y	Y	Y	Y	Y	Y	Y	N								
	t statistic	0.20	1.23	0.37	0.05	2.03	1.20	1.20	4.68	3.60	3.42	0.07	3.00	2.09	9.22	8.88							
16	Significance	N	N	N	N	N	N	N	Y	N	N	N	N	N	Y	Y							
	t statistic	2.88	4.30	3.41	3.13	1.07	1.89	1.86	1.56	0.52	0.34	3.01	0.08	0.98	6.11	5.74	3.05						
17	Significance	N	Y	N	N	N	N	N	N	N	N	N	N	N	Y	Y	N						
	t statistic	2.02	3.44	2.56	2.27	0.18	1.01	0.99	2.47	1.41	1.23	2.14	0.81	0.99	7.05	6.69	2.19	0.88					
18	Significance	N	N	N	N	N	N	N	N	N	N	N	N	N	Y	Y	N	N					
	t statistic	2.47	3.90	3.01	2.72	0.64	1.47	1.44	2.01	0.96	0.78	2.59	0.36	0.55	6.60	6.24	2.64	0.43	0.54				
19	Significance	N	Y	N	N	N	N	N	N	N	N	N	N	N	Y	Y	N	N	N				
	t statistic	5.01	6.43	5.53	5.26	3.20	4.02	3.97	0.57	1.59	1.78	5.14	2.19	3.09	4.02	3.63	5.16	2.09	2.99	2.54			
20	Significance	Y	Y	Y	Y	N	Y	Y	N	N	N	Y	N	N	Y	N	Y	N	N	N			
	t statistic	0.73	2.15	1.28	0.98	1.11	0.27	0.29	3.76	2.69	2.50	0.85	2.09	1.18	8.31	7.96	0.92	2.14	1.28	1.73	4.25		
21	Significance	N	N	N	N	N	N	N	Y	N	N	N	N	N	Y	Y	N	N	N	N	Y		
	t statistic	0.80	0.63	0.23	0.54	2.63	1.80	1.80	5.28	4.20	4.01	0.67	3.60	2.69	9.80	9.47	0.59	3.64	2.79	3.24	5.75	1.51	
22	Significance	N	N	N	N	N	N	N	Y	Y	Y	N	N	N	Y	Y	N	N	N	N	Y	N	
	t statistic	0.69	2.11	1.24	0.94	1.14	0.31	0.33	3.80	2.73	2.54	0.81	2.13	1.22	8.35	8.00	0.88	2.18	1.32	1.77	4.29	0.04	1.47
23	Significance	N	N	N	N	N	N	N	Y	N	N	N	N	N	Y	Y	N	N	N	N	Y	N	N
VOI		1	2	3	4	5	6	7	8	9	10	11	12	13	14	15	16	17	18	19	20	21	22

Full statistical data from one way analysis of variance with pairwise multiple comparison procedures for structural model index (SMI). t statistic is representative of parametric distribution of data.

	DA																						
	Q statistic	0.35																					
2	Significance	N																					
	Q statistic	2.20	1.86																				
3	Significance	N	N																				
	Q statistic	0.84	0.49	1.37																			
4	Significance	N	N	N																			
	Q statistic	0.29	0.06	1.92	0.55																		
5	Significance	N	N	N	N																		
	Q statistic	0.54	0.20	1.67	0.30	0.26																	
6	Significance	N	N	N	N	N																	
	Q statistic	5.03	4.68	2.80	4.20	4.74	4.49																
7	Significance	Y	Y	N	Y	Y	Y																
	Q statistic	0.57	0.22	1.64	0.27	0.28	0.03	4.46															
8	Significance	N	N	N	N	N	N	Y															
	Q statistic	2.02	1.67	0.19	1.18	1.73	1.48	2.98	1.45														
9	Significance	N	N	N	N	N	N	N	N														
	Q statistic	0.09	0.44	2.27	0.92	0.37	0.63	5.07	0.65	2.09													
10	Significance	N	N	N	N	N	N	Y	N	N													
	Q statistic	0.72	0.37	1.50	0.13	0.43	0.17	4.32	0.15	1.31	0.80												
11	Significance	N	N	N	N	N	N	Y	N	N	N												
	Q statistic	4.00	3.66	1.78	3.17	3.72	3.46	1.02	3.44	1.97	4.06	3.29											
12	Significance	Y	N	N	N	N	N	N	N	N	Y	N											
	Q statistic	7.11	6.76	4.86	6.27	6.82	6.57	2.06	6.54	5.04	7.13	6.40	3.08										
13	Significance	Y	Y	Y	Y	Y	Y	N	Y	Y	Y	Y	N										
	Q statistic	1.61	1.27	0.57	0.78	1.33	1.08	3.34	1.05	0.39	1.68	0.91	2.33	5.38									
14	Significance	N	N	N	N	N	N	N	N	N	N	N	N	Y									
	Q statistic	1.72	1.37	0.48	0.89	1.44	1.18	3.28	1.16	0.30	1.79	1.01	2.26	5.34	0.09								
15	Significance	N	N	N	N	N	N	N	N	N	N	N	N	Y	N								
	Q statistic	1.08	0.74	1.11	0.25	0.80	0.54	3.91	0.52	0.93	1.16	0.37	2.90	5.97	0.53	0.63							
16	Significance	N	N	N	N	N	N	Y	N	N	N	N	N	Y	N	N							
	Q statistic	8.66	8.32	6.42	7.84	8.38	8.13	3.65	8.11	6.61	8.68	7.96	4.66	1.61	6.93	6.90	7.53						
17	Significance	Y	Y	Y	Y	Y	Y	N	Y	Y	Y	Y	Y	N	Y	Y	Y						
	Q statistic	7.92	7.58	5.67	7.09	7.64	7.38	2.87	7.36	5.85	7.94	7.21	3.89	0.81	6.18	6.15	6.78	0.81					
18	Significance	Y	Y	Y	Y	Y	Y	N	Y	Y	Y	Y	Y	N	Y	Y	Y	N					
	Q statistic	8.23	7.89	5.97	7.40	7.95	7.69	3.18	7.67	6.16	8.25	7.52	4.19	1.12	6.49	6.45	7.09	0.51	0.31				
19	Significance	Y	Y	Y	Y	Y	Y	N	Y	Y	Y	Y	Y	N	Y	Y	Y	N	N				
	Q statistic	6.08	5.74	3.87	5.26	5.80	5.55	1.09	5.52	4.05	6.12	5.38	2.10	0.95	4.39	4.34	4.97	2.54	1.75	2.05			
20	Significance	Y	Y	Y	Y	Y	Y	N	Y	Y	Y	Y	N	N	Y	Y	Y	N	N	N			
	Q statistic	7.21	6.87	6.96	6.38	6.93	6.67	2.16	6.65	5.15	7.24	6.50	3.18	0.11	5.49	5.44	6.08	1.51	0.70	1.01	1.05		
21	Significance	Y	Y	Y	Y	Y	Y	N	Y	Y	Y	Y	N	N	Y	Y	Y	N	N	N	N		
	Q statistic	5.81	5.46	3.57	4.97	5.52	5.27	0.77	5.24	3.76	5.84	5.10	1.79	1.29	4.11	4.05	4.68	2.89	2.10	2.40	0.33	1.39	
22	Significance	Y	Y	N	Y	Y	Y	N	Y	Y	Y	Y	N	N	Y	Y	Y	N	N	N	N	N	
	Q statistic	7.45	7.11	5.20	6.62	7.17	6.91	2.40	6.89	5.39	7.47	6.74	3.42	0.34	5.72	5.68	6.31	1.27	0.47	0.77	1.29	0.24	1.63
23	Significance	Y	Y	Y	Y	Y	Y	N	Y	Y	Y	Y	N	N	Y	Y	Y	N	N	N	N	N	N
VOI		1	2	3	4	5	6	7	8	9	10	11	12	13	14	15	16	17	18	19	20	21	22

Full statistical data from one way analysis of variance with pairwise multiple comparison procedures for degree of anisotropy (DA). Q statistic is representative of the non-parametric distribution of data.

APPENDIX 3: Raw cortical bone thickness data

		GLUTEAL THICKNESS (mm)																						
	ROI	1	2	3	4	5	6	7	8	9	10	11	12	13	14	15	16	17	18	19	20	21	22	23
Specimen																								
SS3 Right		0.17	0.16	0.39	1.09	0.61	0.3	0.81	1.38	1.24	0.54	0.18	0.68	1.48	1.35	0.95	0.17	1.92	1.64	1.24	0.76	0.22	0.22	0.22
		0.175	0.17	0.36	1.01	0.59	0.28	0.75	1.19	1.3	0.41	0.17	0.75	1.35	1.31	0.82	0.2	1.69	1.74	1.15	0.73	0.21	0.21	0.21
		0.17	0.17	0.37	1.02	0.58	0.26	0.78	1.32	1.29	0.52	0.17	0.72	1.39	1.3	0.92	0.2	1.73	1.67	1.22	0.73	0.23	0.22	0.22
		0.17	0.17	0.37	1.04	0.59	0.27	0.76	1.36	1.25	0.5	0.17	0.73	1.4	1.3	0.89	0.18	1.76	1.65	1.2	0.72	0.23	0.23	0.22
SS3 Left		0.16	0.17	0.36	0.99	0.62	0.28	0.81	1.36	1.24	0.54	0.18	0.7	1.45	1.3	0.93	0.18	1.87	1.6	1.29	0.74	0.22	0.22	0.22
		0.18	0.18	0.33	0.96	0.62	0.29	0.78	1.14	1.25	0.47	0.18	0.75	1.36	1.26	0.99	0.18	1.63	1.39	1.23	0.72	0.22	0.22	0.22
		0.17	0.18	0.36	1	0.6	0.28	0.78	1.2	1.24	0.48	0.18	0.72	1.4	1.31	0.95	0.18	1.72	1.59	1.24	0.73	0.23	0.23	0.22
		0.18	0.17	0.35	0.95	0.61	0.28	0.79	1.29	1.25	0.5	0.18	0.73	1.39	1.3	0.9	0.17	1.74	1.61	1.26	0.69	0.23	0.22	0.23
STHB1 Right		0.15	0.16	0.36	1.05	0.76	0.26	0.82	1.34	1.24	0.56	0.16	0.7	1.37	1.32	0.73	0.16	1.75	1.45	1.25	0.7	0.21	0.24	0.22
		0.17	0.17	0.36	0.95	0.53	0.26	0.79	1.22	0.93	0.51	0.17	0.69	1.28	1.19	0.76	0.17	1.55	1.27	0.98	0.69	0.22	0.22	0.22
		0.17	0.17	0.35	0.96	0.56	0.27	0.8	1.26	1.1	0.49	0.17	0.7	1.31	1.25	0.8	0.17	1.64	1.49	1.21	0.73	0.22	0.23	0.23
		0.17	0.17	0.36	1.02	0.59	0.26	0.8	1.28	0.98	0.52	0.17	0.71	1.36	1.28	0.79	0.18	1.59	1.52	1.01	0.7	0.22	0.22	0.23
STHB1 Left		0.16	0.16	0.35	0.99	0.78	0.27	0.78	1.38	1.17	0.6	0.16	0.69	1.41	1.32	0.84	0.17	1.75	1.41	1.2	0.65	0.21	0.23	0.22
		0.17	0.17	0.37	0.89	0.62	0.24	0.71	1.25	1.08	0.45	0.17	0.68	1.24	1.22	0.85	0.17	1.69	1.28	1.15	0.68	0.21	0.23	0.23
		0.17	0.17	0.35	0.92	0.69	0.26	0.81	1.29	1.21	0.56	0.16	0.69	1.38	1.31	0.9	0.17	1.58	1.45	1.2	0.67	0.22	0.22	0.23
		0.17	0.17	0.36	0.96	0.64	0.27	0.78	1.32	1.13	0.57	0.17	0.7	1.41	1.32	0.89	0.17	1.7	1.39	1.22	0.69	0.22	0.23	0.23
STHB2 Right		0.16	0.15	0.38	1.03	0.69	0.28	0.78	1.41	1.26	0.62	0.16	0.72	1.4	1.4	0.76	0.18	1.66	1.48	1.32	0.68	0.22	0.22	0.23
		0.17	0.17	0.37	1.01	0.67	0.29	0.79	1.41	1.24	0.6	0.17	0.69	1.39	1.39	0.88	0.17	1.64	1.45	1.33	0.68	0.22	0.23	0.23
		0.17	0.17	0.37	0.99	0.72	0.28	0.82	1.43	1.22	0.58	0.17	0.71	1.4	1.38	0.79	0.17	1.6	1.55	1.35	0.69	0.22	0.23	0.23
		0.17	0.17	0.36	1.03	0.64	0.28	0.79	1.42	1.26	0.57	0.17	0.73	1.38	1.41	0.81	0.17	1.63	1.49	1.36	0.64	0.22	0.22	0.23
STHB2 Left		0.16	0.16	0.35	1.08	0.67	0.27	0.8	1.43	1.24	0.6	0.16	0.72	1.38	1.42	0.75	0.16	1.68	1.45	1.3	0.65	0.22	0.22	0.23
		0.17	0.17	0.36	1.01	0.69	0.28	0.78	1.39	1.24	0.57	0.17	0.68	1.38	1.4	0.8	0.17	1.7	1.5	1.32	0.68	0.22	0.22	0.23
		0.17	0.17	0.34	1.05	0.7	0.28	0.78	1.4	1.22	0.58	0.17	0.68	1.36	1.42	0.82	0.17	1.72	1.48	1.34	0.65	0.22	0.22	0.23
		0.17	0.17	0.35	1	0.7	0.29	0.79	1.42	1.24	0.58	0.17	0.7	1.36	1.46	0.82	0.17	1.76	1.45	1.35	0.66	0.22	0.22	0.23
IP Left		0.16	0.16	0.37	1.01	0.72	0.32	0.77	1.47	1.2	0.58	0.16	0.7	1.47	1.48	0.88	0.17	1.76	1.44	1.36	0.7	0.21	0.2	0.21
		0.17	0.17	0.37	0.99	0.69	0.3	0.76	1.44	1.21	0.58	0.17	0.69	1.43	1.46	0.86	0.17	1.76	1.44	1.34	0.69	0.21	0.22	0.2
		0.17	0.17	0.36	0.98	0.73	0.31	0.77	1.38	1.2	0.57	0.17	0.7	1.4	1.44	0.88	0.18	1.78	1.48	1.32	0.68	0.21	0.22	0.2
		0.17	0.17	0.35	1.04	0.71	0.3	0.79	1.43	1.26	0.58	0.17	0.71	1.36	1.4	0.89	0.17	1.75	1.46	1.3	0.7	0.21	0.22	0.2
LTH/G Right		0.15	0.15	0.35	1.03	0.65	0.28	0.8	1.42	1.3	0.56	0.16	0.69	1.35	1.46	0.89	0.15	1.7	1.6	1.37	0.8	0.21	0.2	0.21
		0.16	0.17	0.35	0.99	0.69	0.29	0.79	1.4	1.29	0.56	0.17	0.71	1.38	1.46	0.9	0.17	1.72	1.54	1.34	0.75	0.21	0.2	0.21
		0.17	0.17	0.33	1.01	0.66	0.3	0.78	1.38	1.3	0.57	0.17	0.68	1.37	1.39	0.92	0.17	1.76	1.56	1.32	0.73	0.21	0.21	0.22
		0.17	0.17	0.36	1.03	0.67	0.29	0.75	1.32	1.28	0.56	0.17	0.68	1.35	1.36	0.88	0.17	1.78	1.52	1.3	0.77	0.21	0.2	0.21
NP4 Right		0.18	0.16	0.36	0.93	0.54	0.29	0.76	1.19	0.93	0.57	0.16	0.66	1.2	1.17	0.7	0.16	1.58	1.41	1.32	0.65	0.21	0.23	0.23
		0.17	0.17	0.37	0.96	0.6	0.29	0.79	1.25	1.19	0.56	0.17	0.65	1.3	1.29	0.76	0.17	1.68	1.4	1.3	0.7	0.21	0.22	0.23
		0.18	0.17	0.38	0.99	0.59	0.28	0.78	1.26	1.18	0.56	0.17	0.65	1.32	1.3	0.78	0.17	1.65	1.45	1.3	0.68	0.21	0.22	0.23
		0.18	0.17	0.37	1	0.61	0.29	0.76	1.22	1.2	0.55	0.17	0.68	1.35	1.25	0.78	0.17	1.64	1.45	1.32	0.66	0.21	0.22	0.23
NP4 Left		0.17	0.16	0.36	0.9	0.48	0.3	0.72	1.26	0.96	0.51	0.18	0.67	1.16	1.17	0.8	0.17	1.48	1.45	1.36	0.71	0.21	0.2	0.22
		0.18	0.18	0.35	0.96	0.55	0.29	0.75	1.22	1.1	0.54	0.17	0.68	1.38	1.25	0.8	0.17	1.58	1.48	1.36	0.7	0.21	0.22	0.23
		0.18	0.18	0.37	0.93	0.54	0.3	0.74	1.27	1.08	0.56	0.18	0.65	1.34	1.32	0.78	0.17	1.55	1.49	1.34	0.71	0.21	0.22	0.22
		0.18	0.18	0.36	0.99	0.51	0.3	0.79	1.3	1.05	0.54	0.18	0.68	1.33	1.29	0.76	0.17	1.56	1.47	1.34	0.69	0.21	0.22	0.22

		GLUTEAL THICKNESS (mm)																						
	ROI	1	2	3	4	5	6	7	8	9	10	11	12	13	14	15	16	17	18	19	20	21	22	23
Specimen																								
LTH/E Right		0.18	0.16	0.36	1.05	0.61	0.31	0.76	1.48	1.08	0.58	0.18	0.68	1.41	1.43	0.79	0.17	1.83	1.48	1.18	0.79	0.21	0.22	0.22
		0.18	0.18	0.36	1.02	0.63	0.3	0.79	1.46	1.05	0.56	0.18	0.69	1.4	1.36	0.83	0.17	1.8	1.46	1.2	0.75	0.22	0.22	0.22
		0.18	0.18	0.39	1.02	0.65	0.3	0.78	1.4	1.01	0.55	0.18	0.69	1.42	1.34	0.85	0.17	1.76	1.42	1.26	0.74	0.22	0.22	0.22
		0.18	0.18	0.38	1.04	0.67	0.3	0.76	1.39	1.1	0.56	0.17	0.64	1.39	1.32	0.81	0.17	1.73	1.44	1.28	0.72	0.22	0.22	0.22
LTH/E Left		0.18	0.18	D	D	0.68	0.32	D	1.42	1.15	0.58	0.18	0.62	1.43	1.42	0.7	0.18	1.88	1.45	1.22	0.76	0.21	0.21	0.2
		0.18	0.18	D	D	0.7	0.3	D	1.4	1.21	0.57	0.18	0.65	1.38	1.4	0.76	0.18	1.76	1.44	1.3	0.76	0.22	0.21	0.22
		0.18	0.18	D	D	0.69	0.31	D	1.38	1.19	0.56	0.18	0.66	1.4	1.39	0.78	0.18	1.74	1.5	1.28	0.75	0.22	0.21	0.22
		0.18	0.18	D	D	0.73	0.3	D	1.39	1.21	0.58	0.18	0.67	1.46	1.45	0.78	0.18	1.78	1.51	1.26	0.75	0.22	0.21	0.22
NP2 Right		0.17	0.18	0.36	1.01	0.72	0.29	0.8	1.41	1.27	0.55	0.18	0.68	1.45	1.47	0.72	0.18	1.86	1.55	1.22	0.66	0.21	0.21	0.22
		0.18	0.18	0.36	1.06	0.71	0.29	0.79	1.4	1.23	0.56	0.17	0.67	1.46	1.45	0.78	0.18	1.78	1.46	1.26	0.7	0.21	0.21	0.21
		0.18	0.18	0.38	1.03	0.74	0.3	0.78	1.38	1.26	0.56	0.18	0.68	1.46	1.45	0.8	0.18	1.79	1.48	1.28	0.65	0.22	0.22	0.22
		0.18	0.18	0.35	1.01	0.72	0.3	0.8	1.37	1.18	0.58	0.18	0.69	1.44	1.46	0.76	0.18	1.76	1.45	1.3	0.68	0.21	0.21	0.21
NP2 Left		0.17	0.18	0.38	1.08	0.75	0.28	0.8	1.46	1.19	0.68	0.18	0.7	1.5	1.48	0.73	0.18	1.87	1.57	1.18	0.68	0.19	0.2	0.21
		0.18	0.18	0.39	1.12	0.72	0.3	0.79	1.41	1.19	0.61	0.18	0.69	1.48	1.46	0.79	0.18	1.77	1.5	1.26	0.68	0.21	0.21	0.21
		0.18	0.18	0.38	1.11	0.73	0.3	0.81	1.38	1.18	0.63	0.18	0.68	1.47	1.45	0.76	0.18	1.78	1.49	1.3	0.66	0.22	0.22	0.22
		0.18	0.18	0.39	1.05	0.75	0.31	0.82	1.45	1.25	0.66	0.18	0.66	1.48	1.43	0.75	0.18	1.8	1.47	1.3	0.69	0.21	0.21	0.21
LTH/F Right		0.19	0.19	0.49	1.25	0.8	0.38	0.87	1.76	1.35	0.74	0.19	0.8	1.54	1.7	1.06	0.19	1.98	1.73	1.51	0.97	0.21	0.21	0.21
		0.19	0.18	0.5	1.15	0.79	0.35	0.82	1.7	1.3	0.69	0.18	0.69	1.56	1.61	1.1	0.18	2.01	1.68	1.45	0.9	0.21	0.21	0.21
		0.18	0.18	0.47	1.19	0.78	0.36	0.84	1.68	1.29	0.7	0.18	0.72	1.55	1.58	1.09	0.18	2.11	1.68	1.48	0.95	0.22	0.22	0.22
		0.18	0.18	0.48	1.06	0.8	0.32	0.86	1.71	1.35	0.68	0.18	0.74	1.54	1.63	1.11	0.18	1.98	1.69	1.45	0.95	0.21	0.21	0.21
LTH/F Left		0.19	0.19	0.48	1.19	0.83	0.38	0.91	1.81	1.41	0.68	0.19	0.76	1.49	1.58	1.14	0.19	2.1	1.66	1.57	1	0.21	0.21	0.21
		0.19	0.18	0.49	1.3	0.81	0.36	0.84	1.75	1.35	0.65	0.18	0.73	1.38	1.55	1.11	0.18	1.96	1.64	1.52	0.98	0.22	0.21	0.21
		0.18	0.18	0.46	1.12	0.8	0.36	0.85	1.72	1.32	0.66	0.19	0.71	1.39	1.52	1.05	0.18	2.03	1.64	1.48	0.98	0.22	0.22	0.22
		0.18	0.18	0.43	1.21	0.85	0.38	0.85	1.8	1.31	0.67	0.18	0.74	1.4	1.5	1.13	0.18	2.13	1.62	1.54	0.97	0.22	0.21	0.22
SA/A Right		0.2	0.2	D	1.56	0.9	0.39	D	1.97	1.3	0.68	0.2	0.76	1.44	1.69	1.09	0.2	2.36	1.86	1.41	1.29	0.25	0.24	0.24
		0.19	0.18	D	1.28	0.86	0.34	D	1.83	1.35	0.67	0.19	0.75	1.38	1.63	1.1	0.19	2.16	1.8	1.46	1.05	0.25	0.24	0.25
		0.18	0.18	D	1.32	0.82	0.36	D	1.85	1.3	0.67	0.18	0.74	1.39	1.64	1.05	0.19	2.19	1.78	1.48	1.1	0.25	0.24	0.25
		0.19	0.18	D	1.19	0.88	0.36	D	1.79	1.3	0.68	0.19	0.73	1.45	1.69	1.15	0.19	2.06	1.8	1.48	1.12	0.25	0.24	0.25
SA/E Right		0.19	0.19	0.42	1.11	0.82	0.39	0.84	1.68	1.53	0.78	0.2	0.72	1.48	1.6	0.93	0.21	2.09	1.79	1.61	1.27	0.26	0.26	0.27
		0.19	0.18	0.4	1.19	0.81	0.38	0.83	1.76	1.4	0.7	0.19	0.74	1.46	1.54	1.01	0.2	2.04	1.8	1.56	1.15	0.25	0.25	0.25
		0.19	0.18	0.39	1.22	0.79	0.37	0.83	1.75	1.48	0.73	0.19	0.74	1.44	1.59	0.99	0.21	2.01	1.74	1.56	1.2	0.25	0.25	0.25
		0.19	0.18	0.42	1.15	0.82	0.39	0.86	1.71	1.49	0.72	0.19	0.74	1.45	1.58	0.98	0.2	1.99	1.75	1.54	1.18	0.25	0.25	0.25
SA/E Left		0.2	0.2	0.45	1.12	0.91	0.4	0.91	1.8	1.42	0.79	0.2	0.8	1.52	1.65	1.19	0.21	2.15	1.83	1.82	1.31	0.26	0.26	0.26
		0.19	0.19	0.42	1.15	0.85	0.36	0.84	1.79	1.4	0.78	0.19	0.78	1.48	1.6	1.15	0.2	2.04	1.83	1.72	1.23	0.25	0.25	0.25
		0.18	0.19	0.41	1.08	0.84	0.39	0.86	1.76	1.38	0.74	0.19	0.76	1.59	1.58	1.15	0.2	2.14	1.83	1.74	1.25	0.25	0.25	0.25
		0.19	0.19	0.4	1.23	0.82	0.39	0.88	1.79	1.39	0.76	0.2	0.75	1.56	1.54	1.05	0.21	2.01	1.78	1.76	1.26	0.25	0.25	0.25
NP1 Right		0.19	0.19	0.4	1.27	0.84	0.42	0.92	1.8	1.37	0.69	0.2	0.78	1.58	1.7	1.02	0.2	2.03	1.88	1.6	1.15	0.28	0.26	0.28
		0.19	0.18	0.39	1.21	0.8	0.38	0.89	1.69	1.4	0.72	0.2	0.76	1.58	1.67	1.05	0.2	2.06	1.82	1.55	1.21	0.26	0.26	0.26
		0.19	0.19	0.38	1.2	0.79	0.38	0.9	1.78	1.39	0.72	0.19	0.76	1.54	1.64	1.1	0.19	1.99	1.78	1.6	1.18	0.26	0.26	0.26
		0.18	0.19	0.37	1.18	0.8	0.39	0.86	1.76	1.35	0.7	0.19	0.77	1.52	1.69	1.08	0.2	2	1.82	1.6	1.17	0.26	0.26	0.26

		GLUTEAL THICKNESS (mm)																						
	ROI	1	2	3	4	5	6	7	8	9	10	11	12	13	14	15	16	17	18	19	20	21	22	23
Specimen																								
NP1 Left		0.21	0.2	0.4	1.15	0.81	0.41	0.88	1.74	1.38	0.68	0.2	0.8	1.6	1.65	1.01	0.2	2.1	1.9	1.63	1.1	0.27	0.26	0.27
		0.19	0.19	0.39	1.18	0.83	0.4	0.88	1.76	1.36	0.7	0.19	0.77	1.58	1.6	1.04	0.2	2.05	1.88	1.63	1.18	0.26	0.26	0.26
		0.2	0.2	0.4	1.12	0.78	0.38	0.89	1.79	1.37	0.73	0.19	0.76	1.56	1.59	1.04	0.19	2.16	1.85	1.6	1.2	0.26	0.26	0.26
		0.19	0.2	0.4	1.28	0.79	0.38	0.9	1.8	1.38	0.72	0.2	0.76	1.57	1.63	1.09	0.2	2.03	1.88	1.65	1.22	0.26	0.26	0.26
SA/F Right		0.2	0.2	0.4	1.15	0.93	0.37	0.98	1.85	1.39	0.75	0.21	0.79	1.49	1.73	1.24	0.2	2.03	1.88	1.64	1.24	0.25	0.26	0.26
		0.19	0.2	0.38	1.25	0.86	0.34	0.94	1.8	1.4	0.72	0.2	0.78	1.48	1.69	1.12	0.2	1.99	1.84	1.6	1.25	0.26	0.26	0.26
		0.19	0.19	0.39	1.24	0.84	0.36	0.96	1.79	1.4	0.73	0.19	0.79	1.48	1.67	1.2	0.19	1.89	1.83	1.58	1.2	0.26	0.26	0.26
		0.19	0.19	0.4	1.19	0.83	0.38	0.99	1.78	1.41	0.73	0.19	0.8	1.46	1.65	1.18	0.2	2.03	1.8	1.6	1.18	0.26	0.26	0.26
SA/F Left		0.19	0.19	0.43	1.1	0.91	0.4	1	1.78	1.43	0.72	0.2	0.81	1.48	1.75	1.2	0.2	2.11	1.8	1.68	1.2	0.24	0.26	0.26
		0.18	0.19	0.42	1.13	0.79	0.38	0.89	1.78	1.39	0.73	0.19	0.79	1.48	1.7	1.2	0.2	2.05	1.78	1.65	1.18	0.26	0.26	0.26
		0.19	0.19	0.4	1.24	0.84	0.39	0.93	1.8	1.41	0.72	0.2	0.74	1.44	1.72	1.17	0.19	1.96	1.76	1.58	1.18	0.26	0.26	0.26
		0.19	0.19	0.39	1.26	0.85	0.38	0.95	1.85	1.42	0.7	0.2	0.75	1.46	1.72	1.19	0.2	2.03	1.72	1.62	1.25	0.26	0.26	0.26
SA/J Right		0.21	0.21	0.41	1.2	0.96	0.4	1	1.97	1.4	0.78	0.21	0.8	1.53	1.75	1.17	0.21	2.13	1.78	1.66	1.23	0.26	0.26	0.26
		0.2	0.2	0.38	1.25	0.86	0.38	0.97	1.9	1.4	0.74	0.2	0.78	1.55	1.65	1.17	0.2	1.97	1.82	1.64	1.2	0.26	0.26	0.26
		0.2	0.2	0.37	1.23	0.9	0.38	0.96	1.92	1.38	0.76	0.19	0.78	1.54	1.64	1.2	0.21	2.05	1.84	1.6	1.19	0.26	0.26	0.26
		0.19	0.2	0.39	1.24	0.89	0.37	0.99	1.93	1.37	0.75	0.19	0.76	1.5	1.63	1.2	0.2	2.01	1.78	1.62	1.18	0.26	0.26	0.26
SA/J Left		0.2	0.2	0.42	1.25	0.93	0.41	1.01	1.99	1.36	0.75	0.2	0.78	1.54	1.78	1.2	0.2	2.04	1.8	1.61	1.2	0.25	0.28	0.26
		0.19	0.19	0.4	1.17	0.89	0.39	0.98	1.85	1.39	0.72	0.19	0.76	1.5	1.7	1.18	0.19	2.01	1.8	1.65	1.18	0.26	0.27	0.26
		0.19	0.19	0.41	1.2	0.88	0.39	0.96	1.79	1.36	0.7	0.19	0.73	1.52	1.72	1.18	0.2	1.99	1.83	1.64	1.18	0.27	0.27	0.27
		0.19	0.19	0.39	1.21	0.88	0.34	0.97	1.89	1.36	0.75	0.2	0.76	1.54	1.68	1.2	0.2	1.96	1.84	1.64	1.23	0.27	0.27	0.27
P1 Right		0.21	0.24	0.42	1.1	0.95	0.52	0.87	1.95	1.41	0.64	0.2	0.72	1.6	1.65	1.15	0.24	2.22	1.86	1.69	1.19	0.28	0.27	0.28
		0.2	0.21	0.39	1.18	0.89	0.4	0.89	1.89	1.41	0.7	0.2	0.74	1.58	1.68	1.15	0.22	2.1	1.84	1.65	1.2	0.26	0.27	0.27
		0.19	0.2	0.4	1.12	0.9	0.42	0.88	1.9	1.4	0.69	0.2	0.72	1.56	1.7	1.2	0.23	2.08	1.82	1.62	1.2	0.27	0.28	0.27
		0.19	0.2	0.42	1.13	0.88	0.43	0.87	1.91	1.38	0.68	0.1	0.72	1.58	1.67	1.2	0.22	2.13	1.86	1.65	1.18	0.27	0.27	0.28
P1 Left		0.2	0.24	0.41	1.11	1	0.41	0.85	1.82	1.44	0.62	0.19	0.76	1.61	1.74	1.08	0.23	1.9	1.94	1.54	1.17	0.29	0.24	0.27
		0.19	0.2	0.39	1.3	0.86	0.4	0.86	1.8	1.4	0.64	0.19	0.78	1.58	1.68	1.15	0.22	1.91	1.9	1.58	1.15	0.28	0.25	0.26
		0.19	0.2	0.39	1.49	0.83	0.4	0.85	1.85	1.42	0.66	0.19	0.76	1.56	1.66	1.15	0.22	1.95	1.86	1.58	1.15	0.28	0.26	0.28
		0.19	0.19	0.38	1.26	0.87	0.39	0.84	1.84	1.4	0.69	0.2	0.76	1.58	1.62	1.16	0.23	1.98	1.8	1.56	1.12	0.28	0.25	0.28
SA/B Right		0.26	0.22	0.42	1.11	0.86	0.4	0.89	2.01	1.41	0.72	0.22	0.78	1.48	1.77	1.2	0.22	2.1	D	D	D	D	D	D
		0.2	0.19	0.41	1.25	0.83	0.39	0.88	1.94	1.4	0.7	0.21	0.78	1.5	1.6	1.2	0.22	2.05	D	D	D	D	D	D
		0.2	0.19	0.4	1.24	0.8	0.41	0.87	1.91	1.39	0.72	0.2	0.76	1.47	1.68	1.18	0.23	2.07	D	D	D	D	D	D
		0.19	0.19	0.4	1.18	0.89	0.36	0.88	1.89	1.38	0.73	0.19	0.76	1.48	1.74	1.2	0.22	1.99	D	D	D	D	D	D
SA/B Left		0.24	0.22	0.41	1.31	0.83	0.41	0.89	2.05	1.37	0.68	0.21	0.8	1.46	1.8	1.16	0.21	2.09	1.99	1.6	1.16	0.28	0.27	0.26
		0.2	0.19	0.4	1.28	0.85	0.41	0.89	1.95	1.38	0.7	0.2	0.75	1.48	1.76	1.16	0.22	2.01	1.85	1.62	1.05	0.27	0.27	0.27
		0.2	0.19	0.38	1.25	0.84	0.39	0.85	1.95	1.38	0.76	0.19	0.76	1.46	1.75	1.15	0.22	1.96	1.82	1.6	1.1	0.28	0.27	0.27
		0.2	0.2	0.39	1.31	0.8	0.4	0.88	1.96	1.4	0.75	0.2	0.78	1.48	1.78	1.16	0.22	1.94	1.89	1.6	1.1	0.28	0.28	0.28
SA/D Right		0.21	0.19	0.41	1.16	0.83	0.42	0.85	1.61	1.44	0.66	0.21	0.73	1.56	1.5	1.13	0.21	1.97	1.66	1.54	0.9	0.29	0.26	0.29
		0.2	0.2	0.38	1.2	0.86	0.4	0.86	1.8	1.42	0.7	0.2	0.7	1.5	1.68	1.2	0.22	1.95	1.72	1.6	0.97	0.28	0.27	0.28
		0.2	0.19	0.38	1.19	0.81	0.41	0.86	1.79	1.4	0.73	0.19	0.71	1.49	1.72	1.19	0.21	2	1.74	1.6	0.95	0.28	0.28	0.28
		0.2	0.19	0.38	1.38	0.8	0.42	0.86	1.75	1.39	0.72	0.19	0.73	1.52	1.78	1.2	0.22	1.98	1.7	1.59	0.9	0.28	0.27	0.28

		PELVIC THICKNESS (mm)																						
	ROI	1	2	3	4	5	6	7	8	9	10	11	12	13	14	15	16	17	18	19	20	21	22	23
Specimen																								
SS3 Right		0.17	0.18	0.25	0.32	0.24	0.2	0.27	0.25	0.4	0.27	0.17	0.31	0.34	0.7	0.46	0.18	0.88	0.75	0.76	0.38	0.24	0.24	0.24
		0.175	0.17	0.22	0.28	0.22	0.17	0.24	0.29	0.41	0.26	0.17	0.27	0.38	0.73	0.41	0.18	0.75	0.72	0.7	0.34	0.22	0.22	0.22
		0.17	0.17	0.2	0.29	0.24	0.18	0.27	0.24	0.38	0.31	0.18	0.27	0.35	0.68	0.45	0.18	0.85	0.75	0.68	0.41	0.24	0.22	0.23
		0.17	0.17	0.23	0.3	0.23	0.18	0.26	0.25	0.4	0.28	0.17	0.28	0.36	0.69	0.42	0.17	0.82	0.7	0.72	0.37	0.22	0.23	0.23
SS3 Left		0.17	0.18	0.25	0.34	0.24	0.2	0.27	0.25	0.39	0.27	0.18	0.32	0.33	0.71	0.45	0.18	0.87	0.77	0.74	0.37	0.23	0.23	0.24
		0.18	0.18	0.21	0.3	0.23	0.25	0.25	0.28	0.39	0.27	0.18	0.35	0.34	0.73	0.43	0.17	0.75	0.75	0.65	0.4	0.24	0.22	0.23
		0.17	0.18	0.23	0.3	0.22	0.2	0.26	0.28	0.4	0.28	0.17	0.31	0.36	0.7	0.42	0.17	0.8	0.73	0.68	0.36	0.22	0.22	0.23
		0.17	0.17	0.24	0.32	0.23	0.2	0.25	0.29	0.39	0.27	0.18	0.3	0.35	0.69	0.42	0.18	0.81	0.75	0.7	0.38	0.23	0.23	0.23
STHB1 Right		0.18	0.16	0.24	0.3	0.23	0.22	0.27	0.23	0.38	0.28	0.18	0.33	0.35	0.67	0.46	0.18	0.91	0.71	0.75	0.32	0.25	0.26	0.26
		0.17	0.17	0.24	0.28	0.26	0.2	0.27	0.23	0.4	0.3	0.17	0.31	0.28	0.62	0.5	0.17	0.96	0.67	0.7	0.37	0.24	0.25	0.25
		0.17	0.17	0.23	0.29	0.26	0.2	0.26	0.28	0.4	0.28	0.17	0.3	0.32	0.68	0.45	0.17	0.82	0.7	0.67	0.39	0.23	0.22	0.23
		0.17	0.17	0.24	0.29	0.24	0.19	0.25	0.27	0.39	0.29	0.17	0.29	0.31	0.64	0.46	0.17	0.86	0.73	0.69	0.38	0.24	0.23	0.23
STHB1 Left		0.16	0.16	0.26	0.28	0.22	0.21	0.24	0.24	0.35	0.27	0.16	0.32	0.34	0.68	0.47	0.16	0.84	0.68	0.71	0.38	0.25	0.26	0.26
		0.17	0.17	0.21	0.28	0.2	0.21	0.24	0.24	0.31	0.28	0.17	0.3	0.28	0.55	0.48	0.17	0.76	0.66	0.66	0.38	0.25	0.26	0.25
		0.17	0.17	0.24	0.28	0.22	0.21	0.25	0.25	0.34	0.27	0.17	0.32	0.3	0.58	0.45	0.17	0.8	0.68	0.71	0.36	0.23	0.24	0.25
		0.17	0.17	0.24	0.28	0.23	0.21	0.25	0.26	0.34	0.27	0.17	0.3	0.3	0.59	0.49	0.17	0.85	0.68	0.76	0.37	0.23	0.24	0.25
STHB2 Right		0.15	0.15	0.25	0.28	0.23	0.21	0.25	0.24	0.36	0.27	0.16	0.34	0.31	0.64	0.5	0.18	0.87	0.69	0.77	0.33	0.25	0.26	0.26
		0.17	0.17	0.24	0.28	0.23	0.21	0.24	0.25	0.25	0.28	0.17	0.31	0.3	0.62	0.46	0.17	0.83	0.68	0.75	0.36	0.24	0.25	0.25
		0.17	0.17	0.25	0.29	0.22	0.2	0.25	0.26	0.35	0.28	0.17	0.31	0.31	0.66	0.49	0.17	0.84	0.69	0.75	0.36	0.24	0.26	0.25
		0.17	0.17	0.25	0.28	0.22	0.21	0.25	0.26	0.34	0.28	0.17	0.31	0.31	0.65	0.48	0.17	0.85	0.7	0.74	0.35	0.23	0.25	0.25
STHB2 Left		0.16	0.16	0.26	0.28	0.22	0.21	0.26	0.24	0.36	0.28	0.16	0.34	0.32	0.66	0.49	0.17	0.86	0.7	0.78	0.34	0.26	0.26	0.26
		0.17	0.17	0.25	0.28	0.22	0.21	0.25	0.25	0.33	0.28	0.17	0.33	0.3	0.7	0.48	0.17	0.85	0.68	0.75	0.33	0.24	0.25	0.25
		0.17	0.17	0.25	0.28	0.23	0.2	0.26	0.25	0.36	0.28	0.17	0.32	0.28	0.65	0.48	0.17	0.84	0.68	0.76	0.34	0.24	0.24	0.24
		0.17	0.17	0.25	0.28	0.22	0.21	0.26	0.26	0.36	0.28	0.17	0.32	0.3	0.62	0.48	0.17	0.83	0.75	0.75	0.34	0.24	0.24	0.24
IP Left		0.18	0.17	0.24	0.29	0.24	0.2	0.26	0.26	0.42	0.27	0.17	0.34	0.29	0.76	0.48	0.18	0.84	0.77	0.75	0.35	0.2	0.22	0.23
		0.18	0.17	0.25	0.29	0.24	0.2	0.26	0.26	0.38	0.28	0.17	0.33	0.3	0.7	0.46	0.17	0.82	0.75	0.74	0.35	0.21	0.25	0.23
		0.18	0.17	0.24	0.3	0.23	0.21	0.26	0.3	0.38	0.28	0.17	0.33	0.28	0.75	0.46	0.17	0.81	0.77	0.71	0.34	0.21	0.23	0.23
		0.18	0.17	0.24	0.29	0.23	0.2	0.26	0.27	0.38	0.28	0.17	0.32	0.3	0.73	0.47	0.18	0.8	0.75	0.68	0.34	0.21	0.22	0.22
LTH/G Right		0.16	0.16	0.24	0.31	0.23	0.21	0.27	0.29	0.41	0.3	0.16	0.35	0.27	0.73	0.46	0.18	0.8	0.78	0.75	0.37	0.21	0.22	0.22
		0.17	0.17	0.25	0.3	0.24	0.2	0.26	0.28	0.4	0.29	0.17	0.34	0.28	0.72	0.45	0.17	0.82	0.77	0.68	0.37	0.21	0.21	0.21
		0.17	0.17	0.25	0.3	0.24	0.2	0.26	0.28	0.4	0.29	0.17	0.34	0.3	0.7	0.45	0.17	0.84	0.75	0.65	0.36	0.21	0.22	0.22
		0.17	0.17	0.24	0.29	0.23	0.2	0.26	0.28	0.39	0.3	0.17	0.32	0.3	0.73	0.46	0.18	0.86	0.74	0.69	0.36	0.21	0.22	0.22
NP4 Right		0.17	0.18	0.24	0.28	0.23	0.2	0.26	0.24	0.38	0.27	0.16	0.33	0.32	0.65	0.48	0.17	0.89	0.8	0.7	0.35	0.21	0.22	0.22
		0.17	0.18	0.24	0.29	0.23	0.2	0.26	0.25	0.38	0.28	0.17	0.32	0.3	0.7	0.48	0.17	0.9	0.76	0.67	0.35	0.21	0.23	0.21
		0.18	0.18	0.24	0.28	0.23	0.2	0.26	0.25	0.38	0.28	0.17	0.31	0.31	0.68	0.48	0.17	0.85	0.75	0.65	0.34	0.21	0.23	0.22
		0.17	0.18	0.24	0.28	0.23	0.2	0.26	0.26	0.4	0.28	0.17	0.31	0.3	0.68	0.45	0.18	0.86	0.76	0.68	0.34	0.21	0.23	0.22
NP4 Left		0.18	0.17	0.25	0.28	0.23	0.2	0.26	0.25	0.48	0.26	0.18	0.32	0.31	0.68	0.47	0.17	0.89	0.69	0.72	0.33	0.22	0.22	0.22
		0.18	0.18	0.25	0.28	0.24	0.21	0.26	0.26	0.45	0.28	0.18	0.32	0.28	0.67	0.44	0.17	0.8	0.7	0.7	0.33	0.21	0.23	0.21
		0.18	0.18	0.24	0.29	0.24	0.21	0.26	0.26	0.45	0.28	0.18	0.32	0.29	0.68	0.49	0.17	0.86	0.75	0.73	0.34	0.21	0.23	0.22
		0.18	0.18	0.24	0.29	0.23	0.2	0.26	0.25	0.44	0.28	0.18	0.31	0.29	0.65	0.48	0.17	0.84	0.76	0.71	0.34	0.21	0.23	0.22

		PELVIC THICKNESS (mm)																						
	ROI	1	2	3	4	5	6	7	8	9	10	11	12	13	14	15	16	17	18	19	20	21	22	23
Specimen																								
LTH/E Right		0.18	D	0.26	D	D	D	0.25	0.26	D	D	D	0.32	0.29	0.72	0.5	0.18	0.87	0.82	0.64	D	D	D	D
		0.18	D	0.25	D	D	D	0.26	0.26	D	D	D	0.31	0.3	0.7	0.48	0.18	0.85	0.8	0.69	D	D	D	D
		0.18	D	0.25	D	D	D	0.26	0.26	D	D	D	0.31	0.31	0.72	0.48	0.18	0.85	0.79	0.68	D	D	D	D
		0.18	D	0.26	D	D	D	0.26	0.26	D	D	D	0.31	0.28	0.72	0.48	0.18	0.86	0.76	0.64	D	D	D	D
LTH/E Left		0.18	0.18	D	D	0.23	0.21	D	0.26	0.4	0.27	0.17	0.32	0.28	0.74	0.45	0.18	0.86	0.78	0.68	0.36	0.22	0.23	0.23
		0.18	0.18	D	D	D	0.21	D	0.26	0.38	0.28	0.17	0.32	0.27	0.72	0.48	0.18	0.82	0.76	0.63	0.35	0.21	0.23	0.22
		0.18	0.18	D	D	D	0.2	D	0.26	0.4	0.28	0.17	0.32	0.28	0.7	0.48	0.18	0.85	0.75	0.63	0.35	0.21	0.23	0.22
		0.18	0.18	D	D	D	0.2	D	0.26	0.4	0.28	0.17	0.32	0.3	0.75	0.46	0.18	0.86	0.78	0.68	0.35	0.21	0.23	0.23
NP2 Right		0.18	0.18	0.24	0.29	0.24	0.2	0.26	0.25	0.4	0.26	0.18	0.35	0.35	0.72	0.46	0.18	0.85	0.82	0.71	0.37	0.23	0.24	0.24
		0.18	0.18	0.24	0.29	0.24	0.2	0.26	0.26	0.38	0.28	0.18	0.34	0.34	0.74	0.48	0.18	0.82	0.78	0.69	0.35	0.22	0.23	0.23
		0.18	0.18	0.25	0.29	0.24	0.2	0.26	0.26	0.38	0.28	0.18	0.32	0.34	0.75	0.46	0.18	0.86	0.75	0.67	0.36	0.23	0.23	0.23
		0.18	0.18	0.25	0.29	0.24	0.2	0.26	0.26	0.39	0.28	0.18	0.32	0.32	0.72	0.47	0.18	0.84	0.75	0.65	0.36	0.23	0.23	0.23
NP2 Left		0.18	0.18	0.24	0.29	0.23	0.2	0.26	0.26	0.41	0.26	0.18	0.35	0.35	0.72	0.45	0.18	0.83	0.73	0.68	0.34	0.23	0.23	0.24
		0.18	0.18	0.25	0.28	0.24	0.2	0.26	0.26	0.4	0.28	0.18	0.34	0.35	0.76	0.46	0.18	0.9	0.8	0.65	0.35	0.23	0.23	0.23
		0.18	0.18	0.25	0.29	0.23	0.2	0.26	0.26	0.4	0.28	0.18	0.34	0.35	0.78	0.46	0.18	0.85	0.79	0.69	0.34	0.23	0.23	0.24
		0.18	0.18	0.25	0.29	0.23	0.2	0.26	0.26	0.4	0.28	0.18	0.32	0.35	0.8	0.48	0.18	0.86	0.78	0.71	0.34	0.22	0.23	0.23
LTH/F Right		0.2	0.19	0.26	0.28	0.26	0.2	0.29	0.32	0.58	0.26	0.19	0.32	0.56	0.96	0.48	0.2	0.96	0.83	0.74	0.37	0.23	0.24	0.25
		0.19	0.18	0.25	0.28	0.26	0.2	0.28	0.29	0.48	0.28	0.18	0.32	0.48	0.85	0.48	0.19	0.9	0.85	0.75	0.36	0.22	0.23	0.24
		0.19	0.19	0.26	0.28	0.25	0.2	0.28	0.3	0.45	0.28	0.18	0.34	0.45	0.88	0.46	0.19	0.95	0.79	0.75	0.36	0.23	0.22	0.24
		0.2	0.19	0.26	0.28	0.26	0.2	0.29	0.25	0.5	0.28	0.18	0.32	0.48	0.82	0.48	0.19	0.91	0.83	0.74	0.36	0.22	0.24	0.24
LTH/F Left		0.2	0.2	0.27	0.29	0.28	0.22	0.28	0.36	0.5	0.32	0.19	0.31	0.49	0.89	0.48	0.18	0.91	0.87	0.77	0.38	0.23	0.24	0.24
		0.2	0.19	0.27	0.29	0.26	0.2	0.28	0.31	0.45	0.31	0.18	0.32	0.45	0.85	0.5	0.18	0.9	0.88	0.78	0.36	0.22	0.24	0.24
		0.19	0.19	0.27	0.29	0.28	0.2	0.28	0.32	0.51	0.3	0.18	0.3	0.45	0.84	0.48	0.19	0.94	0.86	0.75	0.36	0.22	0.24	0.24
		0.19	0.19	0.27	0.29	0.28	0.2	0.28	0.34	0.48	0.3	0.18	0.31	0.46	0.86	0.48	0.18	0.92	0.82	0.76	0.36	0.22	0.23	0.24
SA/A Right		0.19	0.19	D	0.28	0.28	0.21	D	0.35	0.57	0.3	0.19	0.31	0.48	0.85	0.55	0.19	0.86	0.9	0.78	0.36	0.26	0.25	0.25
		0.19	0.21	D	0.29	0.26	0.2	D	0.35	0.53	0.28	0.18	0.31	0.48	0.82	0.52	0.18	0.88	0.86	0.76	0.35	0.25	0.23	0.24
		0.19	0.19	D	0.3	0.26	0.2	D	0.35	0.52	0.3	0.18	0.32	0.5	0.88	0.55	0.19	0.96	0.81	0.76	0.35	0.24	0.23	0.24
		0.19	0.19	D	0.28	0.28	0.2	D	0.34	0.55	0.3	0.18	0.31	0.48	0.84	0.53	0.18	0.83	0.88	0.78	0.35	0.23	0.23	0.24
SA/E Right		0.19	0.19	0.28	0.3	0.24	0.2	0.27	0.31	0.58	0.32	0.2	0.31	0.5	0.9	0.63	0.19	0.93	0.86	0.73	0.36	0.24	0.26	0.28
		0.119	0.19	0.28	0.3	0.26	0.2	0.26	0.3	0.55	0.28	0.19	0.32	0.48	0.89	0.59	0.18	0.9	0.86	0.74	0.35	0.23	0.25	0.24
		0.19	0.19	0.27	0.28	0.26	0.2	0.26	0.31	0.55	0.3	0.19	0.32	0.48	0.85	0.58	0.19	0.84	0.88	0.75	0.35	0.23	0.25	0.24
		0.19	0.19	0.28	0.3	0.25	0.2	0.26	0.31	0.54	0.28	0.19	0.32	0.49	0.83	0.6	0.18	0.85	0.86	0.75	0.35	0.23	0.25	0.24
SA/E Left		0.19	0.2	0.3	0.3	0.24	0.2	0.25	0.32	0.62	0.3	0.18	0.31	0.54	0.92	0.62	0.2	0.89	0.81	0.75	0.34	0.24	0.28	0.27
		0.19	0.2	0.28	0.3	0.26	0.2	0.26	0.31	0.6	0.3	0.18	0.31	0.49	0.9	0.58	0.2	0.9	0.84	0.76	0.35	0.24	0.26	0.24
		0.19	0.2	0.28	0.29	0.25	0.2	0.26	0.32	0.58	0.29	0.18	0.32	0.48	0.85	0.59	0.2	0.85	0.86	0.75	0.35	0.22	0.25	0.24
		0.19	0.19	0.29	0.28	0.24	0.2	0.26	0.32	0.54	0.28	0.18	0.32	0.48	0.84	0.55	0.19	0.86	0.82	0.74	0.35	0.24	0.25	0.24
NP1 Right		0.2	0.21	0.26	0.28	0.23	0.22	0.28	0.32	0.56	0.26	0.2	0.32	0.56	0.89	0.5	0.2	0.93	0.88	0.74	0.35	0.26	0.25	0.26
		0.19	0.2	0.28	0.28	0.26	0.2	0.27	0.32	0.56	0.28	0.19	0.31	0.54	0.89	0.53	0.2	0.9	0.88	0.74	0.35	0.26	0.24	0.24
		0.19	0.2	0.29	0.29	0.26	0.21	0.27	0.3	0.54	0.28	0.19	0.31	0.54	0.87	0.56	0.2	0.88	0.86	0.75	0.35	0.25	0.25	0.24
		0.19	0.21	0.26	0.3	0.24	0.21	0.28	0.31	0.5	0.28	0.19	0.31	0.52	0.88	0.58	0.2	0.86	0.85	0.76	0.35	0.26	0.25	0.24

		PELVIC THICKNESS (mm)																						
	ROI	1	2	3	4	5	6	7	8	9	10	11	12	13	14	15	16	17	18	19	20	21	22	23
Specimen																								
NP1 Left		0.2	0.2	0.26	0.28	0.23	0.22	0.28	0.32	0.55	0.26	0.2	0.31	0.57	0.9	0.51	0.2	0.9	0.86	0.74	0.36	0.26	0.26	0.26
		0.2	0.2	0.26	0.29	0.26	0.21	0.28	0.3	0.5	0.28	0.19	0.31	0.54	0.89	0.55	0.2	0.88	0.84	0.76	0.35	0.24	0.25	0.25
		0.19	0.19	0.27	0.28	0.26	0.21	0.28	0.3	0.52	0.28	0.19	0.31	0.54	0.89	0.56	0.19	0.85	0.84	0.74	0.36	0.26	0.25	0.25
		0.19	0.2	0.26	0.3	0.26	0.21	0.28	0.32	0.54	0.28	0.19	0.31	0.54	0.89	0.58	0.18	0.88	0.83	0.74	0.36	0.26	0.25	0.25
SA/F Right		0.2	0.2	0.32	0.25	0.23	0.22	0.3	0.32	0.61	0.3	0.2	0.3	0.49	0.94	0.67	0.2	0.97	0.83	0.73	0.31	0.25	0.26	0.27
		0.19	0.19	0.29	0.28	0.26	0.22	0.29	0.32	0.58	0.29	0.19	0.31	0.51	0.9	0.6	0.2	0.9	0.84	0.75	0.32	0.25	0.25	0.25
		0.19	0.2	0.3	0.27	0.25	0.22	0.29	0.31	0.59	0.3	0.19	0.31	0.51	0.94	0.63	0.18	0.92	0.85	0.76	0.32	0.26	0.25	0.26
		0.19	0.2	0.32	0.28	0.26	0.22	0.3	0.31	0.56	0.3	0.19	0.31	0.52	0.94	0.63	0.2	0.95	0.85	0.71	0.33	0.26	0.25	0.25
SA/F Left		0.18	0.18	0.3	0.28	0.24	0.22	0.31	0.32	0.65	0.3	0.19	0.32	0.51	0.96	0.65	0.19	0.98	0.85	0.7	0.33	0.26	0.26	0.27
		0.18	0.19	0.3	0.28	0.25	0.22	0.3	0.31	0.6	0.28	0.19	0.31	0.49	0.93	0.59	0.18	0.99	0.83	0.7	0.35	0.24	0.25	0.25
		0.18	0.18	0.3	0.28	0.24	0.21	0.3	0.31	0.6	0.28	0.19	0.31	0.48	0.91	0.53	0.18	0.98	0.84	0.73	0.35	0.25	0.25	0.26
		0.18	0.18	0.29	0.29	0.24	0.22	0.3	0.31	0.58	0.3	0.19	0.31	0.5	0.9	0.68	0.2	0.88	0.83	0.75	0.35	0.26	0.25	0.26
SA/J Right		0.2	0.2	0.28	0.28	0.23	0.23	0.3	0.32	0.58	0.28	0.21	0.32	0.5	0.96	0.55	0.21	0.98	0.79	0.7	0.35	0.26	0.26	0.27
		0.2	0.19	0.29	0.28	0.24	0.22	0.29	0.32	0.54	0.3	0.2	0.31	0.48	0.91	0.62	0.2	0.9	0.8	0.72	0.35	0.26	0.25	0.27
		0.19	0.18	0.3	0.29	0.24	0.21	0.29	0.31	0.56	0.32	0.21	0.31	0.48	0.89	0.62	0.2	0.95	0.75	0.73	0.35	0.25	0.25	0.26
		0.19	0.19	0.3	0.3	0.25	0.22	0.3	0.31	0.58	0.28	0.21	0.31	0.49	0.89	0.59	0.2	0.94	0.76	0.71	0.35	0.24	0.25	0.26
SA/J Left		0.19	0.19	0.3	0.3	0.24	0.22	0.3	0.33	0.56	0.3	0.2	0.32	0.49	0.96	0.62	0.2	0.99	0.8	0.73	0.34	0.26	0.26	0.27
		0.19	0.19	0.3	0.29	0.25	0.21	0.29	0.32	0.56	0.29	0.19	0.31	0.48	0.89	0.6	0.2	0.98	0.82	0.7	0.35	0.26	0.25	0.26
		0.18	0.19	0.31	0.3	0.24	0.21	0.29	0.32	0.55	0.29	0.19	0.31	0.49	0.88	0.6	0.2	0.96	0.82	0.72	0.35	0.25	0.25	0.26
		0.19	0.19	0.29	0.29	0.25	0.21	0.3	0.32	0.55	0.3	0.19	0.31	0.45	0.85	0.59	0.2	0.95	0.83	0.76	0.35	0.26	0.25	0.26
P1 Right		0.2	0.19	0.28	0.28	0.28	0.21	0.29	0.33	0.56	0.28	0.19	0.31	0.47	0.89	0.6	0.19	0.93	0.85	0.73	0.36	0.25	0.25	0.25
		0.2	0.19	0.29	0.29	0.28	0.2	0.29	0.32	0.56	0.28	0.19	0.31	0.45	0.88	0.58	0.2	0.96	0.83	0.72	0.35	0.25	0.25	0.26
		0.2	0.19	0.29	0.28	0.27	0.21	0.29	0.32	0.54	0.28	0.19	0.31	0.48	0.83	0.55	0.2	0.93	0.81	0.71	0.35	0.25	0.25	0.26
		0.2	0.19	0.29	0.28	0.28	0.21	0.3	0.32	0.58	0.28	0.19	0.31	0.48	0.82	0.56	0.2	0.93	0.84	0.73	0.35	0.25	0.25	0.25
P1 Left		0.19	0.19	0.29	0.27	0.24	0.2	0.27	0.33	0.59	0.29	0.2	0.31	0.53	0.88	0.62	0.2	0.93	0.84	0.72	0.35	0.26	0.25	0.25
		0.19	0.19	0.3	0.28	0.26	0.2	0.26	0.32	0.58	0.3	0.19	0.31	0.49	0.83	0.6	0.2	0.9	0.85	0.7	0.35	0.25	0.25	0.26
		0.19	0.19	0.29	0.28	0.25	0.21	0.26	0.32	0.58	0.3	0.19	0.31	0.5	0.85	0.58	0.2	0.95	0.86	0.73	0.35	0.26	0.25	0.25
		0.19	0.19	0.29	0.27	0.25	0.21	0.26	0.32	0.56	0.28	0.19	0.31	0.54	0.85	0.54	0.2	0.94	0.84	0.74	0.35	0.25	0.25	0.26
SA/B Right		0.2	0.2	0.29	0.34	0.24	0.21	0.26	0.3	0.47	0.29	0.2	0.31	0.5	0.89	0.6	0.2	0.86	D	D	D	D	D	D
		0.19	0.19	0.3	0.3	0.25	0.2	0.26	0.29	0.5	0.29	0.19	0.31	0.54	0.85	0.58	0.2	0.9	D	D	D	D	D	D
		0.2	0.2	0.3	0.3	0.25	0.21	0.26	0.3	0.52	0.3	0.19	0.31	0.56	0.86	0.56	0.2	0.88	D	D	D	D	D	D
		0.2	0.2	0.29	0.31	0.25	0.21	0.26	0.3	0.5	0.3	0.19	0.31	0.54	0.89	0.59	0.2	0.95	D	D	D	D	D	D
SA/B Left		0.2	0.2	0.28	0.32	0.25	0.21	0.28	0.29	0.45	0.29	0.2	0.31	0.5	0.89	0.62	0.2	0.94	0.86	0.75	0.32	0.25	0.25	0.25
		0.19	0.2	0.29	0.31	0.25	0.2	0.29	0.28	0.48	0.3	0.19	0.31	0.47	0.85	0.6	0.2	0.94	0.86	0.7	0.36	0.24	0.25	0.25
		0.2	0.19	0.28	0.3	0.26	0.21	0.28	0.28	0.45	0.3	0.19	0.31	0.5	0.85	0.63	0.2	0.96	0.83	0.73	0.35	0.24	0.25	0.24
		0.2	0.19	0.29	0.3	0.26	0.21	0.28	0.28	0.45	0.28	0.19	0.31	0.47	0.86	0.64	0.2	0.94	0.83	0.75	0.36	0.24	0.25	0.24
SA/D Right		0.2	0.2	0.31	0.31	0.23	0.21	0.28	0.3	0.56	0.28	0.21	0.31	0.56	0.81	0.6	0.21	0.89	0.89	0.76	0.38	0.25	0.25	0.25
		0.2	0.19	0.3	0.3	0.23	0.21	0.29	0.32	0.56	0.28	0.2	0.32	0.6	0.8	0.63	0.2	0.9	0.9	0.7	0.36	0.24	0.25	0.24
		0.2	0.2	0.3	0.29	0.22	0.21	0.28	0.32	0.58	0.28	0.2	0.31	0.58	0.8	0.65	0.2	0.85	0.88	0.75	0.36	0.24	0.25	0.25
		0.2	0.2	0.3	0.3	0.23	0.22	0.28	0.28	0.54	0.28	0.21	0.32	0.59	0.81	0.6	0.2	0.84	0.85	0.72	0.38	0.24	0.25	0.24

Appendix 4

Peer reviewed publications in support of this thesis:

Cunningham, C.A. and Black, S.M. (2009). Development of the fetal ilium – challenging concepts of bipedality. *Journal of Anatomy*. **214**:91-99.

Cunningham, C.A. and Black, S.M. (2009). Anticipating bipedalism: Trabecular organisation in the newborn ilium. *Journal of Anatomy*. **214**:817-829.

Cunningham C.A. and Black, S.M. (2009). Iliac cortical thickness in the neonate- the gradient effect. *Journal of Anatomy*. DOI: 10.1111/j.1469-7580.2009.01112.x

Conference papers presented in support of this thesis:

Cunningham, C.A. (2009). Structural maturity in the neonatal ilium. British Association of Clinical Anatomists (BACA). Summer meeting. University of Dundee.

Cunningham, C.A. (2009). Trabecular bone organisation in the neonatal ilium. British Association for Human Identification (BAHID), 10th Annual Conference. University of Dundee.

Cunningham, C.A. (2008). Trabecular quantification of the neonatal ilium - revealing origins of load bearing structures. Forensic Anthropology Society Europe (FASE). Tri-annual meeting.

Cunningham, C.A. (2007). Radiographic Evaluation of Trabecular Patterning in the Fetal and Neonatal Ilium. British Association for Human Identification (BAHID), 9th Annual Conference. University of Surrey.

Scholarships and awards pertaining to the research presented in this thesis:

British Association for Clinical Anatomists (BACA). Conrad Lewin Prize. July 2009.

British Association for Human Identification (BAHID). Scholarship Award. June 2009.

Wenner-Gren Dissertation Fieldwork Grant. Awarded by Wenner-Gren Foundation. August 2007.

Leng Trust. Awarded Overseas Grant. Awarded by Leng Trust Fund. May 2007.